Discrimination between nuclear and cytosolic effects of the small Rho GTPase RAC1 in the DNA damage response

Inaugural-Dissertation

zur Erlangung des Doktorgrades
der Mathematisch-Naturwissenschaftlichen Fakultät
der Heinrich-Heine-Universität Düsseldorf

vorgelegt von

Rebekka Katharina Kitzinger
aus Mainz

Düsseldorf, Dezember 2021

aus dem Institut für Toxikologie
der Heinrich-Heine-Universität Düsseldorf

Gedruckt mit der Genehmigung der
Mathematisch-Naturwissenschaftlichen Fakultät der
Heinrich-Heine-Universität Düsseldorf

Berichterstatter:

1. Prof. Dr. Gerhard Fritz

2. Prof. Dr. Sebastian Wesselborg

Tag der mündlichen Prüfung: 19.10.2022

Innocent – like a fairytale
It started with the blink of an eye
Wonderful – it had to be fate
But the indifference made us say goodbye
It has come to an end now
It is time to say goodbye

Beautiful nightmare
Couldn't survive on the battlefield
But I'm starting to heal
Beautiful nightmare
Lucky that we reached the top
As they say what goes up must come down

Dead by April, "Beautiful Nightmare"

Table of contents

List of abbreviations

% (v/v)	volume-volume percentage
% (w/v)	weight-volume percentage
53BP1	P53-binding protein 1
F-actin	filamentous actin
G-actin	globular actin
ATM	Ataxia telangiectasia mutated
ATR	Ataxia telangiectasia and Rad3-related
bp	base pairs
BSA	bovine serum albumin
$CaCl_2$	calcium chloride
CDC25A	cell division cycle 25A
CDC42	cell division control protein 42 homolog
CHK1	checkpoint kinase 1
CHK2	checkpoint kinase 2
Cre	Cre recombinase
Cre.ER	mutated estrogen receptor fused to Cre
DAPI	4′,6-diamidino-2-phenylindole
DDR	DNA damage response
DMEM	Dulbecco’s Modifies Eagle Medium, high glucose
DNA	deoxyribonucleic acid
DNA DSB	DNA double strand break
DNA-PK	DNA-dependent protein kinase
DNA SSB	DNA single strand break
DOCK6	dedicator of cytokinesis 6
Dox	doxorubicin

EDTA	ethylenediaminetetraacetic acid
EHT 1864	RAC1 inhibitor
FCS	fetal calf serum
GAP	GTPase-activating protein
GAPDH	Glyceraldehyde 3-phosphate dehydrogenase
GDI	guanine-nucleotide dissociation inhibitor
GDP	guanosine-5'-diphosphate
GEF	guanine-nucleotide exchange factor
GFP	green fluorescent protein
GFP-hRAC1(Q61L)	GFP-coupled constitutively active hRAC1
GFP-hRAC1(T17N)	GFP-coupled dominant-negative hRAC1
GFP-hRAC1(WT)	GFP-coupled wild-type hRAC1
GFP-NLS-hRAC1(Q61L)	GFP-hRAC1(Q61L) with additional NLS
GFP-NLS-hRAC1(T17N)	GFP-hRAC1(T17N) with additional NLS
GFP-NLS-hRAC1(WT)	GFP-hRAC1(WT) with additional NLS
GTP	guanosine 5'-triphosphate
Gy	grey (units radiation dose)
γH2AX	phosphorylated histone 2A family member X
HR	homologous recombination
HRP	horseradish peroxidase
IMDM	Iscove's Modified Dulbecco's Medium, without L-glutamine
IR	ionizing radiation
KAP1	KRAB-associated protein-1
L	leucine
MEF	mouse embryonic fibroblasts

mm	*mus musculus*
MRE11	meiotic recombination 11
N	asparagine
NaCL	sodium chloride
NBS1	Nijmegen breakage syndrome 1
NHEJ	non-homologous end joining
NLS	nuclear localisation sequence
NPM	nucleophosmin
4-OHT	(Z)-4-Hydroxytamoxifen, active tamoxifen metabolite
P53	tumor suppressor P53
PBS	phosphate buffered saline
PEI	polyethyleneimine
PI3K	phosphatidylinositol-3-kinases
PBR	polybasic region
Q	glutamine
QVD	Q-VD-OPh hydrate, pan-caspase inhibitor
RAC1	Ras-related C3 botulinum toxin substrate 1
Rac1$^{flx/flx}$	*Rac1* gene is flanked by loxP sites
hRAC1	human RAC1
mRac1/mRAC1	murine *Rac1* (gene)/murine RAC1 (protein)
*mRac1*siRNA	siRNA against murine *Rac1*
Ras	Rat sarcoma
RHOA	Ras homolog gene family member A
Rho GTPase	Ras-homologous GTPase
ROS	reactive oxygen species
RPA	Replication protein A

SD	standard deviation
SDS	sodium dodecyl sulfate
SEM	standard error of the mean
T	threonine
Tam	tamoxifen
TBST	tris buffered saline with Tween 20
TEMED	tetramethylethylenediamine
TIAM1	T-Cell Lymphoma Invasion and Metastasis 1
TIAM2	T-Cell Lymphoma Invasion and Metastasis 2
Top II	Topoisomerase II
TRITC	tetramethyl rhodamine
wt/WT	wild-type
XRCC4	X-ray repair cross-complementing protein 4

List of figures

List of tables

1 Introduction

1.1 Ras homologous GTPases

Ras-homologous GTPases (Rho GTPases) belong to the Ras (rat sarcoma) superfamily of small GTP-binding proteins (Hall 1990). More than 150 monomeric proteins belong to the Ras superfamily (Ferri et al. 2013) and are divided into five families dependent on their structure, sequence and functional similarities (Figure 1.1). The families are: Ras, Rho, Rab, Arf, and Ran (Wennerberg et al. 2005). Activated Ras GTPases interact with various downstream effectors, which are involved in the control of gene expression, as well as regulation of proliferation, differentiation and survival (Wennerberg et al. 2005). Rab (Ras-like proteins in brain) and Arf (ADP-ribosylation factor) proteins are involved in vesicular transport and in traffic of proteins between organelles (Zerial et al. 2001; Memon 2004). The Ran (Ras-like nuclear) proteins function in nucleocytoplasmic transport (Weis 2003) as well as in regulation of the mitotic spindle assembly, DNA replication, and nuclear envelope assembly (Li et al. 2003). In mammals, the Rho family consists of 19 proteins which can be divided into six different subfamilies. Namely, these subfamilies are Rho, Rac, Cdc42, Rnd, RhoBTB, and RhoT/Miro (Bustelo et al. 2007). Based on their sequence homologies (40 % - 95 %), function, and structure (Wennerberg et al. 2004) the proteins are classified into each group. The structure which distinguishes Rho GTPases from other small GTPases is the so-called Rho insert domain. This domain is needed for the activation of Rho-specific signaling pathways (Valencia et al. 1991). Rho GTPases function as molecular switches in various signaling pathways of mammalian cells. As molecular switches, Rho GTPases transduce external stimuli from the cell membrane to diverse kinases, transcription factors, and modulators of the cytoskeleton (Etienne-Manneville et al. 2002). The best characterized representatives of the Rho GTPases are RHOA (Ras homolog gene family member A), RAC1 (Ras-related C3 botulinum toxin substrate 1), and CDC42 (Cell division control protein 42 homolog) (Hall 1998; Wennerberg et al. 2005). In fibroblasts constitutively active mutants of RHO induce stress fiber formation, constitutively active mutants of RAC enhance lamellipodia formation and membrane ruffling, and constitutively active mutants of CDC42 induce the expression of filopodia (Ridley, Paterson, et al. 1992; Machesky et al. 1996; Etienne-Manneville et al. 2002). Due to this specific phenotype of the cells after activation of Rho GTPases, they were characterized as modulators of the actin cytoskeleton, cell motility and polarity, as well as cell growth. Later their influence on cellular apoptosis, gene transcription, proliferation, and stress responses was discovered (Bishop et al. 2000; Ellenbroek et al. 2007).

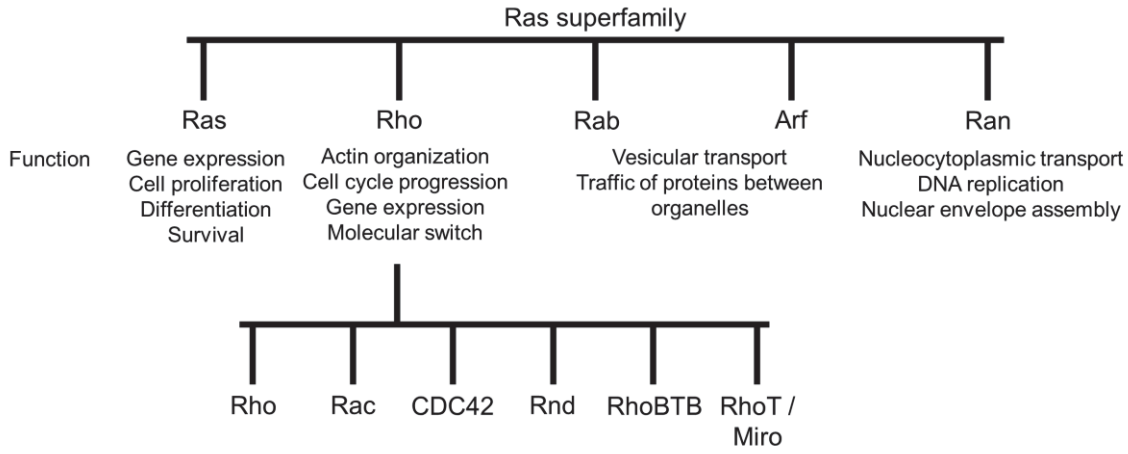

Figure 1.1: Functions of the Ras superfamily and organization of the Rho GTPases.
The various families of the Ras superfamily and their functions as well as the organization of the subfamily of Rho GTPases are shown. The Ras proteins are involved in gene expression, cell proliferation, differentiation, and cell survival (Wennerberg et al. 2005). Vesicular transport and traffic of proteins between organelles belongs to the functions of Rab and Arf proteins (Zerial et al. 2001; Memon 2004). The family of Ran proteins is involved in nucleocytoplasmic transport, DNA replication, and nuclear envelope assembly (Li et al. 2003; Weis 2003). The Rho family members are molecular switches known for actin organization, cell cycle progression, and gene expression (Etienne-Manneville et al. 2002; Wennerberg et al. 2005). The Rho proteins can be divided into six groups, namely Rho, Rac, CDC42, Rnd, RhoBTB, and RhoT/Miro (Bustelo et al. 2007).

1.1.1 The Ras-related C3 botulinum toxin substrate 1

The Ras-related C3 botulinum toxin substrate 1 (RAC1) belongs to the family of small Rho GTPases (Bar-Sagi et al. 2000; Etienne-Manneville et al. 2002; Wennerberg et al. 2005) and is involved in the regulation of a wide range of cellular functions. RAC1 is a molecular switch that cycles between a guanosine-5'-diphosphate (GDP)-bound (inactive) state and a guanosine 5'-triphosphate (GTP)-bound (active) state which allows interaction with effector proteins (Bustelo et al. 2007). Three families of regulatory proteins are controlling the activities of Rho GTPases: guanine-nucleotide exchange factors (GEF) (Cerione et al. 1996; Zheng 2001), GTPase-activating proteins (GAP) (Bokoch et al. 1993; Lamarche et al. 1994), and guanine-nucleotide dissociation inhibitors (GDI) (Olofsson 1999).

Like most Rho GTPases RAC1 possesses a C-terminal hypervariable region ending with the so-called CAAX (C = cysteine residue, A = aliphatic amino acid, X = any amino acid) box (Figure 1.2). This box is a tetrapeptide within the sequence for membrane localization. A requirement for translocation to membranes is the posttranslational modification (isoprenylation) of RAC1. The last amino acid of the CAAX box determines which isoprenoid (farnesyl or geranylgeranyl) will be added (Moores et al. 1991;

Yokoyama et al. 1991). For example, if X is an alanine, cysteine, glutamine, methionine, or serine the protein gets farnesylated (Moores et al. 1991; Baron et al. 2000). An isoleucine, leucine, or phenylalanine on the other hand leads to geranylgeranylation of the protein (Yokoyama et al. 1991; Baron et al. 2000). RAC1 is modified by geranylgeranylation due to the cysteine at its CAAX box (Figure 1.2).

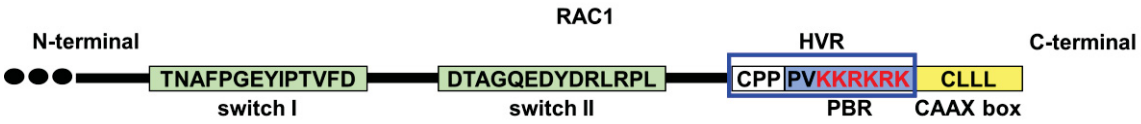

Figure 1.2: Scheme of different domains of RAC1.
The figure shows different domains of RAC1. Switch I and switch II are marked in green, polybasic region (PBR) is marked in light blue, hypervariable region (HVR) is marked with a dark blue frame, CAAX box is marked in yellow, and the canonical NLS sequences (KKRK, RKRK) are marked in red letters. Figure is adapted from Lanning *et al.*, Liang *et al.*, Senyuz *et al*. (Lanning et al. 2004; Liang et al. 2021; Senyuz et al. 2021).

This modification is a prerequisite for translocation to membranes and subsequent activation (Adamson, Marshall, et al. 1992; Adamson, Paterson, et al. 1992; Lin et al. 2015). Without membrane localization there would be no activation of cytosolic RAC1 by GEF and subsequently no signal transduction of extracellular stimuli (Etienne-Manneville et al. 2002; Konstantinopoulos et al. 2007). The prenyl anchor can be masked by RhoGDI, thus cytosolic sequestration of Rho GTPases is preferred (Olofsson 1999; Hoffman et al. 2000). GDI capture and stabilize the inactive GDP-bound form of RAC1 in the cytosol by preventing the dissociation of GDP by interaction of the RhoGDI with the switch regions of RAC1. This in return results in the inability of effectors and GAP to bind to RAC1. The isoprenyl group is shielded and therefore a localization at the membrane is impossible and the activation of RAC1 is prevented (Harding et al. 2010; Bustelo et al. 2012; Cherfils et al. 2013; Lawson et al. 2014; Olson 2016; Porter et al. 2016) (Figure 1.3). GDI are also responsible for the transport and solubility of Rho GTPases in the cytosol (Garcia-Mata et al. 2011). By ubiquitination RAC1 is determined for degradation in the proteasome (Hoffman et al. 2000) which is prevented by being linked to GDI (Boulter et al. 2010). Cytosolic RAC1 is transported to the plasma membrane upon cell stimulation (Bustelo et al. 2007; Bustelo et al. 2012). GEF are responsible for activation of RAC1 and other Rho GTPases. For the Rho family members more than 80 GEF are known by now. RAC1 specific ones are e.g., TIAM1 (T-Cell Lymphoma Invasion and Metastasis 1), VAV proteins, and TRIO (Michiels et al. 1995; Bellanger et al. 1998). GEF are often the targets of biological signals, which induce, inhibit, or modulate their catalytic activity (Bos et al. 2007). Several members of the GEF

family have a PH (plextrin homology) domain, e.g., TIAM1 and VAV proteins. The phospholipid PIP3 (phosphatidylinositol(3,4,5)-triphosphate) can bind to the domain thereby activating the GEF (Welch et al. 2003; Minard et al. 2004; Campa et al. 2015). GEF can also be activated in a PI3K (phosphatidylinositol-3-kinases)-independent manner by tyrosine phosphorylation (Wertheimer et al. 2012). Through catalysis of the exchange of GDP to GTP GEF can activate RAC1. This happens by opening the nucleotide-binding site of RAC1, which is resulting in the dissociation of GDP and binding of GTP. The affinity of RAC1 for GDP and GTP is not changed by GEF, but due to the approximately ten times higher cellular concentration of GTP compared to GDP a binding of GTP to RAC1 is more likely (Welch et al. 2003; Bos et al. 2007). In this active form, the isoprenylated RAC1 is bound to the inner side of the outer cell membrane. GAP can be regulated by protein-protein as well as protein-lipid interactions, and/or posttranslational modifications (Bos et al. 2007). GAP are inactivating RAC1 by accelerating their weak intrinsic GTP hydrolysis rate up to 10^5 (Rittinger et al. 1997; Shutes et al. 2006). The mechanism underlying the GAP-stimulated hydrolysis is that GAP provides an arginine, the so-called arginine finger, to stabilize the partial negative charges that develop at the transition state. Furthermore, it positions the conserved glutamine from the switch II (Q61 in RAC1) to activate a water molecule. This water molecule in turn attacks the γ-phosphate of GTP. Most likely, GAP is released with the P_i during the conformational change of RAC1 (Shutes et al. 2006; Bos et al. 2007; Cherfils et al. 2013). While cycling between the active and the inactive state, the switch I and the switch II region undergo conformation change as a signal of RAC1 being active or inactive which is recognized by downstream effectors (Bishop et al. 2000; Vetter et al. 2001; Dvorsky et al. 2004).

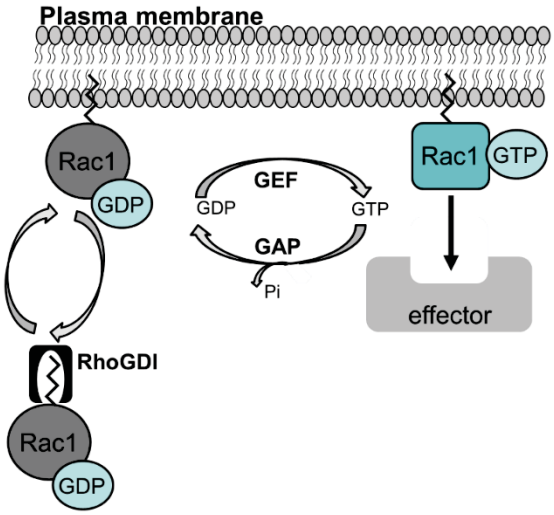

Figure 1.3: Cycling of RAC1 between GTP-bound and GDP-bound state.

RAC1 is a molecular switch that cycles between a guanosine-5'-diphosphate (GDP)-bound (inactive) state and a guanosine 5'-triphosphate (GTP)-bound (active) state which allows interaction with effector proteins (Bustelo et al. 2007). GEF (guanine-nucleotide exchange factors) are activating RAC1 by catalysis of the exchange of GDP to GTP. In this form, the isoprenylated GTP-bound RAC1 is bound to the inner side of the outer cell membrane. GAP (GTPase-activating proteins) are inactivating RAC1 by accelerating their weak intrinsic GTP hydrolysis rate (Shutes et al. 2006). RhoGDI capture and stabilize the inactive form of RAC1 in the cytosol by preventing the dissociation of GDP. The isoprenyl group is shielded and therefore a localization at the membrane is impossible and the activation of RAC1 is prevented (Olson 2016). Cytosolic RAC1 is transported to the plasma membrane upon cell stimulation (Bustelo et al. 2007). The figure is adapted from Onesto *et al.* as well as Fritz and Kaina (Onesto et al. 2008; Fritz et al. 2013).

RAC1 is involved in the regulation of a wide range of cellular functions including cell-cell adhesion, membrane ruffling, cell morphology, cytoskeletal organization, and motility (Bourne et al. 1990; Hall 2012). Due to the crosstalk with other Rho GTPases, RAC1 mediates the motility of a cell (Ridley, Paterson, et al. 1992). Adjustment of the polymerization of actin for the assembly of stress fibers (RHOA), as well as formation of lamellipodia (RAC1) is under control of small Rho GTPases (Nobes et al. 1995). Actin polymerization induces the expansion of rod-like protrusions, named filopodia, as well as sheet-like protrusions, named lamellipodia. Parts of the actin cytoskeleton are monomeric globular actin (G-actin) units, which turn into filamentous actin (F-actin) by polymerization (Lee et al. 2010). Restructuring of F-actin into lamellipodia or membrane ruffles is promoted by RAC1 by control of the ARP2/3 complex (Actin Related Protein 2/3 complex), which mediates actin polymerization (Bisi et al. 2013). The counterparts of RAC1 are RHOA and CDC42. They promote stress fiber and filopodia formation (Karnoub et al. 2001). In addition to the functions of RAC1 regarding the actin cytoskeleton, the small GTPase is also involved in processes like apoptosis (Jin et al. 2006; Yoshida et al. 2010), wound healing (DiPersio 2007; Tscharntke et al. 2007), as well as proliferation, migration and cell cycle progression (Olson et al. 1995; Deplazes et al. 2009; Yoshida et al. 2010; Yan et al. 2012). Beyond that, studies revealed an involvement of RAC1 in response to genotoxic stress (Damrot et al. 2006; Huelsenbeck et al. 2011; Espinha et al. 2015). It modifies cellular responses to genotoxic stress by modulation of the activity of stress kinases (JNK/SAPK, P38) (Coso et al. 1995; Minden et al. 1995; Maundrell et al. 1997) and related transcription factors (e.g., AP1, NF-κB) (Xia et al. 1995; Canman et al. 1996; Ichijo 1999; Gnad et al. 2001; Hall 2012).

1.1.2 Nuclear localization of RAC1

For decades, RAC1 was considered as a purely cytosolic protein, but in the last few years a fraction of RAC1 was identified to translocate into the nucleus (Michaelson et al. 2008; Sandrock et al. 2010; Tong et al. 2013; Zoughlami et al. 2013; Chircop 2014;

Woroniuk et al. 2018; Liu et al. 2019). Recent data suggest a possible involvement in the regulation of nuclear functions as shown by actin-dependent deformation of the nuclear envelope as well as an increase in nuclear plasticity as a result of nuclear RAC1 accumulation (Disanza et al. 2015; Navarro-Lerida et al. 2015). The latest studies also indicate that nuclear RAC1 plays a role in DNA repair, cell survival as well as cell death via regulation of mechanisms of the DDR (DNA damage response) (Fritz et al. 2013; Fritz et al. 2015). Studies focussing on nucleocytoplasmic shuttling of RAC1 revealed a direct interaction of RAC1 with Karyopherin alpha2 which mediates the import of RAC1 into the nucleus (Sandrock et al. 2010). Nucleophosmin (NPM), a nucleolar protein that is involved in various DNA repair pathways, among other things (Box et al. 2016), was discovered as nuclear RAC1 interacting protein and negative regulator of RAC1. NPM limits the GTP loading of RAC1 and NPM silencing inhibited RAC1 accumulation in the nucleus (Zoughlami et al. 2013; Liu et al. 2019). Other identified nuclear proteins that interact with nuclear RAC1 are transcription factor STAT3 (Signal transducer and activator of transcription 3) (Simon et al. 2000) and BCA3 (Breast cancer associated gene 3) (Yao et al. 2017). The activation of STAT3 was inhibited by dominant-negative RAC1 whereas active RAC1 stimulates STAT3 phosphorylation and binds to the transcription factor, thereby regulating its activity (Simon et al. 2000). BCA3 might act as a molecular shuttle for RAC1 translocation to the nucleus (Yao et al. 2017). Lanning *et al.* could show that the polybasic region (PBR) of RAC1 resembles a nuclear localization sequence (NLS) and has significant NLS activity (Lanning et al. 2003; Lanning et al. 2004).The two identified canonical NLS sequences in the C-terminal PBR of RAC1 seem to be necessary for nuclear import (Figure 1.2). A mutant RAC1 harbouring a RHOA PBR (lacking an NLS) showed a stronger localization to the cytoplasm than the wild-type RAC1 (Lanning et al. 2004). Another possible function of nuclear RAC1 is the influence on the DDR by regulation and alteration of the nuclear chromatin structure, the nuclear membrane and the nuclear pores (Butin-Israeli et al. 2013; Fritz et al. 2015; Navarro-Lerida et al. 2015).

The perinuclear actin cap regulates among other things the organization of chromatin in the nucleus. TIAM2 (T-Cell Lymphoma Invasion and Metastasis 2), a RAC1 GEF, localizes to the nuclear envelope and regulates the activity of perinuclear RAC1. The downregulation of TIAM2-regulated RAC1 resulted in disruption of the perinuclear cap (Woroniuk et al. 2018). As certain studies show, nuclear localization of RAC1 is cell-cycle dependent (Michaelson et al. 2008; May et al. 2014). RAC1 was shown to accumulate in the nucleus after treatment with ionizing radiation and to play a role in G2/M checkpoint activation (Yan et al. 2012). Inactive RAC1 was found to be exported from the nucleus

in case of DNA damage/G2 arrest (Hinde et al. 2014). Furthermore, two nuclear export sequences (NES) were identified in the *RAC1* gene. In this study NPM, a nucleocytoplasmic shuttling protein (Borer et al. 1989; Lindstrom 2011), was shown to promote RAC1 nuclear export (Navarro-Lerida et al. 2015). NPM shuttles between the nucleus and the cytoplasm (Colombo et al. 2011) and interacts with RAC1 at the same site as RhoGDI do. The competition between RhoGDI and NPM determines the cytoplasmic/nuclear localization of RAC1. In studies analyzing the activation state of nuclear RAC1 the results revealed predominantly the GTP-bound form in the nucleus (Simon et al. 2000; Michaelson et al. 2008; Hinde et al. 2014). Since the prenylation of the CAAX box competes with the recognition of the NLS by nuclear transport proteins like Karyopherin alpha2 (Michaelson et al. 2008) the found GTP-bound nuclear RAC1 challenges the knowledge about RAC1 activation. The NLS of RAC1 is part of the PBR (Figure 1.2), but the PBR is masked by geranylgeranylation of RAC1 (Abdrabou et al. 2018). This modification is a prerequisite for translocation to membranes and subsequent activation (Adamson, Marshall, et al. 1992; Adamson, Paterson, et al. 1992; Lin et al. 2015).

1.2 Cellular stress response to DNA damage

DNA damage occurs in large quantities every day in every single cell of the body. The damage can be induced by exogenous as well as endogenous factors. UV light, ionizing radiation (IR), and alkylating agents such as nitrosamines are examples for exogenous factors. Reactive oxygen species (ROS), metabolites and replication errors like base mismatches count for endogenous DNA damaging factors (Hoeijmakers 2001). DNA lesions that can occur are, amongst others, base modifications, DNA single strand breaks (SSB) and DNA double strand breaks (DSB). Since unrepaired DSB are a strong pro-apoptotic stimulus (Rich et al. 2000; Khanna et al. 2001; Bohgaki et al. 2010) this work is focused on the DNA damage response after doxorubicin-induced DSB.

1.2.1 DNA damage response

The DNA damage response (DDR) is a complex and fine-tuned network of signaling cascades that are involved in the recognition of DNA damage, DNA repair, cell cycle progression, cell death, and survival (Roos et al. 2013; Roos et al. 2016). In general, the repair involves recognition of the lesion and initiation of a signaling cascade to promote DNA repair. ATM (Ataxia telangiectasia mutated), ATR (ataxia telangiectasia and Rad3-related), and DNA-PK (DNA-dependent protein kinase) belong to a group of PI3 kinases and are initiators of the two main signaling pathways activated by DNA strand breaks (Sancar et al. 2004; Houtgraaf et al. 2006). ATM is mainly activated by DSB and is the

main kinase in the recognition and signaling of IR-induced DSB (Kastan et al. 2004; Lee et al. 2005; Borde et al. 2009) whereas ATR is mainly activated after replicative stress, e.g., replication block, by base damage, and DNA SSB (Zou et al. 2003; Dart et al. 2004; Cimprich et al. 2008). DNA-PK is involved in the repair of IR-induced DSB like ATM, but in contrast to ATM DNA-PK is mainly present in the NHEJ (non-homologous end joining) (Jeggo 1998). The MRN complex, consisting of MRE11 (meiotic recombination 11), RAD50, and NBS1 (Nijmegen breakage syndrome 1), acts as DSB sensor and recruits ATM to the DNA damage site (Lee et al. 2005) (Figure 1.4). The proteins of the MRN complex have different tasks. MRE11 binds to DSB ends and possesses exonuclease as well as endonuclease activity, RAD50 contains zinc hook domains which promote DNA tethering, and NBS1 serves for nuclear transport (Kobayashi et al. 2004; Roset et al. 2014; Shibata et al. 2014). RPA (replication protein A) recognizes SSB and recruits ATR to the damage (Zou et al. 2003). ATM and ATR can bind to open DNA ends and upon activation of their intrinsic kinase activity they selectively phosphorylate and therefore activate the serine-threonine checkpoint effector kinases, checkpoint kinase 1 (CHK1) and checkpoint kinase 2 (CHK2) (Smith et al. 1999; Suzuki et al. 1999; Unsal-Kacmaz et al. 2002) (Figure 1.4). These kinases trigger a variety of specific downstream responses (Bartek et al. 2003). CHK2 is phosphorylated by ATM at Thr68 (Matsuoka et al. 2000; Zhou et al. 2000). This phosphorylation is essential for the activation of the G1/G2 checkpoints of the cell cycle (Lavin et al. 2006). In the event of a blocked transition from G1 to S phase CHK2 phosphorylates CDC25A (cell division cycle 25A) at Ser123 resulting in ubiquitination and degradation of CDC25A. Consequently, CDC25A can no longer activate CDK2 (cyclin dependent kinase 2), which is necessary for G1/S progression (Falck et al. 2001; Zannini et al. 2014). CHK1 is phosphorylated at Ser345 by ATR (Guo et al. 2000; Liu et al. 2000) , thereby leading to G1/S arrest. ATM and ATR are able to phosphorylate P53 at Ser15 and other N-terminal sites directly (Canman et al. 1998) or via CHK1 and CHK2 at Ser20 (Shieh et al. 2000). Direct activation of P53 via ATM and ATR increases its transactivation activity (Canman et al. 1998) and as a result, both pro- as well as anti-apoptotic signals are passed on (Roos et al. 2013). Phosphorylation at Ser15 also prevents the MDM2-regulated degradation of P53 (Shieh et al. 1997). Phosphorylation of P53 via CHK1 and CHK2 results in a blockage of the MDM2-binding site, followed by block of P53 degradation whereby P53 is stabilized (Chehab et al. 1999; Unger et al. 1999; Hirao et al. 2000; Shieh et al. 2000). When P53 is stabilized it accumulates in the nucleus leading to an increase of P21 expression followed by a G1/S arrest (Mailand et al. 2000). KAP1 (KRAB-associated protein-1) is either directly phosphorylated by ATM (White et al. 2012) or indirectly by CHK2 (Hu et al. 2012), thereby promoting transient chromatin relaxation which is essential for

downstream signaling and repair (Ziv et al. 2006; Goodarzi et al. 2008; Goodarzi et al. 2011; Ayrapetov et al. 2014) (Figure 1.4). The phosphorylation of CHK1, CHK2, and P53 are of particular importance, because this is resulting in G1/S and G2/M cell cycle arrest, DNA repair, or apoptosis (Christmann et al. 2003).

Inhibition of topoisomerase II (Top II) by anticancer drugs (e.g., doxorubicin) results in the formation of DNA DSB (Nitiss 2002; Smart et al. 2008), which are highly potent activators of the DDR (Harper et al. 2007). Since the experiments in this work were performed by DSB-inducing agents (doxorubicin, IR) the DDR after DSB formation was of particular interest.

ATM, ATR and DNA-PK do not only regulate the cell cycle checkpoints, they also regulate DNA repair. Different DNA repair associated proteins, e.g., histone 2AX (H2AX), are phosphorylated by ATM, ATR, and DNA-PK (Burma et al. 2001; Wang et al. 2005). The phosphorylation of H2AX on Ser139 (γH2AX) is an early response to the occurrence of DSB (Rogakou et al. 1998) and therefore is a well-accepted surrogate marker for DSB. The induction of DSB results in the rapid formation of γH2AX foci, e.g., within 1 - 3 minutes after IR. The signal can expand up to 30 megabases from the primary lesion and comprises approximately 2,000 γH2AX molecules which can be visualized as a nuclear focus by immunofluorescent staining (Rogakou et al. 1998; Rogakou et al. 1999; Pilch et al. 2003). Each γH2AX focus corresponds to one DNA double-strand break (Rogakou et al. 1999; Sedelnikova et al. 2002). The formation of γH2AX foci takes place in direct proximity of the DSB. Due to phosphorylation of H2AX a loosening of the chromatin structure occurs and therefore the chromatin is more accessible for specific DNA repair proteins which accumulate at the broken DNA ends (Bassing et al. 2004; Kinner et al. 2008; Chapman et al. 2012). Thus, γH2AX leads to the concentration of DNA repair proteins at the DSB (Kinner et al. 2008). 53BP1 (P53-binding protein 1) is also phosphorylated by ATM in response to DNA damage. This phosphorylation is required for ATM-dependent signaling promoted by 53BP1 (Zgheib et al. 2005). 53BP1 is another important player in the DDR and accumulates at DSB sites by recognizing ubiquitylated histone H2A (Lys15) (Setiaputra et al. 2019). 53BP1 promotes NHEJ by blockage of DNA resection performed by CtIP (C-terminal binding protein 1 interacting protein) (Aparicio et al. 2014) leading to DNA repair by NHEJ (Tarsounas et al. 2020). Therefore, 53BP1 can be regarded as another surrogate marker for DSB in general and as an indicative marker for DSB repaired by NHEJ.

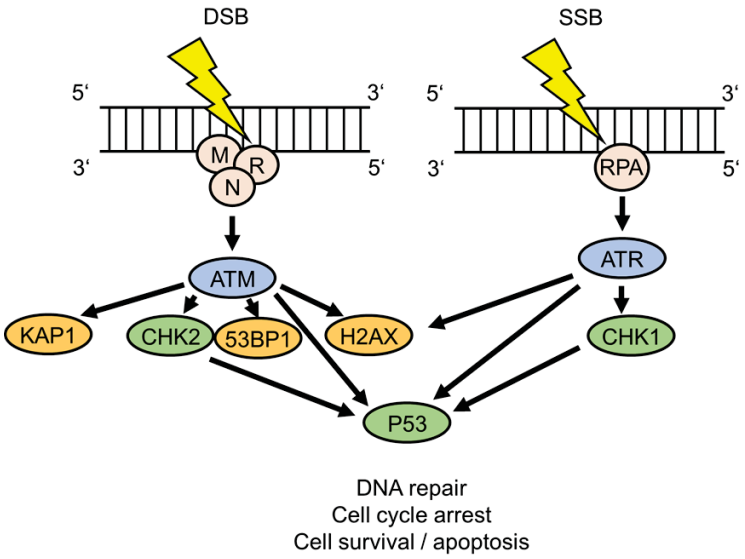

Figure 1.4: Simplified scheme of the DNA damage response (selected subset of proteins). The MRN complex, consisting of MRE11, RAD50, and NBS1 serves as DSB sensor and enables ATM to bind to the damage site (Lee et al. 2005). SSB are recognized by RPA, which then recruits ATR to the damage site (Zou et al. 2003). ATM activates CHK2 whereas ATR activates CHK1, which in return triggers a variety of specific downstream responses (Bartek et al. 2003), e.g. stabilization of P53. The phosphorylation of CHK1, CHK2, and P53 triggers cell cycle arrest, DNA repair, and apoptosis (Christmann et al. 2003). ATM phosphorylates damage indicators such as 53BP1 and H2AX. KAP1 is phosphorylated by ATM or CHK2 (White et al. 2006; Hu et al. 2012), resulting in chromatin relaxation which enables repair proteins to access the damage site (Ziv et al. 2006). Figure is adapted from Christmann *et al.* and Houtgraaf *et al.* (Christmann et al. 2003; Houtgraaf et al. 2006).

1.2.2 RAC1 and the DNA damage response

Besides of being involved in the regulation of the actin cytoskeleton, recent studies also indicate that RAC1 plays a role in DNA repair, cell survival as well as cell death via regulation of mechanisms of the DDR (Lassus et al. 2000; Velaithan et al. 2011; Fritz et al. 2013; Fritz et al. 2015). A signalling pathway which is related to the genotoxin-induced DDR is the RAC1-dependent activation of stress kinases after genotoxic stress (JNK/SAPK, P38) (Coso et al. 1995; Minden et al. 1995; Maundrell et al. 1997; Wartlick et al. 2013) and related transcription factors (e.g., AP1, NF-κB) (Xia et al. 1995; Canman et al. 1996; Ichijo 1999; Gnad et al. 2001; Hall 2012). Activation of the aforementioned kinases and transcription factors is resulting in the induction of apoptosis (Perona et al. 1997; Jin et al. 2006; Wartlick et al. 2013).

A role of RAC1 in the DDR was demonstrated in previous work of our group. Several studies revealed a protection of rat cardiomyocytes (H9c2) and hepatocytes (HepG2), as well as HUVEC (human primary umbilical vein endothelial cells) against Top II poisons such as etoposide and doxorubicin (Dox) by inhibiting RAC1. Inhibition was performed with the lipid lowering drug lovastatin (a non-specific pan-Rho GTPase

inhibitor) (Damrot et al. 2006; Huelsenbeck et al. 2011), with RAC1 inhibitor EHT 1864 (Wartlick et al. 2013), with RAC1 inhibitor NSC23766 (Huelsenbeck et al. 2012) as well as clostridial ADP-ribosylating toxin (Huelsenbeck et al. 2007), that specifically inactivates RAC1. The pharmacological inhibition of RAC1 modulated the Top II poison-induced DDR and protected the cells by reducing the Top II poison-induced DNA damage and cell death. Experiments including mice, characterized by liver-specific RAC1 knock-out, demonstrated a protection of the liver after Dox treatment and less DNA damage (Bopp et al. 2013). In another study the aforementioned mice were treated with DEN (diethyl nitrosamine) to induce liver tumor formation. Mice lacking hepatic RAC1 had tumors of smaller size compared to the mice with hepatic RAC1 expression (Bopp et al. 2015). Other mouse studies displayed a cardioprotective effect of pharmacological RAC1 inhibition upon Dox treatment (Ohlig et al. 2018). The mechanism underlying this protection is currently still unknown. An interaction of RAC1 with proteins of the DDR might be possible since inhibition of RAC1 with NSC23766 blocked various DDR-related signalings, including the ATM-mediated phosphorylation of CHK2 (Fritz et al. 2015). Another possibility is the described link between RAC1 and Top II (Huelsenbeck et al. 2011; Huelsenbeck et al. 2012; Wartlick et al. 2013). Formation of the transient cleavage complex consisting of a cut DNA double-strand covalently linked to Top II and Dox (Lyu et al. 2007) was prevented upon treatment with RAC1 inhibitors (Huelsenbeck et al. 2012; Wartlick et al. 2013). These results make RAC1 a possible target in cancer therapy and several studies support this possibility.

In AML (acute myeloid leukemia) cell lines active RAC1 is associated with Dox-induced apoptosis (Naci et al. 2019) and the study of Hein *et al.* revealed an increased RAC1 expression and an altered pro-survival pathway in breast cancer cells that survived HFR (hyper-fractionated radiation). Inhibition of RAC1 in these cells blocked their survival (Hein et al. 2016). Other studies demonstrated a reduced DNA repair, cell proliferation, as well as cell survival after exposure to UV light or γ-irradiation in RAC1 deficient cells or cells treated with a RAC1 inhibitor (Yan et al. 2014; Espinha et al. 2015). Also a protective role of RAC1 in UV-light-induced skin carcinogenesis and keratinocyte apoptosis was shown (Deshmukh et al. 2017). A hallmark of cancer is the resistance of cells to apoptosis (Hanahan et al. 2000). RAC1 was found overexpressed in certain tumors which correlated with chemoresistance (Schnelzer et al. 2000; Karlsson et al. 2009; De et al. 2020). Moreover, RAC1 promotes anti-apoptotic signaling pathways in cancer cells resulting in therapy resistance (De et al. 2020; Tan et al. 2020). P53 acts as “guardian of the genome” by maintaining genomic integrity as well as preventing the proliferation of cells with damaged DNA (Lane 1992; Toufektchan et al. 2018). Mutations

in P53 can lead to enhanced cell proliferation and survival (Solomon et al. 2011; Mantovani et al. 2019), as well as reduced apoptosis (Blandino et al. 1999; Vogelstein et al. 2000). Yue *et al.* showed that enhanced RAC1 activity is associated with mutant P53 expression and is independent of wild-type P53 function. The mutant P53 DBD (DNA-binding domain) is essential for interaction with RAC1 and increases the SUMOylation of RAC1 which contributes to its activity. As a result of this interaction RAC1 contributes to mutant P53 GOF (gain of function) in promoting cell migration and invasion (Yue et al. 2017). Another study exhibited a MAP kinase-mediated crosstalk between RAC1 and P53 (Lassus et al. 2000). This supports the usefulness role of RAC1 as a possible target in cancer therapy or for the protection of normal tissue (Fritz et al. 2006; Fritz et al. 2011; Henninger et al. 2017).

1.3 DNA double-strand break repair

DNA DSB can be caused by any agent that can break the sugar-phosphate backbone of the DNA. Such agents can be of endogenous origin, such as metabolite products, or exogenous factors such as ionizing radiation or certain chemotherapeutic agents (e.g., doxorubicin). In human cells, the repair of DSB is mediated via two main repair pathways, namely the homologous recombination (HR) and the non-homologous end joining (NHEJ) (Jeggo 1998; Rothkamm et al. 2003). The decision for or against one of these repair pathways is dependent on the cell cycle (Rothkamm et al. 2003; Roos et al. 2006; Lieber 2010). The NHEJ is independent of the cell cycle, but nevertheless is most active in the G0 and G1 phases whereas HR occurs during the late S and G2 phase (Takata et al. 1998; Johnson et al. 2000) since a sister chromatid is needed as template (Rothkamm et al. 2003; Roos et al. 2006; Lieber 2010). HR and NHEJ have the so-called MRN complex, consisting of MRE11, RAD50, and NBS1 as damage sensor in common. The decision for HR or NHEJ is up to the MRN complex, although the exact mechanism is still unclear (Lafrance-Vanasse et al. 2015).

1.3.1 Homologous recombination (HR)

As stated above, HR is initiated by the MRN complex, which performs a nucleolytic resection of the DSB resulting in single-stranded DNA with short 3’ overhangs (Christmann et al. 2003; Sartori et al. 2007). For this purpose, the MRN complex recruits BRCA1 (breast cancer type 1 susceptibility protein) and CtIP which all together regulate the final resection (Limbo et al. 2007; Sartori et al. 2007). The ssDNA is protected against exonucleolytic digestion due to binding of a heptameric ring complex of RAD52 proteins (Stasiak et al. 2000). RAD52 interacts with RAD51 as well as RPA, thereby mediating the DNA strand exchange (Christmann et al. 2003). RAD51 stabilizes SSB and DSB and

promotes ATP-dependent as well as RPA mediated interaction of the lesion with the homologous strand of undamaged DNA (Benson et al. 1994). The strand invasion leads to the formation of the synaptic complex containing the so-called displacement-loop (D-loop). This D-loop is a heteroduplex made up of a damaged DNA strand and its intact homologue (Baumann et al. 1997; Gupta et al. 1998; Qi et al. 2015). After DNA synthesis through the polymerases δ, ε, and η the ends are ligated and the resulting Holliday Junctions (complex of the two DNA double helices) are dissolved (Christmann et al. 2003; Maloisel et al. 2008) (Figure 1.5).

1.3.2 Non-homologous end joining (NHEJ)

The recognition of the DSB begins with binding of the KU70/KU80 complex to the lesion to protect the DSB ends from degradation by exonucleases (Jeggo et al. 1992; Christmann et al. 2003). Afterwards the KU heterodimer associates with DNA-PK_{CS} (DNA-dependent protein kinase catalytic subunit) and the holoenzyme DNA-PK is formed (Gottlieb et al. 1993; Smith et al. 1999). Binding of DNA-PK_{CS} leads to activation of the kinase activity which is required for efficient end joining (Calsou et al. 1999; Yoo et al. 1999). The active DNA-PK phosphorylates numerous target proteins which play a role in DNA repair, cell cycle control, as well as induction of apoptosis (Meek et al. 2004). DNA-PK_{CS} binds to XRCC4 (X-ray repair cross-complementing protein 4) which in turn forms a complex with DNA Ligase IV to re-ligate the broken DNA ends (Grawunder et al. 1997; Leber et al. 1998). The MRN complex processes the DSB before re-ligation by removal of excess DNA at 3’ flaps (Maser et al. 1997; Nelms et al. 1998), whereas flap endonuclease 1 (FEN1) removes excess DNA at 5’ flaps (Christmann et al. 2003). Further overhangs or hairpin structures are processed by the exonuclease Artemis (Ma et al. 2002; Yannone et al. 2008). The ligation of the processed strand ends is performed by the XRCC4/DNA Ligase IV/XLF (XRCC4-like factor)-complex and finally mediates the closure of the DSB (Davis et al. 2014; Waters et al. 2014). During linkage of the DSB ends insertions, deletions, and translocations often occur. Therefore, the NHEJ is an error-prone repair pathway compared to HR which is an error-free pathway (Moore et al. 1996; Wilson et al. 1997) (Figure 1.5).

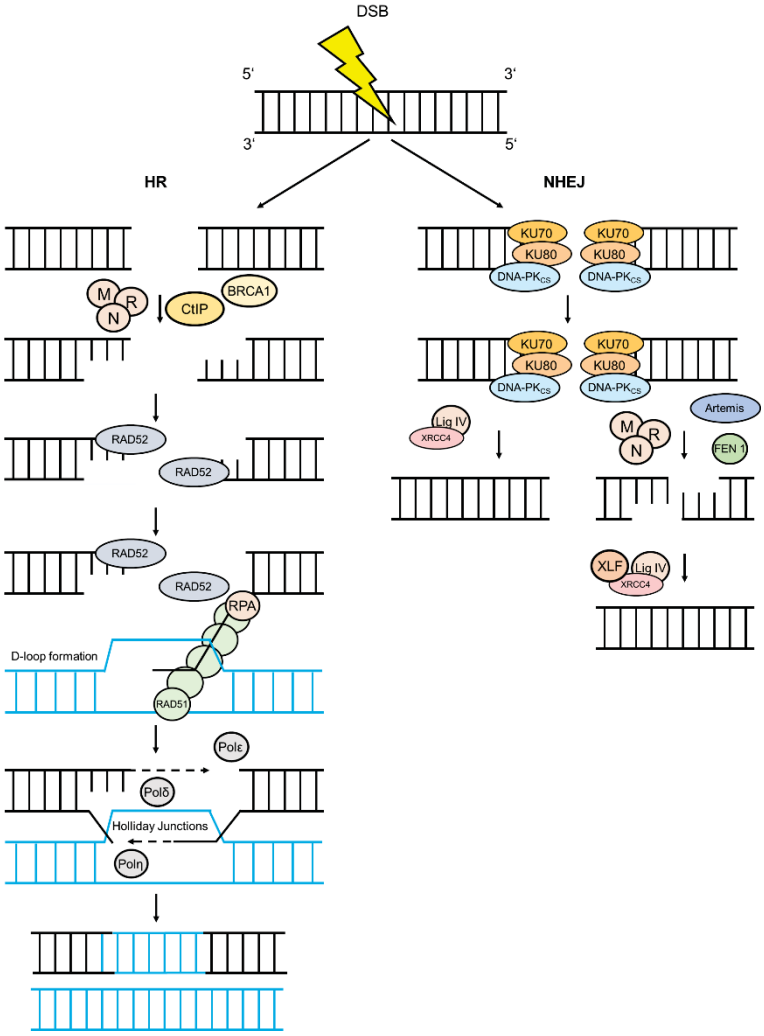

Figure 1.5: Simplified scheme of homologous recombination (HR) and non-homologous end joining (NHEJ) (selected subset of proteins).
HR is initiated by the MRN complex (Christmann et al. 2003) and recruits BRCA1 and CtIP for the final resection (Limbo et al. 2007; Sartori et al. 2007). The ssDNA is protected against digestion through binding of RAD52 proteins (Stasiak et al. 2000). RAD52 interacts with RAD51 as well as RPA, thereby mediating the DNA strand exchange (Christmann et al. 2003). RAD51 stabilizes SSB and DSB and promotes interaction of the lesion with the homologous strand of undamaged DNA (Benson et al. 1994) leading to the formation of the synaptic complex containing the D-loop (Qi et al. 2015). After DNA synthesis through the polymerases δ, ε, and η the ends are ligated and the resulting Holliday Junctions are dissolved (Christmann et al. 2003; Maloisel et al. 2008). **NHEJ** is initiated by binding of the KU70/KU80 complex to the lesion (Jeggo et al. 1992; Christmann et al. 2003). Afterwards the KU heterodimer associates with DNA-PK$_{CS}$ (Gottlieb et al. 1993; Smith et al. 1999) leading to activation of the kinase activity (Calsou et al. 1999; Yoo et al. 1999). DNA-PK$_{CS}$ binds to XRCC4 which in turn forms a complex with DNA Ligase IV to ligate the broken DNA ends (Grawunder et al. 1997; Leber et al. 1998). The MRN complex, Artemis, and FEN1 process the DSB before re-ligation (Maser et al. 1997; Nelms et al. 1998; Christmann et al. 2003; Yannone et al. 2008). The ligation of the processed strand ends is performed by the XRCC4/DNA Ligase IV/XLF-complex and finally mediates the closure of the DSB (Davis et al. 2014; Waters et al. 2014). Figure is adapted from Christmann *et al*. (Christmann et al. 2003).

1.4 DNA damaging agents and the RAC1 inhibitor EHT 1864

1.4.1 Doxorubicin induced DNA damage

Doxorubicin belongs to the group of anthracyclines and is a derivative of daunorubicin which was isolated from *Streptomyces peucetius* in the 1950s (Dimarco et al. 1964). The anthracycline derivative Dox (also known as Adriamycin) was isolated from a mutant *Streptomyces peucetius* strain (Arcamone et al. 2000). It is a highly effective chemotherapeutic agent and is used in cancer therapy for e.g., leukemia, soft tissue sarcoma, solid tumors, as well as breast carcinomas (Blum et al. 1974; Cole et al. 1974). Anthracyclines are characterized by intercalation into the DNA resulting in inhibition of transcription and by inhibition of DNA Top II leading to the formation of DSB (Gewirtz 1999). DNA topoisomerases regulate the DNA topology through transient induction of DNA single or double strand breaks. These enzymes convert the supercoiled DNA into relaxed DNA by transient cleavage of one or both DNA strands during cellular processes like DNA synthesis and transcription and maintain the genomic integrity during these processes. Top II isoform α is essential for survival of proliferating cells. Top II isoform β is ubiquitously expressed (McClendon et al. 2007; Morimoto et al. 2019). The DNA damaging effect resulting from Top II poisoning occurs mainly in the S- and G2-phase of proliferating cells (Ling et al. 1996; Potter et al. 2002) due to the higher expression of Top II α in these cell cycle phases (Goswami et al. 1996). During cellular processes like DNA synthesis and transcription, Top II is regulating the DNA topology thereby passing intact double-stranded DNA through an intentional DSB (Rose 1988) followed by re-ligation of the broken strands (Morimoto et al. 2019). This transient DSB is generated under ATP consumption (Fortune et al. 2000; Wilstermann et al. 2003). The cytotoxic target for Top II poisons, like Dox, is the transient cleavage complex consisting of a cut DNA strand covalently linked to Top II and Dox (Lyu et al. 2007). Dox binds irreversible to Top II and therefore inhibits the ability of Top II to re-ligate the induced DSB leading to the accumulation of cytotoxic DSB (Figure 1.6) (Bromberg et al. 2003; Nitiss 2009). The cleavage complex is finally degraded by proteases. When left unrepaired, these DSB represent a strong apoptotic stimulus (Roos et al. 2013; Roos et al. 2016). Additionally, bulky adducts and DNA crosslinks are formed by anthracyclines resulting in interference with DNA replication and transcription (Gewirtz 1999; Swift et al. 2006) as well as interaction with helicases (Bachur et al. 1992) is reported for Dox. Furthermore, Dox can damage the DNA by generation of reactive oxygen species (ROS) (Bates et al. 1982) which is leading e.g., to DNA single-strand breaks, base mismatches, and point mutations (Simunek et al. 2009; Sterba et al. 2013). Though, generation of ROS only occurs at high doses which are considered as clinically not relevant. According to the

published data of Gewirtz, the lowest Dox concentration at which ROS was detected *in vitro* was 4 µM. However, standard therapy of humans only achieves serum levels of about 1 - 2 µM Dox (Gewirtz 1999). The DNA damaging mechanism of Dox leading to irreversible inhibition of Top II resulting in DSB is the dominant toxic mechanism at doses from 0.5 µM to 5 µM (Gewirtz 1999). In this work Dox was used at a concentration of 1 µM and thus corresponds to the serum levels found in patients.

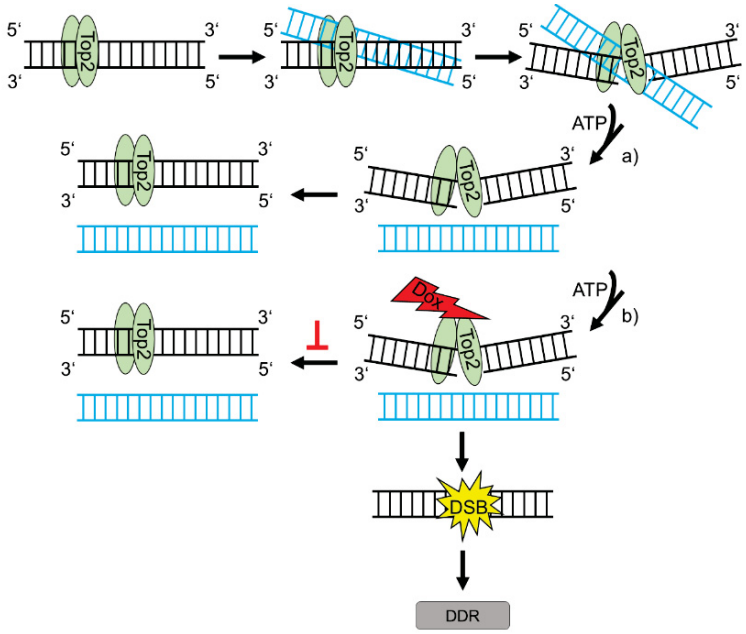

Figure 1.6: Topoisomerase II poisoning by doxorubicin leads to DSB.
To resolve tensions that occur e.g., during replication, topoisomerase II enzymes can pass dsDNA through a transient DSB which has formed in another dsDNA strand. The process takes place under ATP consumption. Topoisomerase II poisons like doxorubicin obstruct re-ligation of the DNA strand (Nitiss 2009) leading to DNA double-strand breaks which can provide a strong apoptotic stimulus (Roos et al. 2013; Roos et al. 2016). Figure is adapted from Nitiss (Nitiss 2009).

1.4.2 Ionizing radiation induced DNA damage

Ionizing radiation (IR) is energetic and is classified as either electromagnetic or particulate, whereas the γ radiation belongs to the electromagnetic radiation (Azzam et al. 2012; Desouky et al. 2015). γ radiation was used in this work on the one hand since it is also used in the context of cancer therapy and, on the other hand, because it induces DSB independent of the Top II. In more than 50 % of cancer patients ionizing radiation is used as cancer therapy, often in combination with chemotherapeutics and surgical resection (Delaney et al. 2005; Begg et al. 2011). Exposure of cells to IR inflicts various types of damage, such as SSB, DSB, DNA-DNA cross-links, and base damage (Cerutti 1974; Steel 1996; Lomax et al. 2013; Belli et al. 2020). The occurring damage can result from direct or indirect radiation effects on the DNA (Goodhead 1994; Nikjoo et al. 1997). Direct DNA damages are resulting from a direct hit of the radiation on the DNA molecule,

thereby disrupting its molecular structure (Desouky et al. 2015). Indirect DNA damage arises from free radicals which are mainly resulting from ionization of intracellular water molecules (Figure 1.7) (Ross 1999). Different types of free radicals are produced, but foremost hydroxyl radicals produce significant damage to the DNA (Dizdaroglu et al. 2012). Regarding γ radiation about 1/3 of DNA damage is due to direct interaction of DNA with the irradiating particle and about 2/3 are resulting from indirect effects (Azzam et al. 2012; Santivasi et al. 2014). The radiation dose is measured in units gray (Gy), a measure of the amount of radiation absorbed by 1 kg of tissue (Borrego-Soto et al. 2015). A dose of 1 Gy induces approximately 20 - 40 DSB, 1,000 SSB, and 1,000 - 1,300 base lesions per cell (Roots et al. 1985; Lomax et al. 2013). The DNA damage is either repaired by HR, BER or by NHEJ (Jeggo 1998; Rothkamm et al. 2003). Unrepaired DNA damage is leading to a cell cycle arrest, followed by senescence and/or apoptosis whereas incorrectly repaired lesions can result in mutations (Zhang et al. 2007).

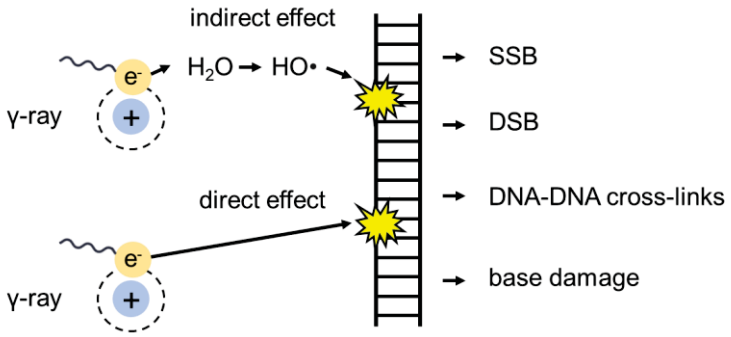

Figure 1.7: Direct and indirect effects of ionizing radiation on the DNA.
The occurring damage can result from direct or indirect radiation effects on the DNA (Goodhead 1994; Nikjoo et al. 1997). Direct DNA damages are resulting from a direct radiation hit on the DNA molecule (Desouky et al. 2015). Indirect DNA damage arises from free radicals which are mainly resulting from ionization of intracellular water (Ross 1999). The resulting types of damage are among others SSB, DSB, DNA-DNA cross-links, and base damage (Lomax et al. 2013). Figure is adapted from Desouky *et al.* (Desouky et al. 2015).

1.4.3 RAC1 inhibitor EHT 1864

Like stated above, GEF are responsible for activation of RAC1 by catalysis of the exchange of GDP to GTP. EHT 1864 is a small molecular inhibitor with high binding affinity for RAC1 as well as its isoforms RAC2 and RAC3. The inhibitor stimulates the nucleotide release of RAC1. By direct binding to RAC1, the protein is put in an inert and inactive state (Shutes et al. 2007; Onesto et al. 2008). The RAC1 inhibition is based on a dissociation of the guanosine nucleotide followed by a conformation change of RAC1. EHT 1864 blocks RAC1-mediated signaling by impairing the ability of RAC1 to activate downstream effectors (Figure 1.8) (Shutes et al. 2007).

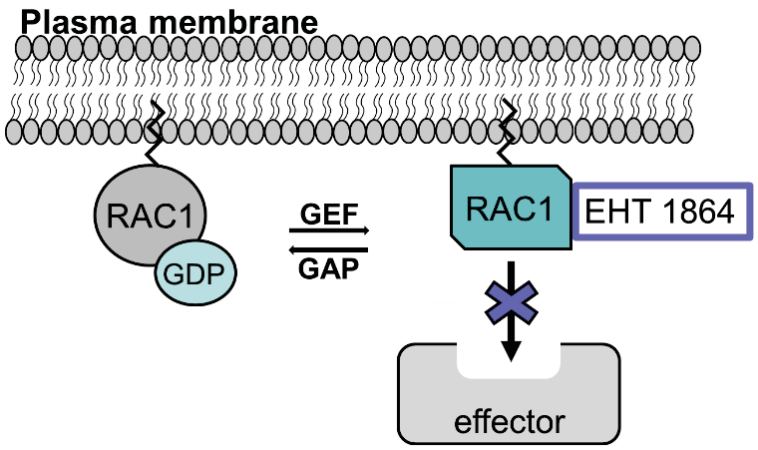

Figure 1.8: Inhibition of RAC1 functions by EHT 1864.
RAC1 cycles between an GDP-bound state and a GTP-bound state, which is regulated by GEF and GAP. Active RAC1 binds to a variety of downstream effectors that regulate signaling networks. EHT 1864 inhibits RAC1 binding to its downstream effectors. The activation of the effector is impossible. Figure is adapted from Onesto *et al.* (Onesto et al. 2008).

1.5 Objectives

The role of the small Rho GTPase RAC1 in the DNA damage response (DDR) is only poorly characterized. Previous work showed a protection against topoisomerase II poison-induced γH2AX foci formation as well as cell death by pharmacological inhibition of RAC1 (Damrot et al. 2006; Huelsenbeck et al. 2011; Huelsenbeck et al. 2012; Wartlick et al. 2013). Until today, it is unclear whether the effects described so far are based on functions of cytosolic and/or nuclear RAC1. Like stated above, RAC1 as well as its guanine nucleotide exchange factors (GEF) were found in the nucleus (Michaelson et al. 2008; Sandrock et al. 2010; Woroniuk et al. 2018), but nuclear-specific functions of Rho GTPases are sparsely characterized so far.

For discrimination between nuclear and cytosolic effects *hRAC1* expression vectors harbouring an additional nuclear localisation sequence (NLS) were cloned. RAC1 possesses a weak C-terminal NLS. To force nuclear localization of hRAC1 an additional, stronger NLS (from SV40 Large T-antigen) was added N-terminal to hRAC1. The hRAC1 proteins without additional NLS should be mainly localized in the cytoplasm, whereas the proteins with an additional NLS should be forced to the nucleus. In the present study mouse embryonic fibroblasts (MEF) were used to analyze the role of wild-type human RAC1 (GFP-hRAC1(WT)), constitutively active human RAC1 (GFP-hRAC1(Q61L)), and dominant-negative human RAC1 (GFP-hRAC1(T17N)) in the Dox-induced DDR. The working hypothesis is that the expression of dominant-negative hRAC1 affects the DDR and DNA repair similar to pharmacological inhibition of RAC1 whereas the expression of wild-type hRAC1 or constitutively active hRAC1 enhances the doxorubicin-induced DDR or does not influence the DDR at all. Pharmacological RAC1 inhibition by EHT 1864 as well as *mRac1* silencing were combined with transfection of *GFP-hRAC1(T17N)* expression vector to answer the questions if cells transfected with dominant-negative *hRAC1* expression vector, *mRac1* siRNA transfected cells and EHT 1864 treated cells show similar results and if it is possible to further enhance the effect of dominant-negative hRAC1, EHT 1864, or *mRac1* siRNA by combining the treatments.

The used MEF(*Rac1*$^{flx/flx}$) cells have a *mRac1* gene which is partially flanked by loxP sites. Therefore, *mRac1* knockout cells were tried to establish for complete exclusion of the endogenous murine RAC1 in the experiments. After successful knockout, the cells could be re-transfected with the human *GFP-RAC1* mutants to analyze the role of the human RAC1 in the DDR.

2 Material and methods

2.1 Material

2.1.1 Devices

Table 2.1: List of used devices

Device	Manufacturer
Analytical balance 3716MP	Sartorius, Göttingen Germany
Centrifuge 5418R	Eppendorf, Hamburg, Germany
Centrifuge Avanti™J-25, high performance centrifuge	Beckman Coulter, Krefeld, Germany
CFX96™ Real-time PCR Detection System	BioRad, Hercules, CA, USA
ChemiDoc™ Touch Imaging System SPR-80	BioRad, Hercules, CA, USA
Clean bench Hera Safe	Thermo Fisher Scientific, Waltham, MA, USA
CO_2-Incubator series CB	Binder, Tuttlingen, Germany
Fine Scale ABS	Kern, Ballingen, Germany
Flow Cytometer BD Accuri™ C6	Becton, Dickinson and Company, Franklin Lakes, NJ; USA
Imaging System Fusion FX7	Peqlab Biotechnologie GmbH, VWR International GmbH, Darmstadt, Germany
Magnetic stirrer Combimag Ret	IKA, Staufen, Germany
Magnetic stirrer MR2002	Heidolph, Schwabach, Germany
Microscope Axiolab	Carl Zeiss AG, Jena, Germany
Microscope BX43	Olympus, Tokyo, Japan
Microscope, inverted CKX41	Olympus, Tokyo, Japan
Mini-PROTEAN® Tetra Vertical Electrophoresis Cell	BioRad, Hercules, CA, USA
Mini Trans-Blot® Cell	BioRad, Hercules, CA, USA
NanoVue™ Plus spectrophotometer	GE Healthcare GmbH, Solingen, Germany

Device	Manufacturer
Radiometer Copenhagen PHM93 Reference pH meter	BioSurplus, San Diego, CA, USA
PowerPac™ Basic Power Supply	BioRad, Hercules, CA, USA
QIAcube	Qiagen, Hilden, Germany
Radiation device Gammacell ® 1000 Elite (γ-emitter, Cs^{137})	Nordion International, Ottawa, Canada
Rocking shaker Mini-Rocker WS21	Hartenstein, Würzburg, Germany
Sonicator EpiShear™ Probe sonicator	Active Motif, La Hulpe, Belgium
Thermal Cycler MyCycler	BioRad, Hercules, CA, USA
Thermomixer® compact	Eppendorf, Hamburg, Germany
Vortex Mixer Vortex-2 Genie	Scientific Industries, Bohemia, NY, USA

2.1.2 Consumables

Table 2.2: List of used consumables

Consumable	Manufacturer
Adhesive PCR Plate Seals	Thermo Fisher Scientific, Waltham, MA, USA
12 well slide	Ibidi GmbH, Graefelfing, Germany
96-Well plate for real-time PCR	Thermo Fisher Scientific, Waltham, MA, USA
Cell culture dishes	Greiner Bio-One International AG, Kremsmuenster, Austria
Cell culture flasks	Greiner Bio-One International AG, Kremsmuenster, Austria
Cell culture plates	Greiner Bio-One International AG, Kremsmuenster, Austria
Coverslips	Marienfeld, Lauda-Königshofen, Germany
Cryo vials	Greiner Bio-One International AG, Kremsmuenster, Austria
Drigalski spatula	neoLab Migge GmbH, Heidelberg, Germany

Consumable	Manufacturer
Falcon tubes	Greiner Bio-One International AG, Kremsmuenster, Austria
Nitrocellulose membrane 0.2 µm	Protran, Amersham, GE Healthcare, Dassel, Germany
Pipette tips	Starlab, Hamburg, Germany
Pipette tips, stuffed, repelling (for PCR)	Starlab, Hamburg, Germany
Plastic pipettes	Carl Roth, Karlsruhe, Germany
Reaction tubes	Sarstedt, Nuembrecht, Germany
Slides	Engelbrecht, Edermuende, Germany
Syringe	B. Braun, Melsungen, Germany
Syringe filter	VWR International GmbH, Darmstadt, Germany
Whatman filter paper	GE Healthcare GmbH, Solingen, Germany

2.1.3 Kits

Table 2.3: List of used kits

Name	Manufacturer
DNeasy Blood & Tissue	Qiagen, Hilden, Germany
High-Capacity cDNA Reverse Transcription Kit	Thermo Fisher Scientific, Waltham, MA, USA
Plasmid Mini Kit/Maxi Kit	Qiagen, Hilden, Germany
QIAquick Gel Extraction Kit	Qiagen, Hilden, Germany
RNeasy Mini Kit	Qiagen, Hilden, Germany
RedTaq Ready Mix	Sigma-Aldrich, Taufkirchen bei Muenchen, Germany
SensiMix SYBR Hi-ROX Kit	Bioline, London, UK

2.1.4 Chemicals

Table 2.4: List of used chemicals

Name	Manufacturer
Acetic acid	Carl Roth, Karlsruhe, Germany
Acetone	Carl Roth, Karlsruhe, Germany
Acrylamide 30 % Rotiphorese Gel	Carl Roth, Karlsruhe, Germany
Agarose	Carl Roth, Karlsruhe, Germany
Ammonium persulfate	Merck, Darmstadt, Germany
Bacto-Agar	Becton, Dickinson and Company, Franklin Lakes, NJ; USA
Bacto-Tryptone	Becton, Dickinson and Company, Franklin Lakes, NJ; USA
BM Chemiluminescence Western Blotting Substrate	Merck, Darmstadt, Germany
Boric acid	Carl Roth, Karlsruhe, Germany
Bovine serum albumin (BSA)	PAN-Biotech, Aidenbach, Germany
Calcium chloride ($CaCl_2$)	ICN Biomedicals GmbH, Eschwege, Germany
Collagen I, rat tail	Santa Cruz Biotechnology Inc., Dallas, TX, USA
Dimethyl sulfoxide (DMSO)	Carl Roth, Karlsruhe, Germany
Doxorubicin	Merck, Darmstadt, Germany
Ethanol	VWR International GmbH, Darmstadt, Germany
Ethidium bromide	Carl Roth, Karlsruhe, Germany
Ethylenediaminetetraacetic acid (EDTA)	Carl Roth, Karlsruhe, Germany
Formaldehyde, 37 %	Merck, Darmstadt, Germany
Gelatin	Merck, Darmstadt, Germany
Glacial acetic acid	Sigma-Aldrich, Taufkirchen bei Muenchen, Germany
Glycerin	Carl Roth, Karlsruhe, Germany
Glycine	Carl Roth, Karlsruhe, Germany

Name	Manufacturer
(Z)-4-Hydroxytamoxifen (4-OHT)	Sigma-Aldrich, Taufkirchen bei Muenchen, Germany
Methanol	VWR International GmbH, Darmstadt, Germany
Milk powder (blotting grade)	Carl Roth, Karlsruhe, Germany
Paraformaldehyde	Merck, Darmstadt, Germany
Phalloidin-TRITC	Santa Cruz Biotechnology Inc., Dallas, TX, USA
Ponceau S	Sigma-Aldrich, Taufkirchen bei Muenchen, Germany
Potassium chloride (KCl)	Merck, Darmstadt, Germany
Potassium dihydrogenphosphate (KH_2PO_4)	Carl Roth, Karlsruhe, Germany
Propidium iodide	Sigma-Aldrich, Taufkirchen bei Muenchen, Germany
Roti-load, 4x	Carl Roth, Karlsruhe, Germany
Sodium citrate	Carl Roth, Karlsruhe, Germany
Sodium chloride (NaCl)	VWR International GmbH, Darmstadt, Germany
Sodium dihydrogen phosphate (NaH_2PO_4)	Merck, Darmstadt, Germany
Sodium dodecyl sulfate (SDS)	Carl Roth, Karlsruhe, Germany
Sodium hydrogen phosphate (Na_2HPO_4)	Carl Roth, Karlsruhe, Germany
Sodium hydroxide (NaOH)	Merck, Darmstadt, Germany
Tetramethylethylenediamine (TEMED)	Carl Roth, Karlsruhe, Germany
Tris-Base	Sigma-Aldrich, Taufkirchen bei Muenchen, Germany
Tris-Hcl	Sigma-Aldrich, Taufkirchen bei Muenchen, Germany
Triton X-100	Sigma-Aldrich, Taufkirchen bei Muenchen, Germany
Tween 20	Merck, Darmstadt, Germany

Name	Manufacturer
Vectashield with DAPI	Vector Laboratories Inc., Burlingame, CA, USA
Yeast extract	Becton, Dickinson and Company, Franklin Lakes, NJ; USA

2.1.5 Cell culture media and supplements

Table 2.5: List of used cell culture media and supplements

Name	Manufacturer
DMEM (Dulbecco's Modifies Eagle Medium, high glucose)	Sigma-Aldrich, Taufkirchen bei Muenchen, Germany
FCS (fetal calf serum)	Merck, Darmstadt, Germany
IMDM (Iscove's Modified Dulbecco's Medium, without L-glutamine)	Sigma-Aldrich, Taufkirchen bei Muenchen, Germany
L-glutamine	Sigma-Aldrich, Taufkirchen bei Muenchen, Germany
Penicillin/Streptomycin	Sigma-Aldrich, Taufkirchen bei Muenchen, Germany

2.1.6 Cell lines

Table 2.6: List of used cell lines

Cell line	Characteristics	Medium
293T	* derived from human embryonic kidney cells (HEK293) * stable expression of SV40 large T antigen * episomal replication of transfected plasmids with SV40 origin of replication possible * neomycin resistance	DMEM + 10 % FCS + 2 mM L-glutamine + 1 % Penicillin/Streptomycin
MEF (mouse embryonic fibroblasts)	* spontaneously immortalized * derived from Cre-loxP system mice * *Rac1* gene is flanked by loxP sites	DMEM + 10 % FCS + 1 % Penicillin/Streptomycin
MEF (198M) (mouse embryonic fibroblasts)	* *Rac1* gene is not flanked by loxP sites	DMEM + 10 % FCS + 1 % Penicillin/Streptomycin

Cell line	Characteristics	Medium
Phoenix-ECO	* derived from 293T cells * additional expression of ecotropic envelope protein	DMEM + 10 % FCS + 2 mM L-glutamine + 1 % Penicillin/Streptomycin

2.1.7 Enzymes

Table 2.7: List of used enzymes

Name	Manufacturer
Cre recombinase Gesicles	Clontech, Mountain View, CA, USA
DNase (RNase free)	Qiagen, Hilden, Germany
EcoRI-HF	New England Biolabs GmbH, Frankfurt am Main, Germany
Proteinase K	Sigma-Aldrich, Taufkirchen bei Muenchen, Germany
Shrimp Alkaline Phosphatase (rSAP)	New England Biolabs GmbH, Frankfurt am Main, Germany
T4 DNA Ligase	New England Biolabs GmbH, Frankfurt am Main, Germany
Trypsin/EDTA solution (10 x)	Sigma-Aldrich, Taufkirchen bei Muenchen, Germany

2.1.8 Bacterial strains

Table 2.8: List of used bacterial strains

Name	Manufacturer
DH5 alpha	Common stock from the institute
One shot® Top10 Competent cells	Thermo Fisher Scientific, Waltham, MA, USA

2.1.9 Antibiotics

Table 2.9: List of used antibiotics

Name	Manufacturer
Ampicillin	Calbiochem, San Diego, CA, USA
Puromycin	Sigma-Aldrich, Taufkirchen bei Muenchen, Germany

2.1.10 Transfection reagents

Table 2.10: List of used transfection reagents

Name	Manufacturer
DreamFect Gold	OZ Biosciences SAS, Marseille, France
EcoTransfect	OZ Biosciences SAS, Marseille, France
Effectene	Qiagen, Hilden, Germany
FuGene HD	Promega GmbH, Walldorf, Germany
GeneJuice	Merck Millipore, Darmstadt, Germany
jetPEI	Polyplus transfection, Illkirch, France
Lipofectamine 3000	Thermo Fisher Scientific, Waltham, MA, USA
Lipofectamine RNAiMAX	Thermo Fisher Scientific, Waltham, MA, USA
Metafectene	Biontex Laboratories GmbH, Munich, Germany
Metafectene Pro	Biontex Laboratories GmbH, Munich, Germany
PEI (polyethyleneimine)	Sigma-Aldrich, Taufkirchen bei Muenchen, Germany
TransIT-X2	Mirus Bio LLC, Madison, WI, USA

2.1.11 Plasmids, vectors, and siRNA

hRAC1 expression vectors

Table 2.11: List of used plasmids for *hRAC1* expression

Name	Characteristics	Manufacturer
pcDNA3-EGFP-Rac1-Q61L	* EGFP-Tag on backbone (N terminal) * human, constitutively active RAC1 * glutamine to leucine substitution (residue 61) * neomycin resistance	pcDNA3-EGFP-Rac1-Q61L was a gift from Gary Bokoch (Addgene plasmid # 12981; http://n2t.net/addgene:12981; RRID:Addgene_12981). Subauste et al. (2000) Map of the plasmid is shown in the appendix (Figure 7.1).
pcDNA3-EGFP-Rac1-T17N	* EGFP-Tag on backbone (N terminal) * human, dominant-negative RAC1 * threonine to asparagine substitution (residue 17) * neomycin resistance	pcDNA3-EGFP-Rac1-T17N was a gift from Gary Bokoch (Addgene plasmid # 12982; http://n2t.net/addgene:12982; RRID:Addgene_12982). (Subauste et al. 2000) Map of the plasmid is shown in the appendix (Figure 7.2).
pcDNA3-EGFP-Rac1(wt)	* EGFP-Tag on insert (N terminal) * human, wild-type RAC1 * neomycin resistance	pcDNA3-EGFP-Rac1(wt) was a gift from Klaus Hahn (Addgene plasmid # 13719; http://n2t.net/addgene:13719; RRID:Addgene_13719). (Kraynov et al. 2000) Map of the plasmid is shown in the appendix (Figure 7.3).
pcDNA3-EGFP-NLS-Rac1-Q61L	* EGFP-Tag on backbone (N terminal) * human, constitutively active RAC1 * glutamine to leucine substitution (residue 61) * additional SV40 nuclear localization sequence * neomycin resistance	Plasmid designed within this study out of pcDNA3-EGFP-Rac1-Q61L. Map of the plasmid is shown in methods (Figure 2.4).
pcDNA3-EGFP-NLS-Rac1-T17N	* EGFP-Tag on backbone (N terminal) * human, dominant-negative RAC1 * threonine to asparagine substitution (residue 17) * additional SV40 nuclear localization sequence * neomycin resistance	Plasmid designed within this study out of pcDNA3-EGFP-Rac1-T17N. Map of the plasmid is shown in methods (Figure 2.4).

Name	Characteristics	Manufacturer
pcDNA3-EGFP-NLS-Rac1(wt)	* EGFP-Tag on insert (N terminal) * human, wild-type RAC1 * additional SV40 nuclear localization sequence * neomycin resistance	Plasmid designed within this study out of pcDNA3-EGFP-Rac1(wt). Map of the plasmid is shown in methods (Figure 2.4).

GFP expression vectors

Table 2.12: List of used plasmids for GFP expression

Name	Characteristics	Manufacturer
pEGFP-C1	* wild-type GFP * neomycin resistance	Clontech, Mountain View, CA, USA Map of the plasmid is shown in the appendix (Figure 7.4).
NLS pEGFP-N3	* GFP * SV40 nuclear localization sequence	Clontech NLS pEGFP-N3 (1299) was a gift from Eric Schirmer (Addgene plasmid # 62043; http://n2t.net/addgene:62043; RRID:Addgene_62043). (Zuleger et al. 2013) Map of the plasmid is shown in the appendix (Figure 7.5).

Lentiviral and retroviral plasmids and expression vectors

Table 2.13: List of used plasmids and expression vectors for lentiviral and retroviral transduction

Name	Characteristics	Manufacturer
pCD/NL-BH	* expression vector for gag/pol * based on HIV isolate HXB2 * deleted for packaging signals, 5' and 3' LTRs, ENV and NEF	The plasmid was kindly provided by Dr. Jakob Reiser, Louisiana State University School of Medicine, New Orleans, USA. (Mochizuki et al. 1998) Map of the plasmid is shown in the appendix (Figure 7.6).

Name	Characteristics	Manufacturer
pcoMEEtm	*expression vector for human codon optimized MEEtm chimeric envelope * based on pALVGalvTM	The plasmid was kindly provided by Prof. Dr. Helmut Hanenberg, Dep. of Otorhinolaryngology and Head/Neck Surgery, Duesseldorf, Germany. Map of the plasmid is shown in the appendix (Figure 7.7).
Puro.Cre empty vector	* encodes for Cre recombinase * Puromycin resistance	Puro.Cre empty vector was a gift from Tyler Jacks (Addgene plasmid # 17408; http://n2t.net/addgene:17408; RRID:Addgene_17408). (Kumar et al. 2008) Map of the plasmid is shown in the appendix (Figure 7.8).
pRetroQ-Cre-ERT2	* inducible Cre recombinase Estrogen receptor (ERT), C terminal on insert * Puromycin resistance	pRetroQ-Cre-ERT2 was a gift from Richard Youle (Addgene plasmid # 59701; http://n2t.net/addgene:59701; RRID:Addgene_59701). Map of the plasmid is shown in the appendix (Figure 7.9).
pSico PGK puro	* Puromycin resistance	pSico PGK puro was a gift from Tyler Jacks (Addgene plasmid # 11586; http://n2t.net/addgene:11586; RRID:Addgene_11586). Map of the plasmid is shown in the appendix (Figure 7.10).

siRNA

Table 2.14: List of used siRNAs

Name	Manufacturer
AllStars Negative Control siRNA (NS siRNA)	Qiagen, Hilden, Germany
GeneSolution siRNA *Rac1*	Qiagen, Hilden, Germany

2.1.12 Inhibitors

Table 2.15: List of used inhibitors

Name	Purpose	Manufacturer
EHT 1864	* RAC1 inhibition * blocks activation by direct binding to RAC1	Bio-Techne GmbH, Wiesbaden-Nordenstadt, Germany
QVD (Q-VD-OPh hydrate)	* Pan-caspase inhibitor * inhibits apoptosis	Sigma-Aldrich, Taufkirchen bei Muenchen, Germany

2.1.13 Nucleotides

Table 2.16: List of primers used for PCR

End point PCR			
Name			**Sequence (5'-3')**
Cre			CGAGTGATGAGGTTCGCAAG TTCACCGGCATCAACGTTTT
Real-time PCR			
Name	**Characteristics**	**NCBI reference sequence**	**Sequence (5'-3')**
Actb (mm)		NM_007393	GCATTGCTGACAGGATGCAG CCTGCTTGCTGATCCACATC
GAPDH (mm)		NM_008084	TCTCCTGCGACTTCAACA TCTCTTGCTCAGTGTCCTT
Rac1 forward (mm)	for evaluation of *Rac1* KO efficiency		GTGCCAAGGACAGTGACAAG
Rac1 reverse 1 (mm)	for evaluation of *Rac1* KO efficiency		GGCTCATGAATGCAGAGTCG
Rac1 reverse 2 (mm)	for evaluation of *Rac1* KO efficiency		GCAATGACAGATGTTCCGCA
Rac1-WT (mm)	binds to uncut floxed *Rac1*		CCTATCATCCTCGTGGGGAC GGTAGGTGATGGGAGTCAGC

Table 2.17: Oligonucleotides used for cloning

Name	Sequence (5'-3')
EcoRI-NLS	AGTCCGGAATTCACTCCTCCAAAAAAGAAGAGAAAGGTAGAATTCCGGTAC GTACCGGAATTCTACCTTTCTCTTCTTTTTTGGAGGAGTGAATTCCGGACT

Table 2.18: List of siRNAs used for *mRac1* knockdown

Name	NCBI reference sequence	Sequence (5'-3')
mm_Rac1_1	NM_009007	ACGGTTAATTTCTGTCAAACA
mm_Rac1_2	NM_009007	GGGCGTTGAGTCCATATTTAA
mm_Rac1_8	NM_009007	ATGGAGTAATTCAACTGAATA

2.1.14 Antibodies

Immunofluorescence

Table 2.19: List of used antibodies for immunofluorescence

Primary Antibody	Origin	Dilution	Company
anti-53BP1	Rabbit polyclonal	1:250	Cell Signaling, Cambridge, UK
anti-phospho-ATM (Ser1981) clone 10H11.E12	Mouse monoclonal	1:250	Merck Millipore, Darmstadt, Germany
anti-GFP [E385], recombinant	Rabbit monoclonal	1:250	Abcam, Cambridge, UK
anti-phospho-Histone H2A.X (Ser139)	Mouse monoclonal	1:500	Merck Millipore, Darmstadt, Germany
anti-RAC1, clone 23A8	Mouse monoclonal	1:500	Merck Millipore, Darmstadt, Germany

Secondary Antibody	Origin	Dilution	Company
Alexa Fluor 488, anti-rabbit IgG (H+L)	Goat	1:500	Thermo Fisher Scientific, Waltham, MA, USA
Alexa Fluor 555, anti-mouse IgG (H+L)	Goat	1:500	Thermo Fisher Scientific, Waltham, MA, USA
Alexa Fluor 647, anti-rabbit IgG (H+L)	Goat	1:250	Thermo Fisher Scientific, Waltham, MA, USA

Western blot analysis

Table 2.20: List of used antibodies for western blot analysis

Primary Antibody	Origin	Dilution	Company
anti-phospho-Chk1 (Ser345)	Rabbit polyclonal	1:1000	Cell Signaling, Cambridge, UK
anti-GFP cloneE385	Mouse monoclonal	1:1000	Epitomics, Burlingame, CA, USA
anti-GAPDH (14C10)	Rabbit monoclonal	1:2000	Cell Signaling, Cambridge, UK
anti-phospho-Histone H2A.X (Ser139)	Mouse monoclonal	1:4000	Merck Millipore, Darmstadt, Germany
anti-phospho KAP-1 (Ser824)	Rabbit polyclonal	1:1000	Bethyl Laboratories Inc., Montgomery, TX, USA
anti-phospho-p53 (Ser15)	Rabbit polyclonal	1:1000	Cell Signaling, Cambridge, UK
anti-RAC1, clone 23A8	Mouse monoclonal	1:4000	Merck Millipore, Darmstadt, Germany

Secondary Antibody	Origin	Dilution	Company
IgG HRP conjugated anti-mouse	Goat	1:2000	Rockland Immunochemicals, Limerick, PA, USA
IgG HRP conjugated anti-rabbit	Goat	1:2000	Rockland Immunochemicals, Limerick, PA, USA

2.1.15 Markers

Table 2.21: List of used markers

Name	Manufacturer
DNA ladder GeneRuler (100 bp, 1 kB)	Thermo Fisher Scientific, Waltham, MA, USA
Protein ladder PageRuler Prestained Plus	Thermo Fisher Scientific, Waltham, MA, USA

2.1.16 Buffers and solutions

Table 2.22: List of used buffers and solutions

Bacteria	
Name	**Compounds**
$CaCl_2$ solution	50 nM $CaCl_2$ in ddH_2O
$CaCl_2$/Glycerin solution	50 nM $CaCl_2$ 10 % Glycerin (v/v) in ddH_2O
LB agar	1.5 % Bacto-Agar (w/v) in LB medium
LB medium	10 g Bacto-Tryptone 5 g yeast extract 5 g NaCl ad 1000 ml ddH_2O

Cloning	
Name	**Compounds**
Annealing buffer	10 mM Tris (pH 7.5-8.0) 50 mM NaCl 1 mM EDTA in ddH_2O
TBE buffer pH 8.0	100 mM Tris 10 mM EDTA 83.34 mM Boric acid in ddH_2O
DNA extraction	
Name	**Compounds**
Lysis buffer	10 mM Tris-Hcl pH 9.0 50 mM KCl 0,1 % Triton X-100 (v/v) in ddH_2O
Immunofluorescence	
Name	**Compounds**
1 % BSA-PBS	1 % BSA (w/v) in PBS
5 % BSA-PBST	0.3 % BSA (w/v) in PBST
4 % Formaldehyde/PBS	4 % formaldehyde (v/v) in PBS
4 % Paraformaldehyde	4 % Paraformaldehyde (w/v) Phosphate buffer ddH_2O
PBS (pH 7.4)	137 mM NaCL 2.7 mM KCl 10 mM Na_2HPO_4 1.79 mM KH_2PO_4 in ddH_2O
PBS high salt	400 mM NaCL in PBS
PBST	0.3 % Triton X-100 (v/v) in PBS
Phosphate buffer (0.2 M)	0.2 M Sodium dihydrogen phosphate (NaH_2PO_4) 0.2 M Sodium hydrogen phosphate (Na_2HPO_4) in ddH_2O

SubG1	
Name	**Compounds**
hypotonic PI solution	50 µg/ml Propidium iodide 0.1 % sodium citrate (w/v) 0.1 % Triton X-100 (v/v) in ddH_2O
western blot	
Name	**Compounds**
Blotting buffer	0.25 M Tris Base 1.92 M Glycine 20 % Ethanol (v/v) in ddH_2O
Electrophoresis buffer	25 mM Tris Base 192 mM Glycine 0.1 % SDS (w/v) in ddH_2O
TBST (pH 7.2)	500 mM Tris Base 1.5 M NaCl 0.05 % Tween 20 (v/v) in ddH_2O
Ponceau S	0.15 % Ponceau S (w/v) 0.5 % glacial acetic acid (v/v) in ddH_2O
Separation Gel (10 %) sufficient for two 1.5 mm gels	7.8 ml ddH_2O 5 ml 1.5 M Tris pH 8.8 6.7 ml Acrylamide 30 % 200 µl SDS 10 % 80 µl TEMED 10 % 200 µl APS 10 %
Separation Gel (15 %) sufficient for two 1.5 mm gels	4.5 ml ddH_2O 5 ml 1.5 M Tris pH 8.8 10 ml Acrylamide 30 % 200 µl SDS 10 % 80 µl TEMED 10 % 200 µl APS 10 %
Stacking Gel (6 %) sufficient for two 1.5 mm gels	5.5 ml ddH_2O 1 ml 1.5 M Tris pH 6.8 1.3 ml Acrylamide 30 % 160 µl SDS 10 % 80 µl TEMED 10 % 800 µl APS 10 %
1.5 M Tris-Base (pH 6.8 and 8.8)	1.5 M Tris Base in ddH_2O

2.1.17 Software

Table 2.23: List of used software

Name	Manufacturer
BD Accuri™ C6	Becton, Dickinson and Company, Franklin Lakes, NJ; USA
CellSens Dimension 1.6	Olympus, Tokyo, Japan
CFX Manager 3.1	BioRad, Hercules, CA, USA
Endnote 20	Thomson Reuters, New York, NY, USA
Fusion Software	Vilber Lourmat Deutschland GmbH, Eberhardzell, Germany
GraphPad Prism 6	GraphPad Software, La Jolla, CA, USA
ImageJ 1.52i	National Institute of Health, USA
Image Lab	BioRad, Hercules, CA, USA
MS Office 2016	Microsoft, Redmond, WA, USA
SnapGene® Viewer 5.0.8	GSL Biotech LLC, San Diego, CA; USA (snapgene.com)

2.2 Methods

2.2.1 Cell biological methods

2.2.1.1 Cell lines and cell culture

Mouse embryonic fibroblasts (MEF) with *mRac1* gene flanked by loxP sites

Primary MEF (mouse embryonic fibroblasts) cells were isolated from embryos of C57BL/6 mice harbouring Mx1-Cre and *Rac1*$^{flox/flox}$. The isolated cells spontaneously immortalized in cell culture. The *Rac1* gene of these cells is flanked by loxP sites (*Rac1*$^{flox/flox}$) (Figure 3.32) and the cells express Cre recombinase under the control of the Mx-1 promoter (Walmsley et al. 2003; Bopp et al. 2015). The Cre/loxP system is a site-specific recombinase technology and Cre, as a site-specific DNA recombinase, catalyzes the recombination of DNA between loxP sequences. In the used MEF the loxP sites are located between exon 3 and 4, as well as between exon 5 and 6 of the *mRac*1 gene (Figure 3.32). Cre recombinase will therefore cut out exon 4 and 5 (1400 bp), which is leading to a frame shift mutation and a non-functional *Rac1* gene product (Walmsley et al. 2003). MEF (*Rac1*$^{flox/flox}$) were grown in Dulbecco's modified Eagle's medium (DMEM) supplemented with 10 % FCS and 1 % Penicillin/Streptomycin. Cells were kept at a constant temperature of 37 °C and a water vapor saturated atmosphere with 5 % CO_2. Passaging of cells was performed two or three times a week at a confluence of 80 % to 90 %. For this purpose, cells were washed with PBS, Trypsin/EDTA was added for detaching the cells. For further cultivation, the cells were diluted in a ratio of 1:10 or seeded for the experiments (for cell number see Table 2.24).

293T kidney cells

293T cells are derived from human embryonic kidney cells (HEK293). They are characterized by stable expression of the SV40 large T antigen which enables these cells for episomal replication of transfected plasmids with SV40 origin of replication (*ori*). They also contain a neomycin resistance gene (DuBridge et al. 1987; Pear et al. 1993). Lentiviral vector production was performed in 293T cells. 293T cells are commonly used, because this cell line is easy to transfect and supports high-level expression of viral proteins (Gama-Norton et al. 2011). 293T were grown on gelatin-coated dishes in Dulbecco's modified Eagle's medium (DMEM) supplemented with 10 % FCS, 1 % Penicillin/Streptomycin, and 2 mM L-glutamine. Cells were kept at a constant temperature of 37 °C and a water vapor saturated atmosphere with 5 % CO_2. Passaging of cells was performed two or three times a week at a confluence of 80 % to 90 %. For this purpose, cells were washed with PBS, Trypsin/EDTA was added for detaching the

cells. For further cultivation, the cells were diluted in a ratio of 1:10 or seeded for the experiments (for cell number see Table 2.24).

Phoenix-ECO

Phoenix-ECO cells are derived from 293T cells and are characterized by their additional expression of an ecotropic envelope protein from CMV (cytomegalovirus) (Pear et al. 1993; Swift et al. 2001). Retroviral vector production was performed in Phoenix-ECO cells. The cells were grown on gelatin-coated dishes in Dulbecco's modified Eagle's medium (DMEM) supplemented with 10 % FCS, 1 % Penicillin/Streptomycin, and 2 mM L-glutamine. Cells were kept at a constant temperature of 37 °C and a water vapor saturated atmosphere with 5 % CO_2. Passaging of cells was performed two or three times a week at a confluence of 80 % to 90 %. For this purpose, cells were washed with PBS, Trypsin/EDTA was added for detaching the cells. For further cultivation, the cells were diluted in a ratio of 1:10 or seeded for the experiments (for cell number see Table 2.24).

Mouse embryonic fibroblasts (MEF) without *mRac1* gene flanked by loxP sites (198M)

Primary MEF (mouse embryonic fibroblasts) were isolated from murine embryos (Lackinger et al. 2001). The isolated cells spontaneously immortalized in cell culture. The cells were used as control cell line for possible cytotoxicity of the viral transduction itself. The *Rac1* gene has no loxP sites ($Rac1^{wt/wt}$) and the cells are not able to express Cre recombinase. MEF ($Rac1^{wt/wt}$) were grown in Dulbecco's modified Eagle's medium (DMEM) supplemented with 10 % FCS and 1 % Penicillin/Streptomycin. Cells were kept at a constant temperature of 37 °C and a water vapor saturated atmosphere with 5 % CO_2. Passaging of cells was performed two or three times a week at a confluence of 80 % to 90 %. For this purpose, cells were washed with PBS, Trypsin/EDTA was added for detaching the cells. For further cultivation, the cells were diluted in a ratio of 1:10 or seeded for the experiments (for cell number see Table 2.24).

2.2.1.2 Cell experiments and treatment with genotoxins

Depending on the experimental setup, treatment with EHT 1864/doxorubicin/IR started at different timepoints.

I) Non-transfected cells were treated with Dox or IR 24 h after seeding. Pre-treatment with EHT 1864 for 3 h hours was performed prior to Dox treatment (Figure 2.1 A, Figure 2.1 C).

II) Cells designated for hRAC1- or GFP- expression were transfected 24 h after seeding and were treated the next day (24 h later) with Dox or IR like

indicated in the figure. Pre-treatment with EHT 1864 for 3 h hours was performed prior to Dox treatment (Figure 2.1 B, Figure 2.1 D).

III) Cells designated for double transfection (siRNA against *mRac1* and hRAC1 expression) were transfected with siRNA while they were seeded and 24 h later a transfection with the various *hRAC1* expression vectors was performed followed by treatment with doxorubicin the next day (24 h later) (Figure 2.1 F). Cells which were only transfected with *mRac1* siRNA were treated with Dox 48 h post-transfection (Figure 2.1 E).

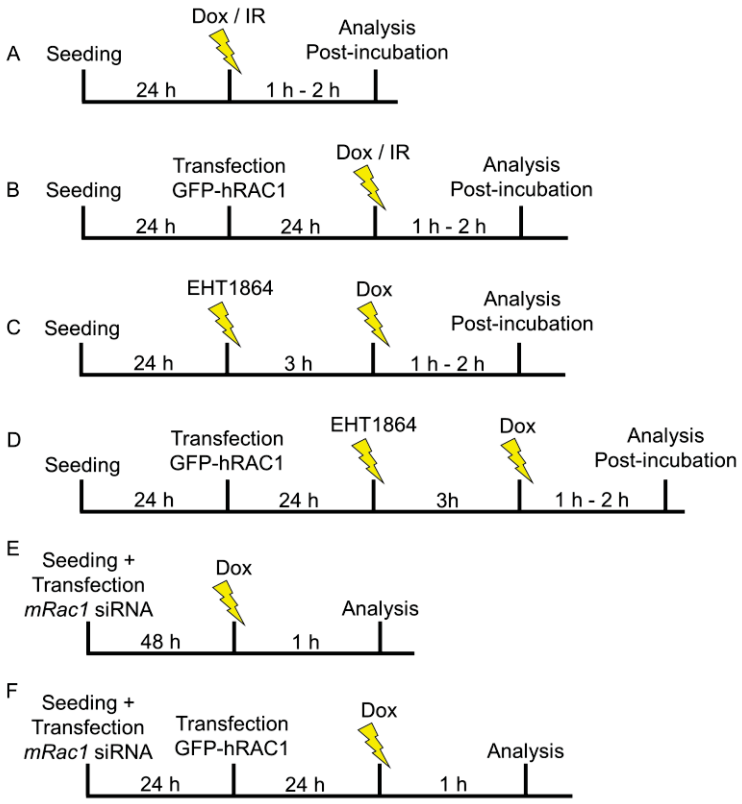

Figure 2.1: Treatment schemes for the performed experiments.
A) Cells were seeded and either 1 h - 2 h pulse-treated with Dox or treated with IR. Treatment with IR was followed by 1 h post-incubation and cells were analyzed directly after. Dox-treated cells were analyzed 0 h, 4 h, or 24 h after treatment. **B**) Cells were seeded and transfected with *GFP-hRAC1* expression vector 24 h later. On the following day cells were 1 h - 2 h pulse-treated with Dox and were analyzed 0 h, 4 h, or 24 h after treatment. If not treated with Dox, cells were irradiated, and analysis was performed 1 h after treatment. **C**) Cells were seeded and 24 h later cells were pre-treated with EHT 1864 for 3 h prior to pulse-treatment with Dox (1 h - 2 h). Cells were analyzed 0 h, 4 h, or 24 h after treatment. **D**) Cells were seeded and transfected with *GFP-hRAC1* expression vector 24 h later. On the next day, cells were pre-treated with EHT 1864 for 3 h prior to pulse-treatment with Dox (1 h - 2 h). Cells were analyzed 0 h, 4 h, or 24 h after treatment **E**) Cells were transfected with siRNA against murine *Rac1* (*mRac1* siRNA) while they were seeded. 48 h later cells were 1 h pulse treated with Dox and analyzed directly after. **F**) Cells were transfected with siRNA against murine *Rac1* (*mRac1* siRNA) while they were seeded, followed by transfection with *GFP-hRAC1* expression vector 24 h later. On the next day, cells were 1 h pulse treated with Dox and analyzed directly afterwards.

Cell numbers were adjusted for each experiment to avoid confluence of the monolayer at the day of analysis (see Table 2.24).

Table 2.24: List of cell numbers used in the experiments

Cell line	Cell number	Culture vessel	Experiment
MEF	15,000 per well	12 well slide	dose kinetics
MEF	25,000 per well	12 well plate	Foci analysis (Dox ± EHT 1864, hRAC1 expression)
MEF	10,000 per well	12 well plate	Foci analysis (*mRac1* siRNA)
MEF	50,000	3.5 cm dish	Foci analysis (IR, hRAC1 expression)
MEF	150,000 300,000	6 cm dish 10 cm dish	Western blot analysis (Dox ± EHT 1864, hRAC1 expression)
293T	5,000,000	10 cm dish	virus production
Phoenix-ECO	6,000,000	10 cm dish	virus production
MEF	500,000	10 cm dish	*mRac1* KO

For genotoxin-induced foci formation analysis, cells were pulse-treated with Dox for 1 h. In case of western blot analysis pulse-treatment was performed for 2 h. Pre-treatment with EHT 1864 was done 3 h prior to Dox treatment. Cells were fixed (for analysis of foci formation) or harvested (for WB analysis) 0 h, 4 h, or 24 h after treatment with Dox. Cells were irradiated in Gammacell® 1000 Elite (Cs^{137} radiation source) and fixed 1 h after IR exposure.

2.2.1.3 Transient transfection of mouse embryonic fibroblasts with *GFP-hRAC1* mutants

2.2.1.3.1 Establishment of a transfection protocol for mouse embryonic fibroblasts

MEF are a challenging cell line to transfect and often show a poor transfection efficiency (Lim et al. 2012; Lee et al. 2017). Only very few comparisons of transfection methods and transfection reagents in MEF according their transfection efficiency are available (Lee et al. 2017). To this end, a transfection reagent needed to be found that allows transfection of MEF cells with a high transfection efficiency. To this end, various

transfection reagents were tested. A brief transfection protocol and the different conditions of the used transfection reagents are stated below.

40,000 cells/well were seeded onto 12-well plates and the transfection procedure was performed according to the respective manufacturer's instructions. The *GFP-hRAC1(WT)* plasmid was chosen for testing of different plasmid DNA:transfection reagent ratios. For detailed information about the ratios for each transfection reagent see Table 2.25. Complexes were formed during the incubation (room temperature). During this time, the medium was removed from the wells, cells were washed with PBS and 1 ml DMEM supplemented with 10 % FCS was added. After incubation, the complexes were added dropwise to the cell's media and the plate was rocked back-and-forth as well as side-to-side for distribution of the complexes. Subsequently, cells were transferred back into the incubator and incubated with the plasmid DNA:transfection reagent complexes for 24 h - 48 h.

Table 2.25: List of transfection conditions for each used transfection reagent.

Transfection reagent	Ratio	Diluent	Incubation time	Medium change
DreamFect Gold	1:2, 1:3, 1:4	serum- and antibiotics-free DMEM	20 min	4 h after transfection
EcoTransfect	1:1, 1:2, 1:3	serum- and antibiotics-free DMEM	20 min	4 h after transfection
Effectene	1:8, 1:20, 1:40	Buffer EC	10 min	5 h after transfection
FuGene HD	1:2, 1:3, 1:4	serum- and antibiotics-free DMEM	15 min	/
GeneJuice	1:2, 1:3, 1:4	serum- and antibiotics-free DMEM	15 min	5 h after transfection
jetPEI	1:1, 1:2, 1:4	150 mM NaCl	15 min	5 h after transfection
Lipofectamine 3000	1:1.5, 1:2.25, 1:3	serum- and antibiotics-free DMEM	15 min	/
Metafectene	1:2, 1:3, 1:4	serum- and antibiotics-free DMEM	15 min	4 h after transfection

Transfection reagent	Ratio	Diluent	Incubation time	Medium change
Metafectene Pro	1:2, 1:3, 1:4	serum- and antibiotics-free DMEM	15 min	4 h after transfection
TransIT-X2	1:2, 1:3, 1:4	serum- and antibiotics-free DMEM	20 min	/

To further increase the transfection efficiency of Lipofectamine 3000 and TransIT-X2 the cell number was reduced to 25,000 per well and the experiment was performed again with plasmid DNA:transfection reagent ratios as stated in Table 2.25. Evaluation of the transfection efficiency was performed 24 h and 48 h after transfection. Representative pictures of the transfected cells were made, total cell number was set to 100 % and the percentage of green fluorescent cells was calculated.

2.2.1.3.2 Transient expression of human RAC1 in mouse embryonic fibroblasts by transfection with *GFP-hRAC1* expression vectors

Transient expression of human RAC1 (hRAC1) was achieved by usage of TransIT-X2, which is a non-liposomal transfection reagent and *GFP-hRAC1* expression vectors. After building complexes of plasmid DNA and TransIT-X2, the complexes are taken up from the cell via endocytosis. The plasmid DNA is only temporarily introduced into the cells and the transfected plasmid DNA remains extrachromosomal (Kim et al. 2010).

Apart from the manufacturer's instructions, 25,000 cells were seeded onto 12-well plates and 150,000 cells were seeded onto a 6 cm dish to improve the transfection efficiency. The remaining transfection procedure was performed in compliance with the manufacturer's instructions. A 3:1 ratio was chosen of TransIT-X2 to DNA.

In brief, cells were seeded on a 6 cm dish (for western blot analysis) or onto coverslips in 12-well plates (for analysis of γH2AX/53BP1 foci formation) 24 h prior to transfection. For transfection of a well in a 12-well plate 100 µl serum- and antibiotics-free DMEM was placed into a collection tube, 1 µl plasmid DNA (1 µg/µl stock) was added and the solution was gently mixed. 3 µl TransIT-X2 were added to the mixture and gently pipetted to mix. Complexes were formed during the incubation period of 20 min (room temperature). During this time, the medium was removed from the cells, cell monolayers were washed with PBS and 1 ml DMEM supplemented with 10 % FCS was re-added. After incubation, the complexes were added dropwise to the cell's media and the plate was rocked back-and-forth as well as side-to-side for equal distribution of the complexes.

Subsequently, cells were transferred back into the incubator and incubated with the Transit-X2:plasmid DNA complexes for 24 h.

2.2.1.4 Knockdown of the intrinsic murine *Rac1* (*mRac1*)

A transient gene knockdown of *mRac1* was induced by transfection with siRNA against *mRac1* (*mRac1* siRNA). To this end, three different siRNAs were combined (see sequences under Table 2.18). Lipofectamine RNAiMAX was used as transfection reagent. 10,000 cells were seeded onto 12-well plates. The final concentration of *mRac1* siRNA was 10 nM. The transfection procedure was performed according to the manufacturer's instructions.

In brief, for each well to be transfected, siRNA and 50 µl serum- and antibiotics-free medium were mixed in the well of the culture plate. 1 µl Lipofectamine RNAiMAX was added, the solution was gently mixed and incubated for 20 min at room temperature. During incubation, the cells were prepared for seeding. 10,000 cells were resuspended in 250 µl DMEM supplemented with 10 % FCS. The cells were added to the well with the Lipofectamine RNAiMAX-siRNA complexes. The plate was rocked back-and-forth as well as side-to-side for distribution of the complexes and the cells. Subsequently, cells were transferred back into the incubator and incubated with the Lipofectamine RNAiMAX-siRNA complexes.

2.2.1.5 Lentiviral vector production and transduction of cells to induce murine *Rac1* (*mRac1*) knockout

Lentiviral vector production was performed in 293T cells. 293T cells are commonly used, because this cell line is easy to transfect and supports high-level expression of viral proteins (Gama-Norton et al. 2011). $5x10^6$ 293T cells were seeded on gelatin-coated 10 cm dishes. On the next day, the cells were transfected using the transfection reagent PEI and various plasmids for production of lentiviruses containing a transgene. For *mRac1* knockout induction Cre recombinase was used as transgene. The viruses were used for induction of *mRac1* knockout in MEF harbouring a *mRac1* gene flanked by loxP sites (see Table 2.6 and 2.2.1.1). The plasmid pCD/NL-BH contains the gene for group-specific antigen (gag), which is a polyprotein and encodes the structural viral proteins, as well as the gene for the replication enzymes (pol) of retroviruses. The gene for the retrovirus envelope (env) is packed in plasmid pcoMEEtm (Elsner et al. 2017). The plasmid "Puro.Cre empty vector" encodes for Cre recombinase, which cuts at loxP sites, and delivers puromycin resistance which is necessary for selection of the transduced cells. For control experiments regarding puromycin-related cell death cells were transduced with virus containing the plasmid "pSico PGK puro" which genes encode for

puromycin resistance only. For transfection two solutions were prepared. Solution A contained 5 µg of the helper plasmids pCD/NL-BH (for gag/pol) and pcoMEEtm (for env), as well as the vector containing the transgene cassette (Puro.Cre empty vector or pSico PGK puro) and 985 µl serum- and antibiotic-free DMEM. Solution B contained the transfection reagent PEI (45 µg) and 955 µl serum- and antibiotic-free DMEM. Both solutions were pooled, vortexed and incubated at room temperature for 20 min. During this time, medium of 293T cells was changed to DMEM supplemented with 15 % FCS (without antibiotics). After incubation, the transfection solution was added to the cells. 24 hours post transfection the medium was changed to IMDM supplemented with 2 mM L-glutamine, 10 % FCS, and 1 % Penicillin/Streptomycin. On the next day, the medium containing the viral supernatant was collected in a falcon tube and filtered through a 0.45 µm syringe filter to get rid of detached cells.

The day before the lentiviral transduction, $5x10^5$ MEF cells were seeded on a 10 cm dish. For transduction of MEF, medium was replaced by undiluted, freshly harvested viral supernatant. On the following day, the medium was changed to DMEM, supplemented with 10 % FCS and 1 % Penicillin/Streptomycin. Additionally, selection with puromycin was started for selection of successfully transduced cells (expressing the puromycin resistance gene) and non-transduced cells (Figure 2.2). Subsequent evaluation of *mRac1* knockout was performed like described under 2.2.2.7.2.

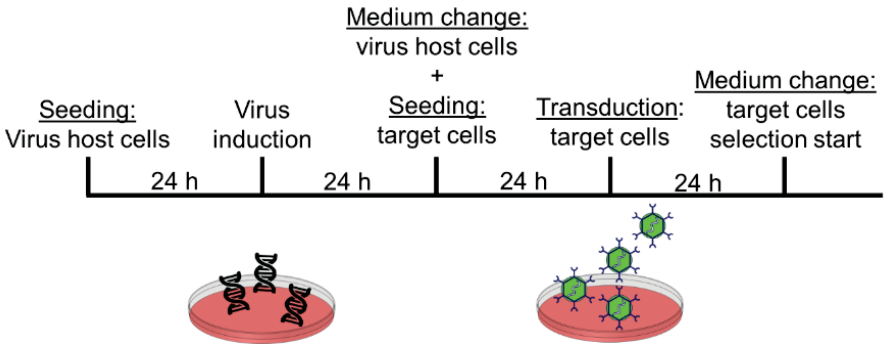

Figure 2.2: Scheme of virus production and transduction of target cells.
Virus host cells were seeded and 24 h later, cells were transfected for induction of virus production. The next day, medium of virus host cells was changed and target cells were seeded. 24 h later target cells were transduced by adding the filtered virus host cell medium containing the virus to the target cells. Medium of the target cells was changed 24 h later and the puromycin [2 µg/ml] selection was started.

2.2.1.6 Retroviral vector production and transduction of cells for stable Cre.ER expression to induce murine *Rac1* (*mRac1*) knockout

Retroviral vector production was performed in Phoenix-ECO cells. Phoenix-ECO cells are based on 293T cells, but in contrast to their parental cell line they stably express

gag/pol and envelope proteins (Swift et al. 2001). For production of a retrovirus containing a transgene, only transfection with the vector containing the transgene cassette is necessary. $6x10^6$ Phoenix-ECO cells were seeded on gelatin-coated 10 cm dishes. 24 h later, the cells were transfected with PEI and pRetroQ-Cre-ERT2. This vector contains the DNA sequence for a mutated estrogen receptor (ER), which is fused to Cre recombinase (Cre.ER). Cre recombinase cuts at loxP sites and therefore induces a *mRac1* knockout in the transduced MEF harbouring the *mRac1* gene flanked by loxP sites (see Table 2.6 and 2.2.1.1). The plasmid also delivers puromycin resistance which allows the selection of successfully transduced cells. For the transfection procedure two solutions were prepared. Solution A contained 10 µg of the vector containing the transgene cassette (pRetroQ-Cre-ERT2) and 990 µl serum- and antibiotic-free DMEM. Solution B contained the transfection reagent PEI (30 µg) and 970 µl serum- and antibiotic-free DMEM. Both solutions were pooled, vortexed and incubated at room temperature for 20 min. During this time, medium of Phoenix-ECO cells was changed to DMEM supplemented with 15 % FCS (without antibiotics). After incubation, the transfection solution was added to the cells. 24 hours post transfection the medium was changed to IMDM supplemented with 2 mM L-glutamine, 10 % FCS, and 1 % Penicillin/Streptomycin. At the next day, the medium containing the viral supernatant was collected in a falcon tube and filtered through a 0.45 µm syringe filter to get rid of detached cells.

2.2.1.7 Generation of a MEF cell line with stable Cre.ER expression for a tamoxifen-inducible *mRac1* KO

The viral transduction with the expression vector pRetroQ-Cre-ERT2 was used for the generation of a stable Cre.ER expressing MEF cell line. The aforementioned vector contains the DNA sequence for a mutated estrogen receptor, which is fused to the Cre recombinase (Cre.ER). Cre.ER stays in an inactive state in the absence of tamoxifen meaning the *mRac1* knockout is inducible upon tamoxifen treatment (Feil et al. 1996; Indra et al. 1999; Chucair-Elliott et al. 2019). Additionally, the vector contains the DNA sequence for puromycin resistance which allows selection between transduced and non-transduced cells. The optimal dose of puromycin was determined beforehand. To this end, MEF cells were treated with different concentrations of puromycin and the dose which induced 100 % cell death within one week (2 µg/ml) was used for further experiments.

The day before the transduction, $5x10^5$ MEF cells were seeded onto a 10 cm dish. For transduction, medium was replaced with undiluted, freshly harvested viral supernatant (described under 2.2.1.7). The next day, medium was changed to DMEM, supplemented

with 10 % FCS and 1 % Penicillin/Streptomycin. Additionally, selection with puromycin (2 µg/ml) was started for generation of a stable Cre.ER expressing cell line. Medium was replaced thrice a week until colonies of puromycin-resistant cell clones formed. A few colonies were picked with a pipette tip under a microscope and each colony was transferred to a well of a 96 well plate. To extend the cell numbers, the cells were transferred to a bigger well plate or a bigger cell culture dish after they were confluent, meaning from a 96-well plate cells were transferred to a 12-well plate, then to a 6-well plate and finally to a 10 cm dish. The clones were kept under constant selection pressure with puromycin. For verification of stable integration of transduced DNA an endpoint PCR was performed like described under 2.2.2.8.

2.2.1.8 Delivery of Cre recombinase via Cre recombinase Gesicles to induce *mRac1* knockout in *Rac1*$^{flx/flx}$ MEF

Cre recombinase Gesicles are nanovesicles produced in 293T cells and were used to deliver the Cre recombinase protein into *Rac1*$^{flx/flx}$ MEF. The Gesicles fuse with the plasma membrane and release active Cre recombinase into the lumen of the cell. After translocating to the nucleus, the active Cre recombinase will then cut at loxP sites. The procedure was performed according to the manufacturer's instructions. In brief, cells were seeded onto a 12 well plate the day before treatment. At a confluency of 60 % - 80 % they were treated with the Gesicles. The Gesicles were thawed and stored on ice. The cell medium was replaced by antibiotics-free DMEM supplemented with protamine phosphate (6 µg/ml) to improve transfection efficiency. Subsequently, Gesicles were added in different concentrations (10 µl, 25 µl) and the cells were incubated overnight (37 °C). On the next day, the medium was changed to DMEM with 10 % FCS and 1 % P/S and cells were harvested 48 h post transfection. Subsequent evaluation of *mRac1* knockout was performed like described under 2.2.2.7.2.

2.2.2 Molecular biology

2.2.2.1 Cloning of *hRAC1* expression vectors with additional nuclear localization sequence

To distinguish between nuclear and cytosolic effects of RAC1 on the DDR, an additional N-terminal NLS was added to *hRAC1* (Figure 2.3). All plasmids (*GFP-hRAC1(WT)*, *GFP-hRAC1(Q61L)*, *GFP-hRAC1(T17N)*) harbor an EcoRI restriction site between the sequence coding for *GFP* and the *hRAC1* insert. Thus, NLS oligonucleotides with EcoRI restriction sites were designed to insert an NLS sequence between the sequence coding for *GFP* and the *hRAC1* insert. NLS Oligonucleotides were dissolved in annealing buffer (for composition of the buffer see Table 2.22). For annealing of the NLS oligonucleotides

100 µM oligonucleotides stock solutions were mixed and incubated for 5 min at 95 °C on a heat block. The reaction tube containing the oligonucleotides was left to allow cool down to room temperature. In the next step the annealed NLS oligonucleotides (≙ insert) and the different *hRAC1* plasmid variants (≙ vector) (Table 2.11) were digested with EcoRI. The linearized plasmids were dephosphorylated with rSAP (shrimp alkaline phosphatase) to prevent re-ligation. Then, dephosphorylated NLS oligonucleotides and dephosphorylated vectors were each loaded into a pocket of the agarose-gel and were electrophoretic separated according to their size. GeneRuler DNA ladder (100 bp and 1 kb) was used in parallel to samples for size verification. By performing this step, the bases which were cut off from the NLS oligonucleotides and the *hRAC1* plasmids by EcoRI were separated from the insert and the vectors needed for ligation. Vectors and oligonucleotides were excised from the gel and purification was performed with the QIAquick Gel Extraction Kit. Afterwards vectors and oligonucleotides were ligated overnight (16 °C). Different ratios of oligonucleotides to vectors were used (1:1, 3:1, 5:1). For ligation a T4 DNA ligase was used, which ligates oligonucleotides and vectors by connecting the 3'-hydroxyl group and the 5'phosphate group and rebuilding phosphodiester bounds (Engler et al. 1982) (Figure 2.3). The next day, competent bacteria (DH5 alpha) were transformed and ~16 h later colonies were picked for plasmid preparation. To confirm the successful integration of the NLS sequence, the newly synthesized plasmids were sent to BMFZ (Biologisch-Medizinisches Forschungszentrum) at the Heinrich Heine University to verify the plasmid sequence identity by Sanger sequencing. Due to the two EcoRI restriction sites in the NLS oligonucleotides the chance of correct orientation of the NLS is 50 %. To this end, also the proper orientation was checked. The obtained sequence was analyzed by SnapGene® to create the following maps (Figure 2.4 A-C). *GFP* is marked bright green, SV40 NLS is marked blue, *hRAC1(WT)* is marked golden (A), *hRAC1(Q61L)* is marked purple (B), and *hRAC1(T17N)* is marked light blue (C).

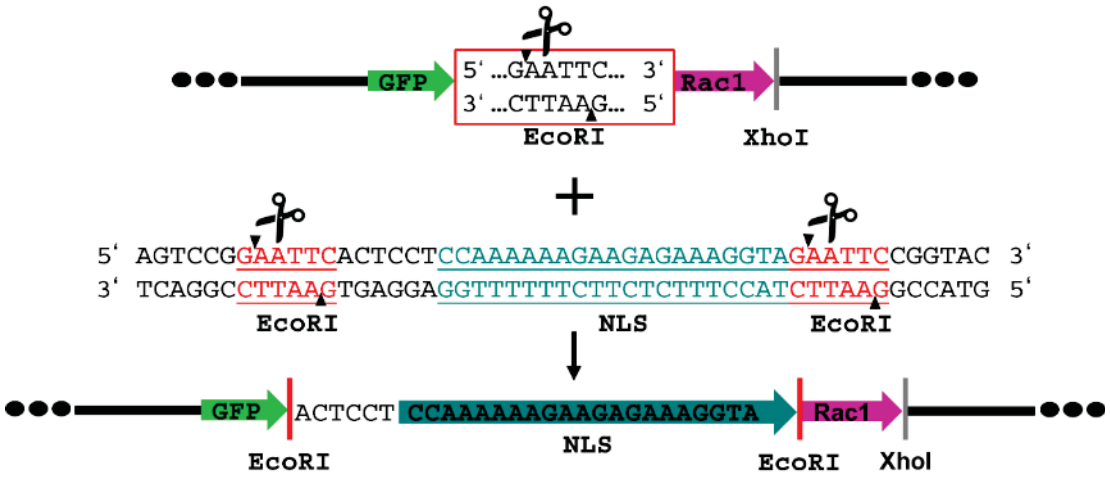

Figure 2.3: Scheme of cloning *GFP-hRAC1* with an additional nuclear localization sequence.
The *GFP-hRAC1* constructs harbor a unique EcoRI restriction site between the *GFP* sequence and the *hRAC1* DNA sequence. To insert the nuclear localization sequence (NLS) between *GFP* and *hRAC1*, oligonucleotides consisting of the NLS sequence and EcoRI restriction sites at each end were ordered. After annealing of the NLS oligonucleotides (≙ insert) they were digested with EcoRI. *GFP-hRAC1* (≙ vector) was also digested with EcoRI and afterwards vector and insert were dephosphorylated. Vector and insert were each loaded into a pocket of the agarose-gel and they were electrophoretic separated according to their size. In this step the bases which were cut off by EcoRI were also separated from the insert and vector. After excision from the gel and purification, vector and insert were ligated overnight. Next day, competent bacteria were transformed with the ligation mix. After plasmid preparation, the constructs were sent to BMFZ for sanger sequencing to verify the plasmid sequence identity and orientation.

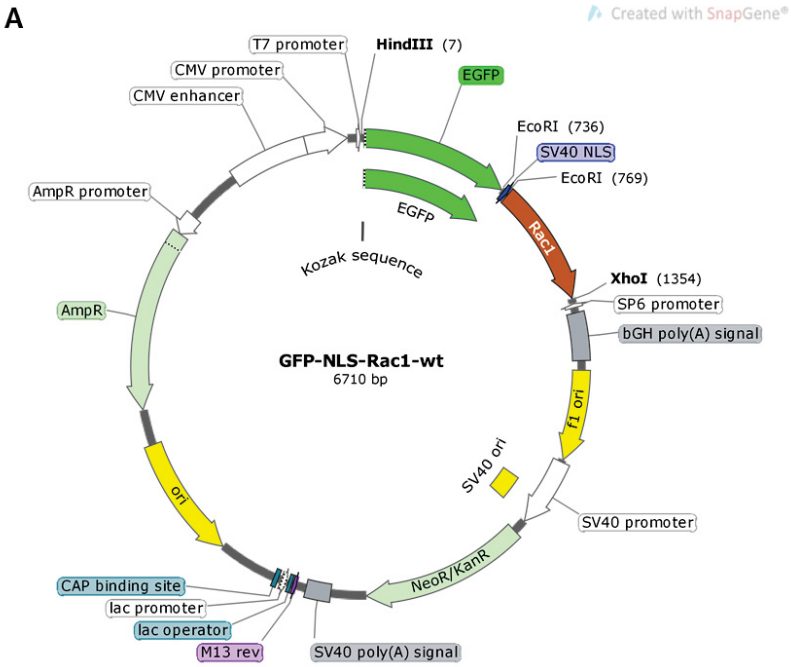

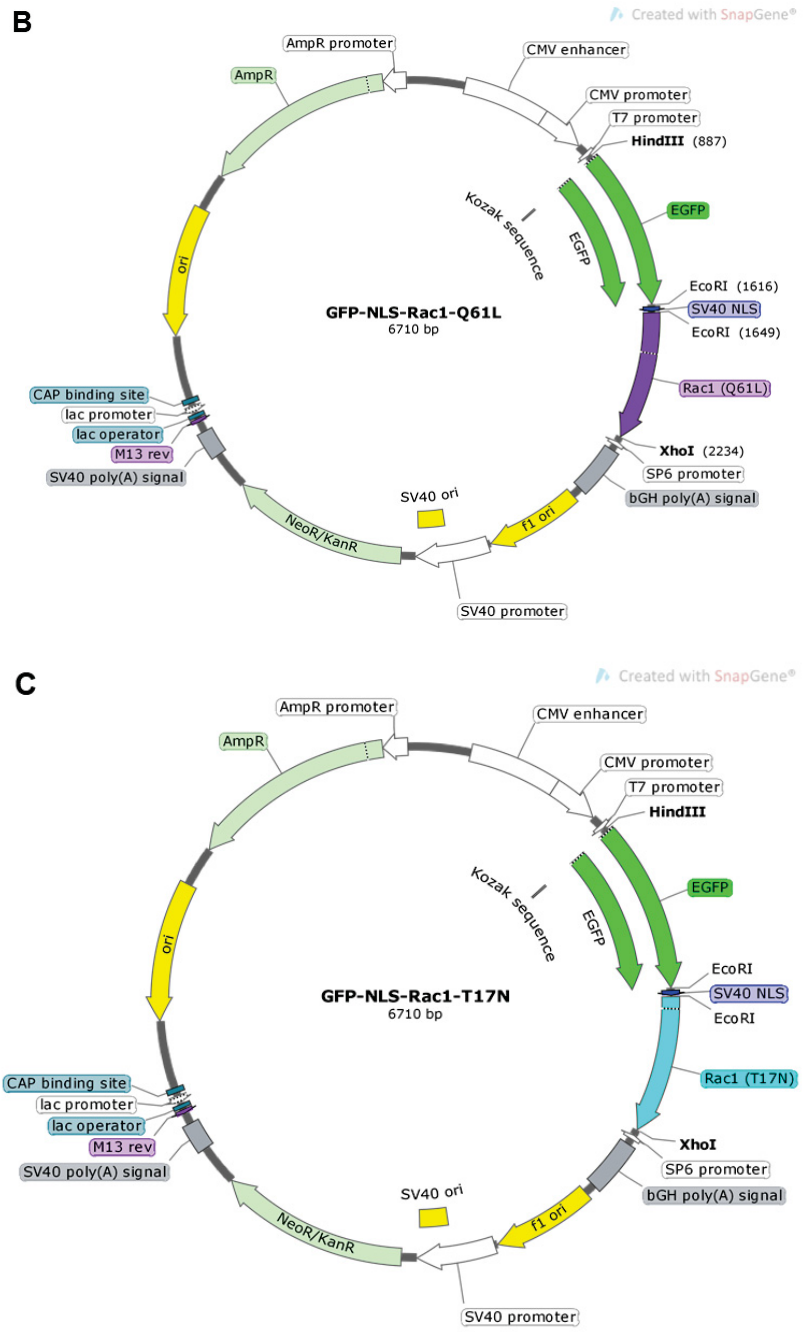

Figure 2.4: Maps of the different *GFP-NLS-hRAC1* expression vectors.
The sequence of the plasmids was analyzed by SnapGene® to create the plasmid maps. *GFP* is marked in bright green, SV40 NLS is marked in blue, *hRAC1(WT)* is marked in golden (**A**), *hRAC1(Q61L)* is marked in purple (**B**), and *hRAC1(T17N)* is marked in light blue (**C**).

2.2.2.2 Transformation of bacteria

The natural competence of bacteria to take up DNA is used in order to amplify plasmid DNA. The competence of bacteria can be enhanced by treatment with calcium chloride.

Frozen bacteria stocks (DH5 alpha or One shot® Top10, see Table 2.8) were thawed on ice. 100 µl of bacteria were carefully mixed with 5 µl ligation reaction and incubated on

ice for 30 min. A short heat shock of 90 s at 42°C was used for enhancement of the permeability of the bacteria to take up DNA. Subsequently, bacteria were put on ice for a short time. After addition of 300 µl pre-warmed LB media, the bacteria were incubated at 37 °C for 60 min at constant shaking, followed by centrifugation (2 min; 4,000 rpm). 300 µl of supernatant were decanted and the pellet was resuspended with the remaining medium. 50 µl of the bacteria were seeded on LB agar plates supplemented with the appropriate antibiotic (depending on the resistance gene of the plasmid) and incubated over night at 37°C.

2.2.2.3 Plasmid preparation

Preparation of purified plasmid DNA in small quantities was performed with the Qiagen Plasmid Mini Kit to test for positive transformed bacterial clones (cloning of *GFP-hRAC1* expression vectors with additional NLS). For isolation of purified plasmid DNA in high quantities the Qiagen Plasmid Maxi Kit was used. In both cases the preparation of the plasmid DNA was performed according to the manufacturer's instructions. The isolation of plasmid DNA is based on the binding of plasmid DNA to a silica membrane in the presence of chaotropic salts. After isolation, the purity and concentration of the plasmid DNA was measured with a NanoVue™ Plus spectrophotometer.

In brief, overnight bacterial culture was centrifuged at 4 °C and the bacterial pellet was resuspended in RNase A containing buffer P1. After addition of buffer P2, the solution was mixed and an incubation of 5 min at room temperature was carried out. Next, buffer P3 was added, the solution was mixed and incubated on ice for 5 min – 20 min (depending on the used kit). Afterwards, the mixture was centrifuged at 4 °C and in the meantime the column was equilibrated with QBT buffer. After centrifugation, the supernatant was applied to the column and allowed to enter the resin by gravity flow. Next, the column was washed two times with QC buffer and elution buffer was added to elute the DNA. Afterwards, the DNA was precipitated through addition of isopropanol and mixing. Then the mixture was centrifuged and the supernatant carefully decanted. This was followed by another washing and centrifugation step. The pellet was air-dried and dissolved in DNase free water.

2.2.2.4 Isolation of genomic DNA

The isolation was performed semi-automatically using the DNeasy Blood & Tissue Kit and QIAcube according to the manufacturer's instructions. In brief, cells were washed with PBS, detached with Trypsin/EDTA and centrifuged. Each cell pellet was resuspended in PBS and proteinase K was added. Next, Buffer AL was added, cells were vortexed and incubated for 10 min at 56 °C. Afterwards pure ethanol was added

and the cells were vortexed again, before they were transferred into a column (included in the DNeasy Blood & Tissue Kit). After centrifugation and washing, the genomic DNA was eluted in DNase free water. After isolation, the purity (absorption ratios of A260/280 and A260/230) and concentration [ng/µl] of the genomic DNA was determined with a NanoVue™ Plus spectrophotometer.

2.2.2.5 RNA isolation

The isolation was performed semi-automatically using the RNeasy Mini Kit and a QIAcube according to the manufacturer's instructions. In brief, cells were washed with PBS, detached with Trypsin/EDTA and centrifuged. Each cell pellet was resuspended in RLT buffer containing DTT and then vortexed for homogenization. After several centrifugation and washing steps, DNase digestion was carried out on the mRNA-binding column. This step was followed again by several centrifugation and washing steps. RNA was finally eluted with RNase free water. After the isolation, the purity (absorption ratios of A260/280 and A260/230) and concentration [ng/µl] of the RNA was determined with a NanoVue™ Plus spectrophotometer.

2.2.2.6 cDNA synthesis

cDNA synthesis was carried out using the High-Capacity cDNA Reverse Transcription Kit according to the manufacturer's instructions. The reverse transcriptase, an RNA-dependent DNA polymerase, is used to synthesize the cDNA complementary to the RNA. Oligo-dT primers were used, that are complementary to the poly-A tail of the mRNA and thus enable the synthesis to start. For cDNA synthesis 500 ng - 2,000 ng RNA were used. The reaction mixture was incubated in a Thermal Cycler for 120 min at 37 °C and stored at -20 °C until use.

2.2.2.7 Real-time PCR

2.2.2.7.1 RT-qPCR for evaluation of mRNA expression

Before the RT-qPCR was performed, mRNA was isolated and cDNA was synthesized with reverse transcription (see 2.2.2.5 and 2.2.2.6). cDNA fragments were amplified using the CFX96TM real-time PCR detection system and the SensiMix SYBR® Hi-ROX kit for semi-quantitative analysis of gene expression. This PCR measurement is based on the fact that the used fluorescent dye (SYBR-Green) intercalates into double-stranded cDNA. The amplification of the target sequence leads to an increase in fluorescence, which is directly proportional to the amount of synthesized DNA. The fluorescence of SYBR-Green was detected after each cycle and a fluorescence threshold value (C_T value) was calculated. The C_T value indicates the cycle at which the exponential phase

of the PCR begins. For each reaction mixture 20 ng - 40 ng cDNA and primers with end concentration of 250 nM were mixed with SensiMix SYBR® Hi-ROX and filled up to a final volume of 20 µl with sterile PCR-grade water. The PCR reaction was carried out in duplicates according to the protocol listed in Table 2.26. Amplified *β-Actin* and *GAPDH* cDNA were used as reference within each experiment based on the ΔΔCq method.

Table 2.26: Real-time PCR protocol

	Step	Temperature	Time [min:sec]
1	TAQ activation /denaturation of cDNA	95 °C	10:00
2	Denaturation	95 °C	0:15
3	Primer hybridization	58 °C	0:15
4	Elongation	72 °C	0:17
		Detection of fluorescence	
5		repeat of step 2 - 4, 44 more times	
6		95 °C	1:00
7		55 °C	1:00
8	Melting curve	65 °C to 95 °C	

2.2.2.7.2 Real-time qPCR for determination of *mRac1* knockout efficiency

This method was used for determination of *mRac1* knockout efficiency after viral transduction/transfection with Cre Recombinase Gesicles. Genomic DNA was isolated from transduced MEF and amplified using the CFX96 real-time PCR detection system and the SensiMix SYBR® Hi-ROX kit. The PCR reaction was carried out in duplicates according to the protocol listed in Table 2.26. The genomic DNA was isolated from cells which harbor loxP sites in the *mRac1* gene (see Table 2.6, 2.2.1.1, and Figure 3.32). After lentiviral transduction (see 2.2.1.6) genomic DNA was isolated like described above (see 2.2.2.4). For discrimination between the non-truncated and the Cre-mediated truncated *mRac1* form, three different *Rac1* primers were used (see Table 2.16 and Figure 2.5). The forward primer binds to a specific site in exon 3 of the *mRac1* gene, reverse primer 1 binds to a specific site in exon 4, and reverse primer 2 binds to a specific site in exon 6. Due to the Cre recombinase induced excision at the loxP sites, exon 4 and 5 are cut out. Thus, with the combination of the forward primer and reverse primer 1 there will be no PCR product detectable in potential *mRac1* knockout cells. Instead, in these cells a product based on the combination of the forward primer and reverse primer 2 (163 bp) will be detectable. In contrast, the cells without *mRac1* gene flanked by loxP sites or cells which were not cut by Cre recombinase a product based on reverse primer 1 (183 bp) will be detectable, but not with reverse primer 2 because of its size (>1600 bp). Products >1000 bp need more time to be completed during the elongation step than given by the used protocol. The used *Taq* polymerase takes about 1 min to generate a

product of 1000 bp length, meaning for a product of 1600 bp a time of about 1.5 min is needed. Due to the fact that the elongation step in the used protocol is only 17 seconds, there is not enough time for the polymerase to build the product of forward primer and reverse primer 2 in cells where the Cre recombinase did not truncate the *mRac1* gene. The mean values of C_T values of potential *mRac1* knockout cells (pKO) and cells with intact *mRac1* gene (WT) were determined. The *mRac1* knockout efficiency was calculated as follows:

$$100/\left(1+\left(\frac{2^{\text{mean Ct pKO}}}{2^{\text{mean Ct WT}}}\right)\right) = \%\ \text{knockout efficiency}.$$

This formula assumes that the PCR products obtained from the use of the different primers must always add up to 100 %. Meaning that the decrease of the WT PCR product (forward primer and reverse primer 1, 183 bp) is direct proportional to an increase of the KO PCR product (forward primer and reverse primer 2, 163 bp) to the same extend.

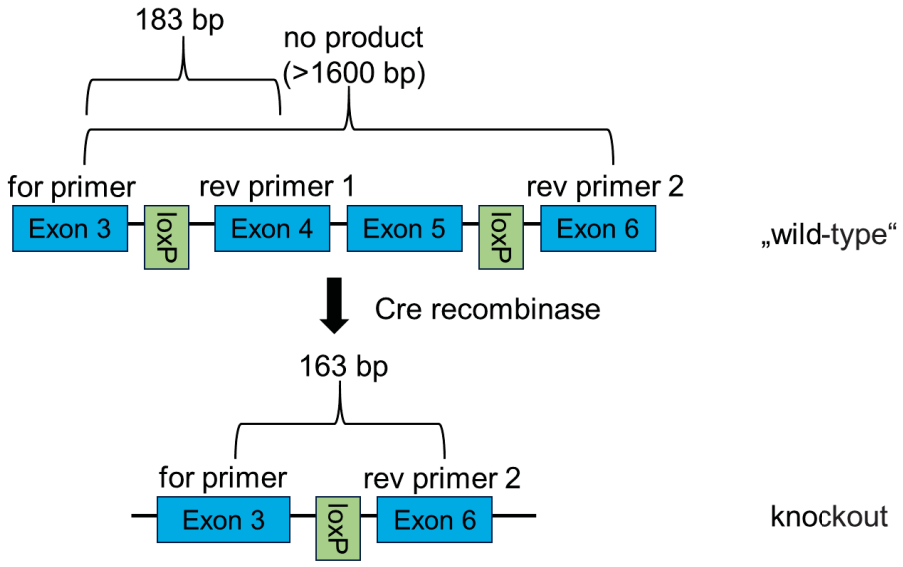

Figure 2.5: Schematic representation of primer binding at non-truncated and Cre-induced truncated *mRac1* form.
The forward primer binds to a specific site in exon 3, the reverse primer 1 binds to a specific site in exon 4, and the reverse primer 2 binds to a specific site in exon 6. PCR with forward primer and reverse primer 1 is resulting in a PCR product of 183 bp in length. PCR with the forward primer and reverse primer 2 generates no PCR product in cells where Cre recombinase did not truncate the *mRac1* gene, because the Taq polymerase is not able to complete the PCR product during the elongation step in the used protocol. Due to the excision of Exon 4 and 5 there will be no binding of reverse primer 1 in cells with *mRac1* gene cut by Cre recombinase. PCR with the forward primer and reverse primer 2 is resulting in a PCR product of 163 bp in length in Cre-induced truncated *mRac1*. Abbreviations: for primer: forward primer, rev primer: reverse primer.

2.2.2.8 End point PCR for detection of stably integrated DNA

For verification of stable integration of transduced plasmid DNA an endpoint PCR was performed. In brief, cells were transduced with Cre.ERT2 vector and 24 h later puromycin selection was started to select for stable Cre.ER expressing cells. Selection was performed until colonies of puromycin resistant cell clones appeared. These clones were harvested, and the cell pellet was resuspended in lysis buffer containing proteinase K [80 µg]. Lysis was performed overnight (55 °C) at constant shaking. On the next day, the proteinase was heat inactivated (10 min, 95 °C) and the sample was prepared for PCR. For this purpose, 500 µg DNA and Cre primers (see Table 2.16) with a final concentration of 250 nM were mixed with RedTaq, $MgCl_2$ and sterile PCR-grade water to a final volume of 20 µl. The PCR reaction was carried out according to the protocol listed in Table 2.27. Finally, the PCR products were separated using an 2 % agarose gel containing ethidium bromide. This dye intercalates into the DNA and allows the detection of bands with the Imaging System Fusion FX7.

Table 2.27: End point PCR protocol.

Step	Temperature	Time [min:sec]
1	94 °C	5:00
2	94 °C	1:00
3	58 °C	1:00
4	72 °C	1:00
5	repeat of step 2 - 4 for 34 more times	
6	72 °C	10:00
7	8 °C	∞

2.2.3 Immunofluorescence

2.2.3.1 Microscopical detection of nuclear γH2AX and 53BP1 foci

For the detection of DNA DSB, the formation of γH2AX and 53BP1 foci (as surrogate markers for DNA DSB) was visualized. However, phosphorylation of H2AX can also occur during certain cellular events that are independent of DSB formation (Turinetto et al. 2015). Therefore, a second marker for DNA DSB was visualized, namely 53BP1 (Panier et al. 2014). Colocalization of γH2AX and 53BP1 foci as markers for DSB is regarded as highly specific for DSB (Schultz et al. 2000; Ward et al. 2003; Chronis et al. 2007).

For foci analysis, cells were seeded onto coverslips in 12-well plates or 3.5 cm dishes. After treatment with Dox or IR, the medium was removed, the cells washed with PBS and fixed with 4 % formaldehyde/PBS (15 min, RT). Subsequently, cells were washed with PBS (3 x 5 min) and incubated with cold methanol at -20 °C for at least 20 min. Then methanol was removed, cells were washed with PBS and 5 % BSA-PBST (PBS with 0.3 % Triton X-100) was added for blockage of unspecific binding sites (60 min, RT, constant shaking). After removal of the blocking solution, primary antibodies were diluted with 5 % BSA-PBST (γH2AX 1:500, 53BP1 1:250), added to the cells and incubated overnight at 4 °C in a humidified chamber. The next day, cells were washed with PBS, PBS high salt (0.4 M NaCl), and PBST before the secondary antibody was added (Alexa Fluor 555 goat anti-mouse 1:500, Alexa Fluor 647 goat anti-rabbit 1:250). Incubation was performed for at least 1 h in the dark (RT), followed by washing with PBS (3 x 5 min; RT; in the dark) and PBST. As final step, cells were mounted with Vectashield containing DAPI, sealed with nail polish and stored at 4 °C until analysis. γH2AX and 53BP1 foci were visualized under a fluorescence microscope due to the fluorophore-coupled secondary antibodies. Pictures were taken and the number of single γH2AX and 53BP1 foci as well as their colocalization was determined using ImageJ (Oeck et al. 2015).

2.2.3.2 Microscopical detection of pATM foci formation after doxorubicin treatment

The ATM kinase is a key regulatory kinase of the DDR and a main mediator of DNA DSB repair, which activates a broad spectrum of proteins (Marechal et al. 2013). For evaluation of ATM activation, the formation of nuclear pATM foci was visualized. For this purpose, cells were plated onto coverslips in 12-well plates. After treatment with Dox, the medium was removed, cells washed with PBS, and then fixed in 4 % formaldehyde/PBS for 15 min at room temperature. Next, cells were washed with PBS and PBST was added for permeabilization of the cells (15 min, RT) at constant shaking. This step was followed by blocking with 5 % BSA-PBST (1 h, RT, constant shaking) to block unspecific binding sites. After removal of the blocking solution, the primary antibody was diluted in 5 % BSA-PBST (1:250), added to the cells and incubated overnight at 4 °C in a humidified chamber. Next day, cells were washed with PBS (3 x 5 min) before the secondary antibody was added (Alexa Fluor 555 goat anti-mouse 1:500). Incubation was performed for at least 1 h in the dark (RT), followed by washing with PBS (3 x 5 min; RT; in the dark). As final step, cells were mounted with Vectashield containing DAPI, sealed with nail polish and stored at 4 °C until analysis. pATM foci were visualized under a fluorescence microscope due to the fluorophore-coupled secondary antibody. Pictures were taken and the number of pATM foci was determined using ImageJ.

2.2.3.3 Staining of the actin cytoskeleton

TRITC-coupled phalloidin is a fluorescent phallotoxin and was used for cytochemical staining of the actin cytoskeleton. The phalloidin toxicity is attributed to the ability to bind filamentous (F-)actin and thereby preventing the depolymerization of actin fibers (Dancker et al. 1975).

Cells were seeded onto coverslips in 12-well plates. After treatment, the cells were washed with PBS for two times and subsequently fixed in freshly prepared 4 % formaldehyde/PBS (methanol-free) for 15 min. Next, cells were washed two times with PBS for 5 min and acetone was added for 3 min. This was followed by two washing steps with PBS (5 min) and by blocking of unspecific binding sites with 1 % BSA-PBS for 1 h. Thereafter, Phalloidin-TRITC was added to the cells (0.1 µg diluted in PBS) for 1 h. Staining was performed in dark at room temperature. After two washing steps with PBS (5 min) the stained cells were mounted with Vectashield containing DAPI and sealed with nail polish before fluorescence microscopy-based analysis was performed.

2.2.4 Protein biochemistry

2.2.4.1 Preparation of protein extracts for SDS-PAGE and western blot analysis

For total cell extracts, cell monolayer was washed with PBS and afterwards 100 µl 1x Roti-load 1 (Roth) (95 °C) was added to a 10 cm dish. For a 6 cm dish 50 µl Roti-load 1 was used. The lysis buffer was spread across the plate followed by short rotation. With the help of a cell scraper, the lysate was transferred to a reaction tube, immediately put on ice and afterwards sonicated for disruption of macromolecules (50 amplitude; 1 s pulse; 1 s pause; 5 bumps; 2 passes; Sonicator EpiShear™ Probe sonicator). The cell debris was pelleted by centrifugation (10,000 x g; 10 min), the supernatant was transferred into a new reaction tube and was used for SDS-PAGE.

2.2.4.2 SDS-PAGE

Electrophoretic separation of the proteins according to their molecular weight was achieved by discontinuous SDS-PAGE. Due to the negative charged detergent SDS in the Roti-load buffer as well as the heating of the samples at 95 °C secondary and tertiary protein structures of the samples are denatured. Furthermore, SDS-protein-complexes are formed. The native protein charge is masked by the negative charged SDS. Hence, the proteins migrate through the gels´ pores to the anode during electrophoresis resulting in their separation according to their molecular weight. The protein ladder PageRuler™ prestained Plus was loaded in the first lane of every gel for protein size verification. The electrophoresis was performed with the help of the Mini-PROTEAN® Tetra Vertical

Electrophoresis Cell system with 15 mA per gel until the dye front of the protein ladder reached the separation gel. Afterwards the electrophoresis was performed with 30 mA per gel.

2.2.4.3 Western blot analysis of proteins involved in the DNA damage response

Transfer of the proteins from the gel onto a nitrocellulose membrane was performed in a tank blot system (Mini Trans-Blot® Cell system) with 300 mA for 90 min. The successful protein transfer, as well as the equal loading of the samples, was verified by staining of the membrane with Ponceau S. To remove the ponceau S staining, the membrane was washed with tab water and afterwards with TBST (Tris buffered saline and Tween20). Subsequently, non-specific antigen binding sites were saturated with 5 % milk powder or 5 % BSA solved in TBST (1 h) at constant shaking. The decision for the usage of milk or BSA for blockage was depending on the protein of interest and the manufacturer's recommendations. Afterwards, the membrane was washed 3 x 5 min with TBST and incubated overnight (4 °C) with the antibody of interest. At the next day, the membrane was washed again 3 x 5 min with TBST to remove excess antibody. Subsequently, the membrane was incubated at constant shaking with a horseradish peroxidase-(HRP) coupled secondary antibody, which is directed against the primary antibody. Incubation was performed for 2 h at room temperature. Membrane was washed again (TBST, 3 x 5 min) before a solution containing luminol was applied. Luminol reacts with HRP and the intensity of the signal was detected with ChemiDoc™. The signals of the target proteins were normalized to the signal of the reference protein GAPDH.

2.2.5 Flow cytometry

2.2.5.1 Analysis of cell cycle distribution and apoptotic cell fraction (SubG1)

Mammalian cells were stained with the DNA-intercalating agent propidium iodide. As a result, the cell cycle status can be determined due to the proportional increase of the PI fluorescence with the DNA content (Crowley et al. 2016). A typical cell cycle profile of untreated cells reveals a G0/G1 peak (2n) and a G2 peak (4n), whereby G2 peak shows double the fluorescence intensity of the G0/G1 peak. The fluorescence intensity of cells in S phase is somewhere between the intensities of G0/G1 peak and G2 peak. The so-called SubG1 fraction represents cells with sub-diploid DNA content and thus these cells are considered as apoptotic (Darzynkiewicz et al. 1997).

After treatment, the medium of each sample was collected in a falcon tube. The monolayer was washed with PBS and the PBS was transferred to the corresponding falcon. After trypsinization the cells were also transferred to the corresponding falcon. Next, cells were pelleted by centrifugation (300 g, 5 min), the supernatant was carefully

decanted, and the remaining cell pellet was resuspended in 1.5 ml hypotonic PI solution. After overnight incubation (4 °C, dark), cells were analyzed using the Flow Cytometer BD Accuri™ C6.

2.2.6 Statistical data evaluation

Statistical comparisons between treatments were made by one-way analysis of variance (ANOVA) with Dunnett post-hoc test or 2-way analysis of variance (ANOVA) with Dunnett or Tukey post-hoc test. Statistical significance was also evaluated using the two-sided, unpaired T-Test according to Student. Statistically significant differences were marked with *, $^{+}$, $^{\#}$, °, $^{\$}$, or $^{\sim}$. *p ≤ 0.05, **p ≤ 0.01, ***p ≤ 0.001, ****p ≤ 0.0001.

3 Results

3.1 Establishment of a transfection protocol for mouse embryonic fibroblasts and dose determinations of doxorubicin as well as of the RAC1 inhibitor EHT 1864

3.1.1 Establishment of a transfection protocol for mouse embryonic fibroblasts

Mouse embryonic fibroblasts (MEF) should be transiently transfected with different human *GFP-RAC1* mutants to analyse the influence of RAC1 on the DNA damage response (DDR) after treatment with doxorubicin (Dox). The used mutants were *GFP-hRAC1(WT)*, *GFP-hRAC1(Q61L)*, and *GFP-hRAC1(T17N)* with and without an additional NLS. GFP-hRAC1(Q61L) is a constitutive active form of RAC1. The endogenous as well as the GAP-stimulated GTPase activity is blocked in this mutant, therefore RAC1 stays in an active state (Khosravi-Far et al. 1995; Bai et al. 2018). GFP-hRAC1(T17N) is permanently in its inactive state, due to a defective GDP to GTP exchange (Feig et al. 1988; Davis et al. 2013). Dominant-negative RAC1 is bound to GDP which sets the protein in its inactive state. MEF are a challenging cell line to transfect and often show a poor transfection efficiency (Lim et al. 2012; Lee et al. 2017). Only very few comparisons of transfection methods and transfection reagents in MEF regarding their transfection efficiency are available (Lee et al. 2017). To this end, a transfection reagent is needed to be found that transfects MEF cells with a high efficiency. Various transfection reagents were tested for transfection of MEF. The *GFP-hRAC1(WT)* plasmid was chosen for the transfection efficacy tests. Transfected cells will appear green under the microscope due to the expressed GFP-hRAC1 fusion protein. As starting point the protocol was performed according to the respective manufacturer's instructions. The following transfection reagents were used: jetPEI, Effectene, GeneJuice, Metafectene, Metafectene Pro, FuGene HD, Dreamfect Gold, Eco Transfect, Lipofectamine 3000, and TransIT-X2 (see material and methods for more details). 40,000 MEF were seeded onto 12 well plates and 24 h later the transfection was performed. For each transfection reagent three different DNA-transfection reagent ratios were tested. To this end, the recommended starting conditions for transfection were chosen as well as further volumes of transfection reagent/DNA which were recommended for optimization. For detailed information see 2.2.1.3.1. If excited with a wavelength in the range of 460 – 495 nm, GFP emits a green fluorescence at 510 – 550 nm (495 nm/519 nm at the used microscope). Due to the expressed GFP-coupled protein, a fluorescence-based evaluation of the transfection efficiency was performed 24 h and 48 h after transfection.

For this purpose, representative pictures of the transfected cells were made and the percentage of green fluorescent cells was calculated. For some of the used transfection reagents a transfection efficiency of 8 % - 13 % in MEF was described (Han et al. 2015). However, as found in the presented study the transfection efficiency for almost all tested reagents was below 5 %. Only two of the transfection reagents reached a transfection efficiency above 10 % (Figure 3.1 A). Pictures taken 24 h and 48 h post-transfection revealed no difference in the transfection efficiency between the two time points.

To further increase the efficiency of the two most promising reagents, namely Lipofectamine 3000 and TransIT-X2, the cell number was reduced to 25,000 cells per well. The protocol for Lipofectamine 3000 recommended to test different volumes of Lipofectamine 3000 reagent, while the volume of DNA should be stable [1 µg]. The tested volumes for the transfection reagent were 1.5 µl, 2.25 µl, and 3 µl. For Lipofectamine 3000 the new protocol did not improve the transfection efficiency. For TransIT-X2 the tested DNA to TransIT-X2 ratios were 1:2, 1:3, and 1:4. The ratio of 1:3 in combination with the reduced cell number increased the transfection efficiency of TransIT-X2 to up to 25 % (Figure 3.1 B). To this end, TransIT-X2 (1:3 ratio) was routineously used as transfection reagent to transiently express human RAC1 mutants in MEF for all following experiments.

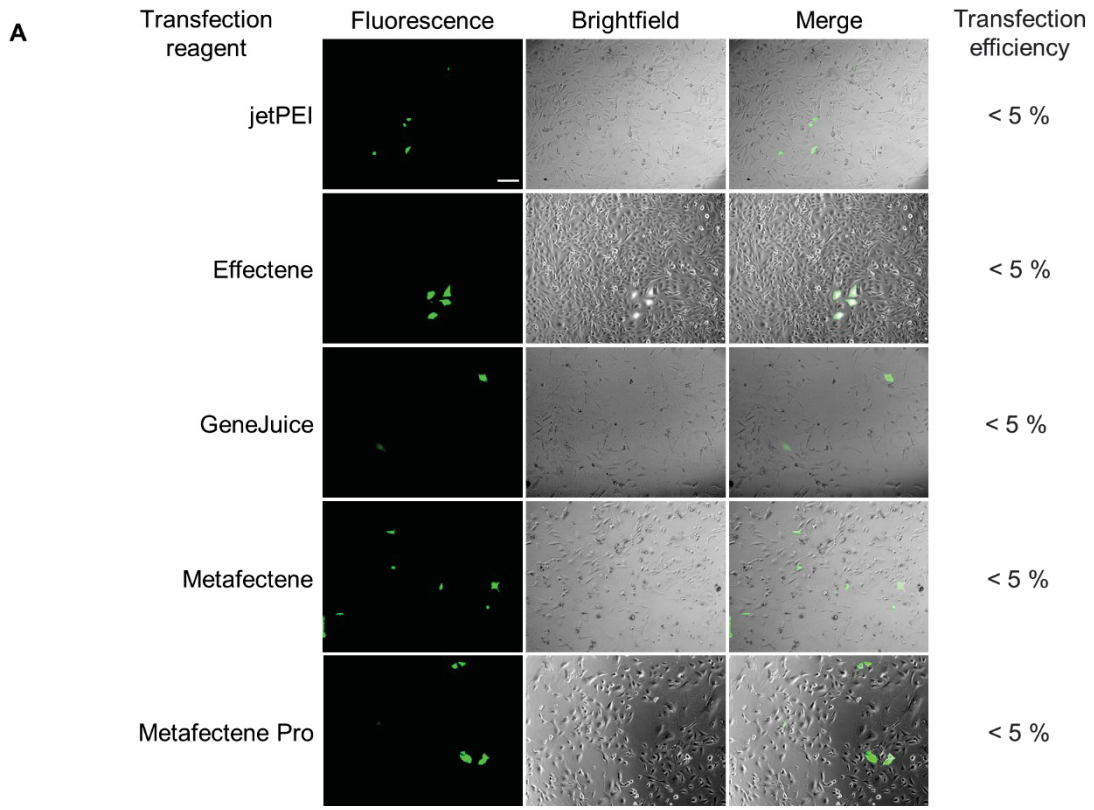

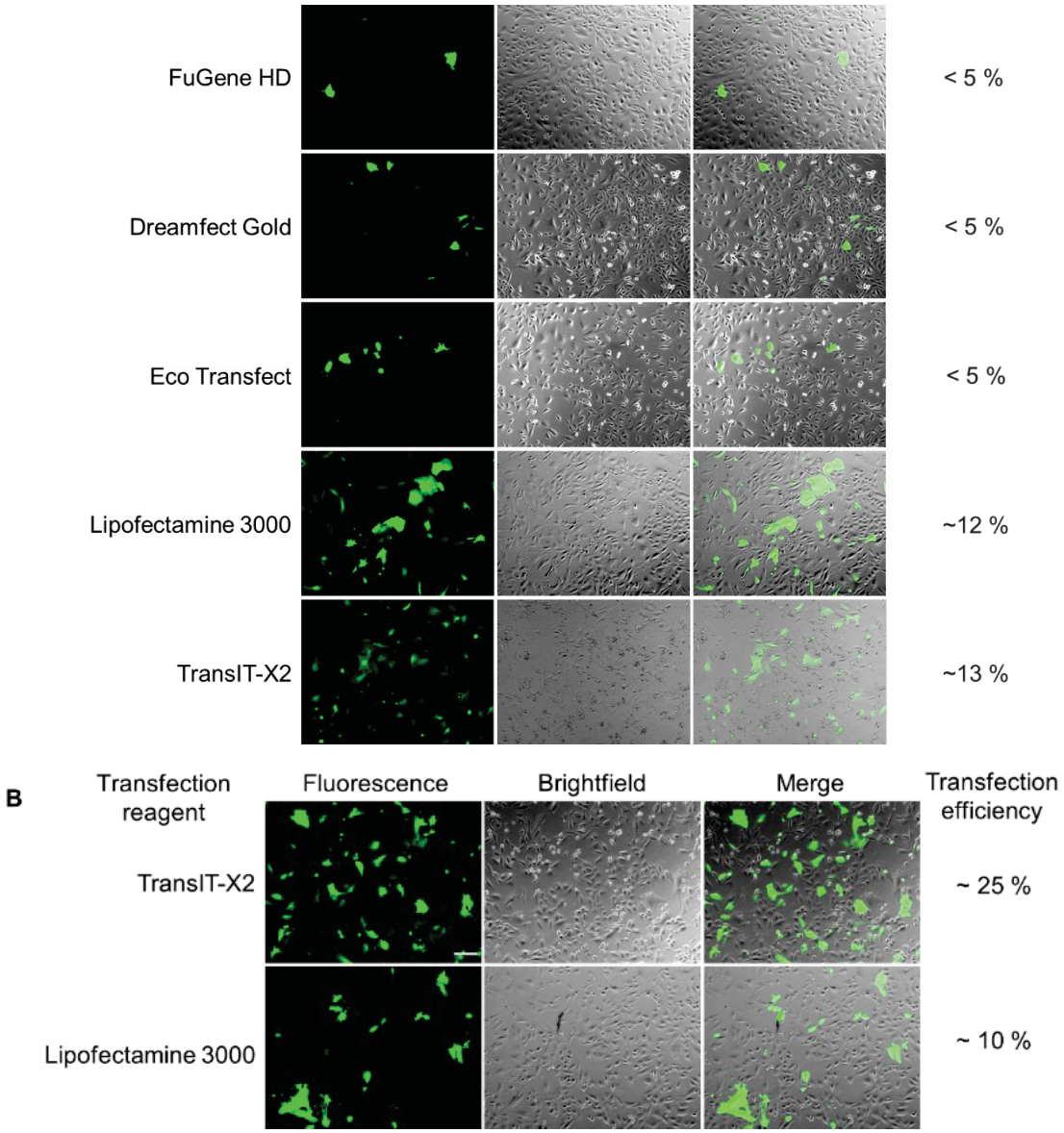

Figure 3.1: Transfection efficiency in mouse embryonic fibroblasts.
A 40,000 cells were seeded per well (12 well plate). Transfection of MEF was performed with various transfection reagents according to the respective manufacturer's instructions. Representative pictures were taken 48 h after transfection with human *GFP-RAC1(WT)* expression vector. Successful transfected cells are shown in green. Ratio of DNA to transfection reagent was 1:2 (jetPEI), 1:50 (Effectene), 1:3 (GeneJuice), 1:4 (Metafectene), 1:4 (Metafectene Pro), 1:3 (FuGeneHD), 1:3 (Dreamfect Gold), 1:3 (Eco Transfect), 1:1.5 (Lipofectamine 3000), and 1:3 (TransIT-X2). Scale bar: 150 µm. **B** 25,000 cells were seeded per well (12-well plate). Transfection of MEF was performed with TransIT-X2 or Lipofectamine 3000 according to the manufacturer's instructions. Representative pictures were taken 48 h after transfection with human *GFP-RAC1(WT)* expression vector. Successful transfected cells reveal a green fluorescence. The ratio of DNA to transfection reagent was 1:3 (TransIT-X2) and 1:1.5 (Lipofectamine 3000). Scale bar: 150 µm.

3.1.2 Dose kinetics of doxorubicin treatment to define a moderate DDR-inducing dose

For investigation of the influence of RAC1 on the doxorubicin-induced DDR suitable doses of Dox have to be used, that induce a strong and well detectable DDR while still allowing to detect a modulation (i.e., potentiation or inhibition) of the DDR. As a consequence of DNA damage various cellular stress responses are activated. DNA repair, cell cycle progression and apoptosis are affected and are collectively quoted as DDR (Harper et al. 2007). A commonly used surrogate marker for detection of DNA double-strand breaks (DNA DSB) is the on serine 139 phosphorylated histone 2A (γH2AX), because it occurs only at sites surrounding the DSB (Olive 2004; Kinner et al. 2008). A Dox dose was needed to be identified which induces a well countable number of distinct γH2AX foci in cell nuclei. For that purpose MEF were treated with 0.1 µM, 0.3 µM, 1 µM, or 3 µM Dox for 1 h because the dominant DSB-inducing effect through irreversible inhibition of Top II were shown to occur at concentrations from 0.5 µM to 5 µM (Gewirtz 1999). Another reason for the used concentrations is the fact that Dox loses its inhibitory effect on topoisomerase II at concentrations above 3 µM Dox (Bodley et al. 1989; Gewirtz 1999; Huelsenbeck et al. 2012).

The number of foci (DNA DSB) was dose-dependent increasing (Figure 3.2). Cells treated with 1 µM Dox had significantly more nuclear γH2AX foci compared to the non-treated cells. The foci were well countable and allowed the detection of an increased or decreased number. 3 µM Dox represented a dose where the cells reached γH2AX foci numbers that were difficult to count as distinct foci in some cases and so this concentration was not considered for further experiments.

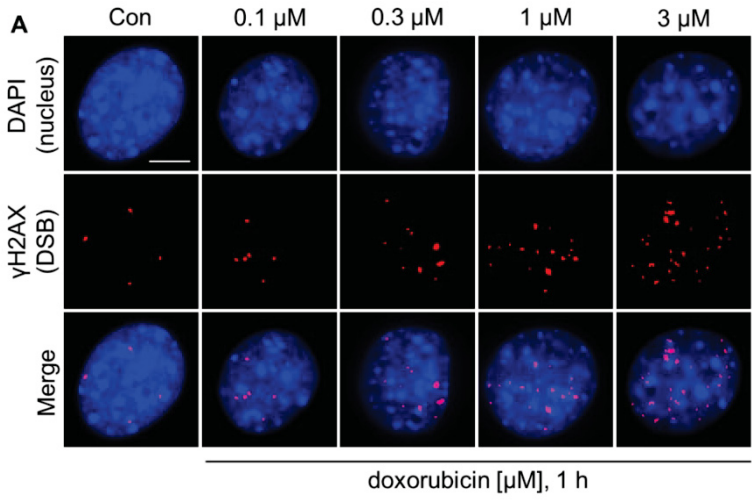

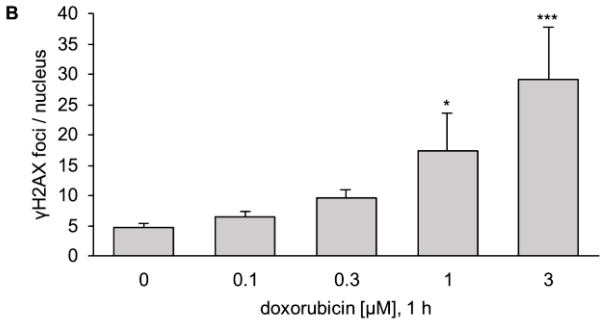

Figure 3.2: Fluorescence-based quantification of doxorubicin-induced DNA double-strand breaks (γH2AX foci).
MEF were treated with 0 µM, 0.1 µM, 0.3 µM, 1 µM, or 3 µM Dox for 1 h. **A** Pictures were taken after the end of the Dox treatment. Representative microscopical fluorescence pictures are shown; blue: DAPI-stained nuclei, red: γH2AX (Ser139) foci (DSB). Scale bar: 10 µm. **B** Quantification of the counted foci. DNA DSB (γH2AX foci) in nuclei were quantified (mean+SD; n=3 with 50 nuclei counted per experiment in each treatment group, *p ≤ 0.05, ***p ≤ 0.001 vs. untreated cells (0 µM Dox); one-way ANOVA with Dunnett post-hoc test). The data underlying the graph are shown in Table 7.1 of the appendix.

To determine a dose of Dox which allows a further modulation of the DDR representative DDR-related proteins were analyzed by western blot analysis. The Dox treatment was prolonged to two hours in case of western blot analysis since 1 h pulse-treatment did not induce a sufficiently strong phosphorylation of the selected DDR proteins. One major mediator of the DSB-induced DDR is the serine/threonine kinase ATM. Substrates for this protein are amongst other the proteins P53 and KAP1 (Banin et al. 1998; White et al. 2012). Therefore, these proteins were selected as representative proteins for the analysis of the doxorubicin-induced DDR.

The signal of phosphorylated KAP1, H2AX, and P53 was dose- and time-dependent intensified by doxorubicin treatment (Figure 3.3). pKAP1 was well detectable early after doxorubicin treatment (0 h - 4 h) but disappeared nearly completely after 24 h post-incubation period independent of the dose used while pP53 and γH2AX were still detectable under identical experimental conditions. Western blot analysis displayed 1 µM Dox as an appropriate dose which led to a strong DDR that still allows to detect a modulation (i.e., potentiation or inhibition) and was therefore used for all following western blot experiments.

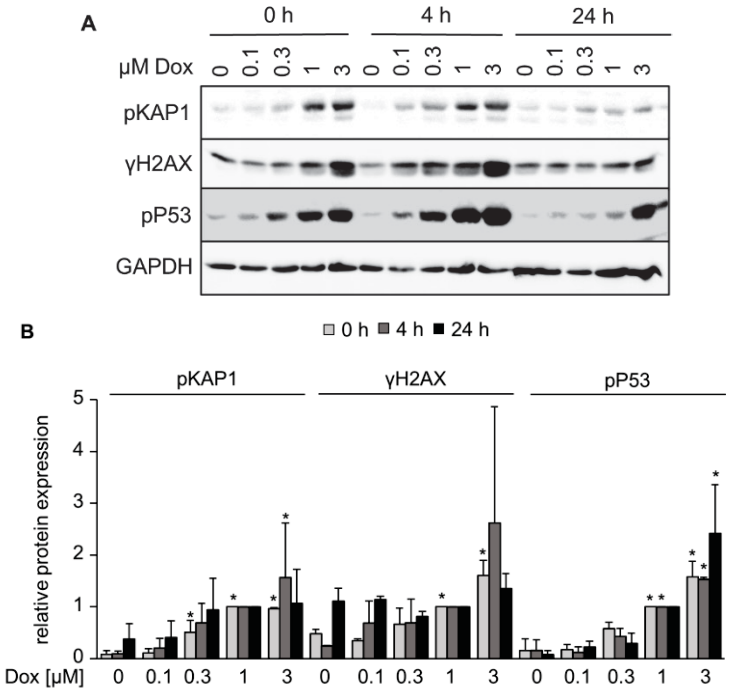

Figure 3.3: Western blot analysis of representative DDR-related proteins after doxorubicin treatment.
MEF were 2 h pulse-treated with 0 µM, 0.1 µM, 0.3 µM, 1 µM, or 3 µM Dox. **A** Cells were harvested after the indicated time points. Afterwards, cells were lysed, and protein extracts were analyzed by western blot analysis as described in methods. GAPDH was used as reference protein. **B** The change in protein expression after Dox treatment was quantified. The protein level of cells treated with 1 µM Dox was normalized to GAPDH and set to 1 (mean+SD; n=3; *p ≤ 0.05 compared to control (0 µM Dox); one-way ANOVA with Dunnett post-hoc test). The data underlying the graph are shown in Table 7.2 of the appendix.

3.1.3 Establishment of a EHT 1864 (RAC1 inhibitor) dose that modulates the doxorubicin induced DNA damage response in mouse embryonic fibroblasts

Previous work already revealed a protection of non-transformed cells against topoisomerase II poisons by inhibiting RAC1 via the lipid lowering drug lovastatin (Damrot et al. 2006; Huelsenbeck et al. 2011) or by direct inhibition of RAC1 with the RAC1 inhibitors EHT 1864 or NSC23766 (Huelsenbeck et al. 2012; Wartlick et al. 2013). This cytoprotection against topoisomerase II poisons was based on less DNA damage and less cell death. In the aforementioned studies MEF were not included. Therefore, a dose of EHT 1864 had to be established for this cell line which weakens the doxorubicin-induced DDR.

As stated above, 1 µM Dox was established as a suitable concentration for induction of the DDR. In this work EHT 1864 will be used as RAC1 inhibitor and therefore as putative

modulator of the DDR. In previous experiments cells were treated with 10 µM EHT 1864 for 1 h prior to treatment with Dox (Wartlick et al. 2013). The used concentration [10 µM] and duration [1 h] were not suitable for MEF cells (Figure 3.4), since the pre-treatment with EHT 1864 did not diminish the Dox-induced signal of pP53 and γH2AX.

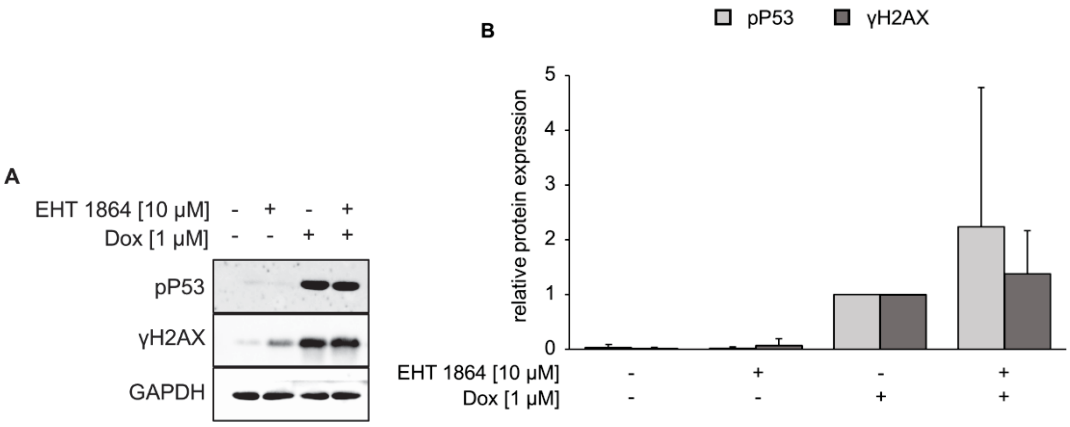

Figure 3.4: Western blot analysis of doxorubicin-induced P53 and H2AX phosphorylation after pre-treatment with EHT 1864.
MEF were pre-treated for 1 h with 10 µM EHT 1864 and afterwards treated with 1 µM Dox for 2 h. **A** Cells were harvested after the end of the Dox treatment. Afterwards cells were lysed, and protein extracts were analyzed by western blot analysis as described in methods. GAPDH was used as reference protein. **B** Changes in signal of phosphorylated proteins was quantified. The protein expression of cells treated with 1 µM Dox was set to 1 (mean+SD; n=3). The data underlying the graph are shown in Table 7.3 of the appendix.

Therefore, the time of EHT 1864 treatment was prolonged and different EHT 1864 concentrations were tested. MEF were pre-treated with 10 µM, 30 µM, or 100 µM of the RAC1 inhibitor for 3 h prior to the treatment with Dox. The evaluation of the different doses was performed by γH2AX foci analyses (Figure 3.5 A, B) and the detection of representative DDR-related proteins by western blot analysis (Figure 3.5 C, D).

All three doses of the RAC1 inhibitor showed similar inhibitory effects on the Dox-stimulated γH2AX foci formation, which was independent of the EHT 1864 concentration (Figure 3.5 A, B).

As detected by western blot analysis, the untreated control cells as well as EHT 1864 treated cells showed no signal of pCHK1, pP53, γH2AX, and pKAP1 (Figure 3.5 C, D). The biggest amount of phosphorylated proteins was detected in the cells treated with Dox alone (mono-treatment). Pre-treatment with the RAC1 inhibitor resulted in a reduced protein level of the evaluated representative DDR proteins. 10 µM and 30 µM EHT 1864 caused a significantly reduced level of phosphorylated CHK1 an P53 as compared to Dox mono-treatment. 100 µM EHT 1864 showed a significant reduction in the signal of all analyzed phosphorylated proteins compared to Dox treatment alone.

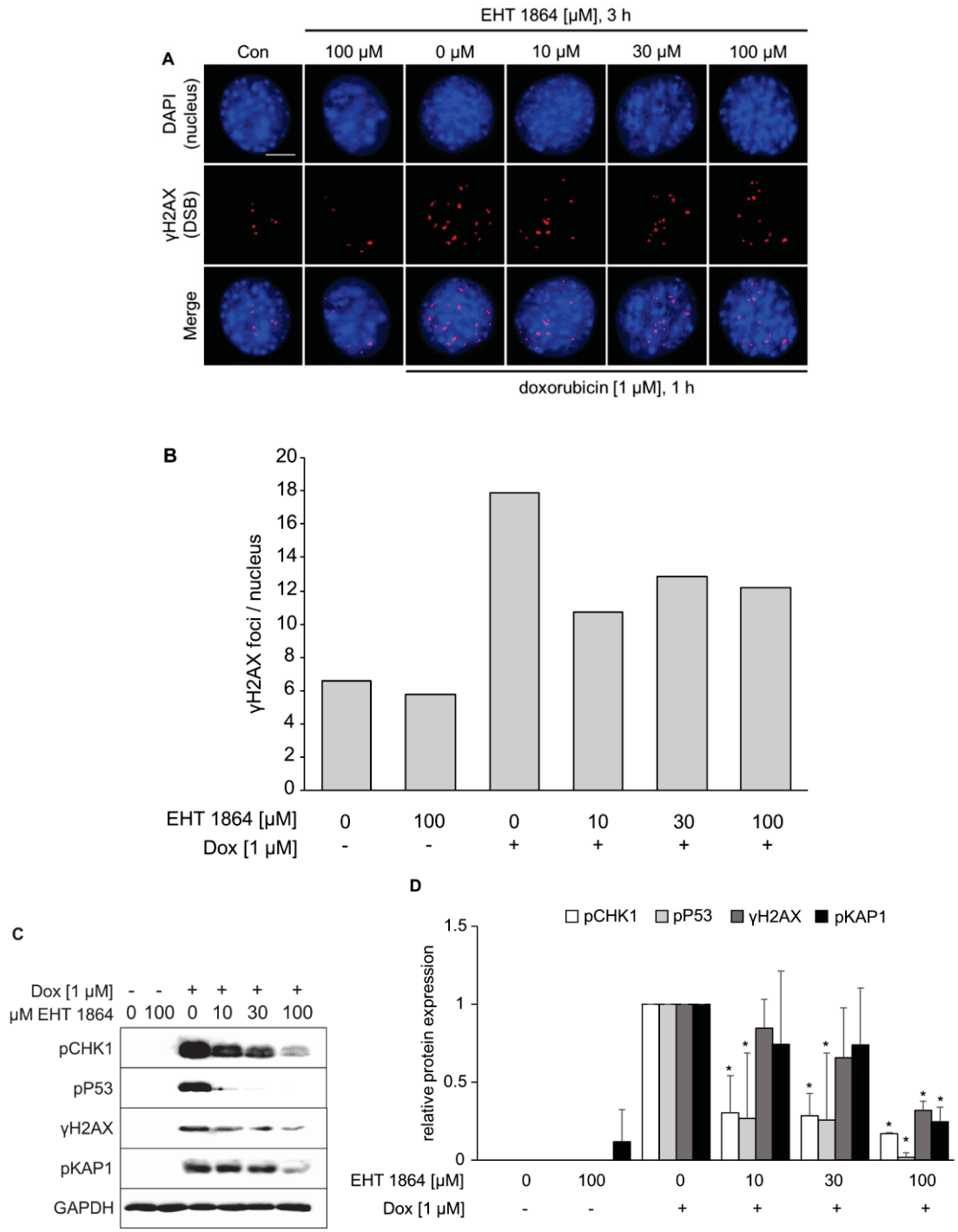

Figure 3.5: Fluorescence-based quantification of doxorubicin-induced DNA double-strand breaks (γH2AX foci) as well as western blot analysis of doxorubicin-induced representative DDR-related proteins after pre-treatment with EHT 1864.
MEF were pre-treated for 3 h with different doses of EHT 1864 [10 µM, 30 µM, or 100 µM] and afterwards treated for 1 h (γH2AX foci) or 2 h (western blot) with 1 µM Dox. **A** Pictures were taken after the end of the Dox treatment. Representative microscopical fluorescence pictures are shown; blue: DAPI-stained nuclei, red: γH2AX (Ser139) foci. Scale bar: 10 µm. **B** Quantification of the counted foci numbers. DNA DSB (γH2AX foci) in nuclei were quantified (mean; n=1 with 50 nuclei counted). The data underlying the graph are shown in Table 7.4 of the appendix. **C** Cells were harvested after the Dox treatment period. Afterwards, cells were lysed, and protein extracts were analyzed by western blot analysis as described in methods. GAPDH was used as reference protein. **D** Change in protein expression was quantified as described in methods. The protein

expression of cells treated with 1 µM Dox was set to 1 (mean+SD; n=3; *p ≤ 0.05 compared to Dox monotreatment; one-way ANOVA with Dunnett post-hoc test). The data underlying the graph are shown in Table 7.5 of the appendix.

Since pre-treatment with 100 µM EHT 1864 would make a further reduction (e.g., by combining two modulators of the DDR) of the selected proteins difficult. For this reason, 30 µM EHT 1864 were chosen for the following western blot experiments. Immunocytochemical staining for γH2AX was repeated with 30 µM EHT 1864 (Figure 3.6). The decrease in foci number of pre-treated cells was significant compared to the cells treated with Dox alone. Consequently, 30 µM EHT 1864 was also chosen for further fluorescence microscopy experiments.

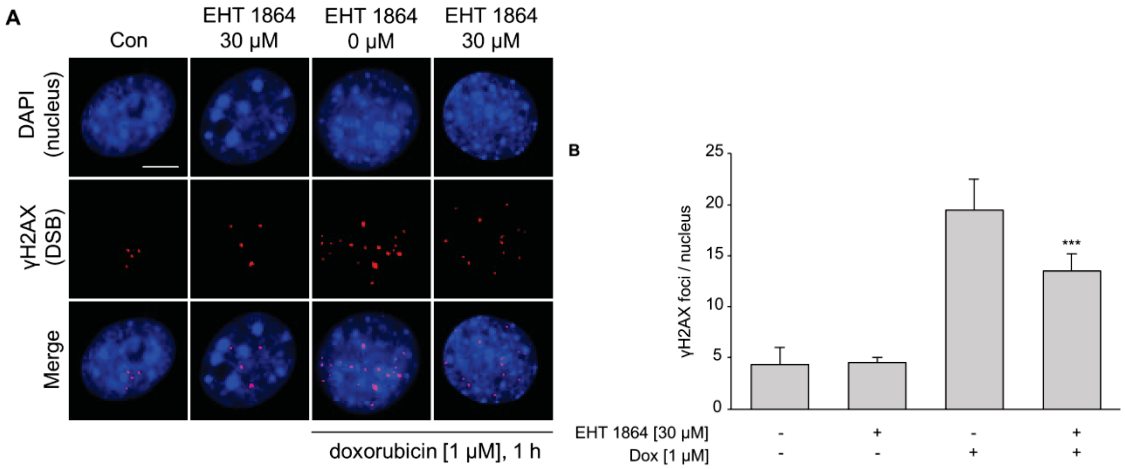

Figure 3.6: Fluorescence-based quantification of doxorubicin-induced DNA double-strand breaks (γH2AX foci) after pre-treatment with EHT 1864.
MEF were pre-treated for 3 h with a single dose of EHT 1864 [30 µM] and afterwards treated with 1 µM Dox for 1 h. **A** Pictures were taken after the end of the Dox treatment. Representative microscopical fluorescence pictures are shown; blue: DAPI-stained nuclei, red: γH2AX (Ser139) foci. Scale bar: 10 µm. **B** Quantification of the counted foci. DNA DSB (γH2AX foci) in nuclei were quantified (mean+SD; n=6 with 50 nuclei counted per experiment, ***p ≤ 0.001 compared to Dox monotreatment; one-way ANOVA with Dunnett post-hoc test). The data underlying the graph are shown in Table 7.6 of the appendix.

3.2 Influence of a forced RAC1 translocation into the nucleus on the doxorubicin-induced DNA damage response

Previous experiments which demonstrated a protection against topoisomerase II poison-induced DNA damage and cell death by pharmacological inhibition of RAC1 (Damrot et al. 2006; Huelsenbeck et al. 2011; Wartlick et al. 2013) are underlying this work. Rho proteins, like RAC1, were recently found inside the nucleus (Sandrock et al. 2010). Until today, it is unclear whether the described protection against topoisomerase II poison-induced DNA damage is dependent on cytosolic RAC1 and/or nuclear RAC1. Nuclear functions of RAC1 are still poorly characterized. In this work various human RAC1 mutants were transiently expressed in MEF prior to Dox or IR treatment. To distinguish between effects promoted by nuclear RAC1 and cytosolic RAC1, the *GFP-hRAC1* mutants were used with and without an additional nuclear localization sequence (NLS). The hypothesis is that expression of wild-type hRAC1 (GFP-hRAC1(WT)) or constitutively active hRAC1 (GFP-hRAC1(Q61L)) does not influence the doxorubicin-induced DDR or even enhances the DDR, while dominant-negative hRAC1 (GFP-hRAC1(T17N)) should dampen the DDR similar to a pharmacological inhibition of RAC1.

3.2.1 Generation of GFP-hRAC1 constructs with an additional nuclear localization sequence

As stated in the introduction, RAC1 possesses a weak C-terminal NLS. The intrinsic murine RAC1 as well as the expressed human RAC1 variants are thought to be mainly localized in the cell's cytoplasm. To force more nuclear localization of hRAC1 an additional, stronger NLS (from SV40 Large T-antigen) was added N-terminal. DNA-sequencing confirmed the presence of the additional NLS in the human *RAC1* expression vectors. The cloning of *GFP-NLS-hRAC1* mutants was performed as described in methods under 2.2.2.1.

3.2.2 Analysis of the subcellular distribution of mRAC1 and GFP-hRAC1 in mouse embryonic fibroblasts transiently transfected with various human *GFP-RAC1* mutants (with and without additional NLS)

To confirm the functionality of the NLS introduced into the *hRAC1* expression vectors and to analyze if there is a difference in localization of GFP-hRAC1 and GFP-NLS-hRAC1 as compared to the endogenous mRAC1, MEF were transiently transfected with *GFP-hRAC1(WT), GFP-NLS-hRAC1(WT)*, *GFP-hRAC1(Q61L)*, *GFP-NLS-hRAC1(Q61L)*, *GFP-hRAC1(T17N),* or *GFP-NLS-hRAC1(T17N)* expression vector. Constructs with additional NLS are thought to be located in the nucleus to a bigger extent than the variants without the additional NLS.

The quantification was performed by measuring the fluorescence intensity of GFP-coupled hRAC1 (with and without additional NLS) in the cytoplasm and the nucleus of successfully transfected cells. The total fluorescence of each cell was set to 100 %. Individual cells that were not successfully transfected following the transfection, and hence were GFP negative, could be included as an additional “intrinsic” control (transfection control; TR Con) in the same experimental setup. In cells without GFP-tagged hRAC1 a fluorescence-coupled secondary antibody which binds to the used primary RAC1 antibody was used to detect the intrinsic mRAC1.

In advance control experiments were performed to answer two questions regarding the subcellular distribution of endogenous mRAC1 as well as of the human GFP-RAC1 variants. (i) Does the transfection method affect the subcellular distribution of the intrinsic mRAC1? (ii) Does the GFP-tag has an impact on the transgenic human RAC1 subcellular distribution? The transfection method itself had no impact on intracellular mRAC1 distribution. Regarding the second question, even though GFP was significantly augmented in the nucleus compared to intrinsic mRAC1 it had no influence on distribution of the transgenic human RAC1 since not all *GFP-hRAC1* mutants were significantly enriched in the nucleus (Figure 3.7, Appendix Figure 7.11).

80 % of the intrinsic mRAC1 was located in the cytoplasm in control cells (Figure 3.7). Transgenic GFP-hRAC1(Q61L) as well as transgenic GFP-hRAC1(T17N) expressing cells showed a similar distribution compared to the distribution of intrinsic mRAC1. In cells expressing GFP-hRAC1(WT) about 70 % of GFP-hRAC1 was located in the cytoplasm. These experiments revealed a similar subcellular distribution of the transgenic human GFP-fused RAC1 and the intrinsic mRAC1 (Figure 3.7). More than 80 % of the GFP-NLS-hRAC1(WT) was localized in the nucleus (Figure 3.7). Cells transfected with *GFP-NLS-hRAC1(Q61L)* expression vector and *GFP-NLS-hRAC1(T17N)* expression vector had about 35 % GFP-NLS-hRAC1 in the nucleus. Summarizing the results, a comparison of hRAC1 localization between *GFP-hRAC1* mutants with and without additional NLS demonstrated a significant increase in nuclear hRAC1 (Figure 3.7) in cells transfected with the NLS constructs. The *hRAC1* constructs with the additional NLS showed a 2 - 4 times stronger nuclear accumulation than their counterpart without additional NLS. This experiment verified that the NLS worked as expected.

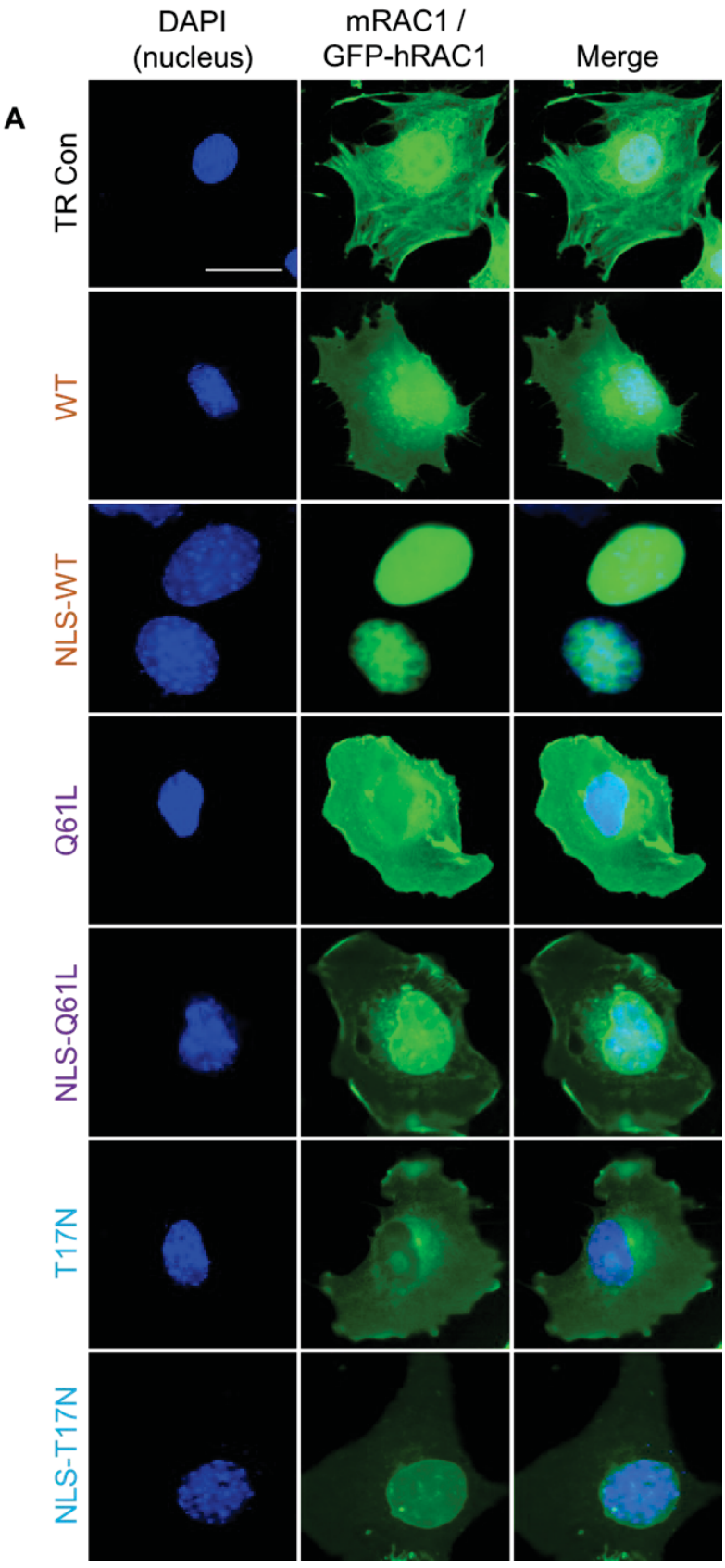
A
DAPI (nucleus)
mRAC1 / GFP-hRAC1
Merge
TR Con
WT
NLS-WT
Q61L
NLS-Q61L
T17N
NLS-T17N

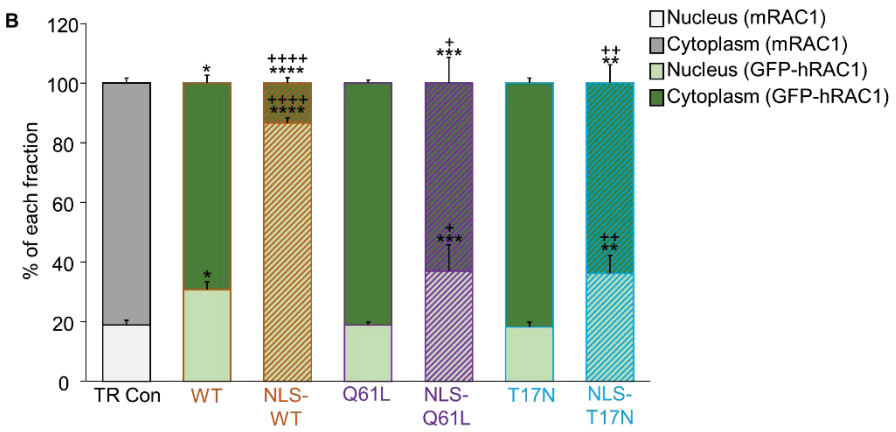

Figure 3.7: Fluorescence-based quantification of intrinsic mRAC1 as well as GFP-hRAC1 distribution in cells expressing human GFP-RAC1 with and without additional NLS.
MEF were transiently transfected with *GFP-hRAC1(WT)*, *GFP-NLS-hRAC1(WT)*, *GFP-hRAC1(Q61L)*, *GFP-NLS-hRAC1(Q61L)*, *GFP-hRAC1(T17N), or GFP-NLS-hRAC1(T17N)* expression vector. Transfection control cells (TR Con) were treated with TransIT-X2. **A** Pictures were taken 24 h after transfection. Representative microscopical pictures are shown; blue: DAPI-stained nuclei, green: GFP signal (GFP-tagged hRAC1 or fluorescence-coupled antibody against primary antibody directed against intrinsic mRAC1). Scale bar: 25 µm**. B** Quantification of the fluorescence. Fluorescence intensity for cytoplasm and nucleus were quantified by measuring the fluorescence intensity of GFP-coupled hRAC1. The total fluorescence of each cell was set to 100 % (mean+SD; n=3 with 50 cells counted per experiment; *p ≤ 0.05; **p ≤ 0.01, ***p ≤ 0.001, ****p ≤ 0.0001 compared to control (TR Con); one-way ANOVA with Dunnett post-hoc test; $^{+}$p ≤ 0.05; $^{++}$p ≤ 0.01, $^{++++}$p ≤ 0.0001 compared to GFP-hRAC1 without NLS; T-Test, unpaired, two-sided): The data underlying the graph are shown in Table 7.7 of the appendix. Abbreviations: TR Con: control cells treated with transfection reagent (TransIT-X2), WT: wild-type RAC1, NLS-WT: wild-type RAC1 with additional NLS, Q61L: constitutively active RAC1, NLS-Q61L: constitutively active RAC1 with additional NLS, T17N: dominant-negative RAC1, NLS-T17N: dominant-negative RAC1 with additional NLS.

3.2.3 Expression of human GFP-RAC1 mutants with and without additional NLS alters lamellipodia and stress fibers formation

It is well-known that RAC1 is involved in the regulation of the actin cytoskeleton. Adjustment of the polymerization of actin for the production of stress fibers (RHOA), as well as formation of lamellipodia (RAC1) and filopodia (CDC42) is under control of small Rho GTPases (Nobes et al. 1995). Actin polymerization induces the expansion of rod-like protrusions, named filopodia, as well as sheet-like protrusions, named lamellipodia. Restructuring of filamentous actin (F-actin) into lamellipodia or membrane ruffles is promoted by RAC1 (Karnoub et al. 2001). The RAC1 inhibitor EHT 1864 was shown to prevent RAC1-dependent lamellipodia formation (Shutes et al. 2007). Changes in the actin cytoskeleton was evaluated in cells transfected with *hRAC1* mutants to confirm that they are functional.

For visualization of changes in the actin cytoskeleton, more precisely the lamellipodia formation, stress fibers formation and membrane ruffles, TRITC-phalloidin was used.

Phalloidin is a phallotoxin used for cytochemical staining of the actin cytoskeleton and binds to F-actin. For quantification, a custom stress fiber score was used (Figure 3.8):

Score 1: no or single stress fibers; thin stress fibers

Score 2: several stress fibers; partly over the whole cell; thin stress fibers

Score 3: “normal condition”; several stress fibers; thicker than in score 2; mainly across the whole cell; free space detectable; sometimes even individual thick stress fibers

Score 4: stress fibers over the whole cell, thicker than in score 3, individual fibers are no longer properly noticeable; partially free space detectable

Score 5: stress fibers all over the cell, pretty thick, individual fibers are no longer noticeable; looks like “a big red mass”

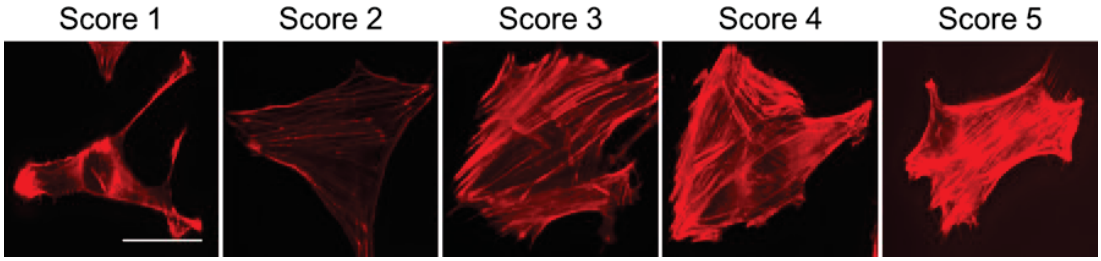

Figure 3.8: Examples for custom stress fibers score.
Cells were stained with Phalloidin-TRITC. Representative microscopical fluorescence pictures of the custom stress fibers score are shown; red: cytoskeleton stained with Phalloidin-TRITC. Scale bar: 25 µm.

For stress fibers score quantification 50 cells per experiment were rated and a mean score was calculated.

In advance the influence of the transfection reagent and GFP as well as NLS-GFP as part of the hRAC1 constructs on the actin cytoskeleton was analyzed. There was no change in lamellipodia formation, stress fibers formation or membrane ruffles upon transfection with *GFP* or *NLS-GFP* expression vector or the treatment with transfection reagent (Appendix, Figure 7.12).

In GFP-hRAC1(WT) and GFP-NLS-hRAC1(WT) expressing cells, there was no change in lamellipodia formation compared to the control cells (Figure 3.9 A, B). An induction of lamellipodia was seen in cells expressing constitutively active hRAC1 with and without additional NLS. Cells transfected with *GFP-hRAC1(Q61L)* expression vector had twice the number of lamellipodia compared to the transfection control cells (TR Con), whereas GFP-NLS-hRAC1(Q61L) expressing cells showed 1.5x the number of lamellipodia compared to the transfection control cells (TR Con) (Figure 3.9 A, B). GFP-

hRAC1(T17N) expression had no influence on lamellipodia formation (Figure 3.9 A, B), whereas dominant-negative hRAC1 with additional NLS led to a decrease in lamellipodia formation.

Furthermore, the impact of hRAC1 expression on stress fiber formation was investigated. Cells transfected with *GFP-hRAC1(WT)* or *GFP-NLS-hRAC1(WT)* expression vector showed no difference in stress fiber formation compared to the transfection control cells (TR Con) (Figure 3.9 A, C). *GFP-hRAC1(Q61L)* expression vector transfected cells revealed a decreased stress fiber score, whereas stress fibers formation remained unaffected by transfection of constitutively active *GFP-hRAC1* harbouring an additional NLS. GFP-hRAC1(T17N) expression led to an increased stress fibers score compared to the transfection control cells (TR Con). Transfection with *GFP-NLS-hRAC1(T17N)* expression vector had no influence on stress fiber formation, whereas the stress fiber formation was significantly decreased compared to GFP-hRAC1(T17N) expressing cells (Figure 3.9 A, C).

In regard of the number of cells with membrane ruffles the transient transfection with the different *hRAC1* mutants with and without additional NLS had no detectable effect. (Figure 3.9 A, D).

Taken together, alteration of the actin cytoskeleton is dependent on the activation status of RAC1. Cells transfected with *GFP-hRAC1(Q61L)* expression vector with and without additional NLS showed a similar number of lamellipodia compared to the transfection control cells (TR Con). Expression of GFP-hRAC1(T17N) but not of GFP-NLS-hRAC1(T17N) augmented the stress fibers formation in contrast to the control cells, whereas expression of GFP-hRAC1(Q61L) led to a decrease in stress fibers formation. hRAC1 constructs with additional NLS had no effect on stress fibers formation, leading to the conclusion that stress fibers formation is depending on the activation status of RAC1.

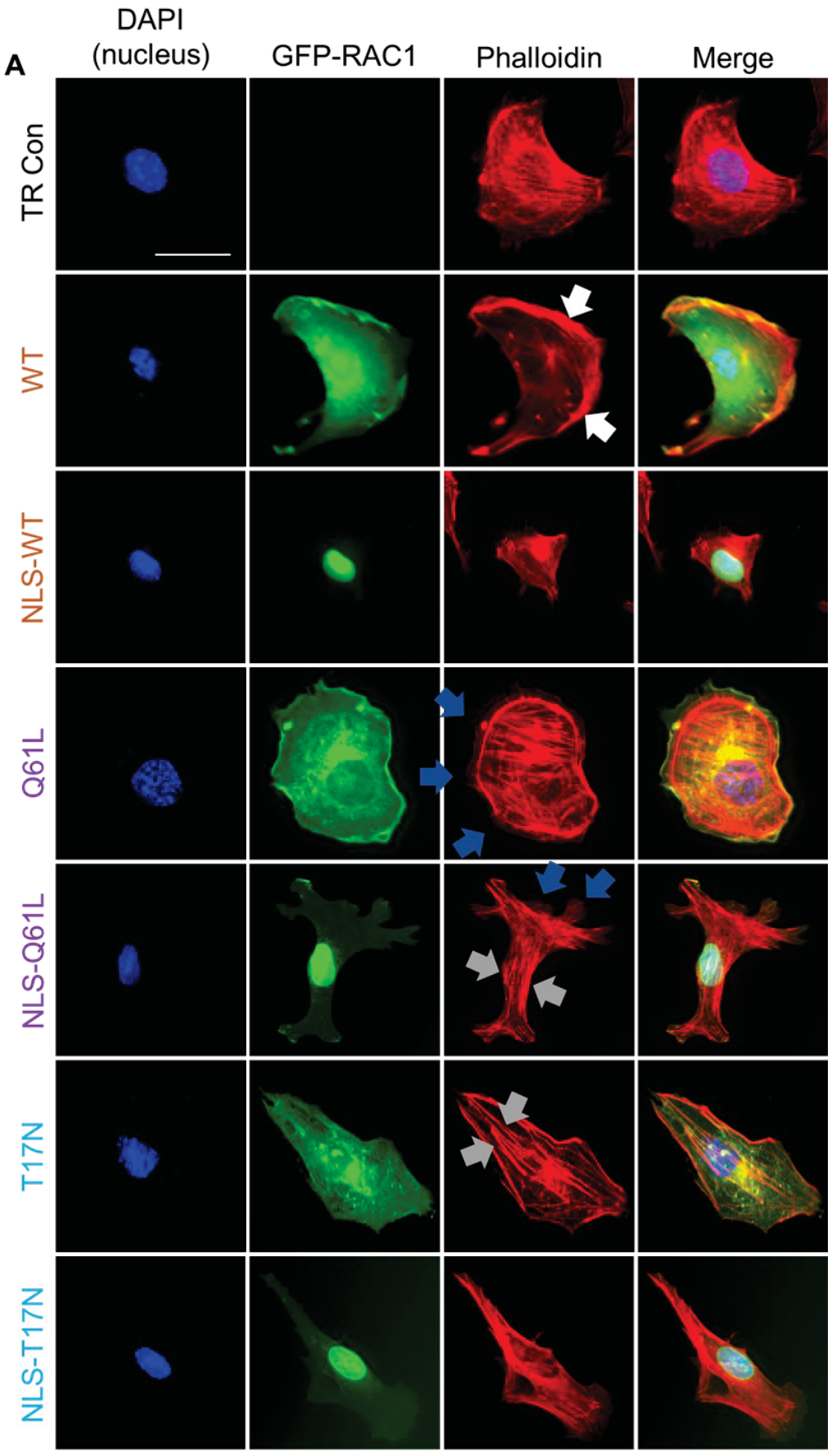
A
DAPI (nucleus)
GFP-RAC1
Phalloidin
Merge
TR Con
WT
NLS-WT
Q61L
NLS-Q61L
T17N
NLS-T17N

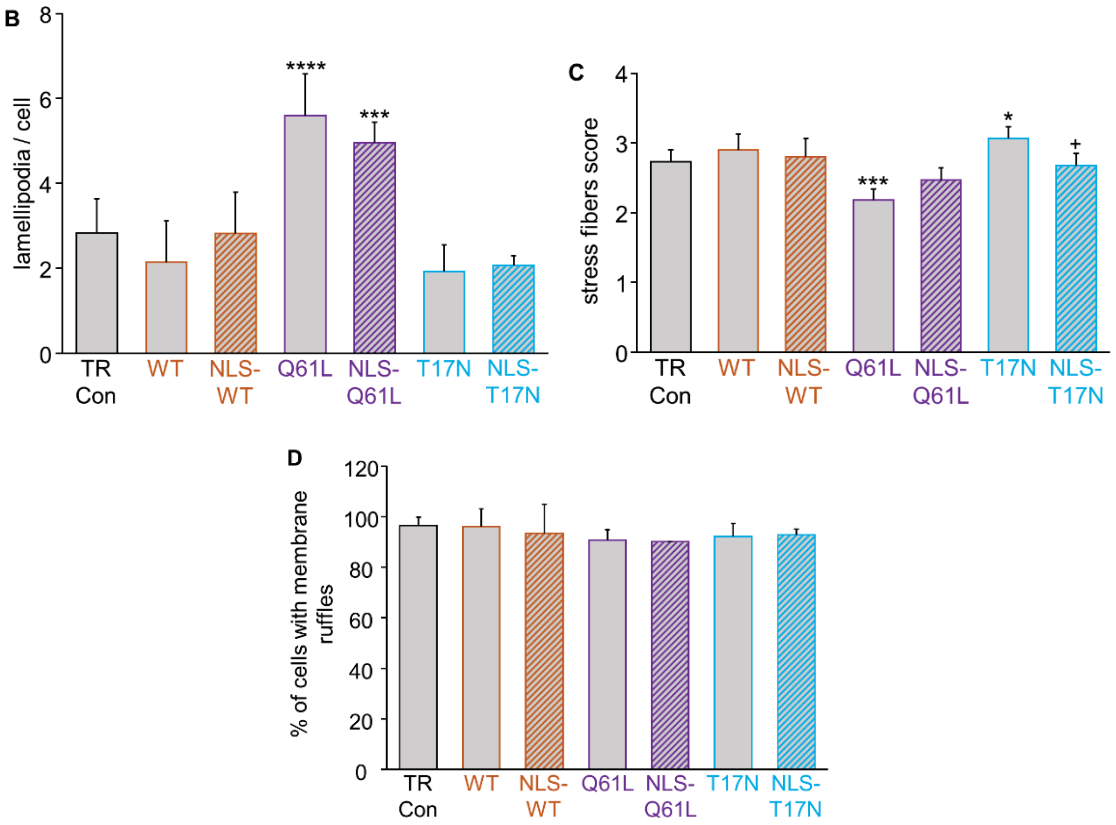

Figure 3.9: Influence of the different human *GFP-RAC1* mutants (with and without additional NLS) on the lamellipodia, stress fibers, and membrane ruffles formation.
MEF were transiently transfected with *GFP-hRAC1(WT)*, *GFP-NLS-hRAC1(WT)*, *GFP-hRAC1(Q61L)*, *GFP-NLS-hRAC1(Q61L)*, *GFP-hRAC1(T17N)*, or *GFP-NLS-hRAC1(T17N)* expression vector. Transfection control cells (TR Con) were treated with TransIT-X2. 24 h after transfection, cells were stained with phalloidin-TRITC. **A** Representative microscopical fluorescence pictures are shown; blue: DAPI-stained nuclei, green: GFP signal, red: cytoskeleton stained with phalloidin-TRITC, white arrow: membrane ruffles, blue arrow: lamellipodia, grey arrow: stress fibers. Scale bar: 25 µm. **B** Quantification of lamellipodia formation. Lamellipodia of each cell were counted (mean+SD; n=3 with 50 cells counted per experiment; ***p ≤ 0.001, ****p ≤ 0.0001 compared to control (TR Con); one-way ANOVA with Dunnett post-hoc test). The data underlying the graph are shown in Table 7.8 of the appendix. **C** Quantification of stress fibers score. Stress fibers score of each cell was rated (mean+SD; n=3 with 50 cells counted per experiment; *p ≤ 0.05, ***p ≤ 0.001 compared to control (TR Con); one-way ANOVA with Dunnett post-hoc test; $^{+}$p ≤ 0.05 compared to GFP-hRAC1 without NLS, (T-test, unpaired, two-sided). The data underlying the graph are shown in Table 7.9 of the appendix. **D** Quantification of cells with membrane ruffles. Counted cells were grouped in cells showing no membrane ruffles or having at least one membrane ruffle (mean+SD; n=3 with 50 cells counted per experiment). The data underlying the graph are shown in Table 7.10 of the appendix. Abbreviations: TR Con: control cells treated with transfection reagent (TransIT-X2), WT: wild-type RAC1, NLS-WT: wild-type RAC1 with additional NLS, Q61L: constitutively active RAC1, NLS-Q61L: constitutively active RAC1 with additional NLS, T17N: dominant-negative RAC1, NLS-T17N: dominant-negative RAC1 with additional NLS.

3.2.4 Influence of a dominant-negative hRAC1 expression on the doxorubicin-induced DNA damage response

Dominant-negative hRAC1 with and without additional NLS was used to scrutinize the results of already published data as well as the data presented in 3.1.3 in this thesis regarding the effect of pharmacological RAC1 inhibition. Pharmacological RAC1 inhibition by EHT 1864 as well as *mRac1* silencing were combined with transfection of *GFP-hRAC1(T17N)* expression vector with and without additional NLS to answer the following questions. (i) Do *GFP-hRAC1(T17N)* and *GFP-NLS-hRAC1(T17N)* expression vector transfected, *mRac1* siRNA transfected and EHT 1864 treated cells show similar results? (ii) Is it possible to further enhance the effect of dominant-negative hRAC1, EHT 1864, or *mRac1* siRNA by combining the treatments?

3.2.4.1 Influence of expression of human dominant-negative GFP-RAC1 with and without additional NLS on doxorubicin-induced γH2AX and 53BP1 foci formation and the DNA damage response

Beforehand control experiments (see appendix) were performed to exclude effects of the used transfection method and plasmids on basal foci formation. Neither the transfection method nor the expression vectors had an impact on the basal foci formation (Appendix, Figure 7.13).

Cells expressing predominantly cytoplasmic dominant-negative hRAC1 showed only half the number of γH2AX and 53BP1 foci as well as colocalized foci compared to the Dox control (TR) cells (Figure 3.10). Forcing the translocation of dominant-negative hRAC1 into the nucleus did not reduce the number of foci any further than GFP-hRAC1(T17N) did. The results of the dominant-negative mutants are similar to the results obtained upon pharmacological RAC1 inhibition in previous work as well as in part 3.1.3 of this thesis. Overall, there was no significant difference in the decline of γH2AX and 53BP1 foci following Dox treatment in cells expressing mainly cytoplasmic dominant-negative hRAC1 or forced nuclear accumulation of dominant-negative hRAC1.

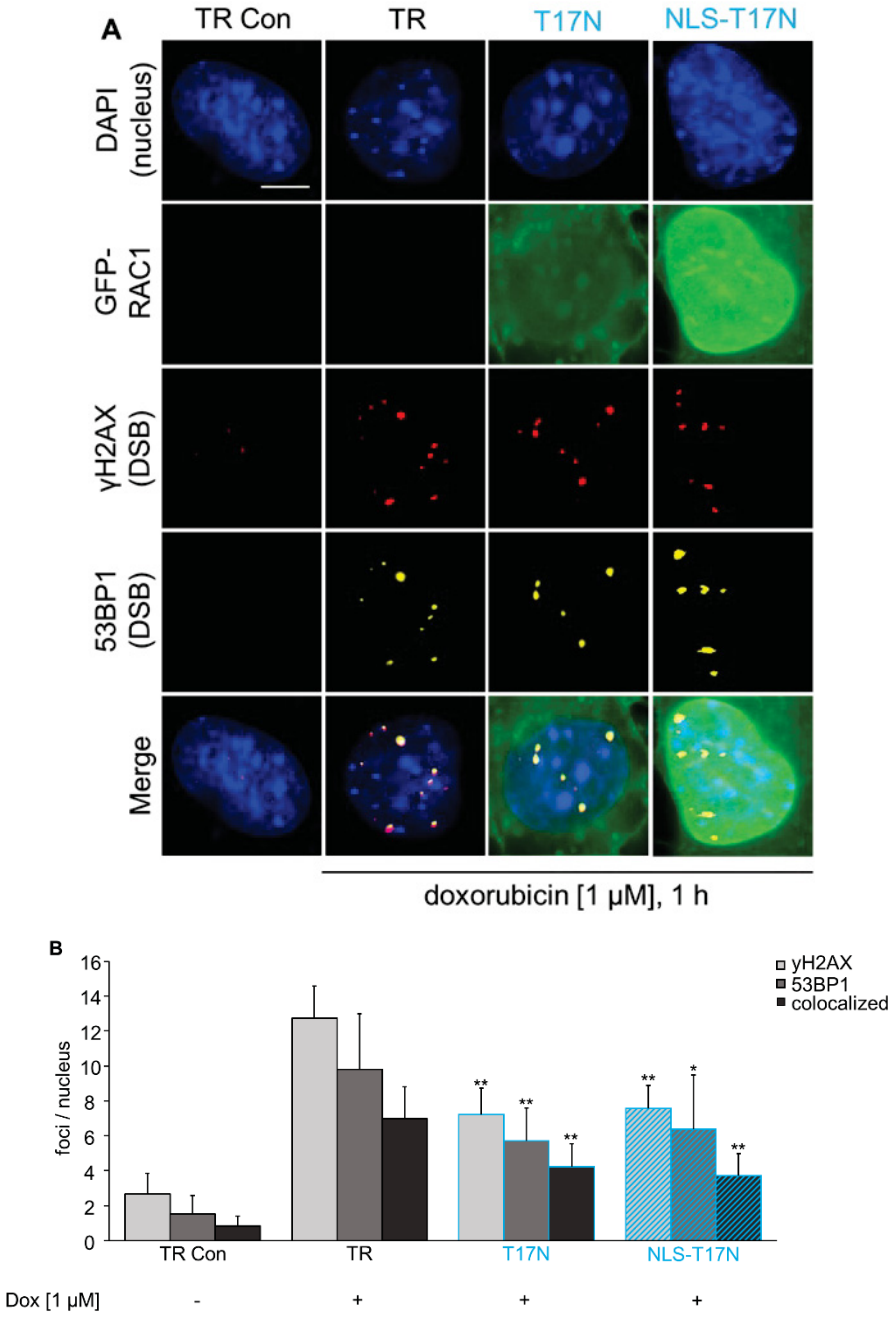

Figure 3.10: Influence of mainly cytosolic and targeted nuclear expression of dominant-negative hRAC1 on doxorubicin-induced γH2AX and 53BP1 foci formation.
MEF were transiently transfected with *GFP-hRAC1(T17N)* or *GFP-NLS-hRAC1(T17N)* expression vector. Transfection control cells (TR Con, TR) were treated with TransIT-X2. 24 h after transfection cells were treated with Dox [1 µM] for 1 h. **A** After the end of the Dox treatment, the staining of γH2AX and 53BP1 foci was carried out as described in methods. Representative microscopical fluorescence pictures are shown; blue: DAPI-stained nuclei, green: GFP signal, red: γH2AX (Ser139), yellow: 53BP1. Scale bar: 10 µm. **B** Quantification of γH2AX and 53BP1 foci formation, as well as colocalization of these foci. Foci of each cell were counted (mean+SD; n=6 - 38 with 50 nuclei counted per experiment; *p ≤ 0.05, **p ≤ 0.01 compared to Dox treated cells (TR); one-way ANOVA with Dunnett post-hoc test). The data underlying the graph are shown in Table 7.11 of the appendix. Abbreviations: TR Con, TR: cells treated with TransIT-X2, T17N: dominant-negative RAC1, NLS-T17N: dominant-negative RAC1 with additional NLS.

For western blot analysis representative DDR-related proteins were chosen to investigate the Dox-induced DDR signalling in cells expressing dominant-negative hRAC1. MEF were transiently transfected with *GFP-hRAC1(T17N)* or *GFP-NLS-hRAC1(T17N)* expression vector. 24 h after transfection cells were pulse-treated with 1 µM Dox (2 h) and harvested after the indicated time-points (Figure 3.11). An antibody against GFP was used to confirm the transfection of the cells. GAPDH was used as reference protein.

Non-transfected Dox-treated cells exhibited high pKAP1 levels which were only slightly decreasing over time. Cells expressing GFP-hRAC1(T17N) revealed a significantly decreased pKAP1 signal 24 h post-treatment (Figure 3.11 A, C), whereas the signal of Dox-induced pKAP1 was completely missing 24 h post-treatment in *GFP-NLS-hRAC1(T17N)* expression vector transfected cells (Figure 3.11 B, C). In mainly cytoplasmic dominant negative hRAC1 expressing cells Dox-induced phosphorylation of H2AX was reduced compared to non-transfected cells. Expression of GFP-NLS-hRAC1(T17N) had no effect on γH2AX expression (Figure 3.11 A, B, D). PP53 expression was decreasing 24 h post-treatment in non-transfected Dox-treated cells, whereas *GFP-hRAC1(T17N)* expression vector transfected cells displayed a significantly reduced Dox-induced pP53 expression directly after treatment as well as 24 h after treatment (Figure 3.11 A, E), whereas cells expressing GFP-NLS-hRAC1(T17N) exhibited a reduction of pP53 protein levels only 24 h post-treatment (Figure 3.11 B, E). Control experiments with sole GFP expression are shown in the appendix and showed no significant change in protein expression (Appendix, Figure 7.14).

Taken together, the dominant-negative *hRAC1* mutant (with or without NLS) showed a tendency to diminish the Dox-induced DDR represented by the depicted set of DDR-related phosphorylated proteins. The decrease in DDR signalling occurred at the same time points, independent of the used plasmids (i.e., with or without NLS) but with different intensities.

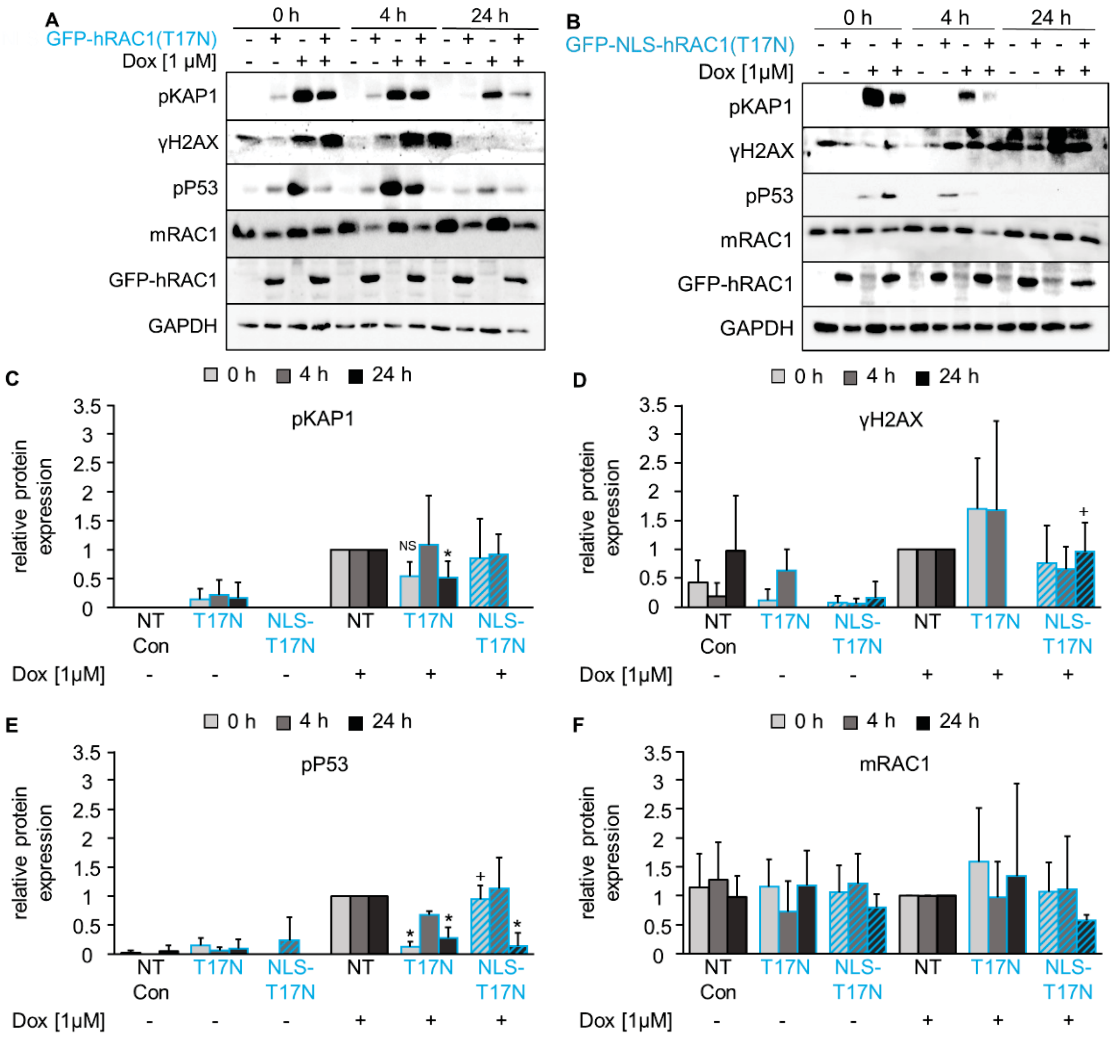

Figure 3.11: Western blot analysis after doxorubicin treatment in dominant-negative hRAC1-expressing cells with and without additional NLS.
MEF were transiently transfected with *GFP-hRAC1(T17N)* (**A**) or *GFP-NLS-hRAC1(T17N)* (**B**) expression vector. 24 h after transfection cells were 2 h pulse-treated with 1 µM Dox. Cells were harvested after indicated time-points. Afterwards cells were lysed, and protein extracts were analyzed by western blot analysis as described in methods. As reference protein GAPDH was used. **C-F** Change in protein expression in *GFP-hRAC1(T17N)* or *GFP-NLS-hRAC1(T17N)* expression vector transfected and non-transfected cells after Dox treatment was quantified as described in methods. The protein expression of non-transfected cells treated with Dox (NT) was set to 1 (mean+SD; n=3; *p ≤ 0.05 compared to non-transfected Dox-treated cells (NT); one-way ANOVA with Dunnett post-hoc test; $^{+}$p ≤ 0.05 compared to GFP-hRAC1(T17N) expression treated with Dox, T-test, unpaired, two-sided). The data underlying the graph are shown in Table 7.12 of the appendix. Abbreviations: NT Con, NT: non-transfected cells, T17N: dominant-negative RAC1, NLS-T17N: dominant-negative RAC1 with additional NLS.

To check if it is possible to further enhance the effect of dominant-negative hRAC1, pharmacological inhibition of RAC1 was combined with the expression of GFP-hRAC1(T17N) with and without additional NLS.

3.2.4.2 Influence of pharmacological RAC1 inhibition on doxorubicin-induced γH2AX and 53BP1 foci formation in cells expressing human GFP-RAC1(T17N) with and without additional NLS

To investigate the effects of a RAC1 inhibitor on Dox-induced DSB formation (foci formation) in MEF, EHT 1864 was included for pharmacological inhibition of RAC1 additionally to the transfection with human *GFP-RAC1(T17N)* expression vector with and without additional NLS. The Dox-induced DDR was investigated by evaluation of γH2AX and 53BP1 foci numbers. 24 h after transfection cells were pre-treated with 30 µM EHT 1864 for 3 h prior to Dox [1 µM, 1 h] treatment. After doxorubicin treatment cells were fixed and stained for γH2AX and 53BP1.

Control experiments are shown in the appendix. Neither the transfection method nor the EHT 1864 treatment had an impact on the basal foci formation (Appendix, Figure 7.15).

EHT 1864 treatment prior to Dox reduced the γH2AX as well as 53BP1 foci numbers by about 50 % in the doxorubicin treated cells treated with transfection reagent (TR) (Figure 3.12). GFP-hRAC1(T17N) expressing cells showed about ~50 % less foci after pre-treatment with EHT 1864. In case of *GFP-NLS-hRAC1(T17N)* expression vector transfected cells pre-treatment with EHT 1864 prior to Dox treatment did not decrease the foci formation any further than GFP-NLS-hRAC1(T17N) expression did. Overall, the data show that the pre-treatment with EHT 1864 could not further decrease the number of foci beyond the inhibitory effect of mainly cytoplasmic dominant-negative hRAC1 or targeted nuclear accumulation of dominant-negative hRAC1 on Dox-stimulated foci formation and *vice versa*.

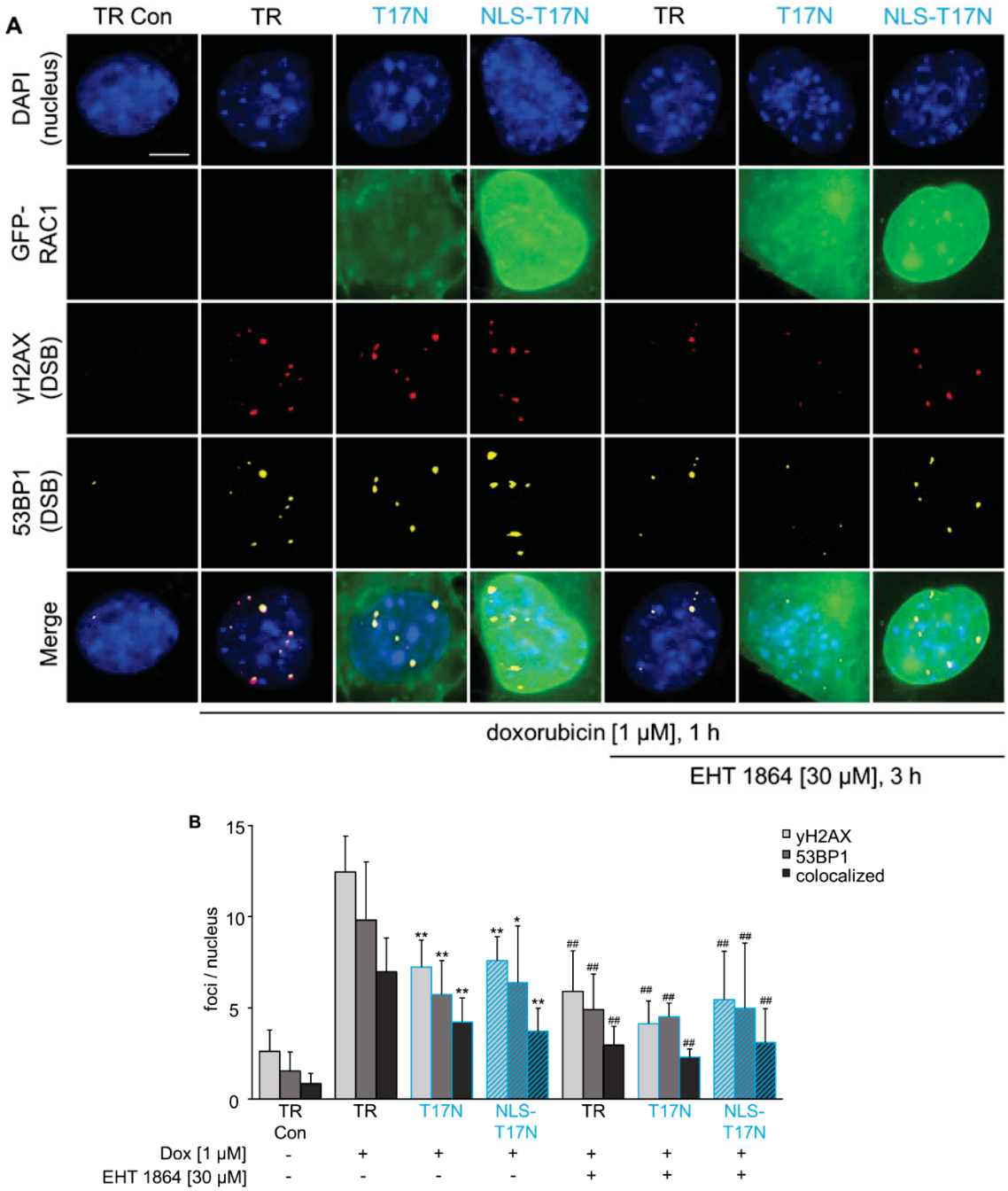

Figure 3.12: Influence of pharmacological RAC1 inhibition on doxorubicin-induced foci formation in cells expressing GFP-hRAC1(T17N) GFP-NLS-hRAC1(T17N).
MEF were transiently transfected with *GFP-hRAC1(T17N)* or *GFP-NLS-hRAC1(T17N)* expression vector. Transfection control cells (TR Con, TR) were treated with TransIT-X2. 24 h after transfection cells were pre-treated with 30 μM EHT 1864 for 3 h prior to treatment with Dox [1 μM, 1 h]. **A** After the end of the Dox treatment, staining of the γH2AX and 53BP1 foci was carried out as described in methods. Representative microscopical fluorescence pictures are shown; blue: DAPI-stained nuclei, green: GFP signal, red: γH2AX (Ser139), yellow: 53BP1. Scale bar: 10 μm. **B** Quantification of γH2AX and 53BP1 foci formation, as well as colocalization of these foci in GFP-hRAC1(T17N) and GFP-NLS-hRAC1(T17N) expressing cells. Foci of each nucleus were counted (mean+SD; n=3 - 38 with 50 nuclei counted per experiment; *p ≤ 0.05, **p ≤ 0.01 compared to cells treated with Dox (TR); one-way ANOVA with Dunnett post-hoc test; ##p ≤ 0.01 compared to cells treated with Dox (TR), 2-way ANOVA with Tukey post-hoc test). The data underlying the graph are shown in Table 7.13 of the appendix. Abbreviations: TR Con, TR:

cells treated with TransIT-X2, T17N: dominant-negative RAC1, NLS-T17N: dominant-negative RAC1 with additional NLS.

In addition, western blot analysis of representative DDR proteins was performed for investigation of the Dox-induced DDR signalling in *GFP-hRAC1(T17N)* expression vector transfected cells with and without EHT 1864 co-treatment. 24 h after transfection cells were pre-treated with EHT 1864 [3 h, 30 µM] prior to treatment with 1 µM Dox (2 h) (Figure 3.13). Non-transfected Dox-treated cells showed an elevated pKAP1 as well as pP53 protein expression which was reduced in the case of pre-treatment with EHT 1864. Cells expressing GFP-hRAC1(T17N) (Figure 3.13) showed a strong signal of pKAP1 right after treatment with Dox and the signal was not weakened by pre-treatment with EHT 1864. In dominant-negative hRAC1 expressing cells the pP53 signal was not detectable (Figure 3.13). Since this experiment was only performed 1 - 2 times, no statistical evaluation was possible. Nevertheless, the results so far do not indicate a further reduction of Dox-induced DDR signalling proteins by linking GFP-hRAC1(T17N) expression and EHT 1864 compared to expression of dominant-negative hRAC1 alone.

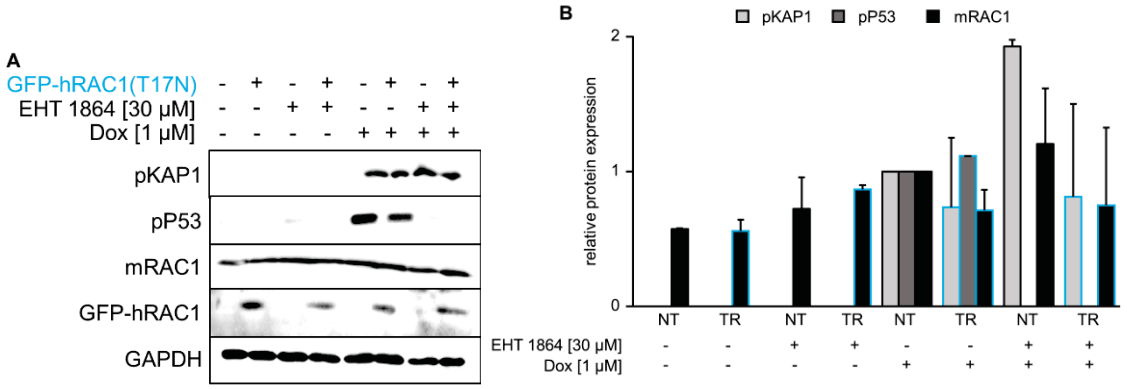

Figure 3.13: Influence of pharmacological RAC1 inhibition on doxorubicin-induced DDR in cells expressing human dominant-negative GFP-RAC1.
MEF were transiently transfected with *GFP-hRAC1(T17N)* expression vector. 24 h after transfection cells were pre-treated with 30 µM EHT 1864 for 3 h prior to treatment with Dox [1 µM, 2 h]. Cells were harvested after the end of the Dox treatment. Afterwards cells were lysed, and protein extracts were analyzed by western blot analysis as described in methods. As reference protein GAPDH was used. **B** Change in protein expression in *GFP-hRAC1(T17N)* expression vector transfected and non-transfected cells after EHT 1864 and Dox treatment was quantified as described in methods. The protein expression of non-transfected cells (NT) treated with Dox was set to 1 (mean+SD; n=1 - 2). The data underlying the graph are shown in Table 7.14 of the appendix. Abbreviations: NT: non-transfected cells, TR: cells transfected with *GFP-hRAC1(T17N)* expression vector.

Since pharmacological RAC1 inhibition could not significantly further reduce the Dox-induced foci formation in cells transfected with dominant-negative *GFP-hRAC1* expression vector with and without additional NLS, a temporary gene knockdown of

mRac1 was combined with the expression of dominant-negative GFP-hRAC1 in the following experiment.

3.2.4.3 Influence of GFP-hRAC1(T17N) (with and without additional NLS) expression on doxorubicin-induced γH2AX and 53BP1 foci formation in cells with silenced *mRac1*

Pharmacological inhibition only blocks the function of a protein, but the protein is still present. EHT 1864 blocks the activity of intrinsic mRAC1 as well as of the transfected *hRAC1*. However, it can also inhibit RAC2 and RAC3 activity as stated above. To exclude the effects of RAC2 and RAC3 inhibition and the resulting possible misinterpretation of RAC1 as relevant target protein a transient gene silencing (*mRac1*) was performed. The transfection with siRNA targets specifically the cell's intrinsic mRAC1 mRNA resulting in a decrease of target protein level. This allows analysis of the impact of hRAC1 on the DDR without interference by the endogenous mRAC1. The procedure of the upcoming experiment is shown in material and methods (Figure 2.1 E, F).

Beforehand control experiments were performed to ensure a specific silencing of *mRac1* without any influence on the transgenic GFP-hRAC1. In summary, the temporary knockdown worked and was specific for the intrinsic mRAC1. Neither the transfection with *hRAC1* expression vectors altered the *mRac1* knockdown efficiency, nor did siRNA against *mRac1* alter the expression of human GFP-RAC1. The transfection methods had no impact on the basal foci formation (Appendix, Figure 7.16, Figure 7.17, Figure 7.18).

The hypothesis was, that the temporary silencing of *mRac1* prevents the cells from Dox-induced γH2AX and 53BP1 foci formation similar to a treatment with EHT 1864 (Figure 3.6, Figure 3.12) and transfection with *GFP-hRAC1(T17N)* and *GFP-NLS-hRAC1(T17N)* expression vector (Figure 3.10). Simultaneous transfection of *GFP-hRAC1(T17N)* or *GFP-NLS-hRAC1(T17N)* expression vector could enhance the prevention of foci formation or does not distress this effect.

Silencing of *mRac1* prevented from Dox-induced γH2AX and 53BP1 foci formation by about 60 %, perfectly mimicking the effect seen with the pharmacological RAC1 inhibitor. Neither the combination of a *mRac1* knockdown and expression of mainly cytoplasmic dominant-negative hRAC1 nor the additional expression of GFP-NLS-hRAC1(T17N) further decreased the Dox-induced foci formation compared to *mRac1* siRNA alone or expression of dominant-negative hRAC1 alone (Figure 3.14).

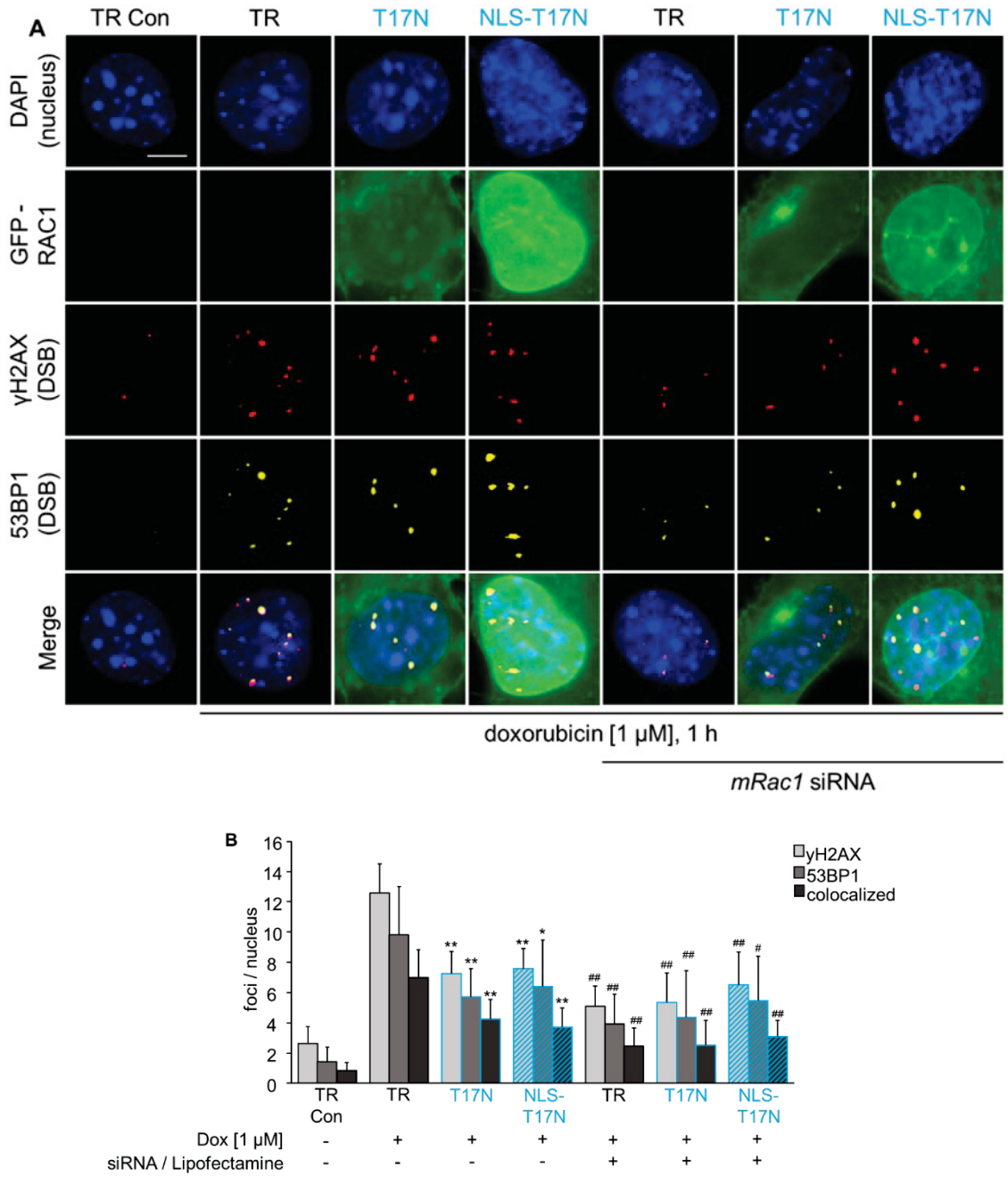

Figure 3.14*:* Influence of GFP-hRAC1(T17N) with or without additional NLS on doxorubicin-induced foci formation in *mRac1* silenced MEF.
mRac1 knockdown was achieved by transfection with *mRac1* siRNA. The treatment scheme is shown in material and methods (Figure 2.1 E, F). Cells were additionally transfected with *GFP-hRAC1(T17N)* or *GFP-NLS-hRAC1(T17N)* expression vector. **A** After the end of the Dox treatment, cells were fixed and staining of γH2AX and 53BP1 foci was carried out as described in methods. Representative microscopical fluorescence pictures are shown; blue: DAPI-stained nuclei, green: GFP signal, red: γH2AX (Ser139), yellow: 53BP1. Scale bar: 10 µm. **B** Quantification of γH2AX and 53BP1 foci formation, as well as colocalization of these foci in *mRac1* silenced cells expressing GFP-hRAC1(T17N) or GFP-NLS-hRAC1(T17N). Foci of each nucleus were counted (mean+SD; n=3-38 with 50 nuclei counted per experiment; *p ≤ 0.05, **p ≤ 0.01 compared to TR; one-way ANOVA with Dunnett post-hoc test; $^{\#}$p ≤ 0.05, $^{\#\#}$p ≤ 0.01 compared to cells treated with Dox (TR), 2-way ANOVA with Tukey post-hoc test). The data underlying the graph are shown in Table 7.15 of the appendix. Abbreviations: TR Con, TR: cells treated with

TransIT-X2 only or treated with Lipofectamine RNAiMAX and TransIT-X2, T17N: dominant-negative RAC1, NLS-T17N: dominant-negative RAC1 with additional NLS.

3.2.4.4 Comparison of mainly cytosolic and targeted nuclear expression of dominant-negative hRAC1, EHT 1864, and *mRac1* siRNA on doxorubicin induced γH2AX and 53BP1 foci formation.

With the performed experiments the published results regarding Dox-induced DSB formation have been confirmed in several ways. MEF transfected with *GFP-hRAC1(T17N)* or *GFP-NLS-hRAC1(T17N)* expression vector exhibited comparable results as cells treated with EHT 1864 or transfected with *mRac1* siRNA regarding Dox-induced γH2AX and 53BP1 foci formation. In all cases γH2AX and 53BP1 foci formation was reduced by ~ 43 - 60 %. Pre-treatment with EHT 1864 as well as transfection with *mRac1* siRNA combined with expression of GFP-hRAC1(T17N) with or without additional NLS could not further decease γH2AX and 53BP1 foci formation (Figure 3.15).

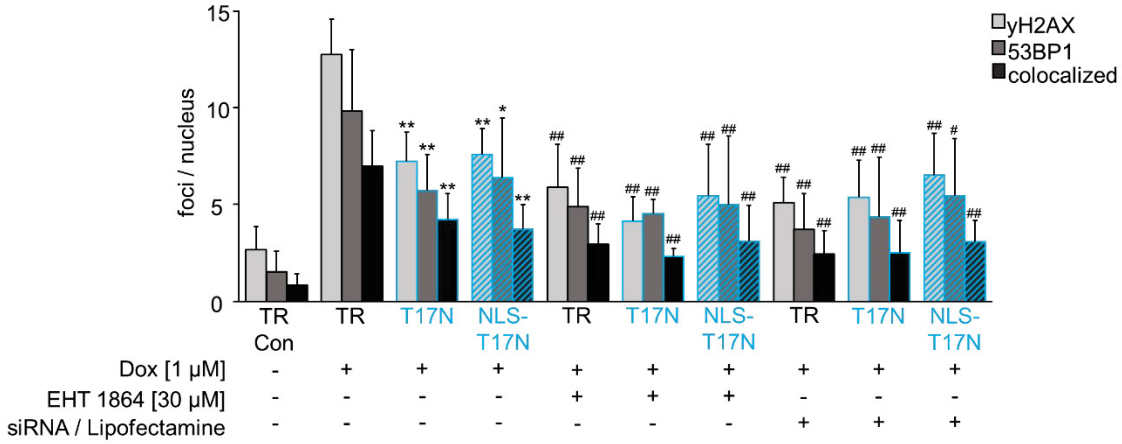

Figure 3.15: Comparison of GFP-hRAC1(T17N) with and without additional NLS, EHT 1864, and *mRac1* siRNA on doxorubicin induced γH2AX and 53BP1 foci formation.
Cells were transfected with *GFP-hRAC1(T17N)* or *GFP-NLS-hRAC1(T17N)* expression vector. Transfection control cells (TR Con, TR) were treated with TransIT-X2 only or with Lipofectamine RNAiMAX and TransIT-X2. 24 h after transfection cells were pre-treated with 30 µM EHT 1864 for 3 h prior to treatment with Dox [1 µM, 1 h] or were only treated with Dox [1 µM, 1 h]. *mRac1* knockdown was achieved by transfection with *mRac1* siRNA. The treatment scheme is shown in material and methods (Figure 2.1 E, F). Cells were additionally transfected with *GFP-hRAC1(T17N)* or *GFP-NLS-hRAC1(T17N)* expression vector. Quantification of γH2AX and 53BP1 foci formation, as well as colocalization of these foci. Foci of each nucleus were counted (mean+SD; n=3 - 38 with 50 nuclei counted per experiment; *p ≤ 0.05, **p ≤ 0.01 compared to cells treated with Dox (TR) one-way ANOVA with Dunnett post-hoc test; $^{\#}$p ≤ 0.05, $^{\#\#}$p ≤ 0.01 compared to cells treated with Dox (TR), 2-way ANOVA with Tukey post-hoc test). The data underlying the graph are shown in Figure 3.10, Figure 3.12,Figure 3.14, and Table 7.16 of the appendix. Abbreviations: TR Con: cells treated with TransIT-X2, TR: cells treated with TransIT-X2 only or treated with Lipofectamine RNAiMAX and TransIT-X2, T17N: dominant-negative RAC1, NLS-T17N: dominant-negative RAC1 with additional NLS.

3.2.4.5 Influence of mainly cytoplasmic and forced nuclear expression of human GFP-RAC1(T17N) on doxorubicin-induced pATM foci formation

Previous publications revealed a potential role of RAC1 in the DDR and the results of this work confirmed this role. Expression of dominant-negative hRAC1 with and without additional NLS altered the doxorubicin-induced foci formation. DSB-inducing chemicals like doxorubicin are known to activate the serine/threonine kinase ATM (Kurz et al. 2004; Huang et al. 2011) which is a major mediator regulator of the DDR (Hoekstra 1997). Substrates for this protein are amongst other proteins H2AX, P53, and KAP1 (Banin et al. 1998; Burma et al. 2001; White et al. 2012) which were altered in cells expressing GFP-hRAC1(T17N) or GFP-NLS-hRAC1(T17N) upon treatment with Dox as seen in the presented data. To analyze whether dominant-negative hRAC1 has an influence on activation (phosphorylation) of ATM in the Dox-induced DDR, pATM foci formation was evaluated.

Control experiments were carried out beforehand. There was no significant change in basal pATM foci number upon transfection (Appendix, Figure 7.19).

Treatment with 1 µM Dox induced pATM foci in all cells. Transfection with *GFP-hRAC1(T17N)* or *GFP-NLS-hRAC1(T17N)* expression vector did not alter the number of pATM foci following Dox treatment compared to cells treated with TransIT-X2 (TR) (Figure 3.16). In conclusion, dominant-negative GFP-hRAC1 had no effect on Dox-induced pATM foci formation.

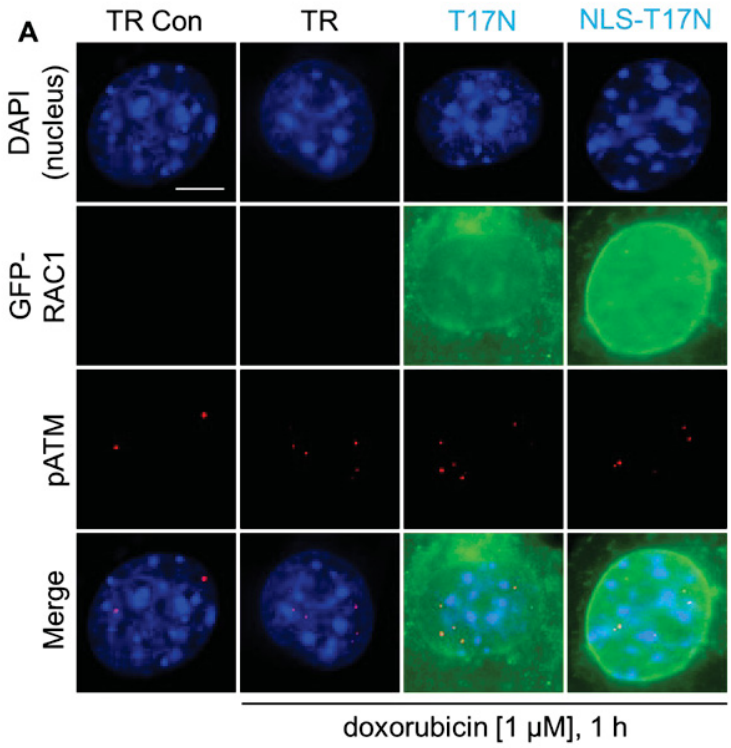

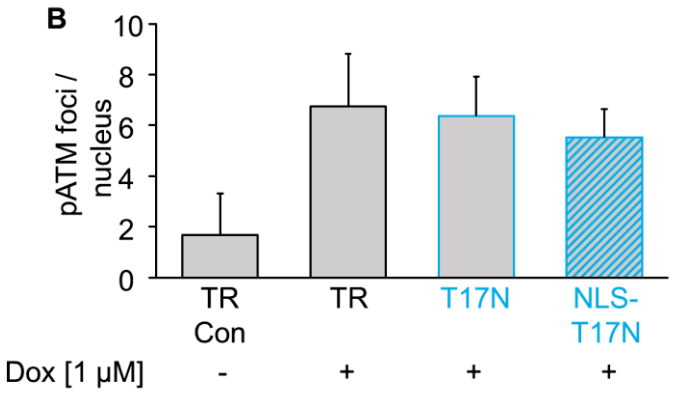

Figure 3.16: Influence of human dominant-negative GFP-RAC1 (with and without additional NLS) on doxorubicin-induced pATM foci formation.
Cells were transiently transfected with *GFP-hRAC1(T17N)* or *GFP-NLS-hRAC1(T17N)* expression vector. Transfection control cells (TR Con, TR) were treated with TransIT-X2. 24 h after transfection cells were treated with Dox [1 µM] for 1 h. **A** After the end of the Dox treatment, cells were fixed and staining of pATM foci was carried out as described in methods. Representative microscopical fluorescence pictures are shown; blue: DAPI-stained nuclei, green: GFP signal, red: pATM. Scale bar: 10 µm. **B** Quantification of pATM foci formation. Foci of each nucleus were counted (mean+SD; n=3 - 18 with 50 nuclei counted per experiment). The data underlying the graph are shown in Table 7.17 of the appendix. Abbreviations: TR Con, TR: cells treated with TransIT-X2, T17N: dominant-negative RAC1, NLS-T17N: dominant-negative RAC1 with additional NLS.

In further experiments wild-type *hRAC1* and constitutively active *hRAC1* variants with and without additional NLS were used to analyze their effects on the Dox-induced DDR. The hypothesis is that expression of wild-type RAC1 or constitutively active RAC1 does not influence the doxorubicin-induced DDR or enhances the DDR. To distinguish between effects promoted by targeted nuclear expression of RAC1 and cytosolic RAC1, human *RAC1* mutants were used with and without an additional NLS.

3.2.5 Influence of wild-type and constitutively active hRAC1 expression on the doxorubicin-induced DNA damage response

3.2.5.1 Influence of expression of human GFP-RAC1 mutants (with and without additional NLS) on doxorubicin-induced γH2AX and 53BP1 foci formation and the DNA damage response

To evaluate the assumption that expression of wild-type RAC1 or constitutively active RAC1 could enhance the doxorubicin-induced DDR or does not affect the DDR at all, the effect of wild-type and constitutively active hRAC1 on Dox-induced DDR and foci formation was analyzed on the one hand, and the difference between forced nuclear expression and mainly cytosolic expression of hRAC1 on the Dox-induced DDR and foci formation was assessed on the other hand.

Beforehand control experiments were performed to exclude effects of the used transfection method and plasmids on basal foci formation. Neither the transfection method nor the plasmids had an impact on the basal foci formation (Appendix, Figure 7.20).

GFP-hRAC1(WT) expressing cell showed a lower number of γH2AX and γH2AX/53BP1 colocalized foci compared to the cells which were treated with TransIT-X2 and treated with Dox (TR) (Figure 3.17). There was no influence on the 53BP1 foci formation following Dox treatment upon expression of GFP-hRAC1(WT). The additional NLS in wild-type hRAC1 only reduced Dox-induced γH2AX foci numbers. GFP-hRAC1(Q61L) did not alter the Dox-induced foci formation at all (Figure 3.17), whereas forcing constitutively active hRAC1 into the nucleus reduced the Dox-induced foci formation even more than GFP-hRAC1(T17N) with and without additional NLS (Figure 3.10, Figure 3.17). Dominant-negative hRAC1 with or without additional NLS reduced the γH2AX foci formation about 43 % - 46 %, while expression of GFP-NLS-hRAC1(Q61L) reduced the γH2AX foci formation about 60 %.

Taken together, mainly cytoplasmic as well as mainly nuclear wild-type hRAC1 reduced the Dox-induced γH2AX foci formation but there was no significant difference between cytoplasmic and nuclear expression of wild-type hRAC1. GFP-NLS-hRAC1(Q61L) reduced the Dox-induced foci formation even more than dominant-negative hRAC1, which implicates that active nuclear RAC1 is essential for a pronounced doxorubicin-induced DDR.

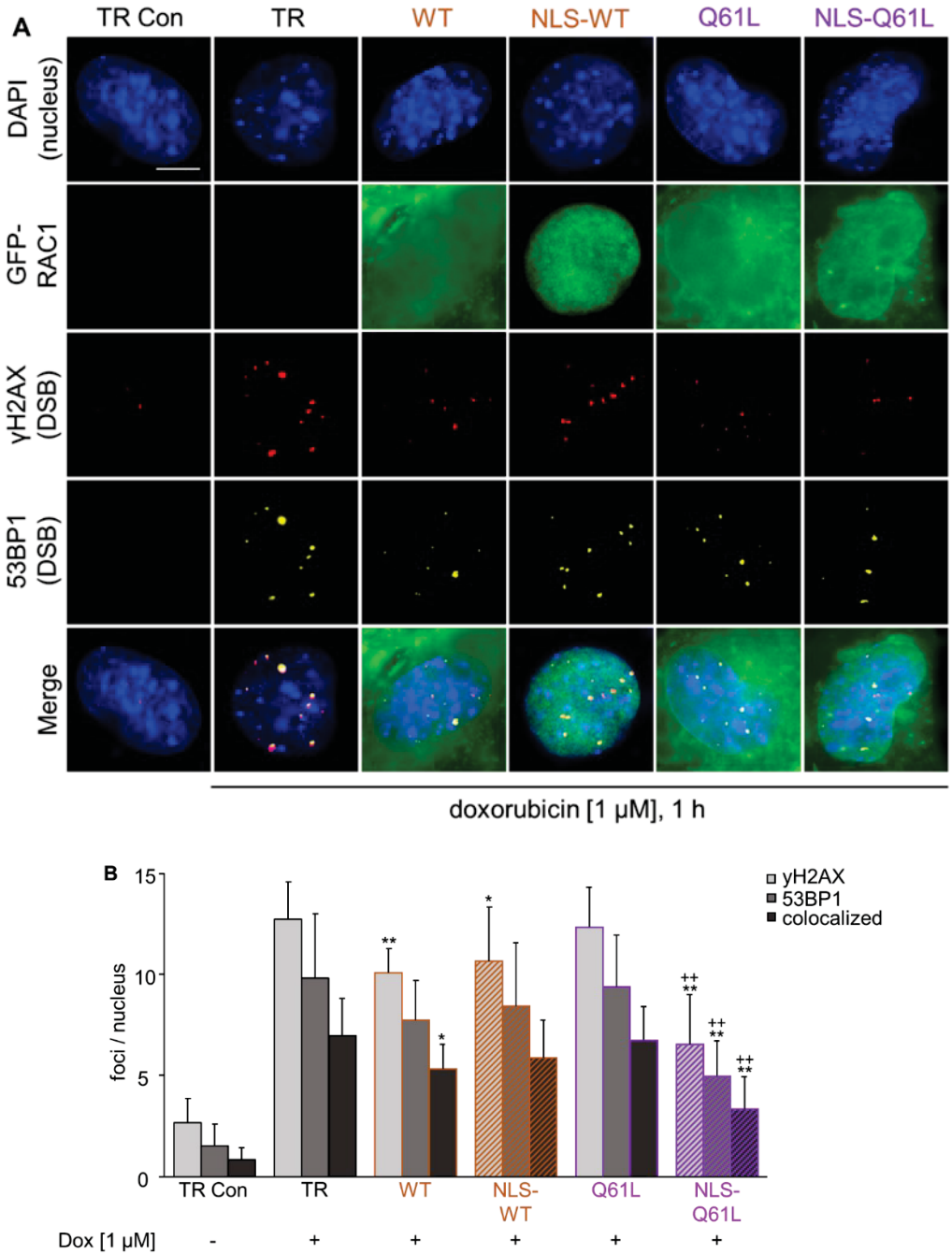

Figure 3.17: Influence of wild-type and constitutively active hRAC1 (with and without additional NLS) expression on doxorubicin-induced foci formation.
MEF were transiently transfected with *GFP-hRAC1(WT)*, *GFP-NLS-hRAC1(WT)*, *GFP-hRAC1(Q61L)* or *GFP-NLS-hRAC1(Q61L)* expression vector. Transfection control cells (TR Con, TR) were treated with TransIT-X2. 24 h after transfection cells were treated with Dox [1 µM] for 1 h. **A** After the end of the Dox treatment, cells were fixed and staining of γH2AX and 53BP1 foci was carried out as described in methods. Representative microscopical fluorescence pictures are shown; blue: DAPI-stained nuclei, green: GFP signal, red: γH2AX (Ser139), yellow: 53BP1. Scale bar: 10 µm. **B** Quantification of γH2AX and 53BP1 foci formation, as well as colocalization of these foci. Foci of each nucleus were counted (mean+SD; n=6 - 38 with 50 nuclei counted per experiment; *p ≤ 0.05, **p ≤ 0.01 compared to TR; one-way ANOVA with Dunnett post-hoc test; $^{++}$p ≤ 0.01 compared to GFP-hRAC1 without NLS, T-test, unpaired, two-sided). The data underlying the graph are shown in Table 7.18 of the appendix. Abbreviations: TR Con, TR: cells

treated with TransIT-X2, WT: wild-type RAC1, NLS-WT: wild-type RAC1 with additional NLS, Q61L: constitutively active RAC1, NLS-Q61L: constitutively active RAC1 with additional NLS.

In addition, western blot analysis of representative DDR-related proteins was performed for investigation of the Dox-induced DDR signalling in GFP-(NLS-)hRAC1 expressing cells. MEF were transiently transfected with *GFP-hRAC1(WT)*, *GFP-NLS-hRAC1(WT)*, *GFP-hRAC1(Q61L)*, or *GFP-NLS-hRAC1(Q61L)* expression vector. 24 h after transfection cells were pulse-treated with 1 µM Dox (2 h) and harvested after the indicated time-points (Figure 3.18, Figure 3.19). An antibody against GFP was used to confirm the successful transfection of the cells. GAPDH was used as reference protein.

Non-transfected Dox-treated cells exhibited high pKAP1 levels which were only slightly decreasing over time. Expression of GFP-hRAC1(WT) significantly decreased Dox-induced pKAP1 protein levels 0 h and 24 h post-treatment (Figure 3.18 A, C), whereas cells transfected with *GFP-NLS-hRAC1(WT)* expression vector revealed a significant reduced level of pKAP1 only 24 h after the end of the pulse-treatment (Figure 3.18 B, C). Non-transfected Dox-treated cells showed γH2AX expression over time. Only GFP-NLS-hRAC1(WT) expressing cells showed a significant decreased level of phosphorylated H2AX 4 h post-treatment (Figure 3.18 B, D). Non-transfected Dox-treated cells showed a pP53 expression over time which was decreasing 24 h post-treatment. Cells transfected with *GFP-hRAC1(WT)* expression vector showed a reduced Dox-induced pP53 expression for all three time-points (Figure 3.18 A, E). The results for cells expressing GFP-NLS-hRAC1(WT) demonstrated a decreased pP53 signal directly after the pulse-treatment with Dox (0 h) as well as 24 h post-treatment (Figure 3.18 B, E). There was no significant difference in Dox induced pP53 expression in cells expressing mainly cytoplasmic or mainly nuclear wild-type hRAC1.

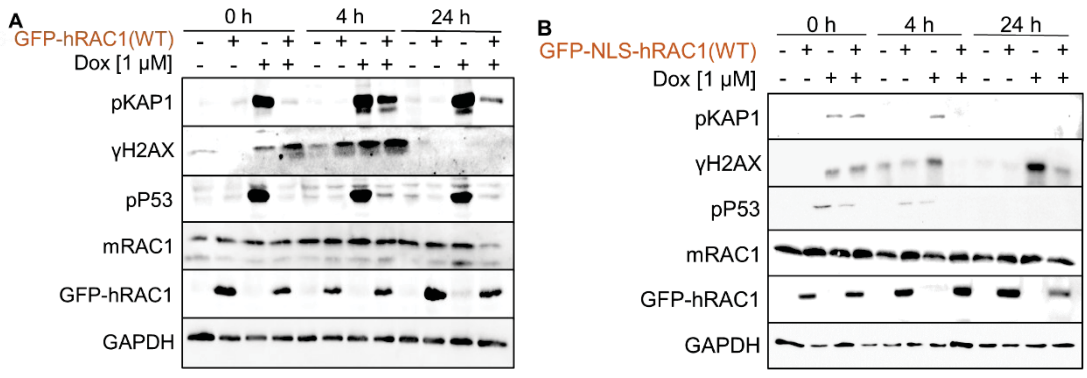

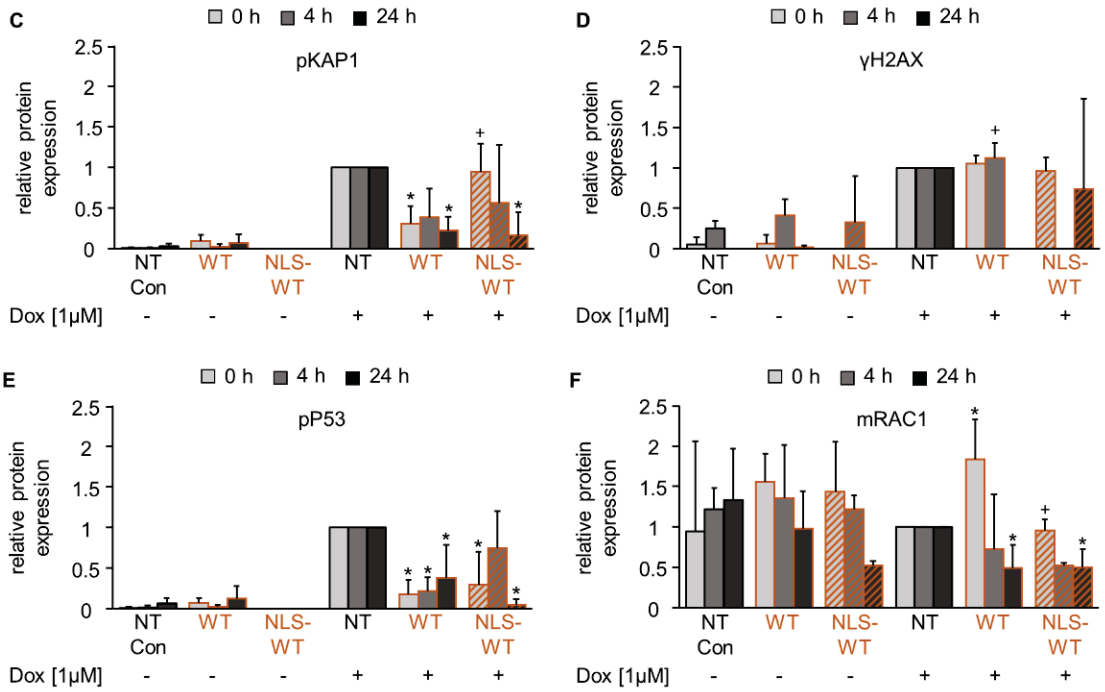

Figure 3.18: Western blot analysis after doxorubicin treatment in wild-type hRAC1-expressing cells with and without additional NLS.
MEF were transiently transfected with *GFP-hRAC1(WT)* (**A**) or *GFP-NLS-hRAC1(WT)* (**B**) expression vector. 24 h after transfection cells were 2 h pulse-treated with 1 µM Dox. Cells were harvested after indicated time-points. Afterwards cells were lysed, and protein extracts were analyzed by western blot analysis as described in methods. As reference protein GAPDH was used. **C - F** Change in protein expression in *GFP-hRAC1(WT)* or *GFP-NLS-hRAC1(WT)* expression vector transfected and non-transfected cells after Dox treatment was quantified as described in methods. The protein expression of non-transfected cells treated with Dox was set to 1 (mean+SD; n=3; *p ≤ 0.05 compared to non-transfected Dox-treated cells (NT); one-way ANOVA with Dunnett post-hoc test; $^{+}$p ≤ 0.05 compared to GFP-hRAC1(WT)/GFP-NLS-hRAC1(WT) expressing cells treated with Dox, T-test, unpaired, two-sided). The data underlying the graph are shown in Table 7.19 of the appendix. Abbreviations: NT Con, NT: non-transfected cells, WT: wild-type RAC1, NLS-WT: wild-type RAC1 with additional NLS.

No significant change in Dox-induced expression of pKAP1, γH2AX, or pP53 was observed in cells transfected with *GFP-hRAC1(Q61L)* expression vector with or without additional NLS (Figure 3.19).

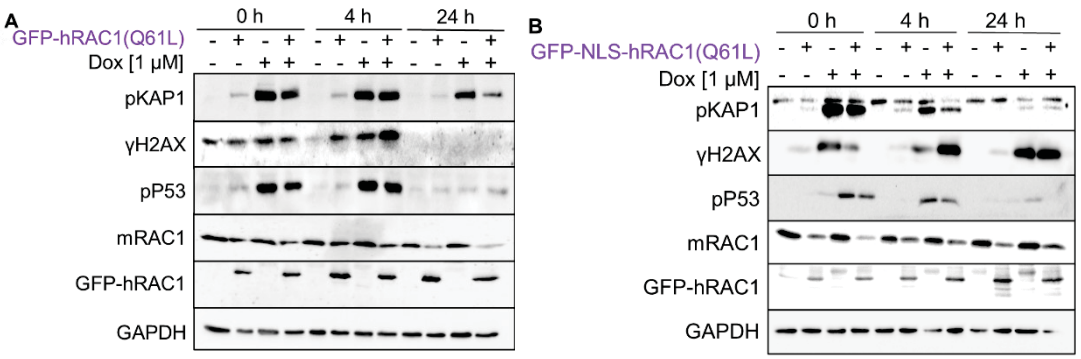

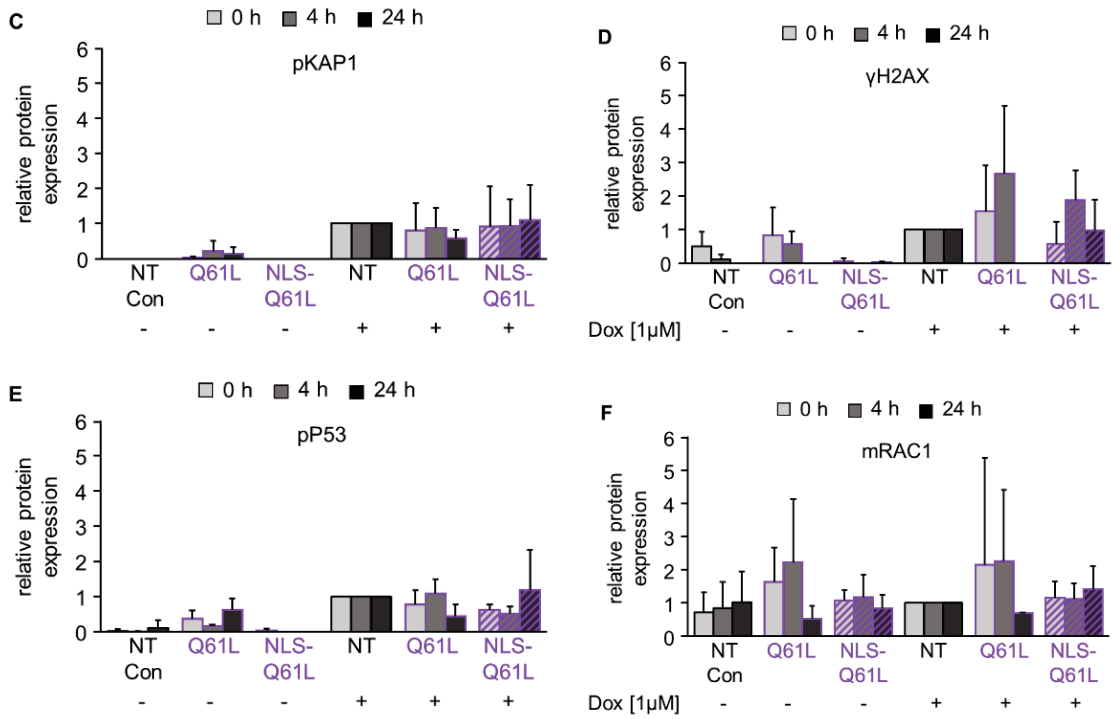

Figure 3.19: Western blot analysis after doxorubicin treatment in constitutively active hRAC1-expressing cells with and without additional NLS.
MEF were transiently transfected with *GFP-hRAC1(Q61L)* (**A**) or *GFP-NLS-hRAC1(Q61L)* (**B**) expression vector. 24 h after transfection cells were 2 h pulse-treated with 1 µM Dox. Cells were harvested after indicated time-points. Afterwards cells were lysed, and protein extracts were analyzed by western blot analysis as described in methods. As reference protein GAPDH was used. **C - F** Change in protein expression in *GFP-hRAC1(Q61L)* or *GFP-NLS-hRAC1(Q61L)* expression vector transfected and non-transfected cells after Dox treatment was quantified as described in methods. The protein expression of non-transfected cells treated with Dox (NT) was set to 1 (mean+SD; n=3). The data underlying the graph are shown in Table 7.20 of the appendix. Abbreviations: NT Con, NT: non-transfected cells, Q61L: constitutively active RAC1, NLS-Q61L: constitutively active RAC1 with additional NLS.

Taken together, only wild-type *hRAC1* mutants diminished the Dox-induced DDR represented by the depicted set of DDR-related phosphorylated proteins. The decrease in protein signalling occurred at the same time points in GFP-hRAC1(WT) and GFP-NLS-hRAC1(WT) expressing cells but in different intensities.

The hypothesis was that expression of wild-type RAC1 or constitutively active RAC1 could enhance the doxorubicin-induced DDR or does not influence the DDR at all. Based on the results of the foci analysis and the western blot analysis, the working hypothesis was both confirmed and refuted. Expression of mainly cytoplasmic constitutively active RAC1 confirmed the working hypothesis and did not influence the DDR, whereas expression of GFP-NLS-hRAC1(Q61L) reduced the Dox induced foci formation but had no influence on the selected proteins analyzed by western blot analysis. Expression of wild-type RAC1 either had no effect or attenuated the DDR.

3.2.5.2 Influence of pharmacological RAC1 inhibition on doxorubicin-induced γH2AX and 53BP1 foci formation in cells expressing cytoplasmic and nuclear human GFP-RAC1 variants

Another question of this work was if expression of wild-type RAC1 or constitutively active RAC1 can revert the inhibitory effect of EHT 1864 on foci formation upon Dox treatment. Like shown above, cells expressing dominant-negative hRAC1 showed no additional effect on foci formation upon treatment with EHT 1864 and Dox independent of the subcellular distribution of hRAC1 (see Figure 3.12).

First of all, the influence of the transfection and the *GFP-hRAC1* mutants in combination with EHT 1864 treatment on the basal foci formation was analyzed. Neither the transfection method nor the EHT 1864 treatment had an impact on the basal foci formation (Appendix, Figure 7.21).

Transfection control cells (TR Con) treated with EHT 1864 prior to Dox showed about 50 % reduced γH2AX as well as 53BP1 foci numbers compared to the doxorubicin treated cells (TR) (Figure 3.20, Figure 3.21). Pre-treatment with EHT 1864 reduced the Dox-induced foci formation independent of the transfected expression vector. Only half as much γH2AX foci and about 1/3 of 53BP1 foci could be detected in mainly cytoplasmic wild-type hRAC1 expressing cells administered with EHT 1864 prior to Dox exposure compared to TR cells as well as the *GFP-hRAC1(WT)* expression vector transfected cells treated with Dox only (Figure 3.20). Cells expressing GFP-NLS-hRAC1(WT) showed 50 % - 60 % less doxorubicin-induced foci after pre-treatment with EHT 1864 compared to the GFP-NLS-hRAC1(WT) expressing cells as well as the TR cells after Dox monotreatment (Figure 3.20).

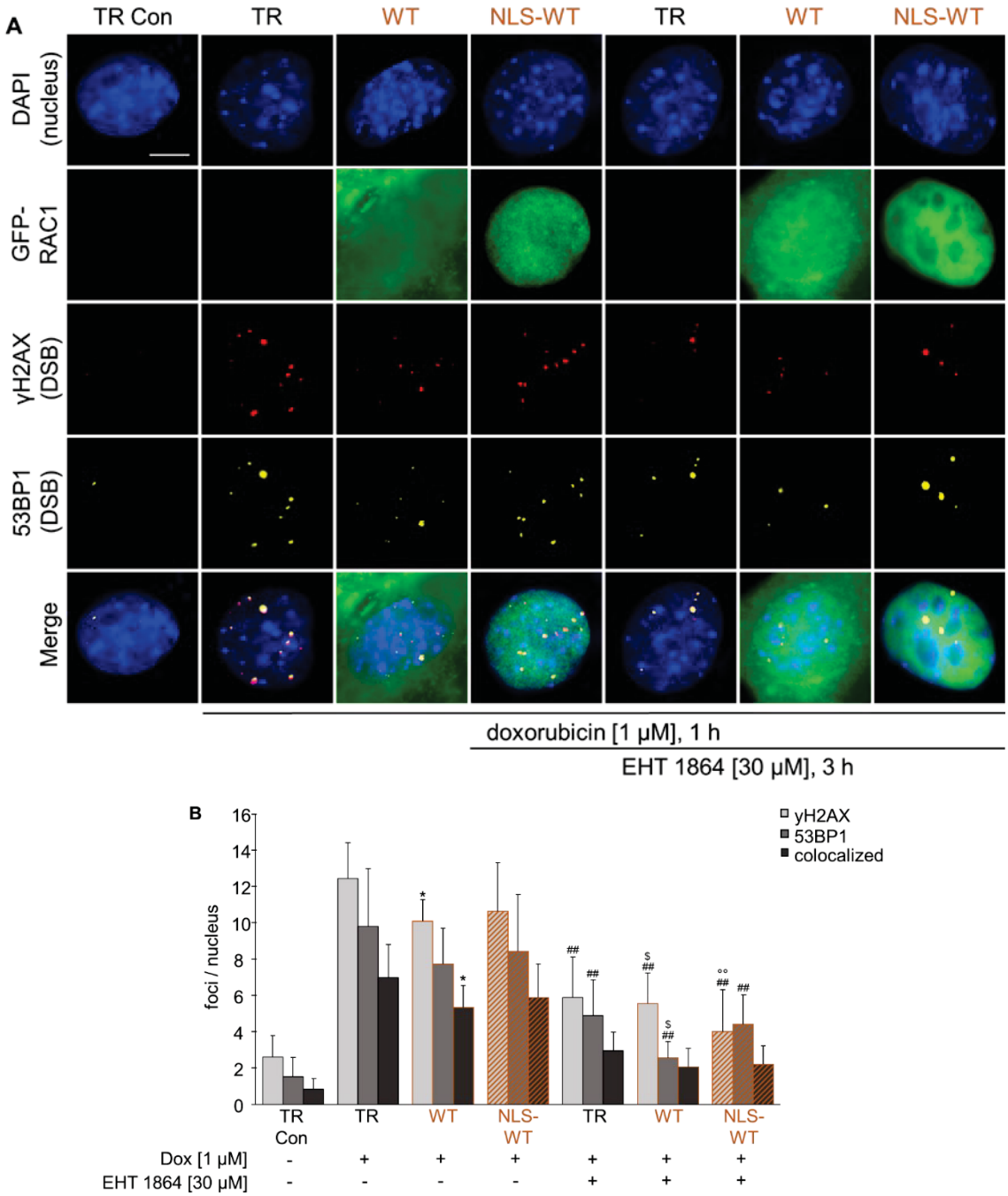

Figure 3.20: Influence of pharmacological RAC1 inhibition on doxorubicin-induced foci formation in cells expressing cytosolic or nuclear human GFP-RAC1(WT).
MEF were transiently transfected with *GFP-hRAC1(WT)* or *GFP-NLS-hRAC1(WT)* expression vector. Transfection control cells (TR Con, TR) were treated with TransIT-X2. 24 h after transfection cells were pre-treated with 30 µM EHT 1864 for 3 h prior to treatment with Dox [1 µM, 1 h]. **A** After the end of the Dox treatment, cells were fixed and staining of γH2AX and 53BP1 foci was carried out as described in methods. Representative microscopical fluorescence pictures are shown; blue: DAPI-stained nuclei, green: GFP signal, red: γH2AX (Ser139), yellow: 53BP1. Scale bar: 10 µm. **B** Quantification of γH2AX and 53BP1 foci formation, as well as colocalization of these foci in GFP-hRAC1(WT) and GFP-NLS-hRAC1(WT) expressing cells. Foci of each nucleus were counted (mean+SD; n=3 - 38 with 50 nuclei counted per experiment; *p ≤ 0.05 compared to cells treated with Dox (TR); one-way ANOVA with Dunnett post-hoc test; ##p ≤ 0.01 compared to cells treated with Dox (TR), 2-way ANOVA with Dunnett post-hoc test, $p ≤ 0.05 compared to GFP-hRAC1(WT) expression treated with Dox, 2-way ANOVA with Tukey post-hoc test; °°p ≤ 0.01 compared to GFP-NLS-hRAC1(WT) expression treated with Dox, 2-way ANOVA with

Dunnett post-hoc test). The data underlying the graph are shown in Table 7.21 of the appendix. Abbreviations: TR Con, TR: cells treated with TransIT-X2, WT: wild-type RAC1, NLS-WT: wild-type RAC1 with additional NLS.

Mainly cytoplasmic constitutively active hRAC1 expressing cells showed about 50 % less foci after pre-treatment with EHT 1864 (Figure 3.21) compared to GFP-hRAC1(Q61L) with Dox monotreatment as well as TR cells. Pre-treatment with EHT 1864 prior to Dox did not make a difference in foci formation in GFP-NLS-hRAC1(Q61L) expressing cells compared to the similarly transfected cells with Dox monotreatment. Under both conditions, the γH2AX and 53BP1 foci formation as well as the colocalized foci were reduced by 50 % compared to TR (Dox monotreatment) (Figure 3.21).

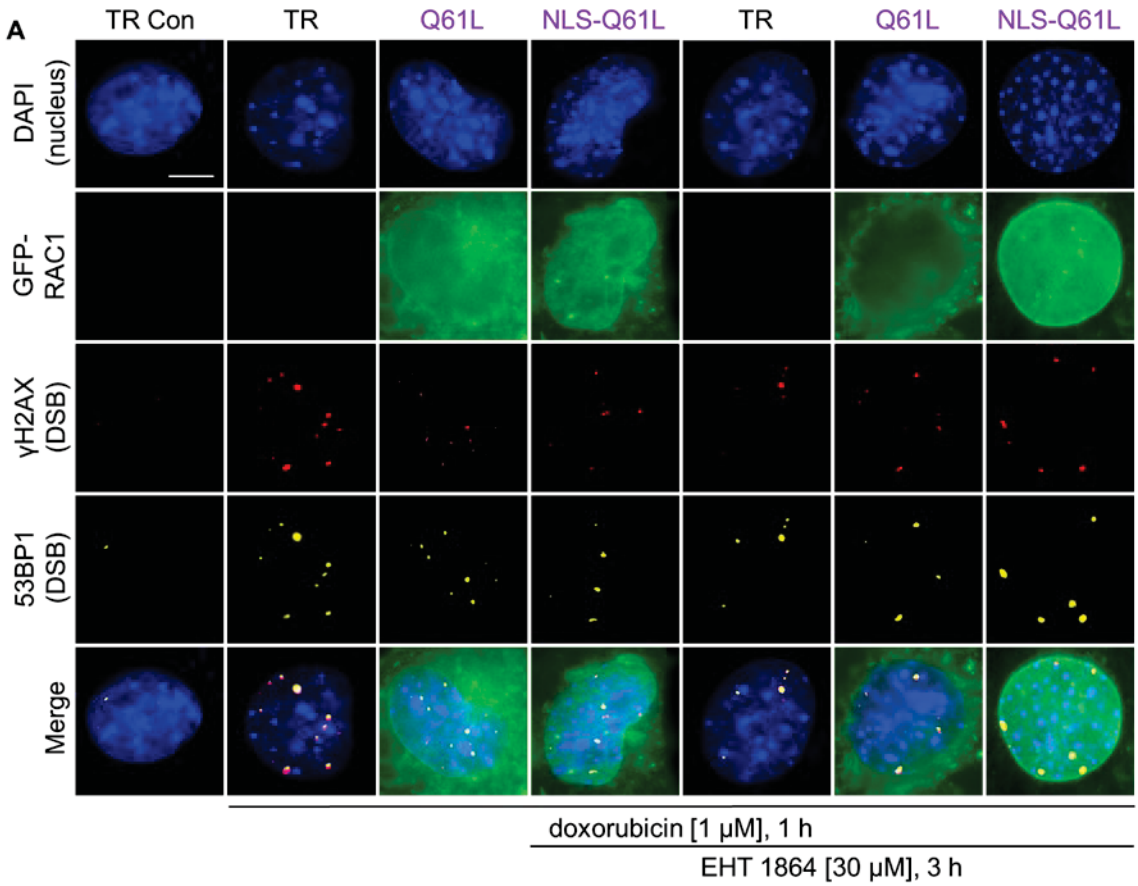

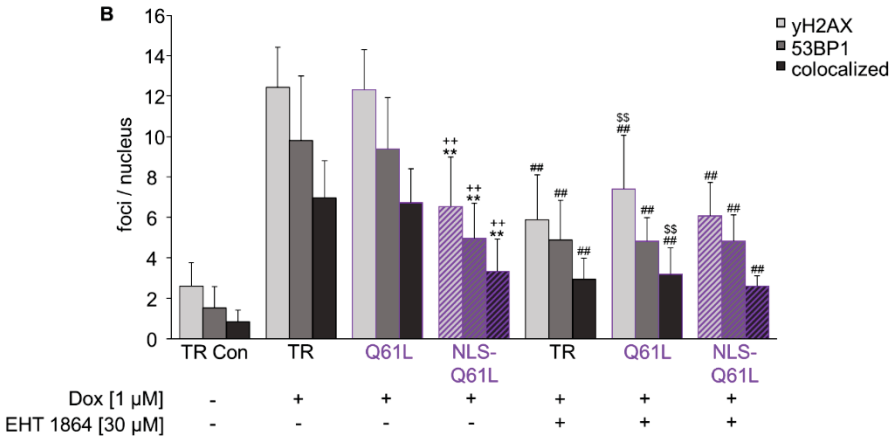

Figure 3.21: Influence of pharmacological RAC1 inhibition on doxorubicin-induced foci formation in cells expressing cytosolic or nuclear human GFP-RAC1(Q61L).
MEF were transiently transfected with *GFP-hRAC1(Q61L)* or *GFP-NLS-hRAC1(Q61L)* expression vector. Transfection control cells (TR Con, TR) were treated with TransIT-X2. 24 h after transfection cells were pre-treated with 30 µM EHT 1864 for 3 h prior to treatment with Dox [1 µM, 1 h]. **A** After the end of the Dox treatment, cells were fixed and staining of γH2AX and 53BP1 foci was carried out as described in methods. Representative microscopical fluorescence pictures are shown; blue: DAPI-stained nuclei, green: GFP signal, red: γH2AX (Ser139), yellow: 53BP1. Scale bar: 10 µm. **B** Quantification of γH2AX and 53BP1 foci formation, as well as colocalization of these foci in GFP-hRAC1(Q61L) and GFP-NLS-hRAC1(Q61L) expressing cells. Foci of each nucleus were counted (mean+SD; n=3 - 38 with 50 nuclei counted per experiment; $^{**}p \leq 0.01$ compared to cells treated with Dox (TR); one-way ANOVA with Dunnett post-hoc test; $^{++}p \leq 0.01$ compared to GFP-hRAC1(Q61L) expression treated with Dox, T-test, unpaired, two-sided; $^{\#\#}p \leq 0.01$ compared to cells treated with Dox (TR), 2-way ANOVA with Dunnett post-hoc test, $^{\$\$}p \leq 0.01$ compared to GFP-hRAC1(Q61L) expression treated with Dox, 2-way ANOVA with Tukey post-hoc test). The data underlying the graph are shown in Table 7.22 of the appendix. Abbreviations: TR Con, TR: cells treated with TransIT-X2, Q61L: constitutively active RAC1, NLS-Q61L: constitutively active RAC1 with additional NLS.

Summarizing, it can be stated that the number of Dox-induced γH2AX and 53BP1 foci was significantly reduced by pre-treatment with EHT 1864. Expression of wild-type hRAC1 and constitutively active hRAC1 could not compensate for the inhibitory effect of EHT 1864 independent of whether RAC1 is expressed mainly in the cytoplasm or the nucleus (Figure 3.20, Figure 3.21).

In addition, western blot analysis of representative DDR proteins was accomplished to investigate the Dox-induced DDR signalling in GFP-hRAC1 expressing cells with and without EHT 1864 treatment. Non-transfected Dox-treated cells showed a pKAP1 as well as pP53 protein expression after treatment which was reduced in the case of pre-treatment with EHT 1864. GFP-hRAC1(WT) expressing cells showed a weak pKAP1 signal after treatment with Dox alone compared to the Dox-treated non-transfected cells. Pre-treatment with EHT 1864 did not make a difference in Dox-induced signal intensity in wild-type hRAC1 expressing cells (Figure 3.22).

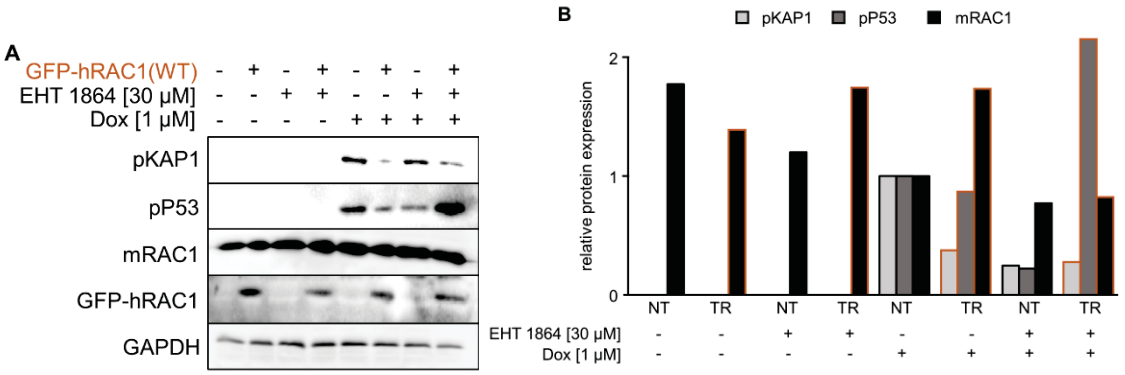

Figure 3.22: Influence of pharmacological RAC1 inhibition on doxorubicin-induced DDR in cells expressing human GFP-RAC1(WT).
MEF were transiently transfected with *GFP-hRAC1(WT)* expression vector. 24 h after transfection cells were pre-treated with EHT 1864 [3 h, 30 µM] prior to treatment with 1 µM Dox for 2 h. Cells were harvested after the end of the Dox treatment. Afterwards cells were lysed, and protein extracts were analyzed by western blot analysis as described in methods. As reference protein GAPDH was used. **B** Change in protein expression in *GFP-hRAC1(WT)* expression vector transfected and non-transfected cells after EHT 1864 and Dox treatment was quantified as described in methods. The protein expression of non-transfected cells treated with Dox (NT) was set to 1 (mean+SD; n=1). The data underlying the graph are shown in Table 7.23 of the appendix. Abbreviations: NT: non-transfected cells, TR: cells transfected with *GFP-hRAC1(WT)* expression vector.

Cells expressing GFP-hRAC1(Q61L) (Figure 3.23) showed a strong signal of pKAP1 right after treatment with Dox and the signal was not weakened by pre-treatment with EHT 1864. Dox-induced phosphorylation of P53 was attenuated after pre-treatment with EHT 1864 in GFP-hRAC1(Q61L) expressing cells (Figure 3.23).

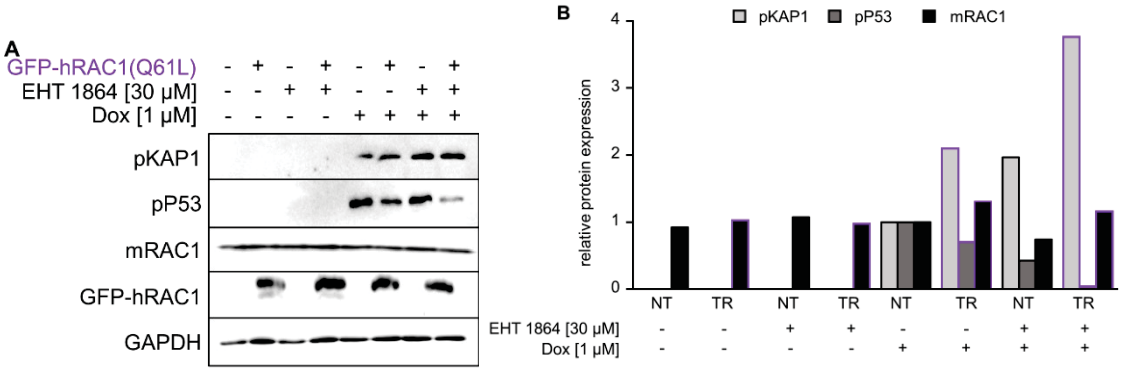

Figure 3.23: Influence of pharmacological RAC1 inhibition on doxorubicin-induced DDR in cells expressing human GFP-RAC1(Q61L).
MEF were transiently transfected with *GFP-hRAC1(Q61L)* expression vector. 24 h after transfection cells were pre-treated with EHT 1864 [3 h, 30 µM] prior to treatment with 1 µM Dox for 2 h. Cells were harvested after the end of the Dox treatment. Afterwards cells were lysed, and protein extracts were analyzed by western blot analysis as described in methods. As reference protein GAPDH was used. **B** Change in protein expression in *GFP-hRAC1(Q61L)* expression vector transfected and non-transfected cells after EHT 1864 and Dox treatment was quantified as described in methods. The protein expression of non-transfected cells treated with Dox (NT) was set to 1 (mean+SD; n=1). The data underlying the graph are shown in Table 7.24 of the appendix.

Abbreviations: NT: non-transfected cells, TR: cells transfected with *GFP-hRAC1(Q61L)* expression vector.

Since this experiment was only performed once, no statistical evaluation was possible, and the results can only be considered with reservations. The results so far do indicate a change in Dox-induced protein expression after pre-treatment with EHT 1864 in cells expressing wild-type or constitutively active hRAC1 as opposed to expression of hRAC1 and Dox treatment alone.

3.2.5.3 Influence of cytoplasmic and nuclear GFP-hRAC1 expression on doxorubicin-induced γH2AX and 53BP1 foci formation in MEF with silenced *mRac1*

For elimination of endogenous mRAC1 a temporary gene knockdown specific for the cell's intrinsic mRAC1 mRNA was performed. The treatment scheme for the following experiments is shown in material and methods (Figure 2.1 E, F). After knockdown of *mRac1*, cells were additionally transfected with *GFP-hRAC1(WT)*, *GFP-NLS-hRAC1(WT), GFP-hRAC1(Q61L)*, or *GFP-NLS-hRAC1(Q61L)* expression vector.

Performed control experiments are shown in the appendix. The used methods did not affect the basal number of foci (Appendix, Figure 7.22).

Silencing of *mRac1* prevented from Dox-induced γH2AX and 53BP1 foci formation by about 60 % in non-transfected cells (TR), perfectly mimicking the effect seen with the pharmacological RAC1 inhibitor (Figure 3.6, Figure 3.12, Figure 3.20, Figure 3.21) or expression of dominant-negative hRAC1 (Figure 3.10). In cells expressing mainly cytoplasmic wild-type hRAC1 with simultaneous *mRac1* knockdown γH2AX foci were reduced by 50 % and 53BP1 foci were even decreased by 70 % in contrast to Dox-treated cells without *mRac1* siRNA transfection (TR). Additional expression of GFP-NLS-hRAC1(WT) during knockdown of *mRac1* decreased the doxorubicin-induced γH2AX and 53BP1 foci formation by 60 % in contrast to Dox-treated cells without *mRac1* siRNA transfection (TR) (Figure 3.24).

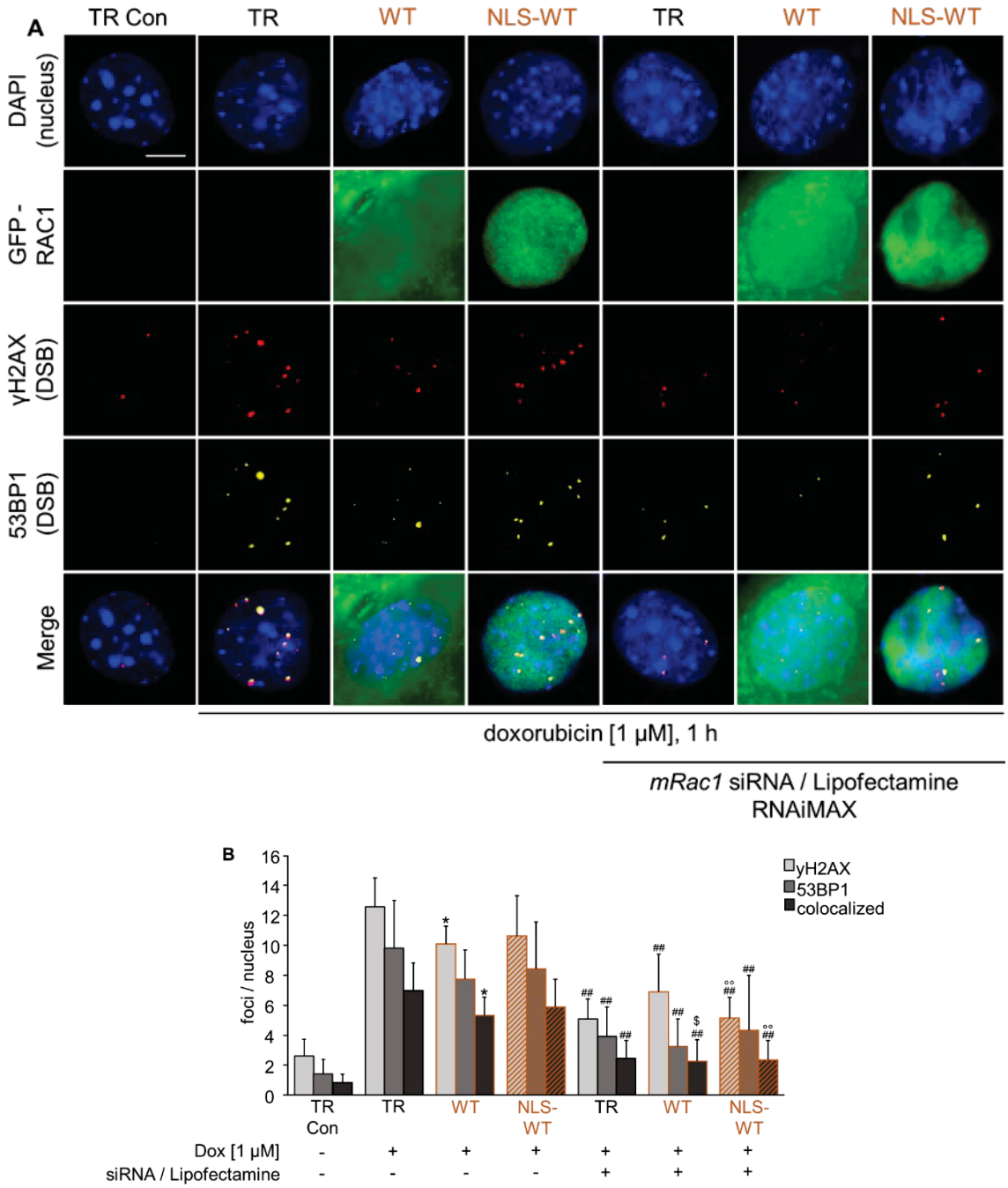

Figure 3.24: Influence of GFP-hRAC1(WT) with or without additional NLS on doxorubicin-induced foci formation in *mRac1* silenced MEF.
mRac1 knockdown was achieved by transfection with *mRac1* siRNA. The treatment scheme is shown in material and methods (Figure 2.1 E, F). Cells were additionally transfected with *GFP-hRAC1(WT)* or *GFP-NLS-hRAC1(WT)* expression vector. **A** After the end of the Dox treatment, cells were fixed and staining of γH2AX and 53BP1 foci was carried out as described in methods. Representative microscopical fluorescence pictures are shown; blue: DAPI-stained nuclei, green: GFP signal, red: γH2AX (Ser139), yellow: 53BP1. Scale bar: 10 µm. **B** Quantification of γH2AX and 53BP1 foci formation, as well as colocalization of these foci in *mRac1* silenced cells expressing GFP-hRAC1(WT) or GFP-NLS-hRAC1(WT). Foci of each nucleus were counted (mean+SD; n=3 - 38 with 50 nuclei counted per experiment; *p ≤ 0.05 compared to cells treated with Dox (TR); one-way ANOVA with Dunnett post-hoc test; ##p ≤ 0.01 compared to cells treated with Dox (TR), 2-way ANOVA with Dunnett post-hoc test; $p ≤ 0.05 compared to GFP-hRAC1(WT) expression treated with Dox, 2-way ANOVA with Tukey post-hoc test; °°p ≤ 0.01

compared to GFP-NLS-hRAC1(WT) expression treated with Dox, 2-way ANOVA with Tukey post-hoc test). The data underlying the graph are shown in Table 7.25 of the appendix. Abbreviations: TR Con, TR: cells treated with TransIT-X2 only or treated with Lipofectamine RNAiMAX and TransIT-X2, WT: wild-type RAC1, NLS-WT: wild-type RAC1 with additional NLS.

Surprisingly, in cells with silenced *mRac1* gene and expression of human GFP-RAC1(Q61L) foci formation was reduced by 70 % (53BP1) to 80 % (γH2AX) as opposed to TR cells with Dox monotreatment. In opposite, expression of GFP-NLS-hRAC1(Q61L) with simultaneous *mRac1* knockdown increased the Dox-induced foci formation compared to the Dox-treated cells with silenced *mRac1* gene. The combination of constitutively active hRAC1 forced to the nucleus and transfection with *mRac1* siRNA restored the foci formation after Dox to the level of cells without *mRac1* knockdown (Figure 3.25). The additional transfection with *GFP-hRAC1(Q61L)* expression vector in cells with silenced *mRac1* decreased the Dox-induced foci formation by about 80 % compared to the mainly cytoplasmic constitutively active hRAC1 expressing cells without *mRac1* manipulation. In contrast to this, the Dox-induced foci formation was induced by about 40 % in *mRac1* silenced MEF expressing GFP-NLS-hRAC1(Q61L) compared to Dox-treated MEF expressing GFP-NLS-hRAC1(Q61L) alone.

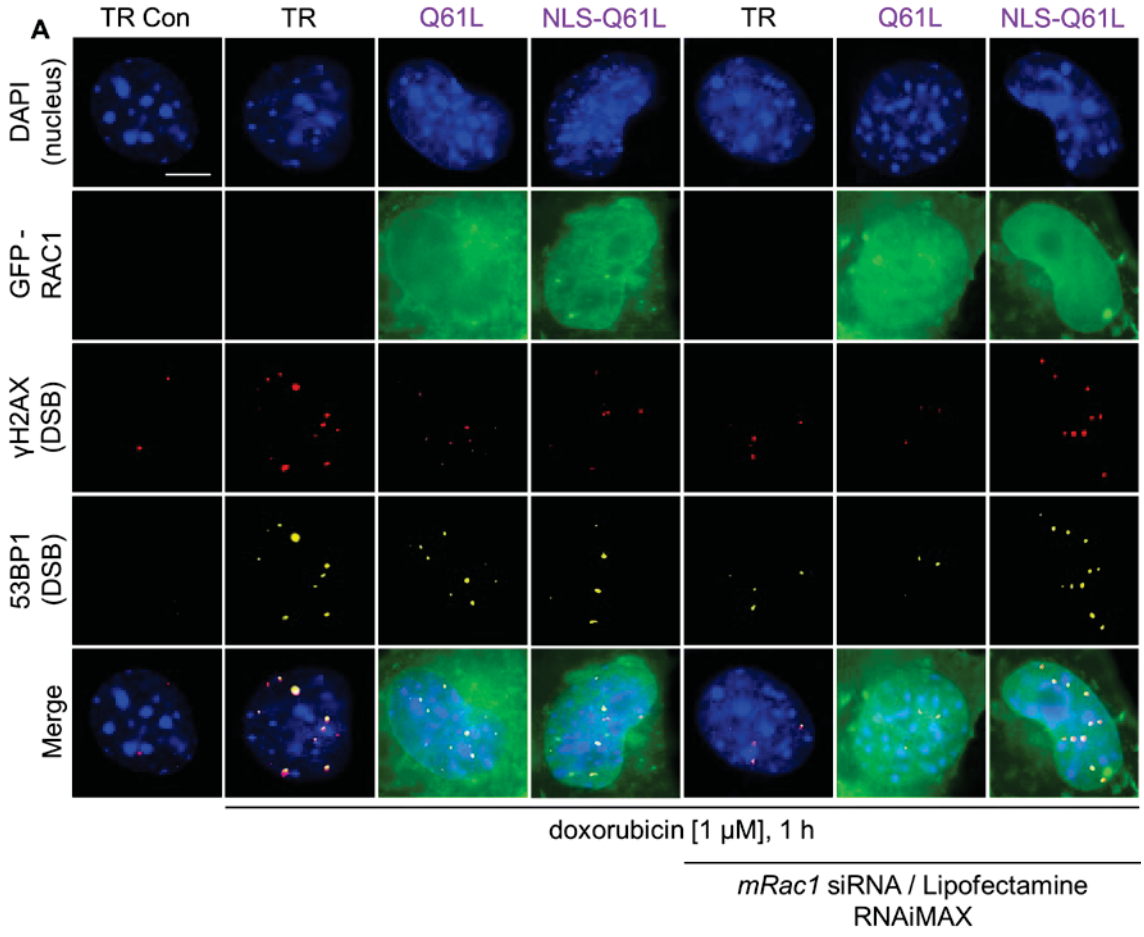

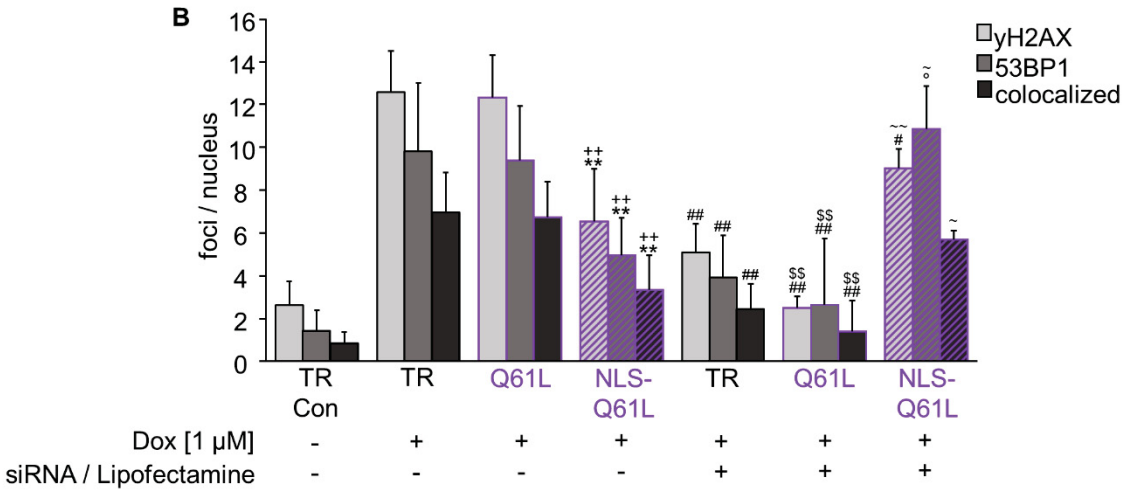

Figure 3.25: Influence of GFP-hRAC1(Q61L) with or without additional NLS on doxorubicin-induced foci formation in *mRac1* silenced.
mRac1 knockdown was achieved by transfection with *mRac1* siRNA. The treatment scheme is shown in material and methods (Figure 2.1 E, F). Cells were additionally transfected with *GFP-hRAC1(Q61L)* or *GFP-NLS-hRAC1(Q61L)* expression vector. **A** After the end of the Dox treatment, cells were fixed and staining of γH2AX and 53BP1 foci was carried out as described in methods. Representative microscopical fluorescence pictures are shown; blue: DAPI-stained nuclei, green: GFP signal, red: γH2AX (Ser139), yellow: 53BP1. Scale bar: 10 µm. **B** Quantification of γH2AX and 53BP1 foci formation, as well as colocalization of these foci in *mRac1* silenced cells expressing GFP-hRAC1(Q61L) or GFP-NLS-hRAC1(Q61L). Foci of each nucleus were counted (mean+SD; n=3 - 38 with 50 nuclei counted per experiment; $^{**}p \leq 0.01$ compared to cells treated with Dox (TR); one-way ANOVA with Dunnett post-hoc test; $^{++}p \leq 0.01$ compared to GFP-hRAC1(Q61L) expression treated with Dox, T-test, unpaired, two-sided; $^{\#}p \leq 0.05$, $^{\#\#}p \leq 0.01$ compared to cells treated with Dox (TR), 2-way ANOVA with Dunnett post-hoc test, $^{\$\$}p \leq 0.01$ compared to GFP-hRAC1(Q61L) expression treated with Dox, 2-way ANOVA with Tukey post-hoc test, $^{\sim}p \leq 0.0$, $^{\sim\sim}p \leq 0.01$ compared to GFP-hRAC1(Q61L) expression and m*Rac1* silencing treated with Dox, 2-way ANOVA with Tukey post-hoc test; $^{\circ}p \leq 0.05$ compared to GFP-NLS-hRAC1(Q61L) expression treated with Dox, 2-way ANOVA with Tukey post-hoc test). The data underlying the graph are shown in Table 7.26 of the appendix. Abbreviations: TR Con, TR: cells treated with TransIT-X2 only or treated with Lipofectamine RNAiMAX and TransIT-X2, Q61L: constitutively active RAC1, NLS-Q61L: constitutively active RAC1 with additional NLS.

Since expression of GFP-NLS-hRAC1(Q61L) decreased the Dox-induced γH2AX and 53BP1 foci formation (in cells without *mRac1* silencing) whereas expression of GFP-NLS-hRAC1(Q61L) in mRAC1 knockdown cells restored the Dox-induced γH2AX and 53BP1 foci formation to the original level of Dox-treated cells, it can be concluded that nuclear and cytoplasmic constitutively active hRAC1 have different effects on the Dox-induced DDR.

3.2.5.4 Comparison of mainly cytosolic and targeted nuclear expression of wild-type and constitutively active hRAC1, EHT 1864, and *mRac1* siRNA on doxorubicin induced γH2AX and 53BP1 foci formation.

For better comparison of the different DDR modulators in cells transfected with *hRAC1* mutants as well as the difference in mainly cytoplasmic and forced nuclear expression of hRAC1, the results obtained were combined in one single graph. Dox-induced γH2AX and 53BP1 foci formation was reduced by ~15 - 25 % in wild-type hRAC1 expressing cells independent of an additional NLS. Pre-treatment with EHT 1864 as well as transfection with *mRac1* siRNA combined with expression of GFP-hRAC1(WT) with or without additional NLS reduced the Dox-induced foci formation by ~55 - 75 %. There was no significant difference between mainly cytoplasmic and forced nuclear expression of wild-type hRAC1 (Figure 3.26).

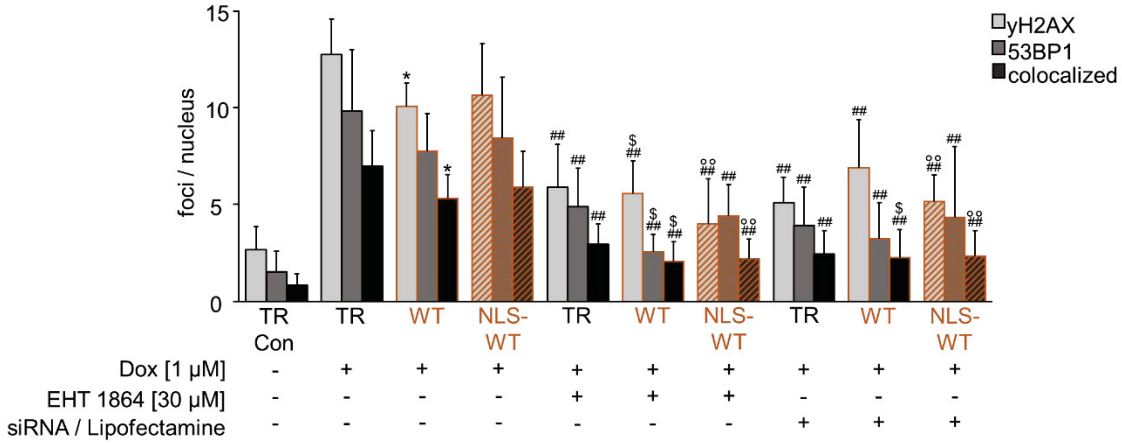

Figure 3.26: Comparison of GFP-hRAC1(WT) with and without additional NLS, EHT 1864, and *mRac1* siRNA on doxorubicin induced γH2AX and 53BP1 foci formation.
Cells were transfected with *GFP-hRAC1(WT)* or *GFP-NLS-hRAC1(WT)* expression vector. Transfection control cells (TR Con, TR) were treated with TransIT-X2 only or with Lipofectamine RNAiMAX and TransIT-X2. 24 h after transfection cells were pre-treated with 30 µM EHT 1864 for 3 h prior to treatment with Dox [1 µM, 1 h] or were only treated with Dox [1 µM, 1 h]. *mRac1* knockdown was achieved by transfection with *mRac1* siRNA. The treatment scheme is shown in material and methods (Figure 2.1 E, F). Cells were additionally transfected with *GFP-hRAC1(WT)* or *GFP-NLS-hRAC1(WT)* expression vector. Quantification of γH2AX and 53BP1 foci formation, as well as colocalization of these foci. Foci of each nucleus were counted (mean+SD; n=3 - 38 with 50 nuclei counted per experiment; *$p \leq 0.05$ compared to cells treated with Dox (TR) one-way ANOVA with Dunnett post-hoc test; $^{\#\#}p \leq 0.01$ compared to cells treated with Dox (TR), 2-way ANOVA with Tukey post-hoc test; $^{\$}p \leq 0.05$ compared to GFP-hRAC1(WT) treated with Dox, 2-way ANOVA with Tukey post-hoc test; $^{\circ\circ}p \leq 0.01$ compared to GFP-NLS-hRAC1(WT) expressing cells treated with Dox, 2-way ANOVA with Tukey post-hoc test). The data underlying the graph are shown in Table 7.27 of the appendix. Abbreviations: TR Con: cells treated with TransIT-X2, TR: cells treated with TransIT-X2 only or treated with Lipofectamine RNAiMAX and TransIT-X2, WT: wild-type RAC1, NLS-WT: wild-type RAC1 with additional NLS.

Pre-treatment with EHT 1864 reduced the Dox-induced foci formation by ~40 - 60 % in constitutively active hRAC1 expressing cells (with and without additional NLS). Expression of GFP-NLS-hRAC1(Q61L) exhibited the same phenotype regarding Dox-induced foci formation as cells expressing mainly cytoplasmic or forced nuclear dominant-negative hRAC1. Monotreatment with Dox reduced the foci formation by ~50 % in GFP-NLS-hRAC1(Q61L) expressing cells whereas cells expressing mainly cytoplasmic constitutively active hRAC1 exhibited no change in Dox-induced foci formation in comparison to non-transfected cells. Transfection with *mRac1* siRNA combined with the expression of GFP-NLS-hRAC1(Q61L) restored the foci formation after Dox to the level of cells without *mRac1* knockdown. Combined transfection of *mRac1* siRNA with *GFP-hRAC1(Q61L)* expression vector could not restore the Dox-induced foci formation. The combination rather decreased the foci by ~75 - 80 % compared to cells without *mRac1* knockdown (Figure 3.27). This implicates that active (GTP-bound) nuclear RAC1 is essential for a pronounced doxorubicin-induced DDR.

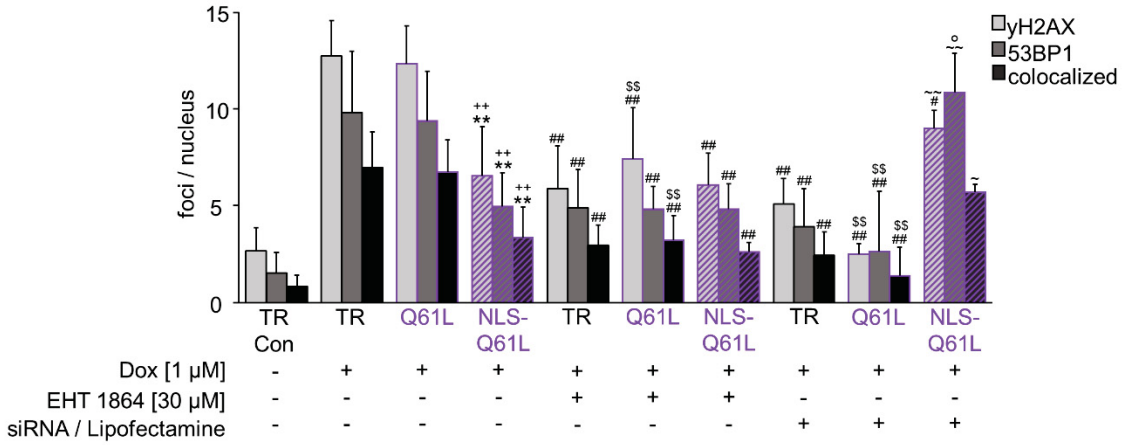

Figure 3.27: Comparison of GFP-hRAC1(Q61L) with and without additional NLS, EHT 1864, and *mRac1* siRNA on doxorubicin induced γH2AX and 53BP1 foci formation.
Cells were transfected with *GFP-hRAC1(Q61L)* or *GFP-NLS-hRAC1(Q61L)* expression vector. Transfection control cells (TR Con, TR) were treated with TransIT-X2 only or with Lipofectamine RNAiMAX and TransIT-X2. 24 h after transfection cells were pre-treated with 30 µM EHT 1864 for 3 h prior to treatment with Dox [1 µM, 1 h] or were only treated with Dox [1 µM, 1 h]. *mRac1* knockdown was achieved by transfection with *mRac1* siRNA. The treatment scheme is shown in material and methods (Figure 2.1 E, F). Cells were additionally transfected with *GFP-hRAC1(Q61L)* or *GFP-NLS-hRAC1(Q61L)* expression vector. Quantification of γH2AX and 53BP1 foci formation, as well as colocalization of these foci. Foci of each nucleus were counted (mean+SD; n=3 - 38 with 50 nuclei counted per experiment; $^{**}p \leq 0.01$ compared to cells treated with Dox (TR) one-way ANOVA with Dunnett post-hoc test; $^{\#}p \leq 0.05$, $^{\#\#}p \leq 0.01$ compared to cells treated with Dox (TR), 2-way ANOVA with Tukey post-hoc test; $^{++}p \leq 0.01$ compared to GFP-hRAC1(Q61L) treated with Dox, T-test, unpaired, two-sided; $^{\$\$}p \leq 0.01$ compared to GFP-hRAC1(Q61L) treated with Dox, 2-way ANOVA with Tukey post-hoc test; $^{\sim}p \leq 0.05$, $^{\sim\sim}p \leq 0.01$ compared to *mRac1* siRNA + GFP-hRAC1(Q61L) treated with Dox, 2-way ANOVA with Tukey post-hoc test; $^{\circ}p \leq 0.05$ compared to GFP-NLS-hRAC1(Q61L) treated with Dox, 2-way ANOVA with Tukey post-hoc test). The data underlying the graph are shown in Table 7.28 of the appendix. Abbreviations: TR Con: cells treated with TransIT-X2, TR: cells treated with TransIT-X2 only or

treated with Lipofectamine RNAiMAX and TransIT-X2, Q61L: constitutively active RAC1, NLS-Q61L: constitutively active RAC1 with additional NLS.

3.2.5.5 Influence of human GFP-RAC1(WT) and human GFP-RAC1(Q61L) with and without additional NLS on doxorubicin-induced pATM foci formation

Forced nuclear accumulation as well as cytoplasmic hRAC1 expression affected ATM-activated proteins (Figure 3.18, Figure 3.19). To investigate the hRAC1 involvement in activation of ATM in the Dox-induced DDR, pATM foci formation was evaluated.

Control experiments were performed beforehand and are shown in the appendix. There was no significant change in basal pATM foci number upon the used methods (Appendix, Figure 7.23).

Treatment with 1 µM Dox induced pATM foci in all transfected and non-transfected cells. Transfection with *GFP-hRAC1* expression vectors with and without additional NLS did not alter the amount of Dox-induced pATM foci as opposed to cells treated with TransIT-X2 and Dox (TR) (Figure 3.28). Cells with silenced *mRac1* showed a significant increase in pATM foci counts after doxorubicin contrary to non-transfected cells.

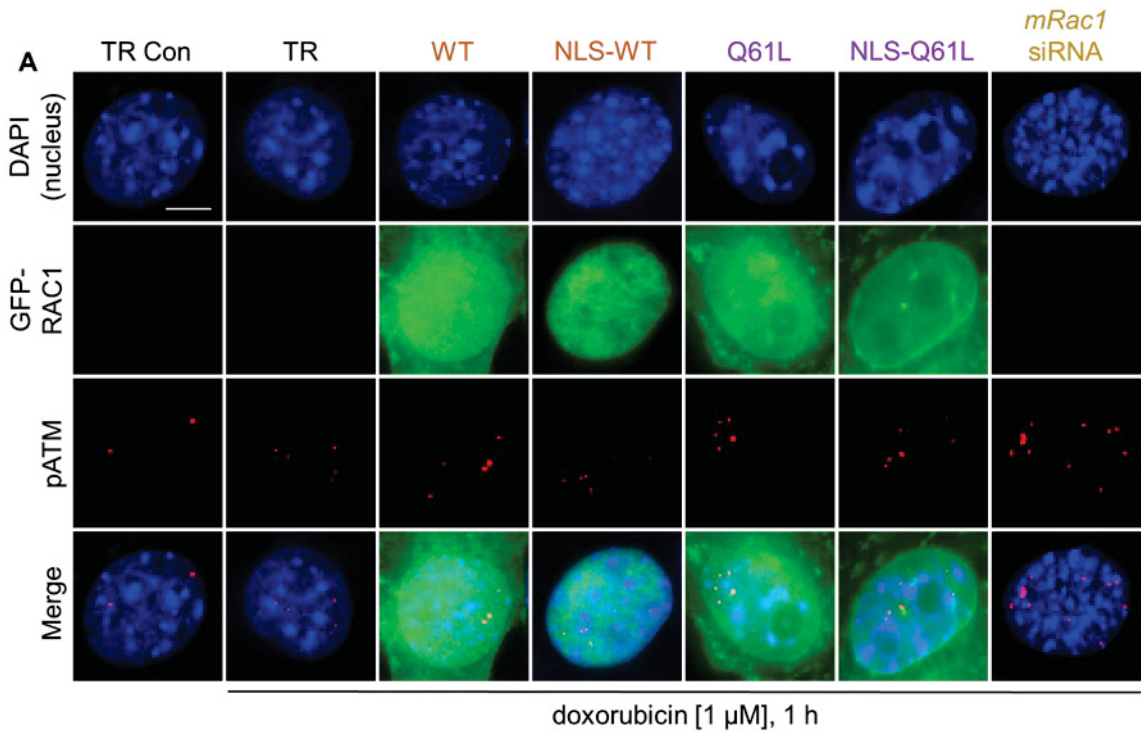

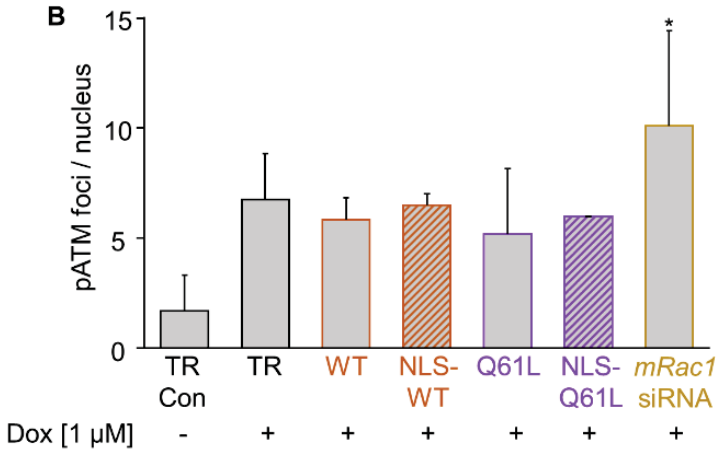

Figure 3.28: Influence of human GFP-RAC1 expression and *mRac1* gene silencing on doxorubicin-induced pATM foci formation.
Cells were transiently transfected with *GFP-hRAC1(WT)*, *GFP-NLS-hRAC1(WT)*, *GFP-hRAC1(Q61L)* or *GFP-NLS-hRAC1(Q61L)* expression vector or *mRac1* siRNA. Transfection control cells (TR Con, TR) were treated with TransIT-X2. 24 h after transfection with *GFP-hRAC1* expression vectors or 48 h after transfection with *mRac1* siRNA cells were treated with Dox [1 µM, 1 h]. **A** After the end of the Dox treatment, cells were fixed and staining of pATM foci was carried out as described in methods. Representative microscopical fluorescence pictures are shown; blue: DAPI-stained nuclei, green: GFP signal, red: pATM. Scale bar: 10 µm. **B** Quantification of pATM foci formation. Foci of each nucleus were counted (mean+SD; n=1 - 18 with 50 nuclei counted per experiment; *p ≤ 0.05 compared to Dox treated cells (TR), one-way ANOVA with Dunnett post-hoc test). The data underlying the graph are shown in Table 7.29 of the appendix. Abbreviations: TR Con, TR: cells treated with TransIT-X2, WT: wild-type RAC1, NLS-WT: wild-type RAC1 with additional NLS, Q61L: constitutively active RAC1, NLS-Q61L: constitutively active RAC1 with additional NLS, *mRac1* siRNA: siRNA against murine *Rac1*.

In conclusion, mainly cytoplasmic as well as forced nuclear expression of wild-type/constitutively active hRAC1 had no effect on pATM foci formation. Nevertheless, RAC1 might influence Dox-induced origination of the aforementioned foci since *mRac1* silencing induced appearance of pATM foci. It would have been expected that cells transfected with *GFP-hRAC1(T17N)* expression vector with and without additional NLS (Figure 3.16) show a similar phenotype as cells transfected with *mRac1* siRNA in Dox-induced pATM foci formation. Since this is not the case, the role of RAC1 in Dox-induced pATM foci formation needs to be further investigated in future experiments.

3.3 Influence of a forced RAC1 translocation to the nucleus on the ionizing radiation-induced foci formation

The data so far show a role of RAC1 in the doxorubicin-induced DDR. Previous work already presented a connection between RAC1 and Top II poisons (Henninger et al. 2012; Huelsenbeck et al. 2012; Wartlick et al. 2013). To answer the question whether the observed effects are specific for Top II poisons like doxorubicin or if they are similar for different types of DSB-inducing agents, IR was used since it induces DSB independent of Top II.

Performed control experiments are shown in the appendix. Even though IR-induced 53BP1 foci were significantly decreased in *GFP* expression vector transfected cells compared to non-transfected cells it had no influence on foci formation upon IR treatment since this decrease was not observed in all cells expressing GFP-hRAC1 mutants (Appendix, Figure 7.24).

For DSB-induction doses of 1 Gy and 3 Gy were used. Irradiation with 1 Gy induced an average formation of ~17 γH2AX and ~13 53BP1 foci per cell in TR control cells (TR). Expression of mainly cytoplasmic human GFP-RAC1(WT) as well as predominantly nuclear expression of wild-type hRAC1 had no influence on IR-induced γH2AX and 53BP1 foci formation (Figure 3.29).

Irradiation with 3 Gy induced an average formation of ~25 γH2AX and 20 53BP1 foci per cell in TR control cells (TR). A similar number of foci was visible in irradiated cells transfected with *GFP-hRAC1(WT)* expression vector contrary to the TR control cells (TR) (Figure 3.29). The number of colocalized γH2AX and 53BP1 foci was significantly decreased in GFP-hRAC1(WT) expressing cells. However, upon irradiation with 3 Gy γH2AX and 53BP1 foci formation as well as colocalization of these foci was significantly reduced in GFP-NLS-hRAC1(WT) expressing cells (Figure 3.29).

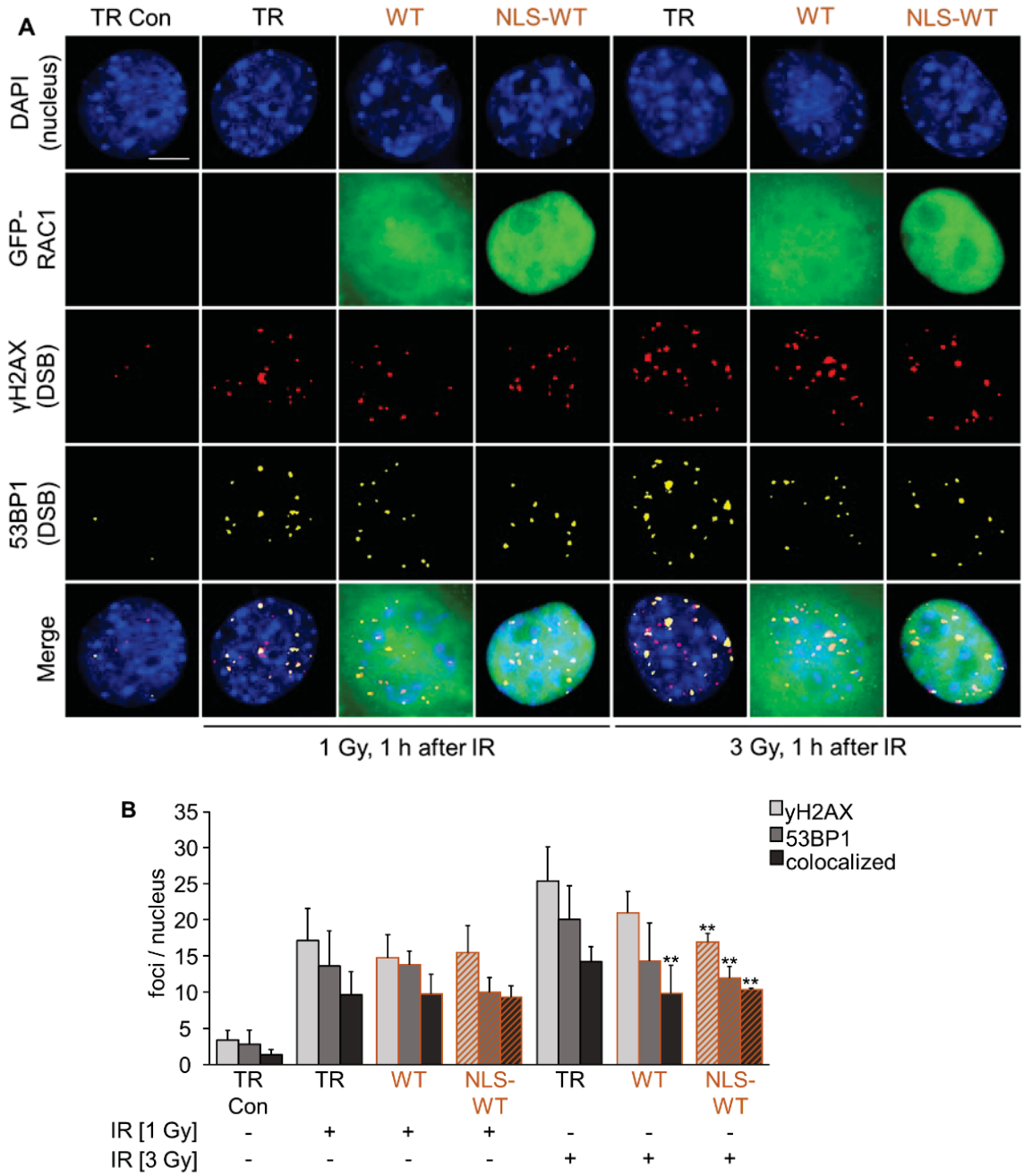

Figure 3.29: Influence of GFP-hRAC1(WT) with or without additional NLS on IR-induced γH2AX and 53BP1 foci formation.
Cells were transiently transfected with *GFP-hRAC1(WT)* or *GFP-NLS-hRAC1(WT)* expression vector. Transfection control cells (TR Con, TR) were treated with TransIT-X2. 24 h after transfection cells were irradiated [1 Gy, 3 Gy]. **A** 1 h after treatment with IR, cells were fixed and staining of γH2AX and 53BP1 foci was carried out as described in methods. Representative microscopical fluorescence pictures are shown; blue: DAPI-stained nuclei, green: GFP signal, red: γH2AX (Ser139), yellow: 53BP1. Scale bar: 10 µm. **B** Quantification of γH2AX and 53BP1 foci formation, as well as colocalization of these foci. Foci of each nucleus were counted (mean+SD; n=3 - 18 with 50 nuclei counted per experiment; **p ≤ 0.01 compared to TR [3 Gy]; one-way ANOVA with Dunnett post-hoc test). The data underlying the graph are shown in Table 7.30 of the appendix. Abbreviations: TR Con, TR: cells treated with TransIT-X2, WT: wild-type RAC1, NLS-WT: wild-type RAC1 with additional NLS.

Expression of GFP-hRAC1(Q61L) or GFP-NLS-hRAC1(Q61L) had no influence on foci formation following irradiation with 1 Gy as well as 3 Gy (Figure 3.30).

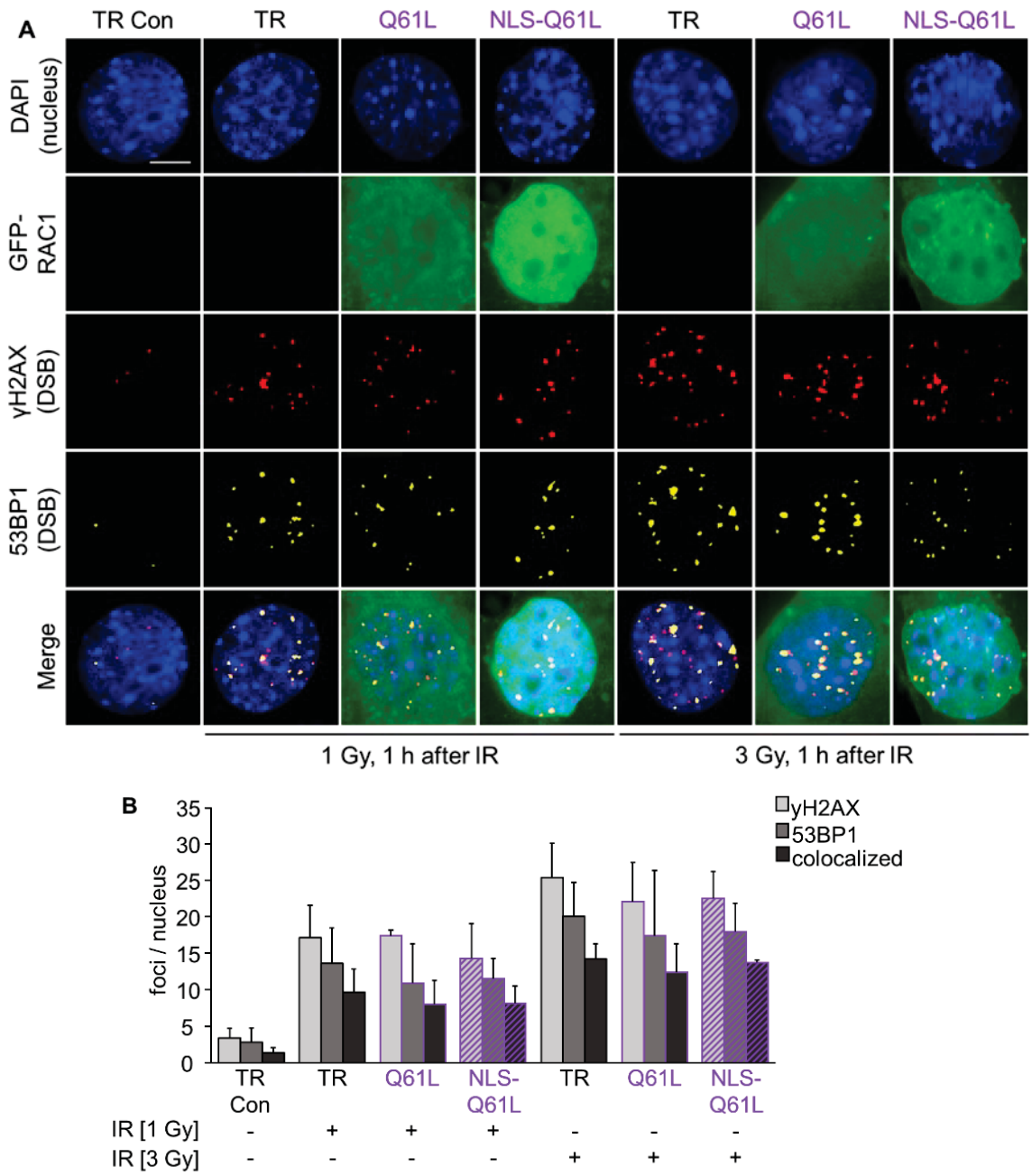

Figure 3.30: Influence of GFP-hRAC1(Q61L) with or without additional NLS on IR-induced γH2AX and 53BP1 foci formation.
Cells were transiently transfected with *GFP-hRAC1(Q61L)* or *GFP-NLS-hRAC1(Q61L)* expression vector. Transfection control cells (TR Con, TR) were treated with TransIT-X2. 24 h after transfection cells were irradiated [1 Gy, 3 Gy]. **A** 1 h after treatment with IR, cells were fixed and staining of γH2AX and 53BP1 foci was carried out as described in methods. Representative microscopical fluorescence pictures are shown; blue: DAPI-stained nuclei, green: GFP signal, red: γH2AX (Ser139), yellow: 53BP1. Scale bar: 10 µm. **B** Quantification of γH2AX and 53BP1 foci formation, as well as colocalization of these foci. Foci of each nucleus were counted (mean+SD; n=3 - 18 with 50 nuclei counted per experiment). The data underlying the graph are shown in Table 7.31 of the appendix. Abbreviations: TR Con, TR: cells treated with TransIT-X2, Q61L: constitutively active RAC1, NLS-Q61L: constitutively active RAC1 with additional NLS.

Expression of GFP-hRAC1(T17N) had no influence on 1 Gy-induced γH2AX and 53BP1 foci formation (Figure 3.31). The only significant reduction of γH2AX foci (about 35 % less foci) compared to TR control cells (TR) was seen upon irradiation with 1 Gy of GFP-NLS-hRAC1(T17N) expressing cells (Figure 3.31). Expression of dominant-negative hRAC1 (with and without additional NLS) had no influence on foci formation following irradiation with 3 Gy (Figure 3.31)

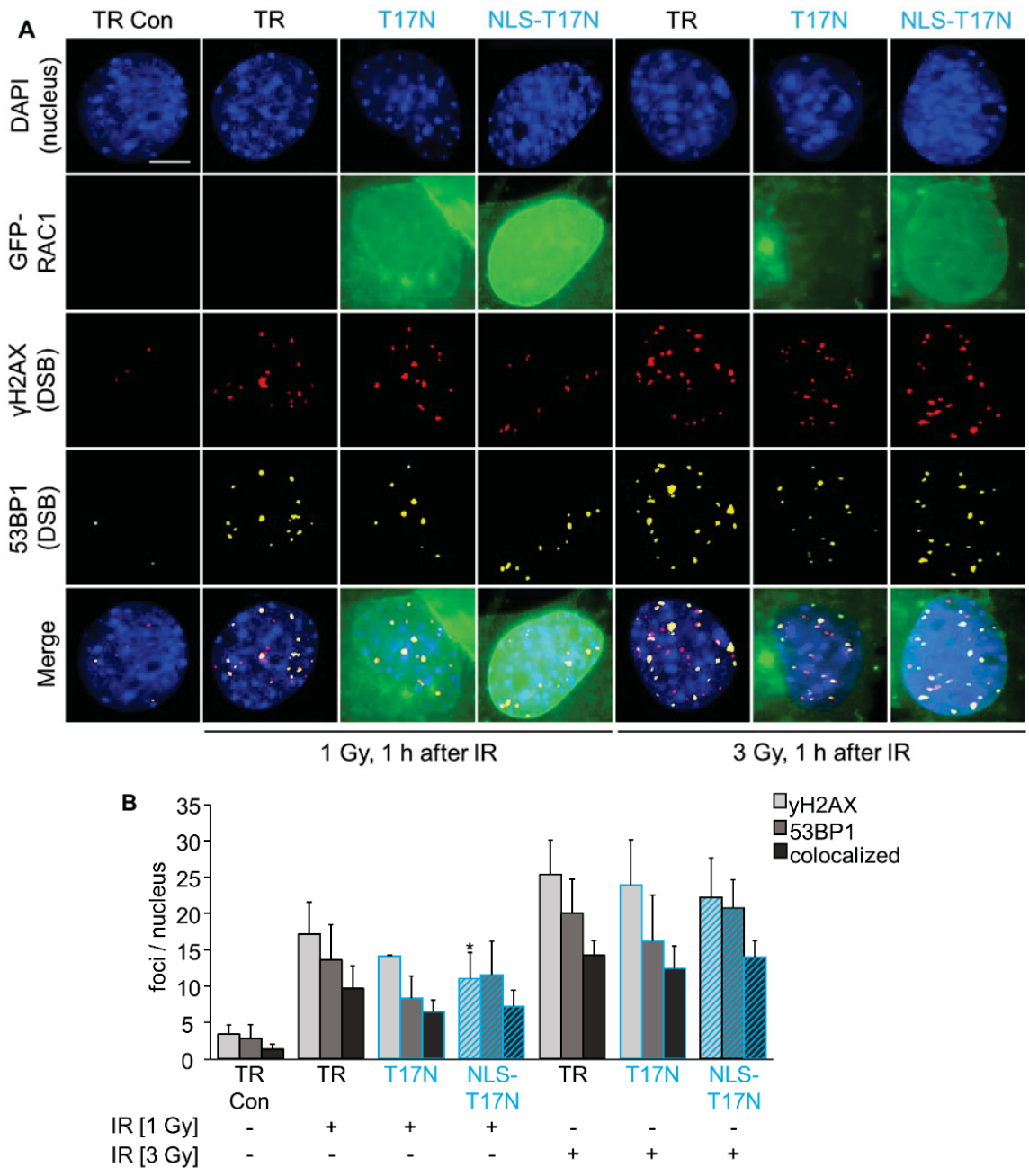

Figure 3.31: Influence of GFP-hRAC1(T17N) with or without additional NLS on IR-induced γH2AX and 53BP1 foci formation.
Cells were transiently transfected with *GFP-hRAC1(T17N)* or *GFP-NLS-hRAC1(T17N)* expression vector. Transfection control cells (TR Con, TR) were treated with TransIT-X2. 24 h after transfection cells were irradiated [1 Gy, 3 Gy]. **A** 1 h after treatment with IR, cells were fixed and staining of γH2AX and 53BP1 foci was carried out as described in methods. Representative

microscopical fluorescence pictures are shown; blue: DAPI-stained nuclei, green: GFP signal, red: γH2AX (Ser139), yellow: 53BP1. Scale bar: 10 µm. **B** Quantification of γH2AX and 53BP1 foci formation, as well as colocalization of these foci. Foci of each nucleus were counted (mean+SD; n=3 - 18 with 50 nuclei counted per experiment; *p ≤ 0.05 compared to TR [1 Gy]; one-way ANOVA with Dunnett post-hoc test). The data underlying the graph are shown in Table 7.32 of the appendix. Abbreviations: TR Con, TR: cells treated with TransIT-X2, T17N: dominant-negative RAC1, NLS-T17N: dominant-negative RAC1 with additional NLS.

It can be stated that the detected effects of both mainly cytoplasmic and forced nuclear hRAC1 on the DDR seem to be rather doxorubicin-specific, although a dose-dependent effect on the IR-induced DDR was seen in GFP-hRAC1(WT) as well as GFP-NLS-hRAC1(WT) expressing cells.

In summary, targeted nuclear expression of dominant-negative hRAC1 as well as constitutively active hRAC1 disclosed similar effects, namely a reduced number of Dox-induced γH2AX and 53BP1 foci. Only cells expressing constitutively active hRAC1 showed a difference between mainly cytosolic and forced nuclear hRAC1 expression in regard to Dox-induced foci formation. This implicates that active (GTP-bound) nuclear RAC1 is essential for a pronounced doxorubicin-induced DDR. Furthermore, RAC1 seems to have downstream DDR functions beyond the involvement in DSB formation. The signal of phosphorylated protein (pP53, pKAP1, γH2AX) was depending on the time-point of analysis and/or the presence or absence of an additional NLS in the fusion proteins. Apparently RAC1 not only influences the formation of DSB following Dox treatment but also the DDR signaling after the DSB are formed. Since cells expressing hRAC1 mutants exhibited no influence on the Dox-induced pATM Ser1981 foci formation, RAC1 seems to act downstream of ATM in the DDR. The following experiments were made to generate a stable *mRac1* knockout cell line and to completely eliminate the endogenous mRAC1 for further elucidation of the role of RAC1 in the DDR.

3.4 Generation of *mRac1* knockout cells

3.4.1 Lentiviral transduction with Puro.Cre vector to induce *mRac1* knockout in mouse embryonic fibroblasts with *mRac1* gene flanked by loxP sites

For reduction of endogenous mRAC1 different approaches were used so far. The pharmacological inhibition of endogenous mRAC1 was achieved with EHT 1864. For downregulation of endogenous *mRac1*, MEF were transfected with *mRac1* siRNA. The aim of the following experiments was to generate *mRac1* knockout cells. Hereby, the influence of endogenous murine RAC1 should be completely excluded in the experiments, leading to a cleaner experimental setup. After successful knockout, the cells could be re-transfected with the human *GFP-RAC1* mutants with and without additional NLS to analyze the role of the human RAC1 in the DDR.

The used MEF cells were derived from $Rac1^{flx/flx}$ Mx1-Cre-loxP mice which have been described in previous work (Bopp et al. 2015). The *mRac1* gene of the cells is partially flanked by loxP sites. The Cre/loxP system is a site-specific recombinase technology and Cre, as a site-specific DNA recombinase, catalyzes the recombination of DNA between loxP sequences. In the used MEF the loxP sites are located between exon 3 and 4, as well as between exon 5 and 6 of the *mRac1* gene (Figure 3.32). Cre recombinase will therefore cut out exon 4 and 5 (1400 bp), which is leading to a truncation and a frame shift mutation causing a non-functional *Rac1* gene product (Walmsley et al. 2003). The used cells have an intrinsic Cre recombinase which is under control of the Mx-1 promoter as described under 2.2.1.1 (Bopp et al. 2015). The Mx-1 promoter/the intrinsic Cre recombinase can be induced by treatment with Poly(I:C) or interferon. Since the cells were not interferon responsive *in vitro*, the Cre remained in its inactive state (data not shown). Due to the already existing loxP sites the decision was made to use lentiviral transduction of and additional Cre recombinase as tool to induce a genetic *mRac1* knockout in MEF.

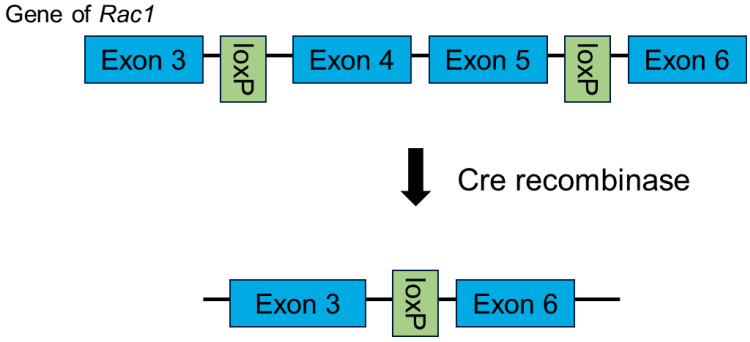

Figure 3.32: Schematic representation of the *mRac1* gene flanked by loxP sites.

LoxP sites were inserted between exon 3 and 4, as well as between exon 5 and 6 (Walmsley et al. 2003; Bopp et al. 2015). After addition of Cre recombinase (in the following experiments by viral transduction) exon 4 and 5 should be cut out, leading to a frameshift mutation in the *mRac1* gene.

A lentivirus containing the gene for Cre recombinase as well as a transgene cassette with a resistance gene (puromycin) was used for the generation of *mRac1* knockout MEF. The vector which delivered the genes for Cre recombinase and puromycin resistance was a Puro.Cre empty vector. The lentivirus/viral supernatant for introducing the *mRac1* knockout was produced as described under 2.2.1.5. 24 h after viral transduction a selection with puromycin was started to discriminate between transduced and non-transduced cells and afterwards cells were analyzed for knockout efficiency and/or cell cycle distribution. Calculation of knockout efficiency is described under 2.2.2.7.2.

As no published data were available of the used cell line regarding viral transduction, different concentrations of the virus supernatant were used to define the optimal amount of lentivirus. With the different concentrations (diluted and undiluted virus supernatant) a low transduction efficiency should be avoided, which can occur due to insufficient amount of lentivirus (Shalem et al. 2014). Another reason for testing different dilutions of the virus supernatant is the possible sensitive reaction of the MEF cells to lentiviral treatment which could result in low viability. Protamine phosphate (PP) was added during transduction to some samples to check whether this improves the transduction efficiency. PP is a positively charged polycation and reduces the repulsion forces between the virus and the cell (Denning et al. 2013; Gouvarchin Ghaleh et al. 2020). 24 h after the transduction puromycin was added for selection for puromycin resistant (Cre expressing and potential *mRac1* knockout) cells. The selection dose of puromycin was determined beforehand. For this, MEF without puromycin resistance were treated with ascending concentrations of puromycin and the dose which caused 100 % cell death [2 µg/ml] within one week was used for further experiments. Incubation with puromycin [2 µg/ml] was continued for 144 h.

As control for a possible cytotoxicity of the viral transduction itself, MEF without loxP sites (*Rac1*$^{wt/wt}$) were transduced with different dilutions of Puro.Cre expression vector. The viral supernatant used for transduction itself is not cytotoxic (Appendix, Figure 7.25).

Viral supernatant was applied undiluted and 1:2 diluted to MEF with loxP sites (*Rac1*$^{flx/flx}$) to define a suitable concentration to induce *mRac1* knockout and to exclude non-specific cytotoxicity. After puromycin-based selection and consecutive DNA-extraction a real-

time qPCR was performed to evaluate the *mRac1* knockout efficiency (Figure 3.33). The highest achieved knockout efficiency was ~50 % in cells transduced with the undiluted Puro.Cre vector and without protamine phosphate. Using 1:2 diluted Puro.Cre vector a knockout efficiency of almost 40 % was achieved. The addition of protamine phosphate did not significantly affect the knockout efficiency and was omitted in following experiments.

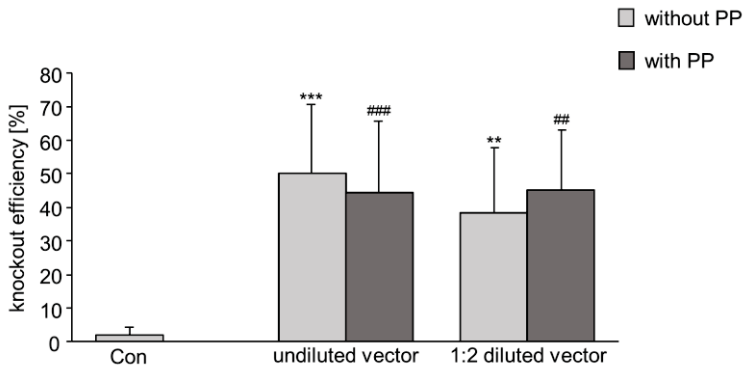

Figure 3.33: Real-time qPCR analysis of *mRac1* knockout efficiency after lentiviral transduction with Puro.Cre vector in mouse embryonic fibroblasts with *mRac1* flanked by loxP sites (*Rac1*$^{flx/flx}$).
Cells were transduced with two concentrations of Puro.Cre vector (undiluted, 1:2 diluted) with and without protamine phosphate. Control cells (*Rac1*$^{flx/flx}$) were left non-transduced. 24 h later puromycin selection was started. 144 h post transduction cells were analyzed by real-time qPCR. Mean values and standard deviation are shown (mean+SD; n=5 - 7; **p ≤ 0.01, ***p ≤ 0.001; compared to Con; one-way ANOVA with Dunnett post-hoc test; ##p ≤ 0.01, ###p ≤ 0.001 compared to Con, 2-way ANOVA with Dunnett post-hoc test). Abbreviations: Con: non-transduced control cells (*Rac1*$^{flx/flx}$), PP: protamine phosphate. The data underlying the graph are shown in Table 7.33 of the appendix.

Furthermore, the cell cycle distribution and apoptotic fraction of cells (*Rac1*$^{flx/flx}$) transduced with undiluted Puro.Cre vector was analyzed by flow cytometry. For this purpose, cells were lysed, and the nuclei were stained with the DNA-intercalating agent propidium iodide. A typical cell cycle profile of untreated cells reveals a G0/G1 peak (2n) and a G2 peak (4n), whereby G2 peak shows double the fluorescence intensity of the G0/G1 peak. The fluorescence intensity of cells in S phase is somewhere between the intensities of G0/G1 peak and G2 peak. The so-called SubG1 fraction represents cells with sub-diploid DNA content and thus are considered as apoptotic cells (Darzynkiewicz et al. 1997).

Control samples (non-transduced MEF (*Rac1*$^{flx/flx}$)) and Puro.Cre transduced samples were harvested 144 h after transduction. The potential *mRac1* knockout in puromycin resistant cells resulted in a drastic increase in SubG1 fraction, which represents the apoptotic cell population (Figure 3.34). Unfortunately, puromycin resistant cells exhibited

over 90 % cells in the apoptotic fraction. The question which arose was what is responsible for the cell death of transduced cells, since the viral supernatant itself was not cytotoxic. Two possibilities are conceivable (i) the used concentration of puromycin killed the cells, (ii) caspases might get activated upon transduction. Since the MEF without loxP sites (*Rac1*$^{wt/wt}$) did not show an increased cell death upon transduction (Appendix, Figure 7.25), the possible activation of caspases is probably associated with *mRac1* knockout. The aim was at least 75 % *mRac1* knockout efficiency. Due to the fact, that RAC1 is involved in the adherence of cells and previously published work described a round cell type after treatment with statins (pan Rho GTPases inhibitor) (Koch et al. 1997), cells with *mRac1* knockout might not be as firmly attached to the surface of the cell culture dishes as cells without *mRac1* knockout. In consequence, *mRac1* knockout cells could be lost by washing steps during the selection procedure leading to a negative impact on the *mRac1* knockout efficiency.

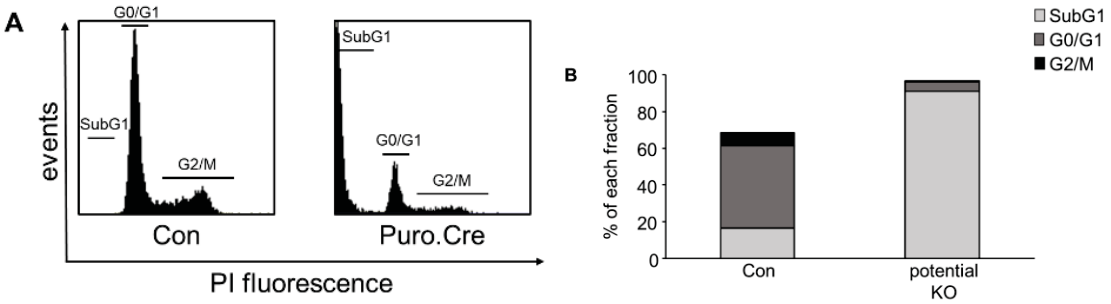

Figure 3.34: Flow cytometric analysis of cell cycle distribution and apoptosis after lentiviral transduction with Puro.Cre vector in mouse embryonic fibroblasts with *mRac1* flanked by loxP sites *(Rac1*$^{flx/flx}$*)*.
Cells were transduced with undiluted Puro.Cre vector and analyzed 144 h after puromycin selection. Control cells (*Rac1*$^{flx/flx}$) were left non-transduced. Cells were lysed and the nuclei were stained with the DNA-intercalating agent propidium iodide. The cell cycle distribution was determined using a flow cytometer. Shown is the evaluation of the different fractions. Shown are representative cell cycle distributions (**A**) and the evaluation of the different fractions (**B**) (n=1). Abbreviations: Con: non-transduced control cells (*Rac1*$^{flx/flx}$), potential KO: cells transduced with Puro.Cre and selected with puromycin. The data underlying the graph are shown in Table 7.34 of the appendix. Abbreviations: SubG1: apoptotic cell fraction, G0/G1: fraction of cells in state of quiescence/growth phase, G2/M: fraction of cells in growth phase (preparation for mitosis)/mitosis.

To check whether a fraction of *mRac1* knockout cells were accidently excluded from evaluation, cells were washed with PBS after the selection procedure and detached cells were collected as “supernatant” for analysis. After indicated time-points a real-time qPCR was performed to evaluate the *mRac1* knockout efficiency (Figure 3.35). *mRac1* knockout efficiency increased over time in “supernatant” cells. This experiment confirmed that cells with *mRac1* knockout were not as properly attached to the surface of the cell culture dishes as cells without *mRac1* knockout and that there was a risk of

losing them. In consequence, these cells of interest might be washed away easily while changing the medium during the time until the cells were collected for analysis.

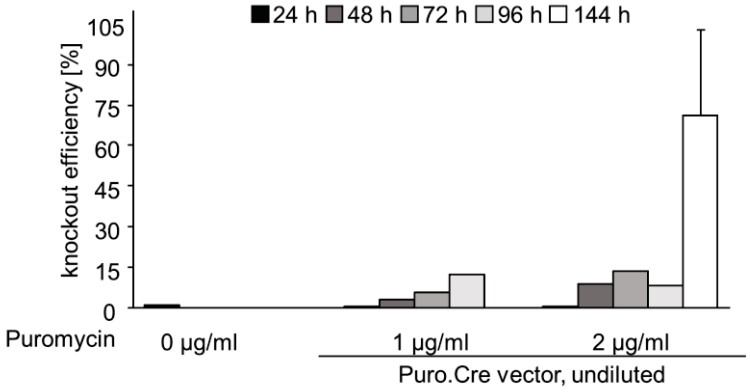

Figure 3.35: Real-time qPCR analysis of the *mRac1* knockout efficiency after lentiviral transduction with Puro.Cre vector in not properly attached mouse embryonic fibroblasts (*Rac1*$^{flx/flx}$).
Cells were transduced with undiluted Puro.Cre vector. 24 h later puromycin selection was started. 24 h - 144 h after transduction cells were washed with PBS and collected for real-time qPCR. Control cells (*Rac1*$^{flx/flx}$) were non-transduced. Mean values and standard deviation are shown (mean+SD; n=1 - 4). The data underlying the graph are shown in Table 7.35 of the appendix.

Regarding the previously asked questions whether the puromycin selection could be responsible for the detected cell death, MEF (*Rac1*$^{flx/flx}$) were transduced with an expression vector containing only puromycin resistance in the transgene cassette (Puro vector). Transduced cells without puromycin treatment showed about 15 % cells in the SubG1 fraction, this fraction was not significantly after treatment with puromycin (Figure 3.36). This increase might be due to the fact that not 100 % of the cells are transduced. Nevertheless, this experiment demonstrated that neither viral transduction nor puromycin selection is the reason for the increased cell death in MEF (*Rac1*$^{flx/flx}$) transduced with Puro.Cre expression vector.

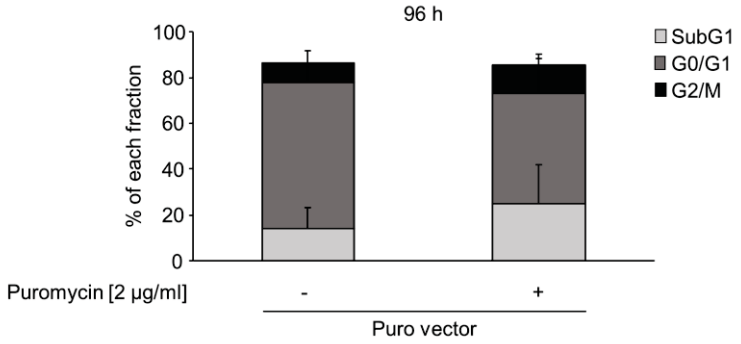

Figure 3.36: Impact of the transduction itself and/or puromycin treatment on cell death in MEF *(Rac1*$^{flx/flx}$*)* transduced with Puro vector (puromycin resistance only).
MEF *(Rac1*$^{flx/flx}$*)* were transduced with Puro vector and harvested 96 h later. Meanwhile puromycin selection was performed [2 µg/ml]. Cells were lysed and the nuclei were stained with the DNA-

intercalating agent propidium iodide. The cell cycle distribution was determined using a flow cytometer. Shown is the evaluation of the different fractions. Mean values and standard deviation are shown (mean+SD; n=3). The data underlying the graph are shown in Table 7.36 of the appendix. Abbreviations: SubG1: apoptotic cell fraction, G0/G1: fraction of cells in state of quiescence/growth phase, G2/M: fraction of cells in growth phase (preparation for mitosis)/mitosis.

Caspase activation plays a major role in apoptosis. Caspases are normally inactive and must be activated so a cell can undergo apoptosis. They are divided into pro-inflammatory caspases (caspase 1, 4, 5, 11, 12) and pro-apoptotic caspases (caspase 2, 3, 6, 7, 8, 9, 10). The pro-apoptotic caspases can be further divided into initiator caspases (caspase 2, 8, 9, 10) and effector caspases (caspase 3, 6, 7). Initiator caspases are linked to the initiation of apoptosis whereas effector caspases cleave cellular substrates which are needed for the survival of the cell. External and internal stimuli can trigger the activation of initiator caspases which in turn activate their substrates, the effector caspases. Afterwards cleavage of survival proteins as well as DNA is performed by effector caspases resulting in apoptotic cell death (Li et al. 2008; Keoni et al. 2015). To prevent *mRac1* knockout cells from undergoing apoptosis, the pan caspase inhibitor Q-VD-OPh hydrate (QVD) was used. QVD binds irreversibly to the catalytic site of caspase proteases and inhibits apoptosis, inhibited caspases are 1, 3,7, 8, 9, 10, and 12.

To prevent the detachment of the transduced cells, MEF (*Rac1*$^{flx/flx}$) were plated on dishes with or without collagen-coated surface. 24 h after lentiviral transduction with Puro.Cre expression vector, cells were permanently treated with 10 µM QVD and puromycin. 24 h - 120 h post-transduction cells were analyzed by flow cytometry and real-time qPCR. QVD prevented apoptosis at early time-points (24 h and 48 h), SubG1 fraction was reduced by about 70 % (Figure 3.37). In later time-points (72 h, 96 h, and 120 h) there was no difference between cells treated with or without QVD. In both cases 50 % of the cells were in SubG1 fraction 72 h and 96 h after lentiviral transduction, 120 h post transduction showed 70 % apoptotic cells.

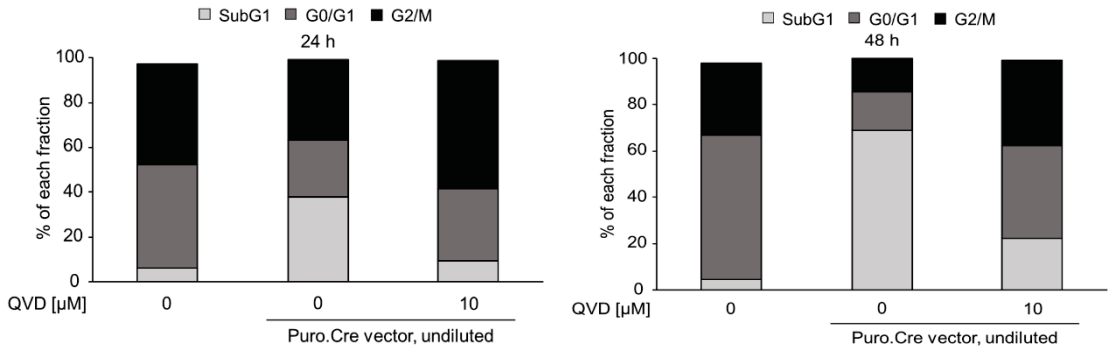

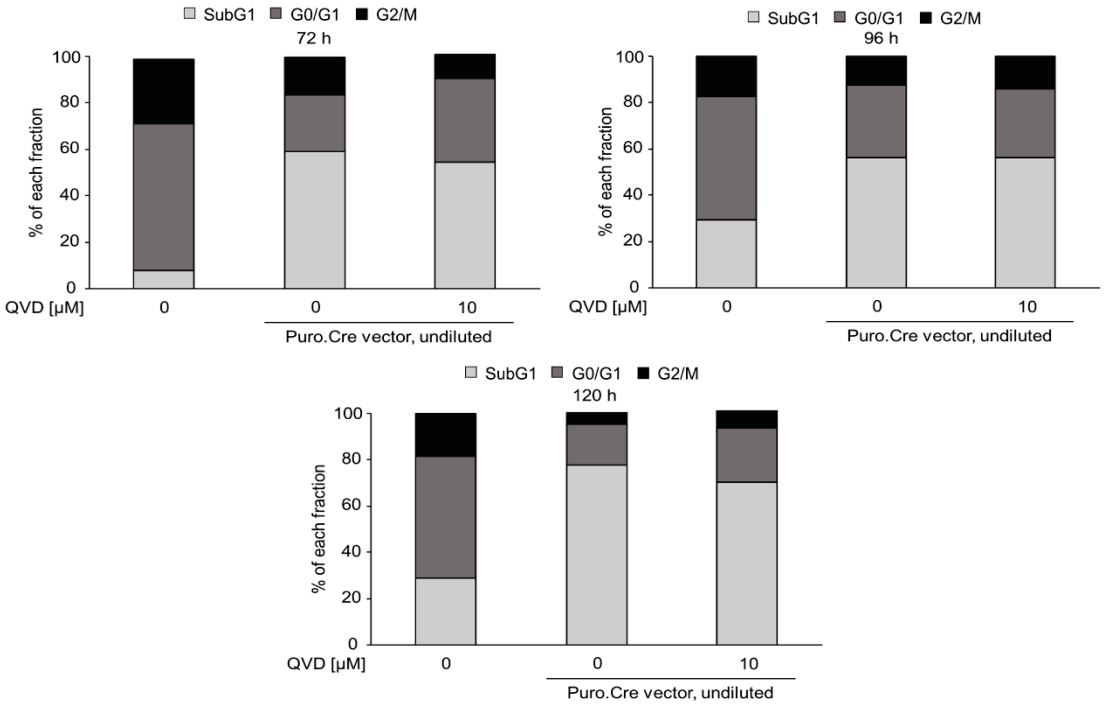

Figure 3.37: Flow cytometric analysis of cell cycle distribution after lentiviral transduction with Puro.Cre vector and treatment with pan caspase inhibitor QVD.
MEF (*Rac1*$^{flx/flx}$) were plated on collagen-coated dishes, transduced with Puro.Cre vector and 24 h later permanently treated with QVD and puromycin. Cells were harvested after indicated time-points. Cells were lysed and the nuclei were stained with the DNA-intercalating agent propidium iodide. The cell cycle distribution was determined using a flow cytometer. Control cells (*Rac1*$^{flx/flx}$) were non-transduced. Shown is the evaluation of the different fractions (n=1). The data underlying the graph are shown in Table 7.37 of the appendix. Abbreviations: QVD: Q-VD-OPh hydrate (pan caspase inhibitor). Abbreviations: SubG1: apoptotic cell fraction, G0/G1: fraction of cells in state of quiescence/growth phase, G2/M: fraction of cells in growth phase (preparation for mitosis)/mitosis.

A real-time qPCR was performed to evaluate *mRac1* knockout efficiency under permanent treatment with QVD (Figure 3.38). Cells without pan caspase inhibitor reached a maximal *mRac1* knockout of 70 % after 72 h, afterwards the amount of puromycin-selected cells with *mRac1* knockout decreased. *mRac1* knockout efficiency peaked highest with 25 % 48 h post transduction in pan caspase inhibitor treated cells, all other time-points demonstrated 8 % - 15 %. In total, QVD prevented apoptosis at early time-points, but unfortunately also reduced the *mRac1* knockout efficiency.

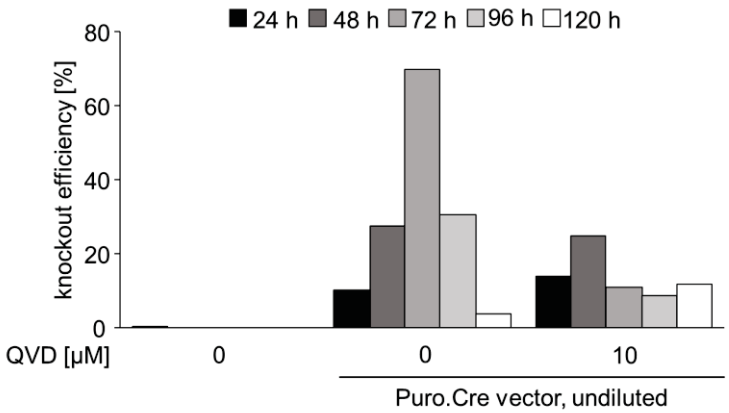

Figure 3.38: Real-time qPCR analysis of *mRac1* knockout after lentiviral transduction with Puro.Cre vector and permanent treatment with a pan caspase inhibitor.
MEF (*Rac1*$^{flx/flx}$) were transduced with undiluted Puro.Cre vector. 24 h later puromycin selection and QVD treatment were started. 24 h - 120 h after transduction cells were harvested for real-time qPCR. Control cells (*Rac1*$^{flx/flx}$) were non-transduced. Mean values are shown (mean; n=1 in duplicates). The data underlying the graph are shown in Table 7.38 of the appendix. Abbreviations: QVD: Q-VD-OPh hydrate (pan caspase inhibitor).

In conclusion, a *mRac1* knockout in MEF (*Rac1*$^{flx/flx}$) is possible, but it seems to be lethal for the cells and could not be prevented by addition of a pan caspase inhibitor (Figure 3.37). Previous work of groups investigating RAC1 already discovered *mRac1* knockout to be embryonic lethal (Sugihara et al. 1998; Tan et al. 2008). The lentiviral transduction itself was non-toxic, because control cells without loxP sites (*Rac1*$^{wt/wt}$) survived (Appendix, Figure 7.25). Also the puromycin concentration is non-toxic for cells tranfected with a gene for puromycin resistance, which was evaluated through lentiviral transduction of puromycin resistance only (Figure 3.36).

Another possibility for the observed cell death might be the Cre activity. According to literature the permanent presence of active Cre recombinase could lead to cell death (Loonstra et al. 2001; Pfeifer et al. 2001; Naiche et al. 2007). To test this hypothesis, two other methods were used to generate *mRac1* knockout cells. In one method, the Cre recombinase will be active, but not permanently present and in the other method the Cre recombinase will be permanently present but needs to be activated.

3.4.2 Transfection with Cre Recombinase Gesicles to induce *mRac1* knockout in mouse embryonic fibroblasts (*Rac1*$^{flx/flx}$)

To test the hypothesis that the *mRac1* knockout cells underwent apoptosis due to a permanent present and active Cre recombinase, *Rac1*$^{flx/flx}$ cells were transfected with Cre Recombinase Gesicles which are cell-derived nanovesicles. They deliver active Cre recombinase, which will be eliminated after time and will not be permanently active or even present in the cells. Transfection was performed according to the manufacturer's

instructions and described under 2.2.1.8. Two different volumes of Cre Recombinase Gesicles were used and cells were harvested for analysis 48 h after transfection. This early time point was chosen according to the manufacturer's instructions. Experiments with lentiviral transduction revealed, that cells with *mRac1* knockout can be loosely attached. Not properly attached cells were collected as "supernatant" for analysis. 10 µl of Cre recombinase Gesicles induced 6 % *mRac1* knockout in attached cells, whereas the loosely attached cells showed 13 % *mRac1* knockout (Figure 3.39). After transfection with 25 µl Cre Recombinase Gesicles, the attached cells showed 20 % *mRac1* knockout, whereas the loosely attached cells showed only 3 % *mRac1* knockout. This knockout efficiency was not sufficient for further experiments and a system with not permanently active Cre Recombinase was tested to induce *mRac1* knockout.

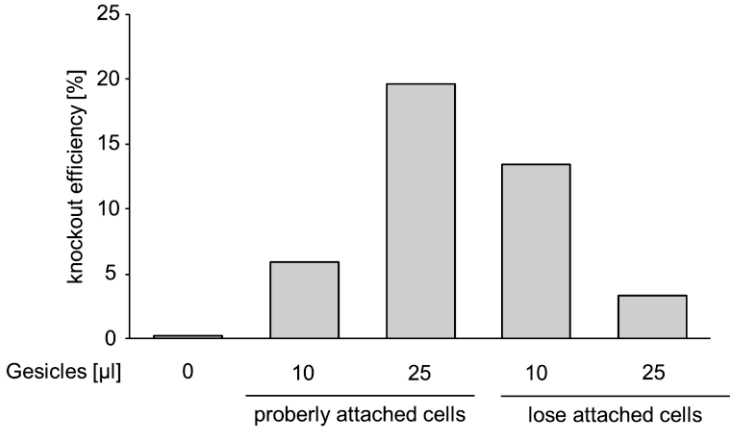

Figure 3.39: Real-time qPCR analysis of *mRac1* knockout after transfection with Cre Recombinase Gesicles in mouse embryonic fibroblasts (*Rac1*$^{flx/flx}$).
MEF (*Rac1*$^{flx/flx}$) were transfected with Cre recombinase Gesicles (10 µl and 25 µl). 48 h after transfection cells were analyzed by real-time qPCR. Control cells (*Rac1*$^{flx/flx}$) were left non-transfected. Mean values are shown (mean; n=1). The data underlying the graph are shown in Table 7.39 of the appendix.

3.4.3 Retroviral transduction with Cre.ER to establish a tamoxifen-inducible *mRac1* knockout in mouse embryonic fibroblasts (*Rac1*$^{flx/flx}$)

Another option to generate *mRac1* knockout cells without permanent present and active Cre recombinase, was the creation of a tamoxifen-inducable knockout system. To this end, cells were transduced with a retrovirus. The used vector was pRetroQ-Cre-ERT2 (Cre.ERT2). This vector contains the DNA sequence for a mutated estrogen receptor, which is fused to Cre recombinase (Cre.ER). In the absence of tamoxifen (Tam), the Cre recombinase stays in an inactive state. Activation is possible only by the addition of the active tamoxifen metabolite 4-hydroxytamoxifen (4-OHT). After activation Cre.ER translocates into the nucleus (Feil et al. 1997; Kim et al. 2018) (Figure 3.40). The vector

also contains a transgene cassette with a gene for puromycin resistance. Virus production was performed as described under 2.2.1.6.

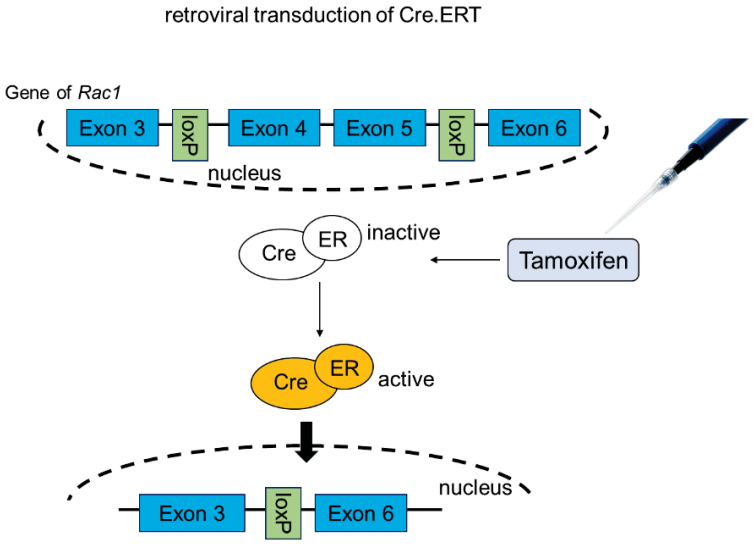

Figure 3.40: Schematic representation of the *mRac1* with loxP sites and activation of Cre recombinase by tamoxifen.
LoxP sites are located between exon 3 and 4, as well as between exon 5 and 6. Cre is fused to a mutated estrogen receptor (Cre.ER). It is inactive until tamoxifen binds to the receptor. After activation Cre.ER translocates into the nucleus. The cut out of exon 4 and 5 is leading to a frameshift mutation in the *mRac1* gene.

As starting point, MEF (*Rac1*$^{flx/flx}$) were transduced with Cre.ERT2 expression vector and 24 h later puromycin selection was started to create stable Cre.ER expressing cells. Puromycin selection was performed until colonies of puromycin-resistant cell clones formed. The tested clones were approved positive for stable Cre.ER expression by Endpoint PCR (Figure 3.41). Clone no. 1 (Cre.ER #1) and clone no. 4 (Cre.ER #4) were used for further experiments.

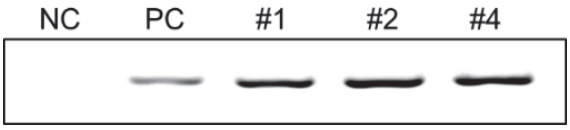

Figure 3.41: Endpoint RT-PCR of Cre.ER to select clones with stable Cre.ER expression.
An endpoint RT-PCR for Cre.ER expression was performed to test for stable Cre.ER expression of the three clones. All the clones were tested positive. Abbreviations: NC: negative control (non-transduced MEF (*Rac1*$^{flx/flx}$)), PC: positive control (Cre.ERT2 vector), #1: clone no. 1, #2: clone no. 2, #4: clone no.4.

The clones were tretated with 1 µM 4-OHT for 5 min, 45 min, 90 min, 3 h, 6 h, 24 h, and 48 h. Cells treated for 24 h and 48 h were harvested after treatment, the other samples were post-incubated for 24 h before they were harvested. *mRac1* expression was

analyzed by real-time RT-qPCR. Due to active Cre exon 4 and 5 should be cut out, leading to a decrease in *mRac1* wild-type expression. In Cre.ER #1 *mRac1* wild-type expression was deacreasing in samples treated for 5 min, 45 min, and 90 min with 4-OHT, then peaked in cells treated for 3 h with 4-OHT, followed by an decrease. In cells treated for 48 h the expression increased again (Figure 3.42). In Cre.ER #4 cells, the expression of *mRac1* wild-type was decreasing under all conditions with one exception. It was increased in cells treated for 48 h. The expression of *mRac1* wild-type was never below 0.5 (50 %) in both clones. Because of the insufficient decrease in *mRac1* wild-type expression, different concentrations of 4-OHT were tested and also a test with multiple 4-OHT treatments (1 µM) was performed. Already a 5 min and a 45 min treatment with 4-OHT followed by 24 h post-incubation was adequate for a decrease of *mRac1* wild-type by 50 %, therefore these time-points were used to evaluate the different concentrations of 4-OHT.

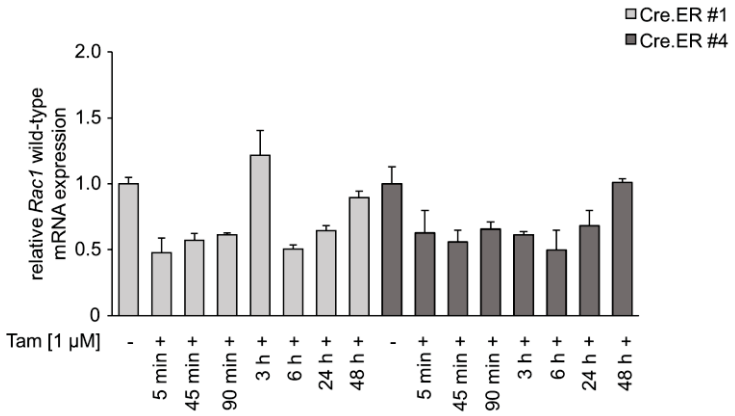

Figure 3.42: Influence of tamoxifen (4-OHT) treatment on expression of *mRac1* in stable Cre.ER expressing cells.
Cells were treated with 1 µM tamoxifen (4-OHT) for 5 min, 45 min, 90 min, 3 h, 6 h, 24 h, or 48 h. Cells treated for 24 h and 48 h were harvested after treatment, the other samples were post-incubated for 24 h before they were harvested. The mRNA expression of *mRac1*-wild-type was examined using quantitative real-time PCR. The relative mRNA expression of untreated, non-transduced cells was set to 1. Mean values and standard error of the mean are shown (mean+SEM; n=1 in duplicates). The data underlying the graph are shown in Table 7.40 of the appendix. Abbreviations: Tam: Tamoxifen (4-OHT).

In the aforementioned experiment with 4-OHT (Figure 3.42) a decrease of *mRac1* wild-type mRNA expression was seen after treatment with 1 µM 4-OHT for 5 min and 45 min and 24 h post-incubation in Cre.ER #1 cells. Here, no change in expression was seen under these conditions (Figure 3.43 A). 5 min treatment with 10 µM 4-OHT (+ 24 h post-incubation) reduced the expression by 70 %, whereas treatment for 45 min (+ 24 h post-incubation) resulted in a 7-fold rise compared to the control (Figure 3.43 A). 100 µM 4-OHT caused an 8-fold increase after 5 min (+ 24 h post-incubation) and even a 25-fold

increase after 45 min (+ 24 h post-incubation) (Figure 3.43 A). Cre.ER #4 cells did not show the lowering effect of *mRac1* wild-type expression after treatment with 1 µM 4-OHT (Figure 3.43 B). 5 min treatment and 24 h post-incubation with 10 µM did not change the expression, whereas 45 min treatment (+ 24 h post-incubation) resulted in an expression which was reduced by 60 % (Figure 3.43 B). Treatment with 100 µM 4-OHT for 45 min and 24 h post-incubation decreased the expression about 50 %, however 5 min treatment (+ 24 h post-incubation) did not change the expression compared to the control (Figure 3.43 B). In conclusion, the two clones showed no similar result regarding the time of treatment or the concentration of 4-OHT to achieve a *mRac1* knockout in stable Cre.ER expressing MEF (*Rac1*$^{flx/flx}$).

For the multiple treatment, cells were treated with 1 µM 4-OHT on two consecutive days or they were treated three times per week (Monday, Wednesday, Friday) for two weeks. Again, the results of Cre.ER #1 and Cre.ER #4 were not similar (Figure 3.43 C). Cre.ER #1 showed an increase of 50 % compared to the control after treatment on two consecutive days, whereas Cre.ER #4 showed a decrease of 50 %. The treatment for two weeks resulted in a reduced expression (85 % less) in Cre.ER #1 but did not change the expression in Cre.ER #4. No conditions regarding the concentration of 4-OHT or the duration of treatment could be validated as suitable or not for *mRac1* KO induction.

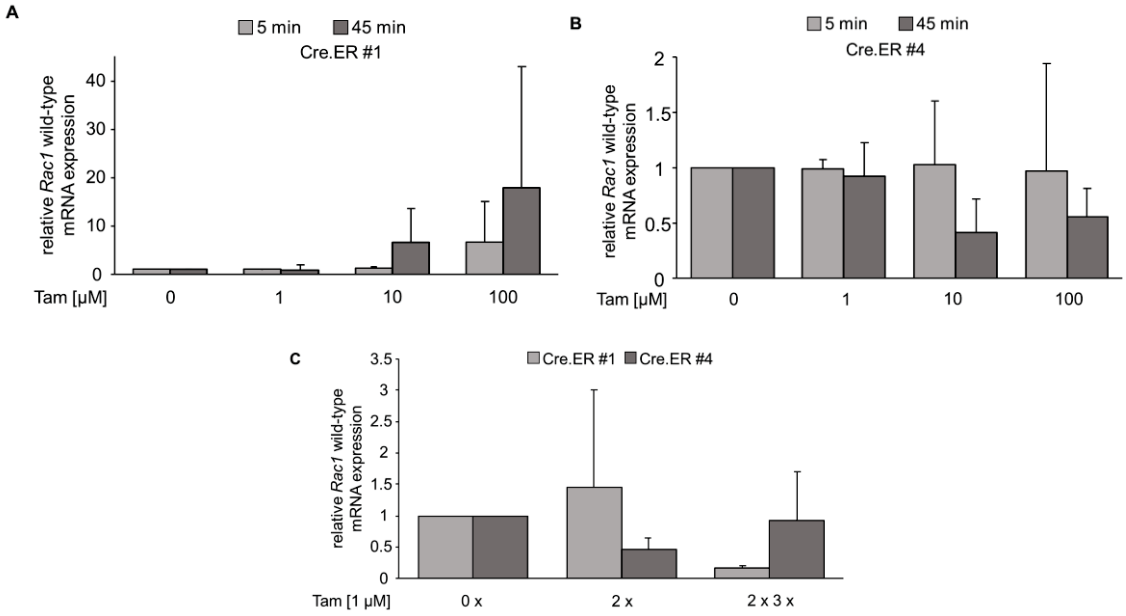

Figure 3.43: Influence of tamoxifen (4-OHT) treatment on expression of *mRac1* in stable Cre.ER expressing MEF (*Rac1*$^{flx/flx}$).
Cells were treated with 1 µM, 10 µM, or 100 µM Tam (4-OHT) for 5 min, or 45 min and post-incubated for 24 h (**A, B**) or cells were treated with 1 µM Tam (4-OHT) on two consecutive days or three times (Monday, Wednesday, Friday) per week for two weeks (**C**). The mRNA expression of *mRac1*-wild-type was examined using real-time RT-qPCR. The relative mRNA expression of untreated, non-transduced cells was set to 1. **A** Mean values and standard deviation are shown (mean+SD; n=2 in duplicates) for Cre.ER #1. Abbreviations: Tam: Tamoxifen (4-OHT). The data

underlying the graph are shown in Table 7.41 of the appendix. **B** Mean values and standard deviation are shown (mean+SD; n=2 in duplicates) for Cre.ER #4. Abbreviations: Tam: Tamoxifen (4-OHT). The data underlying the graph are shown in Table 7.41 of the appendix. **C** Mean values and standard deviation are shown (mean+SD; n=2 in duplicates). Abbreviations: Tam: Tamoxifen (4-OHT), 0 x: no treatment with Tam, 2 x: treatment on two consecutive days, 2 x 3 x: treatment three times per week for two weeks. The data underlying the graph are shown in Table 7.42 of the appendix.

The results of all attempts to generate *mRac1* knockout cells can be summarized as follows, the observed cell death seems to be linked to *mRac1* knockout since the MEF without loxP sites (*Rac1*$^{wt/wt}$) did not show an increased cell death upon transduction. The hypothesis that the Cre activity might lead to cell death as proposed in literature was not evaluated regarding the cell death, sind the used systems (i) with an active, but not permanently present Cre recombinase and (ii) with a permanently present Cre recombinase that needs to be activated did not induce a *mRac1* knockout that was sufficient for further experiments.

4 Discussion

The small Rho GTPase RAC1 was shown to play a role in the doxorubicin-induced DNA damage response (DDR). Previous work showed a protection against doxorubicin (Dox) and etoposide-induced DSB formation as well as cell death by pharmacological inhibition of RAC1 (Damrot et al. 2006; Huelsenbeck et al. 2011; Huelsenbeck et al. 2012; Wartlick et al. 2013). Other studies demonstrated a reduced DNA repair, cell proliferation, as well as cell survival after exposure to UV light or γ-irradiation in RAC1 deficient cells or cells treated with a RAC1 inhibitor (Yan et al. 2014; Espinha et al. 2015). Also a protective role of RAC1 in UV-light-induced skin carcinogenesis and keratinocyte apoptosis was shown (Deshmukh et al. 2017). Recent studies indicated that RAC1 plays a role in DNA repair, cell survival as well as cell death via regulation of mechanism of the DDR (Fritz et al. 2006, 2013; Fritz et al. 2015). While it was initially assumed that these effects are based on interference with RAC1 downstream signaling mechanisms originating from the cell membrane, recently published data challenged that view. In the last few years more and more studies were published where RAC1 as well as certain RAC1-GEF were identified inside the nucleus, at the nuclear envelope, or nuclear membrane (Lanning et al. 2003; Michaelson et al. 2008; Sandrock et al. 2010; Hajas et al. 2013; Tong et al. 2013; Chircop 2014; Woroniuk et al. 2018; Liu et al. 2019). These studies suggest that a more direct interplay between RAC1-regulated nuclear functions and nuclear proteins involved in the DDR is possible. Studies focusing on nucleocytoplasmic shuttling of RAC1 revealed a direct interaction of RAC1 with Karyopherin alpha2 which mediates the import of RAC1 into the nucleus (Sandrock et al. 2010). Recent data suggest an involvement of RAC1 in the regulation of nuclear functions like apoptosis, cell cycle arrest, mitosis (Bar-Sagi et al. 2000; Michaelson et al. 2008; Yoshida et al. 2010), and the modulation of actin polymerization in the nucleus. Nucleophosmin, a nucleocytoplasmic shuttling protein, was identified to promote RAC1 nuclear export (Disanza et al. 2015; Navarro-Lerida et al. 2015). Furthermore, accumulation of nuclear RAC1 was shown to control the nuclear membrane shape and adjusts cytoplasmic RAC1 as well as RHOA activity (Oh et al. 2014).

So far, it was hypothesized that the influence of RAC1-derived modulation of the doxorubicin-induced DDR are based on a modulation of RAC1 downstream signaling from the cell membrane to the nucleus, indicating a rather indirect role of RAC1 in the DDR. Like stated above, RAC1 as well as guanine nucleotide exchange factors were found inside the nucleus (Michaelson et al. 2008; Sandrock et al. 2010; Woroniuk et al. 2018), but nuclear-specific functions of Rho GTPases are sparsely characterized so far.

In this context it is still unknown whether cytosolic RAC1 modulates the Dox-induced DDR or if a nuclear fraction of RAC1 is involved. For the analysis of nuclear and cytoplasmic RAC1 and its role in the Dox-induced DDR, RAC1 was silenced in MEF either pharmacologically with EHT 1864 or by using siRNA against *mRac1*. Additionally, MEF were transiently transfected with *hRAC1* mutants (wild-type, constitutively active, dominant-negative) with or without additional nuclear localization sequence (NLS). Afterwards, the Dox-induced DDR was analyzed by evaluation of fluorescent nuclear γH2AX and 53BP1 foci formation, as well as by detection of activated proteins of the DDR by western blot to elucidate the role of cytoplasmic as well as nuclear RAC1 in the DDR. As already mentioned, the RAC1 protein already harbours a weak C-terminal NLS that can be masked by prenylation (Williams 2003; Lanning et al. 2004; Michaelson et al. 2008; Abdrabou et al. 2018). The intrinsic murine RAC1 as well as the expressed human RAC1 variants are thought to be mainly localized in the cell's cytoplasm. To increase the nuclear localization of hRAC1 a stronger NLS (from SV40 Large T-antigen) (Kalderon et al. 1984) was added N-terminal to the plasmids. The hypothesis was that expression of dominant-negative RAC1 (GFP-hRAC1(T17N)) should dampen the DDR similar to a pharmacological inhibition of RAC1 or knockdown of *Rac1,* while wild-type hRAC1 (GFP-hRAC1(WT)) or constitutively active hRAC1 (GFP-hRAC1(Q61L)) has the opposite effect on the DDR. The aim of the present work was to identify whether cytosolic and/or nuclear RAC1 modulates the doxorubicin-induced DDR. Pharmacological RAC1 inhibition and *mRac1* silencing were included in the examination of the doxorubicin-induced DDR. Mouse embryonic fibroblasts (MEF) served as *in vitro* cell model.

4.1 Dose determinations of doxorubicin as well as of the RAC1 inhibitor EHT 1864

For investigation of the influence of hRAC1 on the doxorubicin-induced DDR doses of Dox had to be found, that induce a strong and well detectable DDR while still allowing a modulation of the DDR, e.g., with the RAC1 inhibitor EHT 1864. MEF were pulse-treated with 0.1 µM, 0.3 µM, 1 µM, or 3 µM Dox for 1 h because the dominant effect of DNA damage induction by irreversible inhibition of Top II mainly occurs at concentrations from 0.5 µM to 5 µM (Gewirtz 1999). Dox is a DSB inducer (Gewirtz 1999; Pommier et al. 2010). To this end γH2AX as surrogate marker for DSB (Olive 2004; Harper et al. 2007; Kinner et al. 2008) as well as a subset of ATM downstream targets were evaluated for finding the appropriate concentration of Dox which led to a strong DDR that could still be further modulated. One major mediator of the DSB-induced DDR is the serine/threonine kinase ATM. Substrates for this protein are amongst other proteins P53 and KAP1 (Banin et al. 1998; White et al. 2012). The phosphorylation of KAP1, H2AX, and P53 was dose-

and time-dependent intensified by doxorubicin treatment and also the number of nuclear γH2AX foci were increasing with dose. The experiments confirmed 1 µM Dox as a strong DDR inducing dose that still allowed a further modulation with EHT 1864. 1 µM Dox was also used in other cell lines to investigate the influence of RAC1 on the Dox-induced DDR (Maiso et al. 2009; Huelsenbeck et al. 2011; Chau et al. 2012; Huelsenbeck et al. 2012; Wartlick et al. 2013; Desantis et al. 2015). Moreover, cancer standard therapy with Dox achieves a serum level of 1 - 2 µM Dox (Gewirtz 1999) meaning the *in vitro* concentration of Dox used in this work is within the clinical relevant range.

Wartlick *et al.* treated the cells with 10 µM EHT 1864 for 1 h (Wartlick et al. 2013). In this publication, treatment with 10 µM EHT 1864 decreased the Dox-stimulated increase in γH2AX as well as Ser15 phosphorylated P53 and attenuated the phosphorylation of stress kinases (pP38, pJNK). The data show that inhibition of RAC1 signaling protects cells present in S- or G-phase from severe DNA damage following doxorubicin treatment as shown by an increase in cell viability. In the present work MEF were pre-treated with 10 µM, 30 µM, or 100 µM of the RAC1 inhibitor for 3 h prior to the treatment with Dox to define an appropriate dose for the used cell line. All three doses of RAC1 inhibitor showed a similar reduction of Dox-induced γH2AX foci, which was reduced independent of the used EHT 1864 concentration by about 30 % - 50 %. Pre-treatment with the RAC1 inhibitor resulted in a significant lower level of the evaluated Dox-induced phosphorylated proteins. Between 10 µM and 30 µM EHT 1864 there was only a slight difference in signal intensity of the selected proteins. This implicates that the treatment of MEF with 30 µM EHT 1864 for 3 h is useful for RAC1 inhibition.

The use of EHT 1864 as a RAC1 inhibitor in general can be criticized since it additionally targets RAC1b, RAC2 and RAC3 (Shutes et al. 2007). However, RAC2 was shown to be expressed in hematopoietic cells only and RAC3 to be mainly expressed in the brain (Shirsat et al. 1990; Moll et al. 1991; Haataja et al. 1997). RAC1b, the splice variant of RAC1, was mainly found in skin as well as epithelial tissues from the intestinal tract and in breast cancer tissues (Jordan et al. 1999; Schnelzer et al. 2000; Melzer et al. 2019). This is important to note, since the experiments presented in this work were performed with mouse embryonic fibroblasts. Therefore, RAC1b, RAC2, and RAC3 can be neglected in the setup used in the present study.

Dütting *et al.* described off-target effects of EHT 1864 when this inhibitor was used at concentrations >30 µM. 100 µM EHT 1864 altered platelet viability in RAC1-deficient mouse platelets and led to RAC1-independent inhibition of PAK1/PAK2 (downstream effectors of RAC1) activation after stimulation with thrombin. Treatment with 200 µM EHT 1864 resulted in induced apoptosis in platelets (Dutting et al. 2015). EHT 1864 did

not block CDC42 or RHOA (Dutting et al. 2015), suggesting that the inhibitor is specific for RAC1. A potent RAC1 inhibition with EHT 1864 was described already at the concentration of 5 µM (Onesto et al. 2008). The concentration of EHT 1864 which was applied in different studies ranged from 5 µM to 100 µM and the duration of treatment ranged from 30 min to 24 h (Onesto et al. 2008; Wartlick et al. 2013; Hampsch et al. 2017; Yu et al. 2019; Li et al. 2020; Singh et al. 2020; Wang et al. 2020). Since unspecific side effects only occurred at higher concentrations of EHT 1864 (≥50 µM) (Dutting et al. 2015; Wang et al. 2020), the chosen concentration of 30 µM EHT 1864 for the experiments performed in this work is in the range of non-critical concentrations of EHT 1864. Therefore, it can be assumed that the observed effects result from specific inhibition of RAC1. Unfortunately, the present work lacks a RAC1 pulldown to confirm this assumption. This should be made up in future work.

4.2 Active RAC1 induces lamellipodia formation and is imported into the nucleus

4.2.1 Constitutively active and dominant-negative hRAC1 alter the lamellipodia and stress fibers formation in MEF

It is known that RAC1 is involved in the regulation of the actin cytoskeleton (Ridley, Paterson, et al. 1992; Nobes et al. 1995; Hall 1998). Actin polymerization induces the expansion of rod-like protrusions, named filopodia, as well as sheet-like protrusions, named lamellipodia. Restructuring of filamentous actin (F-actin) into lamellipodia or membrane ruffles is promoted by active RAC1 (Karnoub et al. 2001; Ridley 2011; Steffen et al. 2013). The RAC1 inhibitor EHT 1864 was shown to prevent RAC1-dependent lamellipodia formation (Shutes et al. 2007). To obtain evidence about the functionality of the used *hRAC1* mutants lamellipodia formation was evaluated in cells transfected with *hRAC1* mutants. Cells expressing constitutively active hRAC1 (with and without additional NLS) revealed an increase of lamellipodia formation as anticipated, demonstrating the functionality of the hRAC1 construct. This is in line with published data of Ehrlich *et al.* who showed that MDCK cells expressing constitutively active RAC1 exhibited an increased rate of lamellipodia formation in contrast to cells expressing dominant-negative RAC1 (Ehrlich et al. 2002). Steffen *et al.* could reconstitute the lamellipodia formation in *Rac1*$^{-/-}$ MEF by transfection with constitutively active *RAC1* expression vector (Steffen et al. 2013).

Besides the formation of lamellipodia also the formation of membrane ruffles is promoted by RAC1 (Ridley, Paterson, et al. 1992; Hall 2012). Constitutively active RAC1 was shown to induce membrane ruffles in various fibroblast cell lines (Ridley, Paterson, et al.

1992; Li et al. 1997; Schwartz et al. 1998) and macrophages (Fujii et al. 2013). In contrast expression of dominant-negative RAC1 (Ridley, Paterson, et al. 1992; Schwartz et al. 1998) and RAC1 knockout (Wells et al. 2004) reduced the formation of membrane ruffles. Regarding the results obtained in the present study, it was impossible to count the single membrane ruffles of each cell. Therefore, it was distinguished between cells showing no membrane ruffles or having at least one membrane ruffle. The total number of cells with membrane ruffles was not affected by transfection with the different *GFP-hRAC1* expression vectors. In the aforementioned publications, the number of membrane ruffles per cell was evaluated or a score for membrane ruffles per cell was used. Consequently, the data presented in this work can neither confirm nor refute the publications. The images shown in the results part were taken with a 40x objective, as originally only the stress fibers and the lamellipodia were to be observed. To get a better resolution of the membrane ruffles, the images should be taken with a 100x objective. With these images, the individual membrane ruffles per cell should be visible and it should be possible to evaluate the potential change by manipulating the RAC1 status.

In fibroblasts expression of constitutively active mutants of Rho (RHOA) induce stress fiber formation (Ridley and Hall 1992; Nobes et al. 1995; Machesky et al. 1996; Nobes et al. 1999). In the present work, expression of mainly cytoplasmic constitutively active hRAC1 led to a decrease in stress fibers formation whereas forced nuclear accumulation as well as mainly cytoplasmic expression of dominant-negative hRAC1 led to an increase in stress fibers formation. This is line with the data of Moorman *et al.* who showed that BHK (baby hamster kidney) cells expressing dominant-negative RAC1 exhibited actin microspikes and stress fiber formation. The co-expression of dominant-negative RAC1 and dominant-negative CDC42 led to a phenotype consisting of predominantly stress fibers, similar to cells expressing RHOA (Moorman et al. 1999). This might be due to the mutual relationship between RHOA and RAC1, in which a high RAC1 activity leads to the reduction of RHOA and *vice versa* (Sander et al. 1999; Zondag et al. 2000; O'Connor et al. 2013). The dominant-negative mutation of the transgenic hRAC1 leads to a loss of function of hRAC1 and impairs the function of intrinsic wildtype mRAC1. This dominant-negative effect could increase the expression of RHOA leading to the phenotype shown in the present work. In order to verify this assumption, further experiments could be performed to analyze whether an altered expression of RHOA is seen in MEF transfected with *hRAC1* mutants compared to un-transfected MEF.

4.2.2 GDP to GTP exchange might be a prerequisite for efficient nuclear import

Transport of proteins into the nucleus as well as out of the nucleus occurs through nuclear pore complexes (Stoffler et al. 1999; Allen et al. 2000). Carrier proteins, the so-

called karyopherins or importins and exportins, facilitate the active transport of proteins between the cytoplasm and the nucleus (Radu et al. 1995; Conti et al. 2001) and are responsible for the majority of nucleocytoplasmic transport (Lee et al. 2006). Proteins which are determined for nuclear import possess a nuclear localization sequence (NLS). The NLS is recognized by importin α (adapter protein) which then forms a heterodimer with importin β (transport receptor) resulting in nuclear import (Conti et al. 2001; Leung et al. 2003). RAC1 harbors a weak NLS in the C-terminal polybasic region (PBR) (Lanning et al. 2004; Michaelson et al. 2008; Abdrabou et al. 2018). Even though the NLS can be masked by the prenylation of the CAAX box, activated as well as prenylated RAC1 was found inside the nucleus (Michaelson et al. 2008; Sandrock et al. 2010; Hinde et al. 2014). Studies focusing on nucleocytoplasmic shuttling of RAC1 revealed a direct interaction of RAC1 with Karyopherin alpha2 which mediates the import of RAC1 into the nucleus (Sandrock et al. 2010). The active state of RAC1 seems to be essential for the karyopherin α-mediated nuclear import of RAC1.

In this work the intrinsic murine RAC1 (mRAC1) as well as the expressed human RAC1 (hRAC1) variants (without additional NLS) were found to be mainly localized in the cell's cytoplasm. Only 19 % of the intrinsic mRAC1 was found inside the nucleus. The nuclear localization of the GFP-hRAC1 fusion proteins (without additional NLS) ranged from 19 % - 30 %. Published data (Michaelson et al. 2008; Tong et al. 2013; Navarro-Lerida et al. 2015) stated about 10 % - 40 % of endogenous RAC1 to be localized inside the nucleus in non-stimulated cells, showing that GFP-hRAC1 has a similar subcellular distribution as endogenous mRAC1. The amount of nuclear RAC1 increased upon treatment with apigenin, a plant pigment from the flavone group (Michaelson et al. 2008). Hinde *et al.* described a distribution of RAC1 between the cytoplasm and the nucleus upon micro-irradiation-induced DNA damage, whereby inactive RAC1 was exported from the nucleus and active RAC1 was found inside the nucleus (Hinde et al. 2014). For accumulation of GFP-hRAC1 fusion protein inside the nucleus independent of the activation state an additional NLS originated from SV40 was added to the used *hRAC1* mutants. This modification significantly enhanced the nuclear localization of the GFP-hRAC1 fusion proteins as shown in this work. The GFP-hRAC1 fusion proteins with the additional NLS showed 2 - 4 times more nuclear accumulation than their counterpart without additional NLS. Cells expressing GFP-NLS-hRAC1(WT) showed greater GFP-NLS-hRAC1 enrichment in the nucleus than cells expressing GFP-NLS-hRAC1(Q61L) or GFP-NLS-hRAC1(T17N). The observed pronounced nuclear expression due to the SV40 NLS is in line with published data (Luo et al. 2004; Saito et al. 2004; Li, Wu, et al. 2007; Ray et al. 2015). Up to 40 % increase in nuclear localization of proteins was shown

when SV40 NLS was added (Collins et al. 2007; Ray et al. 2015). The additional NLS increased nuclear accumulation of wild-type hRAC1 about 55 % whereas the nuclear accumulation of constitutively active as well as dominant-negative hRAC1 was increased about 18 %. To further enhance the nuclear expression of the GFP-NLS-hRAC1 fusion proteins, expressing vectors without a NES could be designed. The NLS would force a nuclear accumulation and the deleted NES would prevent the nuclear export.

The capability to exchange GDP to GTP as well as to interact with downstream effectors seems be a prerequisite for efficient nuclear import since the strongest nuclear accumulation was seen in *GFP-NLS-hRAC1(WT)* expression vector transfected cells. The wild-type hRAC1 was the only used *hRAC1* variant, which is able to do both (i) to cycle between an active and an inactive state and (ii) to interact with downstream effectors. The *hRAC1* mutants used in this work only differ in a single amino acid exchange which, however, seems to affect the required prerequisite for nuclear import. By replacing a glutamine (Q) with leucine (L) at residue 61 RAC1 is stabilized in the active state (RAC1(Q61L)) due to the blocked GAP-stimulated and endogenous GTPase activity (Khosravi-Far et al. 1995; Bai et al. 2018). Substitution at residue 17 of threonine (T) to asparagine (N) also appears to impair nuclear import. The mutation mentioned places RAC1 in a permanently inactive state (RAC1(T17N)) due to a defective GDP GTP exchange (Feig et al. 1988; Davis et al. 2013). RAC1(T17N) can also be bound to GEF which are required for activation of endogenous RAC1 (Hansen et al. 2002). In both cases, the possibility to switch between active and inactive state is no longer given.

4.3 Nuclear GTP-bound RAC1 is necessary for doxorubicin-induced double strand break signaling

Expression of mainly cytoplasmic dominant-negative hRAC1 as well as forced nuclear accumulation of dominant-negative hRAC1, pharmacological inhibition of RAC1 with EHT 1864, as well as transfection of MEF with siRNA against *mRac1* reduced the number of Dox-induced γH2AX and 53BP1 foci as well as co-localization of these foci. All three methods caused a qualitatively and quantitatively similar impairment of the Dox-induced DSB formation. It can be concluded that pre-treatment of MEF with 30 µM EHT 1864 is indeed specific for RAC1. Furthermore, this implicates that it is indeed RAC1 that is of utmost relevance for the regulation of Dox-induced mechanisms of the DDR. In addition, this finding indicates that RAC1 might not be the only factor diminishing the Dox-induced DSB formation otherwise the combination of RAC1 inhibition/silencing with dominant-negative hRAC1 should have reached 100 % reduction of Dox-induced foci. To confirm this assumption, future experiments should use a pull-down activity

measurement to biochemically demonstrate that RAC1 activity is 100% inhibited in the combination treatment. Expression of mainly cytosolic dominant-negative hRAC1 mitigated Dox-induced foci formation and targeted nuclear expression of GFP-NLS-hRAC1(T17N) revealed a similar effect. This shows that inhibition of cytosolic mRAC1 is not as important as the impairment of nuclear mRAC1 for the formation of DSB following Dox treatment.

Surprisingly, cells transfected with *GFP-NLS-hRAC1(Q61L)* expression vector showed the same phenotype with respect to Dox-induced foci formation as cells expressing mainly cytoplasmic or targeted nuclear dominant-negative hRAC1. This was not seen in cells expressing cytoplasmic constitutively active hRAC1. In contrast to the dominant-negative mutants the constitutively active mutants are permanently GTP-bound and are able to interact with downstream effectors. Maybe nuclear RAC1 can only interact with DDR-related proteins when it is able to cycle between a GDP/GTP bound state and/or its nuclear import and export works properly. The latter hypothesis is supported by the observation that active (GTP-bound) RAC1 accumulates in the nucleus of G2 arrested cells after treatment with ionizing radiation while GDP-bound inactive RAC1 is exported from the nucleus (Yan et al. 2012; Hinde et al. 2014; Yan et al. 2014; Navarro-Lerida et al. 2015).

The RAC1 inhibitor EHT 1864 targets the intrinsic mRAC1 as well as the transgenic hRAC1. Expression of GFP-hRAC1(WT) or GFP-hRAC1(Q61L) could not revert this effect in the present work. Theoretically, the expression of GFP-hRAC1(WT) or GFP-hRAC1(Q61L) (with or without additional NLS) was anticipated to revert the EHT 1864 mediated decrease of Dox-induced foci formation as these *hRAC1* mutants should neutralize the EHT 1864 mediated effect. However, EHT 1864 stimulates the nucleotide release of RAC1. By direct binding to RAC1, the protein is put in an inert and inactive state (Shutes et al. 2007; Onesto et al. 2008) and therefore also inhibits the activation of transgenic hRAC1, expression of the hRAC1 mutants did not revert the effect of EHT 1864 in the setup used in the present work. Considering that constitutively active hRAC1 has to be activated once and then remains active it is just as affected by EHT 1864 as wild-type hRAC1. Another reason why the decrease of genotoxin-induced foci formation may not be reversed by GFP-hRAC1 expression may be that EHT 1864 might be present in excess. To confirm these statements future experiments with GFP-hRAC1 expressing cells should be performed treated with lower concentrations of EHT 1864 (< 30 µM) prior to doxorubicin treatment. Due to the lower concentration of EHT 1864 it should be no longer present in excess and the neutralizing effect of GFP-hRAC1 expression should be more easily detectable. To verify the inhibitory effect of

EHT 1864 on GFP-hRAC1, GFP-hRAC1 expressing cells treated with EHT 1864 could be studied for interaction with RAC1 downstream effectors since this interaction should be prevented by EHT 1864 treatment.

For silencing of endogenous mRAC1 a transient gene knockdown of *mRac1* was achieved by transfection with small interfering RNA (siRNA) against *mRac1* (*mRac1* siRNA). Based on the observation that pharmacological RAC1 inhibition resulted in reduced foci formation after Dox treatment, a similar effect was expected for Dox-treated cells with silenced *mRac1*. Silencing of *mRac1* in MEF prevented from Dox-induced γH2AX and 53BP1 foci formation and confirmed this expectation. The observed reduced foci formation after Dox treatment in *mRac1* silenced MEF could only be reverted by simultaneous expression of GFP-NLS-hRAC1(Q61L). Wild-type hRAC1 with and without additional NLS as well as GFP-hRAC1(Q61L) were also thought to revert the effects of *mRac1* silencing but they did not. The question remains why only the constitutively active hRAC1 mainly expressed in the nucleus was capable of reversal. An explanation might be that Dox-induced foci formation is modulated by nuclear RAC1, therefore mainly cytosolic expressed hRAC1 was unable to revert the effects of *mRac1* silencing. Since only inactive RAC1 was described to be exported out of the nucleus (Hinde et al. 2014), the constitutively active hRAC1 (GFP-NLS-hRAC1(Q61L)) might have been kept in the nucleus leading to the observed doxorubicin-induced DSB signaling. This implicates, that at least a fraction of active RAC1 in the nucleus is necessary for a full-blown doxorubicin-induced DSB signaling.

4.3.1 RAC1 is involved in the regulation of downstream DDR functions beyond the involvement in DSB formation

After the occurrence of DSB the serine-threonine kinases ATM, ATR, and DNA-PK get activated (Jackson et al. 2009) which in turn phosphorylate their target proteins to initiate the DDR (Matsuoka et al. 2007). Among others downstream targets that are phosphorylated by the serine-threonine kinases after treatment with Dox are the histone 2AX (Burma et al. 2001; Lyu et al. 2007; Huelsenbeck et al. 2012; Wartlick et al. 2013; Deng et al. 2014), the “guardian of the genome” P53 (Banin et al. 1998; Kurz et al. 2004; Thompson et al. 2004; Liu, Mao, et al. 2008), and KAP1 (KRAB-associated protein-1) (Li, Lee, et al. 2007; White et al. 2012; Bhatia et al. 2013; Xu et al. 2015) which were selected for analysis in the presented work.

Only the expression of constitutively active hRAC1 with and without additional NLS showed no effect on Dox-induced phosphorylation of KAP1, H2AX, and P53. Mainly cytosolic and targeted nuclear expression of wild-type or dominant-negative hRAC1

exhibited a tendency to diminish the Dox-induced DDR represented by the selected set of DDR-related phosphorylated proteins. The decrease in protein signaling occurred at the same time points, independent of the used plasmids but to different intensities. This is leading to the assumption that, in addition to the involvement in DSB formation, there also seem to be downstream DDR functions in which RAC1 is involved.

RAC1-deficient cells as well as cells treated with a RAC1 inhibitor or lovastatin (a non-specific pan-Rho GTPase inhibitor) showed a reduced level of phosphorylated P53 after UV-irradiation, IR, or treatment with topoisomerase II poisons (Wartlick et al. 2013; Fritz et al. 2015; Deshmukh et al. 2017; Ziegler et al. 2017). The authors hypothesize that RAC1 deficiency/inhibition hampers the PI3K signaling pathway and/or accelerates the repair of DSB resulting in a lower amount of phosphorylated P53. Published data describe a reduced level of phosphorylated H2AX after genotoxic stress in RAC1-deficient cells as well as cells treated with a RAC1 inhibitor in western blot analysis (Huelsenbeck et al. 2012; Wartlick et al. 2013; Espinha et al. 2015; Deshmukh et al. 2017). In the experiments presented in this work dominant-negative hRAC1 had no significant effect on the Dox-induced protein level of phosphorylated H2AX. The variations between the number of γH2AX foci in the nucleus and the amount of γH2AX at protein level was due to several reasons. First, the transfection efficiency was only 30 %, which may not have been high enough to cause any detectable changes in Dox-induced phosphorylated H2AX on protein level. Second, western blotting is not as sensitive as immunofluorescent-based analysis of γH2AX foci because this biochemical method is unable to detect minor differences in the amount of γH2AX.

RAC1 is essential for activation of stress-activated protein kinases such as SAPK/JNK (Coso et al. 1995; Minden et al. 1995; Coso et al. 1996; Brenner et al. 1997) and is shown to activate P38 (Mainiero et al. 2000; Alsayed et al. 2001; Kim et al. 2008). SAPK/JNK and P38 in turn are known to phosphorylate histone H2AX at serine 139 (Lu et al. 2006; Sluss et al. 2006; Lu et al. 2008; de Feraudy et al. 2010), P53 (Fuchs et al. 1998; Liu et al. 2001; Roux et al. 2004), as well as KAP1 (Cheng et al. 2016; Krischuns et al. 2018). Therefore, phosphorylation of H2AX, P53 and KAP1 might be altered through manipulation of the cell's RAC1 status independent of DDR mechanisms as presented in this work. The underlying mechanism of the influence of RAC1 on the SAPK-dependent P53 phosphorylation needs to be examined more closely since GFP-NLS-hRAC1(Q61L) seems to be of importance for the Dox-induced foci formation whereas predominantly nuclear as well as mainly cytoplasmic wild-type hRAC1 reduced the level of phosphorylated DDR-related proteins. It can be concluded that the activation status of RAC1 is important for its interference with DDR-related functions and that, dependent on

its activation status, RAC1 may performs various tasks. Another possibility is the involvement of RAC1 in dephosphorylation processes of DDR-related proteins by regulation of phosphatases. Protein phosphatase 5 (PP5) is shown to interact with and to dephosphorylate DNA-PK (Wechsler et al. 2004), which could result in an decreased amount of phosphorylated P53, KAP1, as well as H2AX. Therefore, an interaction of RAC1 and PP5 could be considered. In addition, an interaction of RAC1 and PP5 has been described by immunoprecipitation (Gentile et al. 2006; Chatterjee et al. 2010) demonstrating PP5 as a direct effector protein for active RAC1. Another phosphatase which dephosphorylates pP53, pKAP1, and γH2AX is Wip1 (wild-type p53-induced phosphatase 1) (Campos et al. 2020). Overexpression of Wip1 resulted in reduced levels of γH2AX whereas silencing of Wip1 led to an increase in γH2AX after DNA damage (induced by doxorubicin and other agents) (Macurek et al. 2010; Moon et al. 2010). Admittedly, up to now no direct interaction between RAC1 and Wip1 is described.

Pharmacological inhibition of RAC1 as well as genetic *mRac1* inhibition/silencing exhibited qualitatively and quantitatively similar results. The amount of phosphorylated protein (pP53, pKAP1, γH2AX) was depending on the time-point of analysis after Dox treatment and/or presence or absence of an additional NLS in the expressed GFP-hRAC1 fusion proteins. The amount of these phosphorylated proteins was altered by wild-type and dominant-negative *hRAC1* mutants, leading to the assumption that RAC1 not only influences the DSB formation but likely also the DDR signaling downstream of the damaged DNA.

4.3.2 RAC1 acts downstream or independent of ATM

The DDR is a complex and fine-tuned network of signaling cascades that are involved in the recognition of DNA damage, DNA repair, cell cycle progression, cell death and survival (Roos et al. 2013; Roos et al. 2016). DSB-inducing chemicals like doxorubicin are known to activate the serine/threonine kinase ATM (Kurz et al. 2004; Brum et al. 2013) which phosphorylates damage indicators such as 53BP1 and H2AX. Since pharmacological and genetic inhibition/silencing of RAC1, expression of mainly cytoplasmic dominant-negative hRAC1 and forced nuclear accumulation of dominant-negative hRAC1, as well as targeted expression of nuclear constitutively active hRAC1 reduced the doxorubicin-induced γH2AX and 53BP1 foci formation an interaction of RAC1 and ATM might be anticipated.

However, the expression of hRAC1 mutants (with or without additional NLS) in MEF exhibited no influence on the Dox-induced pATM foci formation whereas cells with silenced *mRac1* showed an increase in Dox-induced pATM foci formation. There is no

explanation for the discrepancy. It might be possible that the intrinsic mRAC1 which is still present in cells transfected with *hRAC1* mutants may have intercepted the effect of GFP-hRAC1(T17N). Cells treated with a RAC1 inhibitor, for example EHT 1864 or NSC23766, should show a similar result as cells transfected with siRNA against *mRac1*. This could be verified in a future experiment.

Up to now the location of RAC1 in the DDR signaling cascade is unclear. The presented results upon Dox-induced pATM foci formation lead to different possible options (i) RAC1 might act downstream of ATM (ii) RAC1 does not interact with ATM but with other serine/threonine kinases like DNA-PK or ATR which are among the most important sensor proteins and detect DNA damage within minutes of its occurrence (iii) nuclear RAC1 interacts with enzymes that are involved in posttranslational modification, e.g. phosphorylation and/or dephosphorylation of ATM, H2AX, KAP1, and P53.

A possible interaction of RAC1 and ATM was presented by Oh and colleagues. They showed a reduced activation of ATM after IR in cells with Net1A (neuroepithelial transforming gene 1) knockdown (Oh et al. 2014). RAC1 has been shown to control the functions of the RhoGEF Net1A (Carr et al. 2013; Song et al. 2015). Also a protective role of RAC1 in UV-light-induced skin carcinogenesis and keratinocyte apoptosis was shown (Deshmukh et al. 2017) leading to a possible interaction between RAC1 and ATR. Since phosphorylation of P53 at Ser15 (Lees-Miller et al. 1992; Banin et al. 1998; Tibbetts et al. 1999), KAP1 at Ser824 (White et al. 2006; Lu et al. 2019), and H2AX at Ser139 (Wang et al. 2005; Lu et al. 2019) can also be performed by DNA-PK and ATR these serine/threonine kinases might be responsible for the seen effects instead of ATM.

4.3.3 Nuclear RAC1 plays a role in IR-induced γH2AX and 53BP1 foci formation

Manipulation of the RAC1 status of MEF altered the doxorubicin-induced DDR. To answer the question whether the observed effects are specific for Top II poisons, ionizing radiation (IR) was included in the experiments. IR induces DSB independent of Top II as explained in 0.

Commonly used dosages to irradiate MEF for induction of the DDR are 1 Gy - 10 Gy (Helbig et al. 2011; Tarrade et al. 2015; Elaimy et al. 2016; Dong et al. 2017). For the experiments in this thesis MEF transfected with *hRAC1* mutants with and without additional NLS were irradiated with 1 Gy or 3 Gy and fixed 1 h after treatment. Irradiation with 1 Gy induces 20 - 40 DSB (Roots et al. 1985). Transfection with *GFP-NLS-hRAC1(T17N)* expression vector led to a reduced IR-induced γH2AX foci formation after 1 Gy. This is in line with published data where indirect RAC1 inhibition (inhibition through statins, non-specific pan-Rho GTPase inhibitors) prevented the activation of the DDR in

cells treated with ionizing radiation (Nubel et al. 2006; Mahmoudi et al. 2008; Ziegler et al. 2017). Interestingly, reduced foci formation in cells after irradiation with 3 Gy occurred only in cells expressing mainly cytoplasmic or predominantly nuclear wild-type hRAC1. There are articles describing that RAC1 can be activated by IR treatment in various tumor cells, for example glioblastoma multiforme (Yoon et al. 2011; Zhou et al. 2016), head and neck squamous cell carcinoma (Skvortsov et al. 2014), lung cancer (Tan et al. 2020), pancreatic cancer (Yan et al. 2014), cervical cancer (Espinha et al. 2015), and breast cancer (Yan et al. 2012; Hein et al. 2016). Chi *et al.* reported DOCK6 (dedicator of cytokinesis 6) to be highly expressed in gastric cancers and to be correlated with poor outcomes (Chi et al. 2020). DOCK6 is able to exchange GDP for GTP for RAC1 as well as CDC42 *in vitro* and *in vivo* (Chi et al. 2020). Chi *et al.* could show that overexpression of dominant-negative RAC1 or knockdown of RAC1 suppressed DOCK6-enhanced radioresistance (Chi et al. 2020). Although radioresistance has so far only been described in cancer cells, proteins involved in radioresistance may also underlie the results shown in this work in MEF, since only wild-type hRAC1 could significantly attenuate the IR-induced foci formation. RAC1 was shown to accumulate in the nucleus after treatment with ionizing radiation (Yan et al. 2012). Inactive RAC1 was found to be exported from the nucleus in case of DNA damage/G2 arrest (Hinde et al. 2014). Since the transgenic wild-type hRAC1 used in this work is the only hRAC1 variant still able to cycle between an active and an inactive state, which might be a prerequisite for interaction with DDR-related proteins, this could explain why no change in IR-induced foci was detected in cells expressing constitutively active or dominant-negative hRAC1.

The mechanisms underlying this phenotype needs to be defined in future experiments. Import into the nucleus and export out of the nucleus after DNA damage could be investigated by live cell imaging. Due to the expressed GFP-coupled hRAC1 protein, a fluorescence-based evaluation of the transport is possible. In addition, the GDP/GTP loading of RAC1 in the nucleus and the cytoplasm should be examined before irradiation and at different times after irradiation. To gain further insight in the network of RAC1 signaling an analysis of interaction partners in subcellular fractions by gene expression could be performed.

To summarize all presented data of this work, the functions of RAC1 as a player in the doxorubicin-induced DDR are dependent on the activation status of RAC1 and/or a properly working GDP/GTP exchange. Having a look at all experiments of the present work they have one thing in common, namely only cells expressing wild-type or constitutively active hRAC1 show a difference between mainly cytosolic and targeted nuclear expression in the Dox-induced DDR. Forced expression of nuclear constitutively

active hRAC1 (GFP-NLS-hRAC1(Q61L)) exhibited a diminished Dox-induced foci formation which was not seen in cells expressing cytoplasmic constitutively active RAC1. Silencing of *mRac1* resulted in decreased foci formation after Dox treatment. The observed effects could only be reverted by silencing *mRac1* and simultaneous targeted expression of constitutively active nuclear RAC1. Mainly cytoplasmic and predominantly nuclear expressed wild-type hRAC1 had only a minor effect on the Dox-induced foci formation. Dominant-negative hRAC1 showed a reduced foci formation upon Dox-treatment independent of the subcellular distribution leading to the question if dominant-negative RAC1 alters the DDR *via* unknown interaction partners since mainly cytoplasmic expression as well as forced nuclear accumulation of dominant-negative hRAC1 exhibited the same results. A reduced protein level of Dox-induced pP53, pKAP1, and γH2AX was only seen in cells transfected with *GFP-hRAC1(T17N)* as well as *GFP-NLS-hRAC1(T17N)* expression vector. A possibility for cytoplasmic hRAC1 to interact with DDR-related proteins is *via* stress kinases (P38, JNK). Whether these stress kinases modify RAC1 in the cytosol and the modified RAC1 is subsequently transported into the nucleus or is only modified in the nucleus needs to be clarified in future experiments. The conclusion is that the activity or the possibility to switch between an active and an inactive state is a basic requirement for nuclear RAC1 to interact with DDR-related proteins. Furthermore, RAC1 seems to have downstream DDR functions beyond the involvement in DSB formation.

4.4 Generation of *mRac1* knockout cells

4.4.1 RAC1 is necessary for cell survival

Lentiviruses are ideal for gene transfer into eukaryotic cells, especially into primary cells like MEF (Vigna et al. 2000; Piacibello et al. 2002). To this end, lentiviral transduction was used to induce *mRac1* knockout in MEF. The used transgene codes for Cre recombinase, which should cut at loxP sites inserted in the *mRac1* gene leading to a loss of exons and a frameshift mutation (Figure 3.32, Figure 3.40).

The *mRac1* knockout principally was possible but was leading to cell death which could not be prevented by use of a pan caspase inhibitor (QVD) leading to the assumption that the observed cell death might be caspase-independent. There are different possibilities which could lead to insufficient *mRac1* knockout efficiency (below 75 %) and/or cell death:

1) *Rac1* wild-type cells could overgrow *Rac1* knockout cells
2) Inappropriate concentration and/or duration of tamoxifen treatment
3) A homozygous *Rac1* knockout is lethal

A point which contributes to the mentioned possibly reduced cell growth of *Rac1* knockout cells is the fact that RAC1 mediates the effects of growth factors (Bokoch et al. 1993). Cyclin D1 is involved in cell cycle progression and drives the G1/S phase transition (Baldin et al. 1993; Du et al. 2013). RAC1 is known to promote transcription and translation of cyclin D1, resulting in a possible cell cycle arrest in *Rac1* knockout cells (Etienne-Manneville et al. 2002; Yoshida et al. 2010). This leads to the assumption that *Rac1* wild-type cells are growing faster than *Rac1* knockout cells. Different researchers working on RAC1 observed a reduced proliferation rate in *Rac1* knockout cells (MEF, T-cells) (Vidali et al. 2006; Guo et al. 2008; Steffen et al. 2013) or cells stably expressing dominant-negative RAC1 (HeLa cells) (Espinha et al. 2015) compared to *Rac1* wildtype cells. This in turn has the consequence, that *Rac1* wildtype cells could overgrow *Rac1* knockout cells which could be the case in the experiment where Cre Recombinase Gesicles were used for *Rac1* knockout induction as well as in the experiments with viral transduction. The MEF used in this thesis perform cell division on average every 26 h (data not shown). As stated above, *Rac1* wild-type cells might be faster growing than *Rac1* knockout cells and since the cells transfected with Cre Recombinase Gesicles were harvested 48 h post-transfection, *Rac1* wild-type cells might have overgrown *Rac1* knockout cells leading to the observed low *Rac1* knockout efficiency (20 %). To clarify the hypothesis of reduced proliferation, 5-Ethynyl-2'-deoyuridine (EdU) incorporation could be analyzed in future experiments. EdU is a modified nucleoside, a thymidine analog, that is incorporated into the DNA during S-phase (Yu et al. 2009). By addition of a fluorescent dye, the EdU incorporation can be made visible and can be analyzed under the microscope. Due to the reduced proliferation rate in *Rac1* knockout cells there should be less incorporated EdU than in *Rac1* wild.type cells.

Regarding the possibility of inappropriate concentration and/or duration of tamoxifen treatment, different concentrations of tamoxifen (4-OHT) as well as different durations of treatment were used in published data. Mostly 250 nM - 1 µM 4-OHT for 24 h up to 72 h were applied in MEF (Song et al. 2011; Dimitrova et al. 2014; Gopinathan et al. 2014; Piunti et al. 2014; Poburski et al. 2016). The duration of 4-OHT treatment in MEF is quite different in literature and ranges from 6 h up to 5 days (Li et al. 2010; Sfeir et al. 2012; Zheng et al. 2013; Gopinathan et al. 2014; Di et al. 2017; Xie et al. 2017; Zhou et al. 2020). Therefore, different concentrations of 4-OHT and treatment durations were tested in the experiments performed in this work. The best result achieved with the used conditions was 50 % *Rac1* knockout efficiency. The results for the tested clones with stable Cre.ER expression were highly variable and unfortunately do not allow to draw

conclusions about the efficacy of 4-OHT-induced *mRac1* knockout efficiency. Further experiments should be performed with 4-OHT concentration in a range of 1 µM – 10 µM since the knockout efficiency of 1 µM was up to 50 % and a treatment duration of up to 24 h.

A homozygous *Rac1* knockout might be cytolethal and lead to the observed cell death. It seems like the higher the *Rac1* knockout efficiency the more cells underwent apoptosis. Other groups tried to generate *Rac1* knockout mice and showed that a systemic *Rac1* knockout (*Rac1*-null mice) is embryonic lethal (Sugihara et al. 1998; Tan et al. 2008; Duquette et al. 2014; Abu-Issa 2015). Sugihara *et al.* identified all *Rac1*-null embryos to be not viable. They figured out, that the embryos died before E9.5 (Sugihara et al. 1998). *Rac1*-null embryos or rather the isolated epiblast cells showed no lamellipodia, a slow downed motility, and were completely rounded up (Sugihara et al. 1998), similar to inactivation of Rho proteins with C3 transferase, an ADP-ribosyltransferase from *Clostridium botulinum* (Paterson et al. 1990). In normal developing epiblast cells, the epiblast epithelium is formed after contact with the basement membrane. He and colleagues found immense apoptosis in *Rac1*-null embryoid bodies which came into contact with the basement membrane (He et al. 2010). They could show that RAC1 mediates the survival of epiblast cells after contact with the basement membrane through activation of the PI3K-Akt signaling pathway. This leads to the assumption that *Rac1*-null embryoid bodies have an impaired pro-survival pathway (He et al. 2010). However, a tissue-specific as well as inducible *Rac1* knockout in adult animals is possible (Liu, Kapoor, et al. 2008; Bopp et al. 2013; Nohata et al. 2016; Deshmukh et al. 2017).

RAC1 is known to be involved in both apoptosis and cell survival through interaction with JNK/SAPK and P38 (Coso et al. 1995; Minden et al. 1995) as well as related transcription factors such as NF-κB (Jefferies et al. 2000), PI3K, AKT (Ruggieri et al. 2001; Murga et al. 2002), BAD (BCL-2-Antagonist of cell death) and BCL-2 (B-cell lymphoma 2) (Maundrell et al. 1997; Zhang et al. 2004). Thus, RAC1 is not restricted to either the pro-apoptotic or the anti-apoptotic pathway. Accordingly, it may be possible that deletion of RAC1 leads to apoptosis, as demonstrated in this work, whereas inhibition of RAC1 leads to less apoptosis as shown in previous work (Damrot et al. 2006; Huelsenbeck et al. 2011; Huelsenbeck et al. 2012; Wartlick et al. 2013).

Certain working groups published data from cell culture experiments with *Rac1* knockout cells (Liu, Kapoor, et al. 2008; Tan et al. 2008; Steffen et al. 2013; Kunschmann et al. 2019). Most of those publications lack western blot- or PCR-based experiments which proof the *Rac1* knockout. In some cases, a western blot was performed, but the so-called

Rac1 knockout cells still show weak RAC1 expression (Liu, Kapoor, et al. 2008; Tan et al. 2008). In the few publications where the *Rac1* knockout was experimentally confirmed (Steffen et al. 2013; Kunschmann et al. 2019). Unfortunately, the exact used method and culture conditions are not properly stated.

Maybe a homozygous *Rac1* knockout in cells is impossible without manipulating specific pathways/proteins, e.g., PTEN, at the same time. Migeotte *et al.* could show that apoptosis in *Rac1* knockout cells could be reduced by heterozygous *PTEN* knockout (Migeotte et al. 2011). This provides evidence that *Rac1* acts downstream of the PI3K-Akt pathway/ATM as already stated above.

4.5 Perspective

The experiments described in this thesis have shown that only cells expressing wild-type hRAC1 or constitutively active hRAC1 exhibited a difference between mainly cytosolic and targeted nuclear expression regarding Dox induced foci formation as well as Dox-induced phosphorylation of DDR-related proteins. This leads to the assumption that only active nuclear RAC1 or nuclear RAC1, which is able to cycle between the GDP/GTP bound state, is able to interact with DDR-related proteins. Apparently RAC1 not only influences the DSB formation but also the DDR signaling after the DNA is damaged through influencing phosphorylation or dephosphorylation reactions of e.g., P53 and KAP1. The amount of these phosphorylated proteins was altered upon expression of wild-type and dominant-negative hRAC1 mutants, leading to the assumption that there seem to be also downstream DDR functions of RAC1 beyond the involvement in DSB formation.

The western blot experiments were performed with cells transfected with *hRAC1* mutants but with an intact background of endogenous mRAC1, therefore *GFP-hRAC1* expression vector transfected cells with silenced mRAC1 should be included in future experiments. To gain further insight in the network of RAC1 signaling future studies should also include analysis of interaction partners in subcellular fractions by gene expression and western blot analysis. Furthermore, a RAC1 activation assay could be carried out with these fractions to evaluate the basal GDP/GTP loading of intrinsic RAC1 as well as the GDP/GTP loading of intrinsic RAC1 after treatment with DNA damaging agents to see if there are changes. Furthermore live cell imaging could be used to analyse the import of transgenic hRAC1 into the nucleus and out of the nucleus after DNA damage.

With the aim to investigate the RAC1 import into the nucleus more closely, *RAC1* mutants with deleted CAAX box (ΔCAAX) (with and without additional NLS) could be cloned. The CAAX box is essential for prenylation as well as membrane localization (Adamson, Marshall, et al. 1992; Adamson, Paterson, et al. 1992; Lin et al. 2015). Due to the prenylation the intrinsic NLS is masked (Abdrabou et al. 2018). Transfection of MEF with *GFP-hRAC1ΔCAAX* expression vector could answer the question whether the prenylation and/or the GDP/GTP binding state is a prerequisite for nuclear RAC1 import and the resulting nuclear functions in the doxorubicin induced DDR. Furthermore, expressing vectors with deleted nuclear export sequences (NES) could be designed to force a stronger accumulation of the GFP-NLS-hRAC1 fusion proteins (*GFP-NLS-hRAC1ΔNES* expression vectors*)*, especially of constitutively active and dominant-

negative hRAC1 with additional NLS. The NLS would force a nuclear accumulation and the deleted nuclear export sequences would prevent the nuclear export.

Previous work of this group already revealed a connection between RAC1 and Top II poisons (Henninger et al. 2012; Huelsenbeck et al. 2012; Wartlick et al. 2013). In this published data the effect of RAC1 inhibition on Top II poison-induced DDR was evaluated. For further evaluation of the described link between RAC1 and topoisomerase II (Damrot et al. 2006; Huelsenbeck et al. 2011; Huelsenbeck et al. 2012; Wartlick et al. 2013) a TARDIS assay should be performed. This method allows the detection and quantification of the cleavable complexes (Cowell et al. 2018). RAC1 inhibition prevented the formation of the so-called cleavable complex consisting of doxorubicin, DNA and type II topoisomerases (Huelsenbeck et al. 2012; Wartlick et al. 2013) resulting in less Dox-induced DSB. With the TARDIS assay constitutively active and wild-type RAC1 can be analyzed in regard to their interaction with the cleavable complex and the observations made upon pharmacological RAC1 inhibition can be confirmed with dominant-negative RAC1.

To confirm the results of this thesis that the seen effects of RAC1 in the Dox-induced DDR are specific for Top II poisons, another Top II inhibitor, e.g., etoposide as well as a genotoxin which induces DSB independent of Top II (e.g., IR or temozolomide) should be included in analysis.

A direct interaction of RAC1 and ATM could not be confirmed in this work. Since the analyzed DDR-related proteins (H2AX, KAP1, P53) are also phosphorylated through DNA-PK and ATR (Lees-Miller et al. 1992; Wang et al. 2005; White et al. 2006; Lu et al. 2019), ATM and/or DNA-PK/ATR inhibition through pharmacological inhibition or siRNA silencing, as well as knockout of ATM and/or DNA-PK/ATR (CRISPR-based approach) should be performed to analyze the interaction of RAC1 with PI3K and the DDR-related proteins since ATM, DNA-PK, and ATR are among the most important sensor proteins and detect DNA damage within minutes of its occurrence.

An increased apoptotic rate was seen in experiments described in this thesis and also in published data (He et al. 2010; Migeotte et al. 2011) upon *Rac1* knockout which might be due to a defective pro survival pathway. Thus, to generate a stable *Rac1* knockout cell line, either the pro survival pathway would need to be triggered or the pro apoptotic pathway would need to be inhibited. Migeotte *et al.* showed that apoptosis in *Rac1* knockout cells was reduced by heterozygous *PTEN* knockout (Migeotte et al. 2011). For generation of the *Rac1* knockout cell line, a fluorescent signal which changes the color after Cre recombinase-mediated recombination could be used. For this purpose,

plasmids have been developed which lead to a red fluorescence in the cell after transfection and after Cre recombinase-mediated recombination the fluorescent signal changes to green (Yang et al. 2001; Pfannkuche et al. 2008). Thus, the cells could be sorted on basis of their fluorescence in order to obtain a *Rac1* knockout cell population.

Since *Rac1* knockout cells seem not be able to survive without manipulating other signaling pathways, one consideration would be to generate a stable *Rac1* knockdown cell line using shRNA. While doing so, one could titrate the knockdown to a maximum without lethality for the cells.

5 Summary

RAC1 is a molecular switch that cycles between a guanosine-5'-diphosphate (GDP)-bound (inactive) state and a guanosine 5'-triphosphate (GTP)-bound (active) state which allows interaction with effector proteins. As molecular switch, RAC1 conducts external stimuli from the cell membrane to transcription factors, protein kinases, and modulators of the actin cytoskeleton. Nuclear functions of RAC1 were identified that are related to apoptosis, proliferation, migration and cell cycle progression. Beyond that, studies demonstrated an involvement of RAC1 in response to genotoxic stress. Previous investigations discovered a role of RAC1 in the doxorubicin (Dox)-induced DNA damage response (DDR). Until today, it is unclear whether the described protection against topoisomerase II poison-induced DNA damage and cell death by pharmacological inhibition of RAC1 is dependent on cytosolic RAC1 and/or nuclear RAC1.

To elucidate the role of RAC1 in the DDR RAC1 was pharmacologically inhibited with EHT 1864 or silenced by transfection with siRNA against *mRac1*. Afterwards the Dox-induced double strand break signaling was analyzed by evaluation of fluorescent nuclear γH2AX and 53BP1 foci as well as the Dox-induced DDR by western blot analysis of activated DDR-related proteins. Treatment with EHT 1864 as well as *mRac1* knockdown reduced the Dox-induced DSB-formation to a similar extent. To elucidate the role of nuclear and cytosolic RAC1 in the DDR various human RAC1 mutants (wild-type, constitutively active, dominant-negative) were transiently expressed in mouse embryonic fibroblasts (MEF) prior to Dox treatment in the present work. To distinguish between effects on the Dox-induced DDR promoted by nuclear RAC1 and cytosolic RAC1, the *GFP-hRAC1* expression vectors were used with and without an additional nuclear localization sequence (NLS). To obtain evidence about the functionality of the aforementioned expression vectors in MEF lamellipodia formation was evaluated. For verification of the functionality of the additional NLS RAC1 localization of GFP-hRAC1 with and without additional NLS was quantified by measuring the fluorescence intensity of GFP-coupled hRAC1 in the cytoplasm and the nucleus of successfully transfected cells. Targeted nuclear accumulation of dominant-negative hRAC1 as well as constitutively active hRAC1 disclosed similar effects namely less Dox-induced γH2AX and 53BP1 foci. *hRAC1* mutants altered the Dox-induced DDR in a construct-dependent manner as seen on the amount of pP53 and pKAP1 protein. Since cells expressing hRAC1 mutants exhibited no influence on the Dox-induced pATM Ser1981 foci formation RAC1 seems to act downstream or independent of ATM in the DDR. The presented data are leading to the assumption that RAC1 is required for a substantial activation of the

Dox-induced DDR downstream or independent of ATM and balanced levels of active and inactive RAC1 inside the nucleus are a prerequisite for this response.

Moreover, an attempt was made to generate a stable *mRac1* knockout cell line. Viral transduction was used for induction of the *mRac1* knockout. Creation of the *mRac1* knockout with a Cre-Lox-based system was principally possible but was cytolethal which could not be prevented by use of a pan caspase inhibitor.

Zusammenfassung

RAC1 ist ein molekularer Schalter, der zwischen einem Guanosin-5´-Diphosphat (GDP)-gebundenen (inaktiven) Zustand und einem Guanosin-5´-Triphosphat (GTP)-gebundenen (aktiven) Zustand wechselt, um so die Interaktion mit Effektorproteinen zu ermöglichen. Als molekularer Schalter leitet RAC1 externe Stimuli von der Zellmembran zu Transkriptionsfaktoren, Proteinkinasen und Modulatoren des Cytoskeletts. Es wurden Kernfunktionen von RAC1 identifiziert, die mit Apoptose, Proliferation, Migration und Fortschreiten des Zellzyklus zusammenhängen. Darüber hinaus zeigten Studien eine Beteiligung von RAC1 bei der Reaktion auf genotoxischen Stress. Frühere Untersuchungen ergaben eine Rolle von RAC1 bei der doxorubicin (Dox)-induzierten DNA-Schadensantwort (DDR). Bis heute ist unklar, ob der beschriebene Schutz gegen DNA Schäden und Zelltod, verursacht durch Topoisomerase II-Gifte, durch pharmakologische Hemmung von RAC1 von cytosolischen und/oder nukleärem RAC1 abhängen.

Um die Rolle von RAC1 in der DDR aufzuklären, wurde RAC1 mit EHT 1864 pharmakologisch inhibiert oder durch Transfektion mit siRNA gegen *mRac1* herunterreguliert. Anschließend wurde das Dox-induzierte Doppelstrangbruch *signaling* durch Auswertung fluoreszierender nukleärer γH2AX und 53BP1 Foci sowie der Dox-induzierten DDR durch aktivierte, in die DDR involvierte Proteine mittels Western Blot analysiert. Die Behandlung mit EHT 1864 sowie der *knockdown* von *mRac1* reduzierten die Dox-induzierte DSB-Bildung in ähnlichem Maße. Um die Rolle von nukleärem und cytosolischem RAC1 in der DDR zu klären, wurden in der vorliegenden Arbeit verschiedene humane RAC1 Mutanten (wildtypisch, konstitutiv aktiv, dominant-negativ) transient in embryonalen Fibroblasten der Maus (MEF) exprimiert und anschließend mit Dox behandelt. Zur Unterscheidung zwischen Effekten auf die Dox-induzierte DDR, die durch nukleäres RAC1 und cytosolisches RAC1 hervorgerufen werden, wurden die *GFP-hRAC1* Expressionsvektoren mit und ohne zusätzliche Kernlokalisierungssequenz (*nuclear localisation sequence*, NLS) verwendet. Um Beweise für die Funktionalität der zuvor genannten Expressionsvektoren in MEF zu erhalten, wurde die Bildung von Lamellipodien untersucht. Zur Überprüfung der Funktionalität des zusätzlichen NLS wurde die Lokalisierung von GFP-hRAC1 mit und ohne zusätzliches NLS durch die Messung der Fluoreszenzintensität von GFP-gekoppeltem hRAC1 im Cytoplasma und im Zellkern von zuvor erfolgreich transfizierten Zellen quantifiziert. Die gezielte nukleäre Akkumulation von dominant-negativem hRAC1 sowie von konstitutiv aktivem hRAC1 zeigten ähnliche Effekte, nämlich weniger Dox-induzierte γH2AX und 53BP1 Foci. Die *hRAC1* Mutanten veränderten die Dox-induzierte DDR in Konstrukt-abhängiger Weise,

wie aus der Menge an detektiertem pP53 und pKAP1 hervorgeht. Da Zellen, die hRAC1 Mutanten exprimierten, keinen Einfluss auf die Dox-induzierte Bildung von pATM Ser1981 Foci zeigten, scheint RAC1 in der DDR *downstream* oder unabhängig von ATM zu wirken. Die präsentierten Daten führen zu der Annahme, dass RAC1 für eine Aktivierung der Dox-induzierten DDR *downstream* oder unabhängig von ATM erforderlich ist und eine ausgewogene Menge an aktivem und inaktivem RAC1 im Zellkern eine Voraussetzung für diese Reaktion ist.

Darüber hinaus wurde versucht, eine *mRac1 knockout* Zelllinie zu generieren. Die virale Transduktion wurde zur Induktion des *mRac1 knockout* verwendet. Die Erzeugung des *mRac1 knockout* mit einem Cre-Lox-basierten System war prinzipiell möglich, verlief jedoch zytotoxisch, was auch durch die Verwendung eines Pan-Caspase-Inhibitors nicht verhindert werden konnte.

6 References

Abdrabou, A., and Z. Wang. 2018. 'Post-Translational Modification and Subcellular Distribution of Rac1: An Update', *Cells*, 7.

Abu-Issa, R. 2015. 'Rac1 modulates cardiomyocyte adhesion during mouse embryonic development', *Biochem Biophys Res Commun*, 456: 847-52.

Adamson, P., C. J. Marshall, A. Hall, and P. A. Tilbrook. 1992. 'Post-translational modifications of p21rho proteins', *J Biol Chem*, 267: 20033-8.

Adamson, P., H. F. Paterson, and A. Hall. 1992. 'Intracellular localization of the P21rho proteins', *J Cell Biol*, 119: 617-27.

Allen, T. D., J. M. Cronshaw, S. Bagley, E. Kiseleva, and M. W. Goldberg. 2000. 'The nuclear pore complex: mediator of translocation between nucleus and cytoplasm', *J Cell Sci*, 113 (Pt 10): 1651-9.

Alsayed, Y., S. Uddin, N. Mahmud, F. Lekmine, D. V. Kalvakolanu, S. Minucci, G. Bokoch, and L. C. Platanias. 2001. 'Activation of Rac1 and the p38 mitogen-activated protein kinase pathway in response to all-trans-retinoic acid', *J Biol Chem*, 276: 4012-9.

Aparicio, T., R. Baer, and J. Gautier. 2014. 'DNA double-strand break repair pathway choice and cancer', *DNA Repair (Amst)*, 19: 169-75.

Arcamone, F., G. Cassinelli, G. Fantini, A. Grein, P. Orezzi, C. Pol, and C. Spalla. 2000. 'Adriamycin, 14-hydroxydaunomycin, a new antitumor antibiotic from S. peucetius var. caesius. Reprinted from Biotechnology and Bioengineering, Vol. XI, Issue 6, Pages 1101-1110 (1969)', *Biotechnol Bioeng*, 67: 704-13.

Ayrapetov, M. K., O. Gursoy-Yuzugullu, C. Xu, Y. Xu, and B. D. Price. 2014. 'DNA double-strand breaks promote methylation of histone H3 on lysine 9 and transient formation of repressive chromatin', *Proc Natl Acad Sci U S A*, 111: 9169-74.

Azzam, E. I., J. P. Jay-Gerin, and D. Pain. 2012. 'Ionizing radiation-induced metabolic oxidative stress and prolonged cell injury', *Cancer Lett*, 327: 48-60.

Bachur, N. R., F. Yu, R. Johnson, R. Hickey, Y. Wu, and L. Malkas. 1992. 'Helicase inhibition by anthracycline anticancer agents', *Mol Pharmacol*, 41: 993-8.

Bai, Y., D. Guo, X. Sun, G. Tang, T. Liao, Y. Peng, J. Xu, and L. Shi. 2018. 'Balanced Rac1 activity controls formation and maintenance of neuromuscular acetylcholine receptor clusters', *J Cell Sci*, 131.

Baldin, V., J. Lukas, M. J. Marcote, M. Pagano, and G. Draetta. 1993. 'Cyclin D1 is a nuclear protein required for cell cycle progression in G1', *Genes Dev*, 7: 812-21.

Banin, S., L. Moyal, S. Shieh, Y. Taya, C. W. Anderson, L. Chessa, N. I. Smorodinsky, C. Prives, Y. Reiss, Y. Shiloh, and Y. Ziv. 1998. 'Enhanced phosphorylation of p53 by ATM in response to DNA damage', *Science*, 281: 1674-7.

Bar-Sagi, D., and A. Hall. 2000. 'Ras and Rho GTPases: a family reunion', *Cell*, 103: 227-38.

Baron, R., E. Fourcade, I. Lajoie-Mazenc, C. Allal, B. Couderc, R. Barbaras, G. Favre, J. C. Faye, and A. Pradines. 2000. 'RhoB prenylation is driven by the three carboxyl-terminal amino acids of the protein: evidenced in vivo by an anti-farnesyl cysteine antibody', *Proc Natl Acad Sci U S A*, 97: 11626-31.

Bartek, J., and J. Lukas. 2003. 'Chk1 and Chk2 kinases in checkpoint control and cancer', *Cancer Cell*, 3: 421-9.

Bassing, C. H., and F. W. Alt. 2004. 'H2AX may function as an anchor to hold broken chromosomal DNA ends in close proximity', *Cell Cycle*, 3: 149-53.

Bates, D. A., and C. C. Winterbourn. 1982. 'Deoxyribose breakdown by the adriamycin semiquinone and H2O2: evidence for hydroxyl radical participation', *FEBS Lett*, 145: 137-42.

Baumann, P., and S. C. West. 1997. 'The human Rad51 protein: polarity of strand transfer and stimulation by hRP-A', *EMBO J*, 16: 5198-206.

Begg, A. C., F. A. Stewart, and C. Vens. 2011. 'Strategies to improve radiotherapy with targeted drugs', *Nat Rev Cancer*, 11: 239-53.

Bellanger, J. M., J. B. Lazaro, S. Diriong, A. Fernandez, N. Lamb, and A. Debant. 1998. 'The two guanine nucleotide exchange factor domains of Trio link the Rac1 and the RhoA pathways in vivo', *Oncogene*, 16: 147-52.

Belli, M., and M. A. Tabocchini. 2020. 'Ionizing Radiation-Induced Epigenetic Modifications and Their Relevance to Radiation Protection', *Int J Mol Sci*, 21.

Benson, F. E., A. Stasiak, and S. C. West. 1994. 'Purification and characterization of the human Rad51 protein, an analogue of E. coli RecA', *EMBO J*, 13: 5764-71.

Bhatia, N., T. Z. Xiao, K. A. Rosenthal, I. A. Siddiqui, S. Thiyagarajan, B. Smart, Q. Meng, C. L. Zuleger, H. Mukhtar, S. C. Kenney, M. R. Albertini, and B. Jack Longley. 2013. 'MAGE-C2 promotes growth and tumorigenicity of melanoma cells, phosphorylation of KAP1, and DNA damage repair', *J Invest Dermatol*, 133: 759-67.

Bishop, A. L., and A. Hall. 2000. 'Rho GTPases and their effector proteins', *Biochem J*, 348 Pt 2: 241-55.

Bisi, S., A. Disanza, C. Malinverno, E. Frittoli, A. Palamidessi, and G. Scita. 2013. 'Membrane and actin dynamics interplay at lamellipodia leading edge', *Curr Opin Cell Biol*, 25: 565-73.

Blandino, G., A. J. Levine, and M. Oren. 1999. 'Mutant p53 gain of function: differential effects of different p53 mutants on resistance of cultured cells to chemotherapy', *Oncogene*, 18: 477-85.

Blum, R. H., and S. K. Carter. 1974. 'Adriamycin. A new anticancer drug with significant clinical activity', *Ann Intern Med*, 80: 249-59.

Bodley, A., L. F. Liu, M. Israel, R. Seshadri, Y. Koseki, F. C. Giuliani, S. Kirschenbaum, R. Silber, and M. Potmesil. 1989. 'DNA topoisomerase II-mediated interaction of doxorubicin and daunorubicin congeners with DNA', *Cancer Res*, 49: 5969-78.

Bohgaki, T., M. Bohgaki, and R. Hakem. 2010. 'DNA double-strand break signaling and human disorders', *Genome Integr*, 1: 15.

Bokoch, G. M., and C. J. Der. 1993. 'Emerging concepts in the Ras superfamily of GTP-binding proteins', *FASEB J*, 7: 750-9.

Bopp, A., F. Wartlick, C. Henninger, B. Kaina, and G. Fritz. 2013. 'Rac1 modulates acute and subacute genotoxin-induced hepatic stress responses, fibrosis and liver aging', *Cell Death Dis*, 4: e558.

Bopp, A., F. Wartlick, C. Henninger, M. Schwarz, B. Kaina, and G. Fritz. 2015. 'Rac1 promotes diethylnitrosamine (DEN)-induced formation of liver tumors', *Carcinogenesis*, 36: 378-89.

Borde, V., and J. Cobb. 2009. 'Double functions for the Mre11 complex during DNA double-strand break repair and replication', *Int J Biochem Cell Biol*, 41: 1249-53.

Borer, R. A., C. F. Lehner, H. M. Eppenberger, and E. A. Nigg. 1989. 'Major nucleolar proteins shuttle between nucleus and cytoplasm', *Cell*, 56: 379-90.

Borrego-Soto, G., R. Ortiz-Lopez, and A. Rojas-Martinez. 2015. 'Ionizing radiation-induced DNA injury and damage detection in patients with breast cancer', *Genet Mol Biol*, 38: 420-32.

Bos, J. L., H. Rehmann, and A. Wittinghofer. 2007. 'GEFs and GAPs: critical elements in the control of small G proteins', *Cell*, 129: 865-77.

Boulter, E., R. Garcia-Mata, C. Guilluy, A. Dubash, G. Rossi, P. J. Brennwald, and K. Burridge. 2010. 'Regulation of Rho GTPase crosstalk, degradation and activity by RhoGDI1', *Nat Cell Biol*, 12: 477-83.

Bourne, H. R., D. A. Sanders, and F. McCormick. 1990. 'The GTPase superfamily: a conserved switch for diverse cell functions', *Nature*, 348: 125-32.

Box, J. K., N. Paquet, M. N. Adams, D. Boucher, E. Bolderson, K. J. O'Byrne, and D. J. Richard. 2016. 'Nucleophosmin: from structure and function to disease development', *BMC Mol Biol*, 17: 19.

Brenner, B., U. Koppenhoefer, C. Weinstock, O. Linderkamp, F. Lang, and E. Gulbins. 1997. 'Fas- or ceramide-induced apoptosis is mediated by a Rac1-regulated activation of Jun N-terminal kinase/p38 kinases and GADD153', *J Biol Chem*, 272: 22173-81.

Bromberg, K. D., A. B. Burgin, and N. Osheroff. 2003. 'Quinolone action against human topoisomerase IIalpha: stimulation of enzyme-mediated double-stranded DNA cleavage', *Biochemistry*, 42: 3393-8.

Brum, G., T. Carbone, E. Still, V. Correia, K. Szulak, D. Calianese, C. Best, G. Cammarata, K. Higgins, F. Ji, W. Di, and Y. Wan. 2013. 'N-acetylcysteine potentiates doxorubicin-induced ATM and p53 activation in ovarian cancer cells', *Int J Oncol*, 42: 211-8.

Burma, S., B. P. Chen, M. Murphy, A. Kurimasa, and D. J. Chen. 2001. 'ATM phosphorylates histone H2AX in response to DNA double-strand breaks', *J Biol Chem*, 276: 42462-7.

Bustelo, X. R., V. Ojeda, M. Barreira, V. Sauzeau, and A. Castro-Castro. 2012. 'Rac-ing to the plasma membrane: the long and complex work commute of Rac1 during cell signaling', *Small GTPases*, 3: 60-6.

Bustelo, X. R., V. Sauzeau, and I. M. Berenjeno. 2007. 'GTP-binding proteins of the Rho/Rac family: regulation, effectors and functions in vivo', *Bioessays*, 29: 356-70.

Butin-Israeli, V., S. A. Adam, and R. D. Goldman. 2013. 'Regulation of nucleotide excision repair by nuclear lamin b1', *PLoS One*, 8: e69169.

Calsou, P., P. Frit, O. Humbert, C. Muller, D. J. Chen, and B. Salles. 1999. 'The DNA-dependent protein kinase catalytic activity regulates DNA end processing by means of Ku entry into DNA', *J Biol Chem*, 274: 7848-56.

Campa, C. C., E. Ciraolo, A. Ghigo, G. Germena, and E. Hirsch. 2015. 'Crossroads of PI3K and Rac pathways', *Small GTPases*, 6: 71-80.

Campos, A., and A. Clemente-Blanco. 2020. 'Cell Cycle and DNA Repair Regulation in the Damage Response: Protein Phosphatases Take Over the Reins', *Int J Mol Sci*, 21.

Canman, C. E., and M. B. Kastan. 1996. 'Signal transduction. Three paths to stress relief', *Nature*, 384: 213-4.

Canman, C. E., D. S. Lim, K. A. Cimprich, Y. Taya, K. Tamai, K. Sakaguchi, E. Appella, M. B. Kastan, and J. D. Siliciano. 1998. 'Activation of the ATM kinase by ionizing radiation and phosphorylation of p53', *Science*, 281: 1677-9.

Carr, H. S., C. A. Morris, S. Menon, E. H. Song, and J. A. Frost. 2013. 'Rac1 controls the subcellular localization of the Rho guanine nucleotide exchange factor Net1A to regulate focal adhesion formation and cell spreading', *Mol Cell Biol*, 33: 622-34.

Cerione, R. A., and Y. Zheng. 1996. 'The Dbl family of oncogenes', *Curr Opin Cell Biol*, 8: 216-22.

Cerutti, P. A. 1974. 'Effects of ionizing radiation on mammalian cells', *Naturwissenschaften*, 61: 51-9.

Chapman, J. R., M. R. Taylor, and S. J. Boulton. 2012. 'Playing the end game: DNA double-strand break repair pathway choice', *Mol Cell*, 47: 497-510.

Chatterjee, A., L. Wang, D. L. Armstrong, and S. Rossie. 2010. 'Activated Rac1 GTPase translocates protein phosphatase 5 to the cell membrane and stimulates phosphatase activity in vitro', *J Biol Chem*, 285: 3872-82.

Chau, J. F., D. Jia, Z. Wang, Z. Liu, Y. Hu, X. Zhang, H. Jia, K. P. Lai, W. F. Leong, B. J. Au, Y. Mishina, Y. G. Chen, C. Biondi, E. Robertson, D. Xie, H. Liu, L. He, X. Wang, Q. Yu, and B. Li. 2012. 'A crucial role for bone morphogenetic protein-Smad1 signalling in the DNA damage response', *Nat Commun*, 3: 836.

Chehab, N. H., A. Malikzay, E. S. Stavridi, and T. D. Halazonetis. 1999. 'Phosphorylation of Ser-20 mediates stabilization of human p53 in response to DNA damage', *Proc Natl Acad Sci U S A*, 96: 13777-82.

Cheng, C. T., C. Y. Kuo, C. Ouyang, C. F. Li, Y. Chung, D. C. Chan, H. J. Kung, and D. K. Ann. 2016. 'Metabolic Stress-Induced Phosphorylation of KAP1 Ser473 Blocks Mitochondrial Fusion in Breast Cancer Cells', *Cancer Res*, 76: 5006-18.

Cherfils, J., and M. Zeghouf. 2013. 'Regulation of small GTPases by GEFs, GAPs, and GDIs', *Physiol Rev*, 93: 269-309.

Chi, H. C., C. Y. Tsai, C. S. Wang, H. Y. Yang, C. H. Lo, W. J. Wang, K. F. Lee, L. Y. Lai, J. H. Hong, Y. F. Chang, M. M. Tsai, C. T. Yeh, C. H. Wu, C. C. Hsieh, L. H. Wang, W. J. Chen, and K. H. Lin. 2020. 'DOCK6 promotes chemo- and radioresistance of gastric cancer by modulating WNT/beta-catenin signaling and cancer stem cell traits', *Oncogene*, 39: 5933-49.

Chircop, M. 2014. 'Rho GTPases as regulators of mitosis and cytokinesis in mammalian cells', *Small GTPases*, 5.

Christmann, M., M. T. Tomicic, W. P. Roos, and B. Kaina. 2003. 'Mechanisms of human DNA repair: an update', *Toxicology*, 193: 3-34.

Chronis, F., and E. P. Rogakou. 2007. 'Interplay Between γH2AX and 53BP1 Pathways in DNA Double-Strand Break Repair Response', *Gewirtz D.A., Holt S.E., Grant S. (eds) Apoptosis, Senescence, and Cancer. Cancer Drug Discovery and Development. Humana Press*.

Chucair-Elliott, A. J., S. R. Ocanas, D. R. Stanford, N. Hadad, B. Wronowski, L. Otalora, M. B. Stout, and W. M. Freeman. 2019. 'Tamoxifen induction of Cre recombinase does not cause long-lasting or sexually divergent responses in the CNS epigenome or transcriptome: implications for the design of aging studies', *Geroscience*, 41: 691-708.

Cimprich, K. A., and D. Cortez. 2008. 'ATR: an essential regulator of genome integrity', *Nat Rev Mol Cell Biol*, 9: 616-27.

Cole, M. P., I. D. Todd, and P. M. Wilkinson. 1974. 'A preliminary trial of doxorubicin in advanced breast cancer and other malignant disease', *Br J Cancer*, 29: 114-6.

Collins, E., J. C. Birchall, J. L. Williams, and M. Gumbleton. 2007. 'Nuclear localisation and pDNA condensation in non-viral gene delivery', *J Gene Med*, 9: 265-74.

Colombo, E., M. Alcalay, and P. G. Pelicci. 2011. 'Nucleophosmin and its complex network: a possible therapeutic target in hematological diseases', *Oncogene*, 30: 2595-609.

Conti, E., and E. Izaurralde. 2001. 'Nucleocytoplasmic transport enters the atomic age', *Curr Opin Cell Biol*, 13: 310-9.

Coso, O. A., M. Chiariello, J. C. Yu, H. Teramoto, P. Crespo, N. Xu, T. Miki, and J. S. Gutkind. 1995. 'The small GTP-binding proteins Rac1 and Cdc42 regulate the activity of the JNK/SAPK signaling pathway', *Cell*, 81: 1137-46.

Coso, O. A., H. Teramoto, W. F. Simonds, and J. S. Gutkind. 1996. 'Signaling from G protein-coupled receptors to c-Jun kinase involves beta gamma subunits of heterotrimeric G proteins acting on a Ras and Rac1-dependent pathway', *J Biol Chem*, 271: 3963-6.

Cowell, I. G., and C. A. Austin. 2018. 'Visualization and Quantification of Topoisomerase-DNA Covalent Complexes Using the Trapped in Agarose Immunostaining (TARDIS) Assay', *Methods Mol Biol*, 1703: 301-16.

Crowley, L. C., G. Chojnowski, and N. J. Waterhouse. 2016. 'Measuring the DNA Content of Cells in Apoptosis and at Different Cell-Cycle Stages by Propidium Iodide Staining and Flow Cytometry', *Cold Spring Harb Protoc*, 2016.

Damrot, J., T. Nubel, B. Epe, W. P. Roos, B. Kaina, and G. Fritz. 2006. 'Lovastatin protects human endothelial cells from the genotoxic and cytotoxic effects of the anticancer drugs doxorubicin and etoposide', *Br J Pharmacol*, 149: 988-97.

Dancker, P., I. Low, W. Hasselbach, and T. Wieland. 1975. 'Interaction of actin with phalloidin: polymerization and stabilization of F-actin', *Biochim Biophys Acta*, 400: 407-14.

Dart, D. A., K. E. Adams, I. Akerman, and N. D. Lakin. 2004. 'Recruitment of the cell cycle checkpoint kinase ATR to chromatin during S-phase', *J Biol Chem*, 279: 16433-40.

Darzynkiewicz, Z., G. Juan, X. Li, W. Gorczyca, T. Murakami, and F. Traganos. 1997. 'Cytometry in cell necrobiology: analysis of apoptosis and accidental cell death (necrosis)', *Cytometry*, 27: 1-20.

Davis, A. J., B. P. Chen, and D. J. Chen. 2014. 'DNA-PK: a dynamic enzyme in a versatile DSB repair pathway', *DNA Repair (Amst)*, 17: 21-9.

Davis, M. J., B. H. Ha, E. C. Holman, R. Halaban, J. Schlessinger, and T. J. Boggon. 2013. 'RAC1P29S is a spontaneously activating cancer-associated GTPase', *Proc Natl Acad Sci U S A*, 110: 912-7.

de Feraudy, S., I. Revet, V. Bezrookove, L. Feeney, and J. E. Cleaver. 2010. 'A minority of foci or pan-nuclear apoptotic staining of gammaH2AX in the S phase after UV damage contain DNA double-strand breaks', *Proc Natl Acad Sci U S A*, 107: 6870-5.

De, P., B. J. Rozeboom, J. C. Aske, and N. Dey. 2020. 'Active RAC1 Promotes Tumorigenic Phenotypes and Therapy Resistance in Solid Tumors', *Cancers (Basel)*, 12.

Delaney, G., S. Jacob, C. Featherstone, and M. Barton. 2005. 'The role of radiotherapy in cancer treatment: estimating optimal utilization from a review of evidence-based clinical guidelines', *Cancer*, 104: 1129-37.

Deng, S., T. Yan, C. Jendrny, A. Nemecek, M. Vincetic, U. Godtel-Armbrust, and L. Wojnowski. 2014. 'Dexrazoxane may prevent doxorubicin-induced DNA damage via depleting both topoisomerase II isoforms', *BMC Cancer*, 14: 842.

Denning, W., S. Das, S. Guo, J. Xu, J. C. Kappes, and Z. Hel. 2013. 'Optimization of the transductional efficiency of lentiviral vectors: effect of sera and polycations', *Mol Biotechnol*, 53: 308-14.

Deplazes, J., M. Fuchs, S. Rauser, H. Genth, E. Lengyel, R. Busch, and B. Luber. 2009. 'Rac1 and Rho contribute to the migratory and invasive phenotype associated with somatic E-cadherin mutation', *Hum Mol Genet*, 18: 3632-44.

Desantis, A., T. Bruno, V. Catena, F. De Nicola, F. Goeman, S. Iezzi, C. Sorino, M. P. Gentileschi, S. Germoni, V. Monteleone, M. Pellegrino, M. Kann, P. D. De Meo, M. Pallocca, K. Hopker, F. Moretti, E. Mattei, H. C. Reinhardt, A. Floridi, C. Passananti, T. Benzing, G. Blandino, and M. Fanciulli. 2015. 'Che-1 modulates the decision between cell cycle arrest and apoptosis by its binding to p53', *Cell Death Dis*, 6: e1764.

Deshmukh, J., R. Pofahl, and I. Haase. 2017. 'Epidermal Rac1 regulates the DNA damage response and protects from UV-light-induced keratinocyte apoptosis and skin carcinogenesis', *Cell Death Dis*, 8: e2664.

Desouky, Omar, Nan Ding, and Guangming Zhou. 2015. 'Targeted and non-targeted effects of ionizing radiation', *Journal of Radiation Research and Applied Sciences*, 8: 247-54.

Di, J., J. Tang, H. Qian, D. A. Franklin, C. Deisenroth, Y. Itahana, J. Zheng, and Y. Zhang. 2017. 'p53 upregulates PLCepsilon-IP3-Ca(2+) pathway and inhibits autophagy through its target gene Rap2B', *Oncotarget*, 8: 64657-69.

Dimarco, A., M. Gaetani, P. Orezzi, B. M. Scarpinato, R. Silvestrini, M. Soldati, T. Dasdia, and L. Valentini. 1964. ''Daunomycin', a New Antibiotic of the Rhodomycin Group', *Nature*, 201: 706-7.

Dimitrova, N., J. R. Zamudio, R. M. Jong, D. Soukup, R. Resnick, K. Sarma, A. J. Ward, A. Raj, J. T. Lee, P. A. Sharp, and T. Jacks. 2014. 'LincRNA-p21 activates p21 in cis to promote Polycomb target gene expression and to enforce the G1/S checkpoint', *Mol Cell*, 54: 777-90.

DiPersio, C. M. 2007. 'Double duty for Rac1 in epidermal wound healing', *Sci STKE*, 2007: pe33.

Disanza, A., and G. Scita. 2015. 'Nuclear and cellular plasticity: nuclear RAC1 takes center stage', *Dev Cell*, 32: 261-3.

Dizdaroglu, M., and P. Jaruga. 2012. 'Mechanisms of free radical-induced damage to DNA', *Free Radic Res*, 46: 382-419.

Dong, J., T. Zhang, Y. Ren, Z. Wang, C. C. Ling, F. He, G. C. Li, C. Wang, and B. Wen. 2017. 'Inhibiting DNA-PKcs in a non-homologous end-joining pathway in response to DNA double-strand breaks', *Oncotarget*, 8: 22662-73.

Du, Z., X. Tong, and X. Ye. 2013. 'Cyclin D1 promotes cell cycle progression through enhancing NDR1/2 kinase activity independent of cyclin-dependent kinase 4', *J Biol Chem*, 288: 26678-87.

DuBridge, R. B., P. Tang, H. C. Hsia, P. M. Leong, J. H. Miller, and M. P. Calos. 1987. 'Analysis of mutation in human cells by using an Epstein-Barr virus shuttle system', *Mol Cell Biol*, 7: 379-87.

Duquette, P. M., and N. Lamarche-Vane. 2014. 'Rho GTPases in embryonic development', *Small GTPases*, 5: 8.

Dutting, S., J. Heidenreich, D. Cherpokova, E. Amin, S. C. Zhang, M. R. Ahmadian, C. Brakebusch, and B. Nieswandt. 2015. 'Critical off-target effects of the widely used Rac1 inhibitors NSC23766 and EHT1864 in mouse platelets', *J Thromb Haemost*, 13: 827-38.

Dvorsky, R., and M. R. Ahmadian. 2004. 'Always look on the bright site of Rho: structural implications for a conserved intermolecular interface', *EMBO Rep*, 5: 1130-6.

Ehrlich, J. S., M. D. Hansen, and W. J. Nelson. 2002. 'Spatio-temporal regulation of Rac1 localization and lamellipodia dynamics during epithelial cell-cell adhesion', *Dev Cell*, 3: 259-70.

Elaimy, A. L., A. Ahsan, K. Marsh, W. B. Pratt, D. Ray, T. S. Lawrence, and M. K. Nyati. 2016. 'ATM is the primary kinase responsible for phosphorylation of Hsp90alpha after ionizing radiation', *Oncotarget*, 7: 82450-57.

Ellenbroek, S. I., and J. G. Collard. 2007. 'Rho GTPases: functions and association with cancer', *Clin Exp Metastasis*, 24: 657-72.

Elsner, C., and J. Bohne. 2017. 'The retroviral vector family: something for everyone', *Virus Genes*, 53: 714-22.

Engler, M.J., and C.C. Richardson. 1982. 'DNA Ligases.' in, *The Enzymes*.

Espinha, G., J. H. Osaki, Y. T. Magalhaes, and F. L. Forti. 2015. 'Rac1 GTPase-deficient HeLa cells present reduced DNA repair, proliferation, and survival under UV or gamma irradiation', *Mol Cell Biochem*, 404: 281-97.

Etienne-Manneville, S., and A. Hall. 2002. 'Rho GTPases in cell biology', *Nature*, 420: 629-35.

Falck, J., N. Mailand, R. G. Syljuasen, J. Bartek, and J. Lukas. 2001. 'The ATM-Chk2-Cdc25A checkpoint pathway guards against radioresistant DNA synthesis', *Nature*, 410: 842-7.

Feig, L. A., and G. M. Cooper. 1988. 'Inhibition of NIH 3T3 cell proliferation by a mutant ras protein with preferential affinity for GDP', *Mol Cell Biol*, 8: 3235-43.

Feil, R., J. Brocard, B. Mascrez, M. LeMeur, D. Metzger, and P. Chambon. 1996. 'Ligand-activated site-specific recombination in mice', *Proc Natl Acad Sci U S A*, 93: 10887-90.

Feil, R., J. Wagner, D. Metzger, and P. Chambon. 1997. 'Regulation of Cre recombinase activity by mutated estrogen receptor ligand-binding domains', *Biochem Biophys Res Commun*, 237: 752-7.

Ferri, N., A. Contini, S. K. Bernini, and A. Corsini. 2013. 'Role of small GTPase protein Rac1 in cardiovascular diseases: development of new selective pharmacological inhibitors', *J Cardiovasc Pharmacol*, 62: 425-35.

Fortune, J. M., and N. Osheroff. 2000. 'Topoisomerase II as a target for anticancer drugs: when enzymes stop being nice', *Prog Nucleic Acid Res Mol Biol*, 64: 221-53.

Fritz, G., and C. Henninger. 2015. 'Rho GTPases: Novel Players in the Regulation of the DNA Damage Response?', *Biomolecules*, 5: 2417-34.

Fritz, G., C. Henninger, and J. Huelsenbeck. 2011. 'Potential use of HMG-CoA reductase inhibitors (statins) as radioprotective agents', *Br Med Bull*, 97: 17-26.

Fritz, G., and B. Kaina. 2006. 'Rho GTPases: promising cellular targets for novel anticancer drugs', *Curr Cancer Drug Targets*, 6: 1-14.

———. 2013. 'Rac1 GTPase, a multifunctional player in the regulation of genotoxic stress response', *Cell Cycle*, 12: 2521-2.

Fuchs, S. Y., V. Adler, T. Buschmann, Z. Yin, X. Wu, S. N. Jones, and Z. Ronai. 1998. 'JNK targets p53 ubiquitination and degradation in nonstressed cells', *Genes Dev*, 12: 2658-63.

Fujii, M., K. Kawai, Y. Egami, and N. Araki. 2013. 'Dissecting the roles of Rac1 activation and deactivation in macropinocytosis using microscopic photo-manipulation', *Sci Rep*, 3: 2385.

Gama-Norton, L., L. Botezatu, S. Herrmann, M. Schweizer, P. M. Alves, H. Hauser, and D. Wirth. 2011. 'Lentivirus production is influenced by SV40 large T-antigen and chromosomal integration of the vector in HEK293 cells', *Hum Gene Ther*, 22: 1269-79.

Garcia-Mata, R., E. Boulter, and K. Burridge. 2011. 'The 'invisible hand': regulation of RHO GTPases by RHOGDIs', *Nat Rev Mol Cell Biol*, 12: 493-504.

Gentile, S., T. Darden, C. Erxleben, C. Romeo, A. Russo, N. Martin, S. Rossie, and D. L. Armstrong. 2006. 'Rac GTPase signaling through the PP5 protein phosphatase', *Proc Natl Acad Sci U S A*, 103: 5202-6.

Gewirtz, D. A. 1999. 'A critical evaluation of the mechanisms of action proposed for the antitumor effects of the anthracycline antibiotics adriamycin and daunorubicin', *Biochem Pharmacol*, 57: 727-41.

Gnad, R., B. Kaina, and G. Fritz. 2001. 'Rho GTPases are involved in the regulation of NF-kappaB by genotoxic stress', *Exp Cell Res*, 264: 244-9.

Goodarzi, A. A., T. Kurka, and P. A. Jeggo. 2011. 'KAP-1 phosphorylation regulates CHD3 nucleosome remodeling during the DNA double-strand break response', *Nat Struct Mol Biol*, 18: 831-9.

Goodarzi, A. A., A. T. Noon, D. Deckbar, Y. Ziv, Y. Shiloh, M. Lobrich, and P. A. Jeggo. 2008. 'ATM signaling facilitates repair of DNA double-strand breaks associated with heterochromatin', *Mol Cell*, 31: 167-77.

Goodhead, D. T. 1994. 'Initial events in the cellular effects of ionizing radiations: clustered damage in DNA', *Int J Radiat Biol*, 65: 7-17.

Gopinathan, L., S. L. Tan, V. C. Padmakumar, V. Coppola, L. Tessarollo, and P. Kaldis. 2014. 'Loss of Cdk2 and cyclin A2 impairs cell proliferation and tumorigenesis', *Cancer Res*, 74: 3870-9.

Goswami, P. C., J. L. Roti Roti, and C. R. Hunt. 1996. 'The cell cycle-coupled expression of topoisomerase IIalpha during S phase is regulated by mRNA stability and is disrupted by heat shock or ionizing radiation', *Mol Cell Biol*, 16: 1500-8.

Gottlieb, T. M., and S. P. Jackson. 1993. 'The DNA-dependent protein kinase: requirement for DNA ends and association with Ku antigen', *Cell*, 72: 131-42.

Gouvarchin Ghaleh, H. E., M. Bolandian, R. Dorostkar, A. Jafari, and M. F. Pour. 2020. 'Concise review on optimized methods in production and transduction of lentiviral vectors in order to facilitate immunotherapy and gene therapy', *Biomed Pharmacother*, 128: 110276.

Grawunder, U., M. Wilm, X. Wu, P. Kulesza, T. E. Wilson, M. Mann, and M. R. Lieber. 1997. 'Activity of DNA ligase IV stimulated by complex formation with XRCC4 protein in mammalian cells', *Nature*, 388: 492-5.

Guo, F., J. A. Cancelas, D. Hildeman, D. A. Williams, and Y. Zheng. 2008. 'Rac GTPase isoforms Rac1 and Rac2 play a redundant and crucial role in T-cell development', *Blood*, 112: 1767-75.

Guo, Z., A. Kumagai, S. X. Wang, and W. G. Dunphy. 2000. 'Requirement for Atr in phosphorylation of Chk1 and cell cycle regulation in response to DNA replication blocks and UV-damaged DNA in Xenopus egg extracts', *Genes Dev*, 14: 2745-56.

Gupta, R. C., E. I. Golub, M. S. Wold, and C. M. Radding. 1998. 'Polarity of DNA strand exchange promoted by recombination proteins of the RecA family', *Proc Natl Acad Sci U S A*, 95: 9843-8.

Haataja, L., J. Groffen, and N. Heisterkamp. 1997. 'Characterization of RAC3, a novel member of the Rho family', *J Biol Chem*, 272: 20384-8.

Hajas, G., A. Bacsi, L. Aguilera-Aguirre, M. L. Hegde, K. H. Tapas, S. Sur, Z. Radak, X. Ba, and I. Boldogh. 2013. '8-Oxoguanine DNA glycosylase-1 links DNA repair to cellular signaling via the activation of the small GTPase Rac1', *Free Radic Biol Med*, 61: 384-94.

Hall, A. 1990. 'The cellular functions of small GTP-binding proteins', *Science*, 249: 635-40.

———. 1998. 'Rho GTPases and the actin cytoskeleton', *Science*, 279: 509-14.

———. 2012. 'Rho family GTPases', *Biochem Soc Trans*, 40: 1378-82.

Hampsch, R. A., K. Shee, D. Bates, L. D. Lewis, L. Desire, B. Leblond, E. Demidenko, K. Stefan, Y. H. Huang, and T. W. Miller. 2017. 'Therapeutic sensitivity to Rac GTPase inhibition requires consequential suppression of mTORC1, AKT, and MEK signaling in breast cancer', *Oncotarget*, 8: 21806-17.

Han, N. R., H. Lee, S. Baek, J. I. Yun, K. H. Park, and S. T. Lee. 2015. 'Delivery of episomal vectors into primary cells by means of commercial transfection reagents', *Biochem Biophys Res Commun*, 461: 348-53.

Hanahan, D., and R. A. Weinberg. 2000. 'The hallmarks of cancer', *Cell*, 100: 57-70.

Hansen, M. D., J. S. Ehrlich, and W. J. Nelson. 2002. 'Molecular mechanism for orienting membrane and actin dynamics to nascent cell-cell contacts in epithelial cells', *J Biol Chem*, 277: 45371-6.

Harding, M. A., and D. Theodorescu. 2010. 'RhoGDI signaling provides targets for cancer therapy', *Eur J Cancer*, 46: 1252-9.

Harper, J. W., and S. J. Elledge. 2007. 'The DNA damage response: ten years after', *Mol Cell*, 28: 739-45.

He, X., J. Liu, Y. Qi, C. Brakebusch, A. Chrostek-Grashoff, D. Edgar, P. D. Yurchenco, S. A. Corbett, S. F. Lowry, A. M. Graham, Y. Han, and S. Li. 2010. 'Rac1 is essential for basement membrane-dependent epiblast survival', *Mol Cell Biol*, 30: 3569-81.

Hein, A. L., C. M. Post, Y. M. Sheinin, I. Lakshmanan, A. Natarajan, C. A. Enke, S. K. Batra, M. M. Ouellette, and Y. Yan. 2016. 'RAC1 GTPase promotes the survival of breast cancer cells in response to hyper-fractionated radiation treatment', *Oncogene*, 35: 6319-29.

Helbig, L., J. Damrot, J. Hulsenbeck, B. Koberle, A. Brozovic, M. Osmak, Z. Fiket, B. Kaina, and G. Fritz. 2011. 'Late activation of stress-activated protein kinases/c-Jun N-terminal kinases triggered by cisplatin-induced DNA damage in repair-defective cells', *J Biol Chem*, 286: 12991-3001.

Henninger, C., and G. Fritz. 2017. 'Statins in anthracycline-induced cardiotoxicity: Rac and Rho, and the heartbreakers', *Cell Death Dis*, 8: e2564.

Henninger, C., J. Huelsenbeck, S. Huelsenbeck, S. Grosch, A. Schad, K. J. Lackner, B. Kaina, and G. Fritz. 2012. 'The lipid lowering drug lovastatin protects against doxorubicin-induced hepatotoxicity', *Toxicol Appl Pharmacol*, 261: 66-73.

Hinde, E., K. Yokomori, K. Gaus, K. M. Hahn, and E. Gratton. 2014. 'Fluctuation-based imaging of nuclear Rac1 activation by protein oligomerisation', *Sci Rep*, 4: 4219.

Hirao, A., Y. Y. Kong, S. Matsuoka, A. Wakeham, J. Ruland, H. Yoshida, D. Liu, S. J. Elledge, and T. W. Mak. 2000. 'DNA damage-induced activation of p53 by the checkpoint kinase Chk2', *Science*, 287: 1824-7.

Hoeijmakers, J. H. 2001. 'Genome maintenance mechanisms for preventing cancer', *Nature*, 411: 366-74.

Hoekstra, M. F. 1997. 'Responses to DNA damage and regulation of cell cycle checkpoints by the ATM protein kinase family', *Curr Opin Genet Dev*, 7: 170-5.

Hoffman, G. R., N. Nassar, and R. A. Cerione. 2000. 'Structure of the Rho family GTP-binding protein Cdc42 in complex with the multifunctional regulator RhoGDI', *Cell*, 100: 345-56.

Houtgraaf, J. H., J. Versmissen, and W. J. van der Giessen. 2006. 'A concise review of DNA damage checkpoints and repair in mammalian cells', *Cardiovasc Revasc Med*, 7: 165-72.

Hu, C., S. Zhang, X. Gao, X. Gao, X. Xu, Y. Lv, Y. Zhang, Z. Zhu, C. Zhang, Q. Li, J. Wong, Y. Cui, W. Zhang, L. Ma, and C. Wang. 2012. 'Roles of Kruppel-associated Box (KRAB)-associated Co-repressor KAP1 Ser-473 Phosphorylation in DNA Damage Response', *J Biol Chem*, 287: 18937-52.

Huang, J., J. Yang, B. Maity, D. Mayuzumi, and R. A. Fisher. 2011. 'Regulator of G protein signaling 6 mediates doxorubicin-induced ATM and p53 activation by a reactive oxygen species-dependent mechanism', *Cancer Res*, 71: 6310-9.

Huelsenbeck, J., S. C. Dreger, R. Gerhard, G. Fritz, I. Just, and H. Genth. 2007. 'Upregulation of the immediate early gene product RhoB by exoenzyme C3 from Clostridium limosum and toxin B from Clostridium difficile', *Biochemistry*, 46: 4923-31.

Huelsenbeck, J., C. Henninger, A. Schad, K. J. Lackner, B. Kaina, and G. Fritz. 2011. 'Inhibition of Rac1 signaling by lovastatin protects against anthracycline-induced cardiac toxicity', *Cell death & disease*, 2: e190.

Huelsenbeck, S. C., A. Schorr, W. P. Roos, J. Huelsenbeck, C. Henninger, B. Kaina, and G. Fritz. 2012. 'Rac1 protein signaling is required for DNA damage response stimulated by topoisomerase II poisons', *J Biol Chem*, 287: 38590-9.

Ichijo, H. 1999. 'From receptors to stress-activated MAP kinases', *Oncogene*, 18: 6087-93.

Indra, A. K., X. Warot, J. Brocard, J. M. Bornert, J. H. Xiao, P. Chambon, and D. Metzger. 1999. 'Temporally-controlled site-specific mutagenesis in the basal layer of the epidermis: comparison of the recombinase activity of the tamoxifen-inducible Cre-ER(T) and Cre-ER(T2) recombinases', *Nucleic Acids Res*, 27: 4324-7.

Jackson, S. P., and J. Bartek. 2009. 'The DNA-damage response in human biology and disease', *Nature*, 461: 1071-8.

Jefferies, C. A., and L. A. O'Neill. 2000. 'Rac1 regulates interleukin 1-induced nuclear factor kappaB activation in an inhibitory protein kappaBalpha-independent manner by enhancing the ability of the p65 subunit to transactivate gene expression', *J Biol Chem*, 275: 3114-20.

Jeggo, P. A. 1998. 'Identification of genes involved in repair of DNA double-strand breaks in mammalian cells', *Radiat Res*, 150: S80-91.

Jeggo, P. A., M. Hafezparast, A. F. Thompson, B. C. Broughton, G. P. Kaur, M. Z. Zdzienicka, and R. S. Athwal. 1992. 'Localization of a DNA repair gene (XRCC5) involved in double-strand-break rejoining to human chromosome 2', *Proc Natl Acad Sci U S A*, 89: 6423-7.

Jin, S., R. M. Ray, and L. R. Johnson. 2006. 'Rac1 mediates intestinal epithelial cell apoptosis via JNK', *Am J Physiol Gastrointest Liver Physiol*, 291: G1137-47.

Johnson, R. D., and M. Jasin. 2000. 'Sister chromatid gene conversion is a prominent double-strand break repair pathway in mammalian cells', *EMBO J*, 19: 3398-407.

Jordan, P., R. Brazao, M. G. Boavida, C. Gespach, and E. Chastre. 1999. 'Cloning of a novel human Rac1b splice variant with increased expression in colorectal tumors', *Oncogene*, 18: 6835-9.

Kalderon, D., B. L. Roberts, W. D. Richardson, and A. E. Smith. 1984. 'A short amino acid sequence able to specify nuclear location', *Cell*, 39: 499-509.

Karlsson, R., E. D. Pedersen, Z. Wang, and C. Brakebusch. 2009. 'Rho GTPase function in tumorigenesis', *Biochim Biophys Acta*, 1796: 91-8.

Karnoub, A. E., C. J. Der, and S. L. Campbell. 2001. 'The insert region of Rac1 is essential for membrane ruffling but not cellular transformation', *Mol Cell Biol*, 21: 2847-57.

Kastan, M. B., and J. Bartek. 2004. 'Cell-cycle checkpoints and cancer', *Nature*, 432: 316-23.
Keoni, C. L., and T. L. Brown. 2015. 'Inhibition of Apoptosis and Efficacy of Pan Caspase Inhibitor, Q-VD-OPh, in Models of Human Disease', *J Cell Death*, 8: 1-7.
Khanna, K. K., and S. P. Jackson. 2001. 'DNA double-strand breaks: signaling, repair and the cancer connection', *Nat Genet*, 27: 247-54.
Khosravi-Far, R., P. A. Solski, G. J. Clark, M. S. Kinch, and C. J. Der. 1995. 'Activation of Rac1, RhoA, and mitogen-activated protein kinases is required for Ras transformation', *Mol Cell Biol*, 15: 6443-53.
Kim, H., M. Kim, S. K. Im, and S. Fang. 2018. 'Mouse Cre-LoxP system: general principles to determine tissue-specific roles of target genes', *Lab Anim Res*, 34: 147-59.
Kim, M. J., J. Y. Byun, C. H. Yun, I. C. Park, K. H. Lee, and S. J. Lee. 2008. 'c-Src-p38 mitogen-activated protein kinase signaling is required for Akt activation in response to ionizing radiation', *Mol Cancer Res*, 6: 1872-80.
Kim, T. K., and J. H. Eberwine. 2010. 'Mammalian cell transfection: the present and the future', *Anal Bioanal Chem*, 397: 3173-8.
Kinner, A., W. Wu, C. Staudt, and G. Iliakis. 2008. 'Gamma-H2AX in recognition and signaling of DNA double-strand breaks in the context of chromatin', *Nucleic Acids Res*, 36: 5678-94.
Kobayashi, J., A. Antoccia, H. Tauchi, S. Matsuura, and K. Komatsu. 2004. 'NBS1 and its functional role in the DNA damage response', *DNA Repair (Amst)*, 3: 855-61.
Koch, G., C. Benz, G. Schmidt, C. Olenik, and K. Aktories. 1997. 'Role of Rho protein in lovastatin-induced breakdown of actin cytoskeleton', *J Pharmacol Exp Ther*, 283: 901-9.
Konstantinopoulos, P. A., M. V. Karamouzis, and A. G. Papavassiliou. 2007. 'Post-translational modifications and regulation of the RAS superfamily of GTPases as anticancer targets', *Nat Rev Drug Discov*, 6: 541-55.
Kraynov, V. S., C. Chamberlain, G. M. Bokoch, M. A. Schwartz, S. Slabaugh, and K. M. Hahn. 2000. 'Localized Rac activation dynamics visualized in living cells', *Science*, 290: 333-7.
Krischuns, T., F. Gunl, L. Henschel, M. Binder, J. Willemsen, S. Schloer, U. Rescher, V. Gerlt, G. Zimmer, C. Nordhoff, S. Ludwig, and L. Brunotte. 2018. 'Phosphorylation of TRIM28 Enhances the Expression of IFN-beta and Proinflammatory Cytokines During HPAIV Infection of Human Lung Epithelial Cells', *Front Immunol*, 9: 2229.
Kumar, M. S., S. J. Erkeland, R. E. Pester, C. Y. Chen, M. S. Ebert, P. A. Sharp, and T. Jacks. 2008. 'Suppression of non-small cell lung tumor development by the let-7 microRNA family', *Proc Natl Acad Sci U S A*, 105: 3903-8.
Kunschmann, T., S. Puder, T. Fischer, A. Steffen, K. Rottner, and C. T. Mierke. 2019. 'The Small GTPase Rac1 Increases Cell Surface Stiffness and Enhances 3D Migration Into Extracellular Matrices', *Sci Rep*, 9: 7675.
Kurz, E. U., P. Douglas, and S. P. Lees-Miller. 2004. 'Doxorubicin activates ATM-dependent phosphorylation of multiple downstream targets in part through the generation of reactive oxygen species', *J Biol Chem*, 279: 53272-81.
Lackinger, D., U. Eichhorn, and B. Kaina. 2001. 'Effect of ultraviolet light, methyl methanesulfonate and ionizing radiation on the genotoxic response and apoptosis of mouse fibroblasts lacking c-Fos, p53 or both', *Mutagenesis*, 16: 233-41.
Lafrance-Vanasse, J., G. J. Williams, and J. A. Tainer. 2015. 'Envisioning the dynamics and flexibility of Mre11-Rad50-Nbs1 complex to decipher its roles in DNA replication and repair', *Prog Biophys Mol Biol*, 117: 182-93.
Lamarche, N., and A. Hall. 1994. 'GAPs for rho-related GTPases', *Trends Genet*, 10: 436-40.
Lane, D. P. 1992. 'Cancer. p53, guardian of the genome', *Nature*, 358: 15-6.
Lanning, C. C., J. L. Daddona, R. Ruiz-Velasco, S. H. Shafer, and C. L. Williams. 2004. 'The Rac1 C-terminal polybasic region regulates the nuclear localization and protein degradation of Rac1', *J Biol Chem*, 279: 44197-210.

Lanning, C. C., R. Ruiz-Velasco, and C. L. Williams. 2003. 'Novel mechanism of the co-regulation of nuclear transport of SmgGDS and Rac1', *J Biol Chem*, 278: 12495-506.

Lassus, P., P. Roux, O. Zugasti, A. Philips, P. Fort, and U. Hibner. 2000. 'Extinction of rac1 and Cdc42Hs signalling defines a novel p53-dependent apoptotic pathway', *Oncogene*, 19: 2377-85.

Lavin, M. F., D. Delia, and L. Chessa. 2006. 'ATM and the DNA damage response. Workshop on ataxia-telangiectasia and related syndromes', *EMBO Rep*, 7: 154-60.

Lawson, C. D., and K. Burridge. 2014. 'The on-off relationship of Rho and Rac during integrin-mediated adhesion and cell migration', *Small GTPases*, 5: e27958.

Leber, R., T. W. Wise, R. Mizuta, and K. Meek. 1998. 'The XRCC4 gene product is a target for and interacts with the DNA-dependent protein kinase', *J Biol Chem*, 273: 1794-801.

Lee, B. J., A. E. Cansizoglu, K. E. Suel, T. H. Louis, Z. Zhang, and Y. M. Chook. 2006. 'Rules for nuclear localization sequence recognition by karyopherin beta 2', *Cell*, 126: 543-58.

Lee, J. H., and T. T. Paull. 2005. 'ATM activation by DNA double-strand breaks through the Mre11-Rad50-Nbs1 complex', *Science*, 308: 551-4.

Lee, M., K. Chea, R. Pyda, M. Chua, and I. Dominguez. 2017. 'Comparative Analysis of Non-viral Transfection Methods in Mouse Embryonic Fibroblast Cells', *J Biomol Tech*, 28: 67-74.

Lee, S. H., and R. Dominguez. 2010. 'Regulation of actin cytoskeleton dynamics in cells', *Mol Cells*, 29: 311-25.

Lees-Miller, S. P., K. Sakaguchi, S. J. Ullrich, E. Appella, and C. W. Anderson. 1992. 'Human DNA-activated protein kinase phosphorylates serines 15 and 37 in the amino-terminal transactivation domain of human p53', *Mol Cell Biol*, 12: 5041-9.

Leung, S. W., M. T. Harreman, M. R. Hodel, A. E. Hodel, and A. H. Corbett. 2003. 'Dissection of the karyopherin alpha nuclear localization signal (NLS)-binding groove: functional requirements for NLS binding', *J Biol Chem*, 278: 41947-53.

Li, B., Q. Yu, R. Wang, C. Gratzke, X. Wang, A. Spek, A. Herlemann, A. Tamalunas, F. Strittmatter, R. Waidelich, C. G. Stief, and M. Hennenberg. 2020. 'Inhibition of Female and Male Human Detrusor Smooth Muscle Contraction by the Rac Inhibitors EHT1864 and NSC23766', *Front Pharmacol*, 11: 409.

Li, C., R. C. Wu, L. Amazit, S. Y. Tsai, M. J. Tsai, and B. W. O'Malley. 2007. 'Specific amino acid residues in the basic helix-loop-helix domain of SRC-3 are essential for its nuclear localization and proteasome-dependent turnover', *Mol Cell Biol*, 27: 1296-308.

Li, G., C. D'Souza-Schorey, M. A. Barbieri, J. A. Cooper, and P. D. Stahl. 1997. 'Uncoupling of membrane ruffling and pinocytosis during Ras signal transduction', *J Biol Chem*, 272: 10337-40.

Li, H. Y., K. Cao, and Y. Zheng. 2003. 'Ran in the spindle checkpoint: a new function for a versatile GTPase', *Trends Cell Biol*, 13: 553-7.

Li, J., and J. Yuan. 2008. 'Caspases in apoptosis and beyond', *Oncogene*, 27: 6194-206.

Li, X., C. A. Corsa, P. W. Pan, L. Wu, D. Ferguson, X. Yu, J. Min, and Y. Dou. 2010. 'MOF and H4 K16 acetylation play important roles in DNA damage repair by modulating recruitment of DNA damage repair protein Mdc1', *Mol Cell Biol*, 30: 5335-47.

Li, X., Y. K. Lee, J. C. Jeng, Y. Yen, D. C. Schultz, H. M. Shih, and D. K. Ann. 2007. 'Role for KAP1 serine 824 phosphorylation and sumoylation/desumoylation switch in regulating KAP1-mediated transcriptional repression', *J Biol Chem*, 282: 36177-89.

Liang, J., L. Oyang, S. Rao, Y. Han, X. Luo, P. Yi, J. Lin, L. Xia, J. Hu, S. Tan, L. Tang, Q. Pan, Y. Tang, Y. Zhou, and Q. Liao. 2021. 'Rac1, A Potential Target for Tumor Therapy', *Front Oncol*, 11: 674426.

Lieber, M. R. 2010. 'The mechanism of double-strand DNA break repair by the nonhomologous DNA end-joining pathway', *Annu Rev Biochem*, 79: 181-211.

Lim, J., and J. Dobson. 2012. 'Improved transfection of HUVEC and MEF cells using DNA complexes with magnetic nanoparticles in an oscillating field', *J Genet*, 91: 223-7.

Limbo, O., C. Chahwan, Y. Yamada, R. A. de Bruin, C. Wittenberg, and P. Russell. 2007. 'Ctp1 is a cell-cycle-regulated protein that functions with Mre11 complex to control double-strand break repair by homologous recombination', *Mol Cell*, 28: 134-46.

Lin, Y., and Y. Zheng. 2015. 'Approaches of targeting Rho GTPases in cancer drug discovery', *Expert Opin Drug Discov*, 10: 991-1010.

Lindstrom, M. S. 2011. 'NPM1/B23: A Multifunctional Chaperone in Ribosome Biogenesis and Chromatin Remodeling', *Biochem Res Int*, 2011: 195209.

Ling, Y. H., A. K. el-Naggar, W. Priebe, and R. Perez-Soler. 1996. 'Cell cycle-dependent cytotoxicity, G2/M phase arrest, and disruption of p34cdc2/cyclin B1 activity induced by doxorubicin in synchronized P388 cells', *Mol Pharmacol*, 49: 832-41.

Liu, J., W. Mao, B. Ding, and C. S. Liang. 2008. 'ERKs/p53 signal transduction pathway is involved in doxorubicin-induced apoptosis in H9c2 cells and cardiomyocytes', *Am J Physiol Heart Circ Physiol*, 295: H1956-65.

Liu, L., L. Xiao, H. K. Chung, M. S. Kwon, X. X. Li, N. Wu, J. N. Rao, and J. Y. Wang. 2019. 'RNA-Binding Protein HuR Regulates Rac1 Nucleocytoplasmic Shuttling Through Nucleophosmin in the Intestinal Epithelium', *Cell Mol Gastroenterol Hepatol*, 8: 475-86.

Liu, Q., S. Guntuku, X. S. Cui, S. Matsuoka, D. Cortez, K. Tamai, G. Luo, S. Carattini-Rivera, F. DeMayo, A. Bradley, L. A. Donehower, and S. J. Elledge. 2000. 'Chk1 is an essential kinase that is regulated by Atr and required for the G(2)/M DNA damage checkpoint', *Genes Dev*, 14: 1448-59.

Liu, S., M. Kapoor, X. Shi-wen, L. Kennedy, C. P. Denton, M. Glogauer, D. J. Abraham, and A. Leask. 2008. 'Role of Rac1 in a bleomycin-induced scleroderma model using fibroblast-specific Rac1-knockout mice', *Arthritis Rheum*, 58: 2189-95.

Liu, Y., and M. Kulesz-Martin. 2001. 'p53 protein at the hub of cellular DNA damage response pathways through sequence-specific and non-sequence-specific DNA binding', *Carcinogenesis*, 22: 851-60.

Lomax, M. E., L. K. Folkes, and P. O'Neill. 2013. 'Biological consequences of radiation-induced DNA damage: relevance to radiotherapy', *Clin Oncol (R Coll Radiol)*, 25: 578-85.

Loonstra, A., M. Vooijs, H. B. Beverloo, B. A. Allak, E. van Drunen, R. Kanaar, A. Berns, and J. Jonkers. 2001. 'Growth inhibition and DNA damage induced by Cre recombinase in mammalian cells', *Proc Natl Acad Sci U S A*, 98: 9209-14.

Lu, C., Y. Shi, Z. Wang, Z. Song, M. Zhu, Q. Cai, and T. Chen. 2008. 'Serum starvation induces H2AX phosphorylation to regulate apoptosis via p38 MAPK pathway', *FEBS Lett*, 582: 2703-8.

Lu, C., F. Zhu, Y. Y. Cho, F. Tang, T. Zykova, W. Y. Ma, A. M. Bode, and Z. Dong. 2006. 'Cell apoptosis: requirement of H2AX in DNA ladder formation, but not for the activation of caspase-3', *Mol Cell*, 23: 121-32.

Lu, H., J. Saha, P. J. Beckmann, E. A. Hendrickson, and A. J. Davis. 2019. 'DNA-PKcs promotes chromatin decondensation to facilitate initiation of the DNA damage response', *Nucleic Acids Res*, 47: 9467-79.

Luo, M., C. W. Pang, A. E. Gerken, and T. G. Brock. 2004. 'Multiple nuclear localization sequences allow modulation of 5-lipoxygenase nuclear import', *Traffic*, 5: 847-54.

Lyu, Y. L., J. E. Kerrigan, C. P. Lin, A. M. Azarova, Y. C. Tsai, Y. Ban, and L. F. Liu. 2007. 'Topoisomerase IIbeta mediated DNA double-strand breaks: implications in doxorubicin cardiotoxicity and prevention by dexrazoxane', *Cancer Res*, 67: 8839-46.

Ma, Y., U. Pannicke, K. Schwarz, and M. R. Lieber. 2002. 'Hairpin opening and overhang processing by an Artemis/DNA-dependent protein kinase complex in nonhomologous end joining and V(D)J recombination', *Cell*, 108: 781-94.

Machesky, L. M., and A. Hall. 1996. 'Rho: a connection between membrane receptor signalling and the cytoskeleton', *Trends Cell Biol*, 6: 304-10.

Macurek, L., A. Lindqvist, O. Voets, J. Kool, H. R. Vos, and R. H. Medema. 2010. 'Wip1 phosphatase is associated with chromatin and dephosphorylates gammaH2AX to promote checkpoint inhibition', *Oncogene*, 29: 2281-91.

Mahmoudi, M., I. Gorenne, J. Mercer, N. Figg, T. Littlewood, and M. Bennett. 2008. 'Statins use a novel Nijmegen breakage syndrome-1-dependent pathway to accelerate DNA repair in vascular smooth muscle cells', *Circ Res*, 103: 717-25.

Mailand, N., J. Falck, C. Lukas, R. G. Syljuasen, M. Welcker, J. Bartek, and J. Lukas. 2000. 'Rapid destruction of human Cdc25A in response to DNA damage', *Science*, 288: 1425-9.

Mainiero, F., A. Soriani, R. Strippoli, J. Jacobelli, A. Gismondi, M. Piccoli, L. Frati, and A. Santoni. 2000. 'RAC1/P38 MAPK signaling pathway controls beta1 integrin-induced interleukin-8 production in human natural killer cells', *Immunity*, 12: 7-16.

Maiso, P., E. Colado, E. M. Ocio, M. Garayoa, J. Martin, P. Atadja, A. Pandiella, and J. F. San-Miguel. 2009. 'The synergy of panobinostat plus doxorubicin in acute myeloid leukemia suggests a role for HDAC inhibitors in the control of DNA repair', *Leukemia*, 23: 2265-74.

Maloisel, L., F. Fabre, and S. Gangloff. 2008. 'DNA polymerase delta is preferentially recruited during homologous recombination to promote heteroduplex DNA extension', *Mol Cell Biol*, 28: 1373-82.

Mantovani, F., L. Collavin, and G. Del Sal. 2019. 'Mutant p53 as a guardian of the cancer cell', *Cell Death Differ*, 26: 199-212.

Marechal, A., and L. Zou. 2013. 'DNA damage sensing by the ATM and ATR kinases', *Cold Spring Harb Perspect Biol*, 5.

Maser, R. S., K. J. Monsen, B. E. Nelms, and J. H. Petrini. 1997. 'hMre11 and hRad50 nuclear foci are induced during the normal cellular response to DNA double-strand breaks', *Mol Cell Biol*, 17: 6087-96.

Matsuoka, S., B. A. Ballif, A. Smogorzewska, E. R. McDonald, 3rd, K. E. Hurov, J. Luo, C. E. Bakalarski, Z. Zhao, N. Solimini, Y. Lerenthal, Y. Shiloh, S. P. Gygi, and S. J. Elledge. 2007. 'ATM and ATR substrate analysis reveals extensive protein networks responsive to DNA damage', *Science*, 316: 1160-6.

Matsuoka, S., G. Rotman, A. Ogawa, Y. Shiloh, K. Tamai, and S. J. Elledge. 2000. 'Ataxia telangiectasia-mutated phosphorylates Chk2 in vivo and in vitro', *Proc Natl Acad Sci U S A*, 97: 10389-94.

Maundrell, K., B. Antonsson, E. Magnenat, M. Camps, M. Muda, C. Chabert, C. Gillieron, U. Boschert, E. Vial-Knecht, J. C. Martinou, and S. Arkinstall. 1997. 'Bcl-2 undergoes phosphorylation by c-Jun N-terminal kinase/stress-activated protein kinases in the presence of the constitutively active GTP-binding protein Rac1', *J Biol Chem*, 272: 25238-42.

May, M., I. Schelle, C. Brakebusch, K. Rottner, and H. Genth. 2014. 'Rac1-dependent recruitment of PAK2 to G2 phase centrosomes and their roles in the regulation of mitotic entry', *Cell Cycle*, 13: 2211-21.

McClendon, A. K., and N. Osheroff. 2007. 'DNA topoisomerase II, genotoxicity, and cancer', *Mutat Res*, 623: 83-97.

Meek, K., S. Gupta, D. A. Ramsden, and S. P. Lees-Miller. 2004. 'The DNA-dependent protein kinase: the director at the end', *Immunol Rev*, 200: 132-41.

Melzer, C., R. Hass, H. Lehnert, and H. Ungefroren. 2019. 'RAC1B: A Rho GTPase with Versatile Functions in Malignant Transformation and Tumor Progression', *Cells*, 8.

Memon, A. R. 2004. 'The role of ADP-ribosylation factor and SAR1 in vesicular trafficking in plants', *Biochim Biophys Acta*, 1664: 9-30.

Michaelson, D., W. Abidi, D. Guardavaccaro, M. Zhou, I. Ahearn, M. Pagano, and M. R. Philips. 2008. 'Rac1 accumulates in the nucleus during the G2 phase of the cell cycle and promotes cell division', *J Cell Biol*, 181: 485-96.

Michiels, F., G. G. Habets, J. C. Stam, R. A. van der Kammen, and J. G. Collard. 1995. 'A role for Rac in Tiam1-induced membrane ruffling and invasion', *Nature*, 375: 338-40.

Migeotte, I., J. Grego-Bessa, and K. V. Anderson. 2011. 'Rac1 mediates morphogenetic responses to intercellular signals in the gastrulating mouse embryo', *Development*, 138: 3011-20.

Minard, M. E., L. S. Kim, J. E. Price, and G. E. Gallick. 2004. 'The role of the guanine nucleotide exchange factor Tiam1 in cellular migration, invasion, adhesion and tumor progression', *Breast Cancer Res Treat*, 84: 21-32.

Minden, A., A. Lin, F. X. Claret, A. Abo, and M. Karin. 1995. 'Selective activation of the JNK signaling cascade and c-Jun transcriptional activity by the small GTPases Rac and Cdc42Hs', *Cell*, 81: 1147-57.

Mochizuki, H., J. P. Schwartz, K. Tanaka, R. O. Brady, and J. Reiser. 1998. 'High-titer human immunodeficiency virus type 1-based vector systems for gene delivery into nondividing cells', *J Virol*, 72: 8873-83.

Moll, J., G. Sansig, E. Fattori, and H. van der Putten. 1991. 'The murine rac1 gene: cDNA cloning, tissue distribution and regulated expression of rac1 mRNA by disassembly of actin microfilaments', *Oncogene*, 6: 863-6.

Moon, S. H., L. Lin, X. Zhang, T. A. Nguyen, Y. Darlington, A. S. Waldman, X. Lu, and L. A. Donehower. 2010. 'Wild-type p53-induced phosphatase 1 dephosphorylates histone variant gamma-H2AX and suppresses DNA double strand break repair', *J Biol Chem*, 285: 12935-47.

Moore, J. K., and J. E. Haber. 1996. 'Cell cycle and genetic requirements of two pathways of nonhomologous end-joining repair of double-strand breaks in Saccharomyces cerevisiae', *Mol Cell Biol*, 16: 2164-73.

Moores, S. L., M. D. Schaber, S. D. Mosser, E. Rands, M. B. O'Hara, V. M. Garsky, M. S. Marshall, D. L. Pompliano, and J. B. Gibbs. 1991. 'Sequence dependence of protein isoprenylation', *J Biol Chem*, 266: 14603-10.

Moorman, J. P., D. Luu, J. Wickham, D. A. Bobak, and C. S. Hahn. 1999. 'A balance of signaling by Rho family small GTPases RhoA, Rac1 and Cdc42 coordinates cytoskeletal morphology but not cell survival', *Oncogene*, 18: 47-57.

Morimoto, S., M. Tsuda, H. Bunch, H. Sasanuma, C. Austin, and S. Takeda. 2019. 'Type II DNA Topoisomerases Cause Spontaneous Double-Strand Breaks in Genomic DNA', *Genes (Basel)*, 10.

Murga, C., M. Zohar, H. Teramoto, and J. S. Gutkind. 2002. 'Rac1 and RhoG promote cell survival by the activation of PI3K and Akt, independently of their ability to stimulate JNK and NF-kappaB', *Oncogene*, 21: 207-16.

Naci, D., S. Berrazouane, F. Barabe, and F. Aoudjit. 2019. 'Cell adhesion to collagen promotes leukemia resistance to doxorubicin by reducing DNA damage through the inhibition of Rac1 activation', *Sci Rep*, 9: 19455.

Naiche, L. A., and V. E. Papaioannou. 2007. 'Cre activity causes widespread apoptosis and lethal anemia during embryonic development', *Genesis*, 45: 768-75.

Navarro-Lerida, I., T. Pellinen, S. A. Sanchez, M. C. Guadamillas, Y. Wang, T. Mirtti, E. Calvo, and M. A. Del Pozo. 2015. 'Rac1 nucleocytoplasmic shuttling drives nuclear shape changes and tumor invasion', *Dev Cell*, 32: 318-34.

Nelms, B. E., R. S. Maser, J. F. MacKay, M. G. Lagally, and J. H. Petrini. 1998. 'In situ visualization of DNA double-strand break repair in human fibroblasts', *Science*, 280: 590-2.

Nikjoo, H., P. O'Neill, D. T. Goodhead, and M. Terrissol. 1997. 'Computational modelling of low-energy electron-induced DNA damage by early physical and chemical events', *Int J Radiat Biol*, 71: 467-83.

Nitiss, J. L. 2002. 'DNA topoisomerases in cancer chemotherapy: using enzymes to generate selective DNA damage', *Curr Opin Investig Drugs*, 3: 1512-6.

———. 2009. 'Targeting DNA topoisomerase II in cancer chemotherapy', *Nat Rev Cancer*, 9: 338-50.

Nobes, C. D., and A. Hall. 1995. 'Rho, rac, and cdc42 GTPases regulate the assembly of multimolecular focal complexes associated with actin stress fibers, lamellipodia, and filopodia', *Cell*, 81: 53-62.

———. 1999. 'Rho GTPases control polarity, protrusion, and adhesion during cell movement', *J Cell Biol*, 144: 1235-44.

Nohata, N., Y. Uchida, A. N. Stratman, R. H. Adams, Y. Zheng, B. M. Weinstein, Y. S. Mukouyama, and J. S. Gutkind. 2016. 'Temporal-specific roles of Rac1 during vascular development and retinal angiogenesis', *Dev Biol*, 411: 183-94.

Nubel, T., J. Damrot, W. P. Roos, B. Kaina, and G. Fritz. 2006. 'Lovastatin protects human endothelial cells from killing by ionizing radiation without impairing induction and repair of DNA double-strand breaks', *Clin Cancer Res*, 12: 933-9.

O'Connor, K., and M. Chen. 2013. 'Dynamic functions of RhoA in tumor cell migration and invasion', *Small GTPases*, 4: 141-7.

Oeck, S., N. M. Malewicz, S. Hurst, J. Rudner, and V. Jendrossek. 2015. 'The Focinator - a new open-source tool for high-throughput foci evaluation of DNA damage', *Radiat Oncol*, 10: 163.

Oh, W., and J. A. Frost. 2014. 'Rho GTPase independent regulation of ATM activation and cell survival by the RhoGEF Net1A', *Cell Cycle*, 13: 2765-72.

Ohlig, J., C. Henninger, S. Zander, M. Merx, M. Kelm, and G. Fritz. 2018. 'Rac1-mediated cardiac damage causes diastolic dysfunction in a mouse model of subacute doxorubicin-induced cardiotoxicity', *Arch Toxicol*, 92: 441-53.

Olive, P. L. 2004. 'Detection of DNA damage in individual cells by analysis of histone H2AX phosphorylation', *Methods Cell Biol*, 75: 355-73.

Olofsson, B. 1999. 'Rho guanine dissociation inhibitors: pivotal molecules in cellular signalling', *Cell Signal*, 11: 545-54.

Olson, M. F. 2016. 'Rho GTPases, their post-translational modifications, disease-associated mutations and pharmacological inhibitors', *Small GTPases*: 1-13.

Olson, M. F., A. Ashworth, and A. Hall. 1995. 'An essential role for Rho, Rac, and Cdc42 GTPases in cell cycle progression through G1', *Science*, 269: 1270-2.

Onesto, C., A. Shutes, V. Picard, F. Schweighoffer, and C. J. Der. 2008. 'Characterization of EHT 1864, a novel small molecule inhibitor of Rac family small GTPases', *Methods Enzymol*, 439: 111-29.

Panier, S., and S. J. Boulton. 2014. 'Double-strand break repair: 53BP1 comes into focus', *Nat Rev Mol Cell Biol*, 15: 7-18.

Paterson, H. F., A. J. Self, M. D. Garrett, I. Just, K. Aktories, and A. Hall. 1990. 'Microinjection of recombinant p21rho induces rapid changes in cell morphology', *J Cell Biol*, 111: 1001-7.

Pear, W. S., G. P. Nolan, M. L. Scott, and D. Baltimore. 1993. 'Production of high-titer helper-free retroviruses by transient transfection', *Proc Natl Acad Sci U S A*, 90: 8392-6.

Perona, R., S. Montaner, L. Saniger, I. Sanchez-Perez, R. Bravo, and J. C. Lacal. 1997. 'Activation of the nuclear factor-kappaB by Rho, CDC42, and Rac-1 proteins', *Genes Dev*, 11: 463-75.

Pfannkuche, K., F. T. Wunderlich, M. X. Doss, D. Spitkovsky, M. Reppel, A. Sachinidis, and J. Hescheler. 2008. 'Generation of a double-fluorescent double-selectable Cre/loxP indicator vector for monitoring of intracellular recombination events', *Nat Protoc*, 3: 1510-26.

Pfeifer, A., E. P. Brandon, N. Kootstra, F. H. Gage, and I. M. Verma. 2001. 'Delivery of the Cre recombinase by a self-deleting lentiviral vector: efficient gene targeting in vivo', *Proc Natl Acad Sci U S A*, 98: 11450-5.

Piacibello, W., S. Bruno, F. Sanavio, S. Droetto, M. Gunetti, L. Ailles, F. Santoni de Sio, A. Viale, L. Gammaitoni, A. Lombardo, L. Naldini, and M. Aglietta. 2002. 'Lentiviral gene transfer and ex vivo expansion of human primitive stem cells capable of primary, secondary, and tertiary multilineage repopulation in NOD/SCID mice. Nonobese diabetic/severe combined immunodeficient', *Blood*, 100: 4391-400.

Pilch, D. R., O. A. Sedelnikova, C. Redon, A. Celeste, A. Nussenzweig, and W. M. Bonner. 2003. 'Characteristics of gamma-H2AX foci at DNA double-strand breaks sites', *Biochem Cell Biol*, 81: 123-9.

Piunti, A., A. Rossi, A. Cerutti, M. Albert, S. Jammula, A. Scelfo, L. Cedrone, G. Fragola, L. Olsson, H. Koseki, G. Testa, S. Casola, K. Helin, F. d'Adda di Fagagna, and D. Pasini. 2014. 'Polycomb proteins control proliferation and transformation independently of cell cycle checkpoints by regulating DNA replication', *Nat Commun*, 5: 3649.

Poburski, D., J. B. Boerner, M. Koenig, M. Ristow, and R. Thierbach. 2016. 'Time-resolved functional analysis of acute impairment of frataxin expression in an inducible cell model of Friedreich ataxia', *Biol Open*, 5: 654-61.

Pommier, Y., E. Leo, H. Zhang, and C. Marchand. 2010. 'DNA topoisomerases and their poisoning by anticancer and antibacterial drugs', *Chem Biol*, 17: 421-33.

Porter, A. P., A. Papaioannou, and A. Malliri. 2016. 'Deregulation of Rho GTPases in cancer', *Small GTPases*, 7: 123-38.

Potter, A. J., K. A. Gollahon, B. J. Palanca, M. J. Harbert, Y. M. Choi, A. H. Moskovitz, J. D. Potter, and P. S. Rabinovitch. 2002. 'Flow cytometric analysis of the cell cycle phase specificity of DNA damage induced by radiation, hydrogen peroxide and doxorubicin', *Carcinogenesis*, 23: 389-401.

Qi, Z., S. Redding, J. Y. Lee, B. Gibb, Y. Kwon, H. Niu, W. A. Gaines, P. Sung, and E. C. Greene. 2015. 'DNA sequence alignment by microhomology sampling during homologous recombination', *Cell*, 160: 856-69.

Radu, A., G. Blobel, and M. S. Moore. 1995. 'Identification of a protein complex that is required for nuclear protein import and mediates docking of import substrate to distinct nucleoporins', *Proc Natl Acad Sci U S A*, 92: 1769-73.

Ray, M., R. Tang, Z. Jiang, and V. M. Rotello. 2015. 'Quantitative tracking of protein trafficking to the nucleus using cytosolic protein delivery by nanoparticle-stabilized nanocapsules', *Bioconjug Chem*, 26: 1004-7.

Rich, T., R. L. Allen, and A. H. Wyllie. 2000. 'Defying death after DNA damage', *Nature*, 407: 777-83.

Ridley, A. J. 2011. 'Life at the leading edge', *Cell*, 145: 1012-22.

Ridley, A. J., and A. Hall. 1992. 'The small GTP-binding protein rho regulates the assembly of focal adhesions and actin stress fibers in response to growth factors', *Cell*, 70: 389-99.

Ridley, A. J., H. F. Paterson, C. L. Johnston, D. Diekmann, and A. Hall. 1992. 'The small GTP-binding protein rac regulates growth factor-induced membrane ruffling', *Cell*, 70: 401-10.

Rittinger, K., P. A. Walker, J. F. Eccleston, K. Nurmahomed, D. Owen, E. Laue, S. J. Gamblin, and S. J. Smerdon. 1997. 'Crystal structure of a small G protein in complex with the GTPase-activating protein rhoGAP', *Nature*, 388: 693-7.

Rogakou, E. P., C. Boon, C. Redon, and W. M. Bonner. 1999. 'Megabase chromatin domains involved in DNA double-strand breaks in vivo', *J Cell Biol*, 146: 905-16.

Rogakou, E. P., D. R. Pilch, A. H. Orr, V. S. Ivanova, and W. M. Bonner. 1998. 'DNA double-stranded breaks induce histone H2AX phosphorylation on serine 139', *J Biol Chem*, 273: 5858-68.

Roos, W. P., and B. Kaina. 2006. 'DNA damage-induced cell death by apoptosis', *Trends Mol Med*, 12: 440-50.

———. 2013. 'DNA damage-induced cell death: from specific DNA lesions to the DNA damage response and apoptosis', *Cancer letters*, 332: 237-48.

Roos, W. P., A. D. Thomas, and B. Kaina. 2016. 'DNA damage and the balance between survival and death in cancer biology', *Nat Rev Cancer*, 16: 20-33.

Roots, R., G. Kraft, and E. Gosschalk. 1985. 'The formation of radiation-induced DNA breaks: the ratio of double-strand breaks to single-strand breaks', *Int J Radiat Oncol Biol Phys*, 11: 259-65.

Rose, K. M. 1988. 'DNA topoisomerases as targets for chemotherapy', *FASEB J*, 2: 2474-8.

Roset, R., A. Inagaki, M. Hohl, F. Brenet, J. Lafrance-Vanasse, J. Lange, J. M. Scandura, J. A. Tainer, S. Keeney, and J. H. Petrini. 2014. 'The Rad50 hook domain regulates DNA damage signaling and tumorigenesis', *Genes Dev*, 28: 451-62.

Ross, G. M. 1999. 'Induction of cell death by radiotherapy', *Endocr Relat Cancer*, 6: 41-4.

Rothkamm, K., I. Kruger, L. H. Thompson, and M. Lobrich. 2003. 'Pathways of DNA double-strand break repair during the mammalian cell cycle', *Mol Cell Biol*, 23: 5706-15.

Roux, P. P., and J. Blenis. 2004. 'ERK and p38 MAPK-activated protein kinases: a family of protein kinases with diverse biological functions', *Microbiol Mol Biol Rev*, 68: 320-44.

Ruggieri, R., Y. Y. Chuang, and M. Symons. 2001. 'The small GTPase Rac suppresses apoptosis caused by serum deprivation in fibroblasts', *Mol Med*, 7: 293-300.

Saito, S., X. F. Liu, K. Kamijo, R. Raziuddin, T. Tatsumoto, I. Okamoto, X. Chen, C. C. Lee, M. V. Lorenzi, N. Ohara, and T. Miki. 2004. 'Deregulation and mislocalization of the cytokinesis regulator ECT2 activate the Rho signaling pathways leading to malignant transformation', *J Biol Chem*, 279: 7169-79.

Sancar, A., L. A. Lindsey-Boltz, K. Unsal-Kacmaz, and S. Linn. 2004. 'Molecular mechanisms of mammalian DNA repair and the DNA damage checkpoints', *Annu Rev Biochem*, 73: 39-85.

Sander, E. E., J. P. ten Klooster, S. van Delft, R. A. van der Kammen, and J. G. Collard. 1999. 'Rac downregulates Rho activity: reciprocal balance between both GTPases determines cellular morphology and migratory behavior', *J Cell Biol*, 147: 1009-22.

Sandrock, K., H. Bielek, K. Schradi, G. Schmidt, and N. Klugbauer. 2010. 'The nuclear import of the small GTPase Rac1 is mediated by the direct interaction with karyopherin alpha2', *Traffic*, 11: 198-209.

Santivasi, W. L., and F. Xia. 2014. 'Ionizing radiation-induced DNA damage, response, and repair', *Antioxid Redox Signal*, 21: 251-9.

Sartori, A. A., C. Lukas, J. Coates, M. Mistrik, S. Fu, J. Bartek, R. Baer, J. Lukas, and S. P. Jackson. 2007. 'Human CtIP promotes DNA end resection', *Nature*, 450: 509-14.

Schnelzer, A., D. Prechtel, U. Knaus, K. Dehne, M. Gerhard, H. Graeff, N. Harbeck, M. Schmitt, and E. Lengyel. 2000. 'Rac1 in human breast cancer: overexpression, mutation analysis, and characterization of a new isoform, Rac1b', *Oncogene*, 19: 3013-20.

Schultz, L. B., N. H. Chehab, A. Malikzay, and T. D. Halazonetis. 2000. 'p53 binding protein 1 (53BP1) is an early participant in the cellular response to DNA double-strand breaks', *J Cell Biol*, 151: 1381-90.

Schwartz, M. A., J. E. Meredith, and W. B. Kiosses. 1998. 'An activated Rac mutant functions as a dominant negative for membrane ruffling', *Oncogene*, 17: 625-9.

Sedelnikova, O. A., E. P. Rogakou, I. G. Panyutin, and W. M. Bonner. 2002. 'Quantitative detection of (125)IdU-induced DNA double-strand breaks with gamma-H2AX antibody', *Radiat Res*, 158: 486-92.

Senyuz, S., H. Jang, R. Nussinov, O. Keskin, and A. Gursoy. 2021. 'Mechanistic Differences of Activation of Rac1(P29S) and Rac1(A159V)', *J Phys Chem B*, 125: 3790-802.

Setiaputra, D., and D. Durocher. 2019. 'Shieldin - the protector of DNA ends', *EMBO Rep*, 20.

Sfeir, A., and T. de Lange. 2012. 'Removal of shelterin reveals the telomere end-protection problem', *Science*, 336: 593-7.

Shalem, O., N. E. Sanjana, E. Hartenian, X. Shi, D. A. Scott, T. Mikkelson, D. Heckl, B. L. Ebert, D. E. Root, J. G. Doench, and F. Zhang. 2014. 'Genome-scale CRISPR-Cas9 knockout screening in human cells', *Science*, 343: 84-87.

Shibata, A., D. Moiani, A. S. Arvai, J. Perry, S. M. Harding, M. M. Genois, R. Maity, S. van Rossum-Fikkert, A. Kertokalio, F. Romoli, A. Ismail, E. Ismalaj, E. Petricci, M. J. Neale, R. G. Bristow, J. Y. Masson, C. Wyman, P. A. Jeggo, and J. A. Tainer. 2014. 'DNA double-strand break repair pathway choice is directed by distinct MRE11 nuclease activities', *Mol Cell*, 53: 7-18.

Shieh, S. Y., J. Ahn, K. Tamai, Y. Taya, and C. Prives. 2000. 'The human homologs of checkpoint kinases Chk1 and Cds1 (Chk2) phosphorylate p53 at multiple DNA damage-inducible sites', *Genes Dev*, 14: 289-300.

Shieh, S. Y., M. Ikeda, Y. Taya, and C. Prives. 1997. 'DNA damage-induced phosphorylation of p53 alleviates inhibition by MDM2', *Cell*, 91: 325-34.

Shirsat, N. V., R. J. Pignolo, B. L. Kreider, and G. Rovera. 1990. 'A member of the ras gene superfamily is expressed specifically in T, B and myeloid hemopoietic cells', *Oncogene*, 5: 769-72.

Shutes, A., and C. J. Der. 2006. 'Real-time in vitro measurement of intrinsic and Ras GAP-mediated GTP hydrolysis', *Methods Enzymol*, 407: 9-22.

Shutes, A., C. Onesto, V. Picard, B. Leblond, F. Schweighoffer, and C. J. Der. 2007. 'Specificity and mechanism of action of EHT 1864, a novel small molecule inhibitor of Rac family small GTPases', *J Biol Chem*, 282: 35666-78.

Simon, A. R., H. G. Vikis, S. Stewart, B. L. Fanburg, B. H. Cochran, and K. L. Guan. 2000. 'Regulation of STAT3 by direct binding to the Rac1 GTPase', *Science*, 290: 144-7.

Simunek, T., M. Sterba, O. Popelova, M. Adamcova, R. Hrdina, and V. Gersl. 2009. 'Anthracycline-induced cardiotoxicity: overview of studies examining the roles of oxidative stress and free cellular iron', *Pharmacol Rep*, 61: 154-71.

Singh, S. P., P. A. Thomason, S. Lilla, M. Schaks, Q. Tang, B. L. Goode, L. M. Machesky, K. Rottner, and R. H. Insall. 2020. 'Cell-substrate adhesion drives Scar/WAVE activation and phosphorylation by a Ste20-family kinase, which controls pseudopod lifetime', *PLoS Biol*, 18: e3000774.

Skvortsov, S., J. Dudas, P. Eichberger, M. Witsch-Baumgartner, J. Loeffler-Ragg, C. Pritz, V. H. Schartinger, H. Maier, J. Hall, P. Debbage, H. Riechelmann, P. Lukas, I. Skvortsova, and Eortc PathoBiology Group. 2014. 'Rac1 as a potential therapeutic target for chemo-radioresistant head and neck squamous cell carcinomas (HNSCC)', *Br J Cancer*, 110: 2677-87.

Sluss, H. K., and R. J. Davis. 2006. 'H2AX is a target of the JNK signaling pathway that is required for apoptotic DNA fragmentation', *Mol Cell*, 23: 152-3.

Smart, D. J., H. D. Halicka, G. Schmuck, F. Traganos, Z. Darzynkiewicz, and G. M. Williams. 2008. 'Assessment of DNA double-strand breaks and gammaH2AX induced by the topoisomerase II poisons etoposide and mitoxantrone', *Mutat Res*, 641: 43-7.

Smith, G. C., and S. P. Jackson. 1999. 'The DNA-dependent protein kinase', *Genes Dev*, 13: 916-34.

Solomon, H., S. Madar, and V. Rotter. 2011. 'Mutant p53 gain of function is interwoven into the hallmarks of cancer', *J Pathol*, 225: 475-8.

Song, D., and F. S. Lee. 2011. 'Mouse knock-out of IOP1 protein reveals its essential role in mammalian cytosolic iron-sulfur protein biogenesis', *J Biol Chem*, 286: 15797-805.

Song, E. H., W. Oh, A. Ulu, H. S. Carr, Y. Zuo, and J. A. Frost. 2015. 'Acetylation of the RhoA GEF Net1A controls its subcellular localization and activity', *J Cell Sci*, 128: 913-22.

Stasiak, A. Z., E. Larquet, A. Stasiak, S. Muller, A. Engel, E. Van Dyck, S. C. West, and E. H. Egelman. 2000. 'The human Rad52 protein exists as a heptameric ring', *Curr Biol*, 10: 337-40.

Steel, G. G. 1996. 'From targets to genes: a brief history of radiosensitivity', *Phys Med Biol*, 41: 205-22.

Steffen, A., M. Ladwein, G. A. Dimchev, A. Hein, L. Schwenkmezger, S. Arens, K. I. Ladwein, J. Margit Holleboom, F. Schur, J. Victor Small, J. Schwarz, R. Gerhard, J. Faix, T. E. Stradal, C. Brakebusch, and K. Rottner. 2013. 'Rac function is crucial for cell migration but is not required for spreading and focal adhesion formation', *J Cell Sci*, 126: 4572-88.

Sterba, M., O. Popelova, A. Vavrova, E. Jirkovsky, P. Kovarikova, V. Gersl, and T. Simunek. 2013. 'Oxidative stress, redox signaling, and metal chelation in anthracycline cardiotoxicity and pharmacological cardioprotection', *Antioxid Redox Signal*, 18: 899-929.

Stoffler, D., B. Fahrenkrog, and U. Aebi. 1999. 'The nuclear pore complex: from molecular architecture to functional dynamics', *Curr Opin Cell Biol*, 11: 391-401.

Subauste, M. C., M. Von Herrath, V. Benard, C. E. Chamberlain, T. H. Chuang, K. Chu, G. M. Bokoch, and K. M. Hahn. 2000. 'Rho family proteins modulate rapid apoptosis induced by cytotoxic T lymphocytes and Fas', *J Biol Chem*, 275: 9725-33.

Sugihara, K., N. Nakatsuji, K. Nakamura, K. Nakao, R. Hashimoto, H. Otani, H. Sakagami, H. Kondo, S. Nozawa, A. Aiba, and M. Katsuki. 1998. 'Rac1 is required for the formation of three germ layers during gastrulation', *Oncogene*, 17: 3427-33.

Suzuki, K., S. Kodama, and M. Watanabe. 1999. 'Recruitment of ATM protein to double strand DNA irradiated with ionizing radiation', *J Biol Chem*, 274: 25571-5.

Swift, L. P., A. Rephaeli, A. Nudelman, D. R. Phillips, and S. M. Cutts. 2006. 'Doxorubicin-DNA adducts induce a non-topoisomerase II-mediated form of cell death', *Cancer Res*, 66: 4863-71.

Swift, S., J. Lorens, P. Achacoso, and G. P. Nolan. 2001. 'Rapid production of retroviruses for efficient gene delivery to mammalian cells using 293T cell-based systems', *Curr Protoc Immunol*, Chapter 10: Unit 10 17C.

Takata, M., M. S. Sasaki, E. Sonoda, C. Morrison, M. Hashimoto, H. Utsumi, Y. Yamaguchi-Iwai, A. Shinohara, and S. Takeda. 1998. 'Homologous recombination and non-homologous end-joining pathways of DNA double-strand break repair have overlapping roles in the maintenance of chromosomal integrity in vertebrate cells', *EMBO J*, 17: 5497-508.

Tan, S., P. Yi, H. Wang, L. Xia, Y. Han, H. Wang, B. Zeng, L. Tang, Q. Pan, Y. Tian, S. Rao, L. Oyang, J. Liang, J. Lin, M. Su, Y. Shi, Q. Liao, and Y. Zhou. 2020. 'RAC1 Involves in the Radioresistance by Mediating Epithelial-Mesenchymal Transition in Lung Cancer', *Front Oncol*, 10: 649.

Tan, W., T. R. Palmby, J. Gavard, P. Amornphimoltham, Y. Zheng, and J. S. Gutkind. 2008. 'An essential role for Rac1 in endothelial cell function and vascular development', *FASEB J*, 22: 1829-38.

Tarrade, S., T. Bhardwaj, M. Flegal, L. Bertrand, I. Velegzhaninov, A. Moskalev, and D. Klokov. 2015. 'Histone H2AX Is Involved in FoxO3a-Mediated Transcriptional Responses to Ionizing Radiation to Maintain Genome Stability', *Int J Mol Sci*, 16: 29996-30014.

Tarsounas, M., and P. Sung. 2020. 'The antitumorigenic roles of BRCA1-BARD1 in DNA repair and replication', *Nat Rev Mol Cell Biol*, 21: 284-99.

Thompson, T., C. Tovar, H. Yang, D. Carvajal, B. T. Vu, Q. Xu, G. M. Wahl, D. C. Heimbrook, and L. T. Vassilev. 2004. 'Phosphorylation of p53 on key serines is dispensable for transcriptional activation and apoptosis', *J Biol Chem*, 279: 53015-22.

Tibbetts, R. S., K. M. Brumbaugh, J. M. Williams, J. N. Sarkaria, W. A. Cliby, S. Y. Shieh, Y. Taya, C. Prives, and R. T. Abraham. 1999. 'A role for ATR in the DNA damage-induced phosphorylation of p53', *Genes Dev*, 13: 152-7.

Tong, J., L. Li, B. Ballermann, and Z. Wang. 2013. 'Phosphorylation of Rac1 T108 by extracellular signal-regulated kinase in response to epidermal growth factor: a novel mechanism to regulate Rac1 function', *Mol Cell Biol*, 33: 4538-51.

Toufektchan, E., and F. Toledo. 2018. 'The Guardian of the Genome Revisited: p53 Downregulates Genes Required for Telomere Maintenance, DNA Repair, and Centromere Structure', *Cancers (Basel)*, 10.

Tscharntke, M., R. Pofahl, A. Chrostek-Grashoff, N. Smyth, C. Niessen, C. Niemann, B. Hartwig, V. Herzog, H. W. Klein, T. Krieg, C. Brakebusch, and I. Haase. 2007. 'Impaired epidermal wound healing in vivo upon inhibition or deletion of Rac1', *J Cell Sci*, 120: 1480-90.

Turinetto, V., and C. Giachino. 2015. 'Multiple facets of histone variant H2AX: a DNA double-strand-break marker with several biological functions', *Nucleic Acids Res*, 43: 2489-98.

Unger, T., T. Juven-Gershon, E. Moallem, M. Berger, R. Vogt Sionov, G. Lozano, M. Oren, and Y. Haupt. 1999. 'Critical role for Ser20 of human p53 in the negative regulation of p53 by Mdm2', *EMBO J*, 18: 1805-14.

Unsal-Kacmaz, K., A. M. Makhov, J. D. Griffith, and A. Sancar. 2002. 'Preferential binding of ATR protein to UV-damaged DNA', *Proc Natl Acad Sci U S A*, 99: 6673-8.

Valencia, A., P. Chardin, A. Wittinghofer, and C. Sander. 1991. 'The ras protein family: evolutionary tree and role of conserved amino acids', *Biochemistry*, 30: 4637-48.

Velaithan, R., J. Kang, J. L. Hirpara, T. Loh, B. C. Goh, M. Le Bras, C. Brenner, M. V. Clement, and S. Pervaiz. 2011. 'The small GTPase Rac1 is a novel binding partner of Bcl-2 and stabilizes its antiapoptotic activity', *Blood*, 117: 6214-26.

Vetter, I. R., and A. Wittinghofer. 2001. 'The guanine nucleotide-binding switch in three dimensions', *Science*, 294: 1299-304.

Vidali, L., F. Chen, G. Cicchetti, Y. Ohta, and D. J. Kwiatkowski. 2006. 'Rac1-null mouse embryonic fibroblasts are motile and respond to platelet-derived growth factor', *Mol Biol Cell*, 17: 2377-90.

Vigna, E., and L. Naldini. 2000. 'Lentiviral vectors: excellent tools for experimental gene transfer and promising candidates for gene therapy', *J Gene Med*, 2: 308-16.

Vogelstein, B., D. Lane, and A. J. Levine. 2000. 'Surfing the p53 network', *Nature*, 408: 307-10.

Walmsley, M. J., S. K. Ooi, L. F. Reynolds, S. H. Smith, S. Ruf, A. Mathiot, L. Vanes, D. A. Williams, M. P. Cancro, and V. L. Tybulewicz. 2003. 'Critical roles for Rac1 and Rac2 GTPases in B cell development and signaling', *Science*, 302: 459-62.

Wang, H., M. Wang, H. Wang, W. Bocker, and G. Iliakis. 2005. 'Complex H2AX phosphorylation patterns by multiple kinases including ATM and DNA-PK in human cells exposed to ionizing radiation and treated with kinase inhibitors', *J Cell Physiol*, 202: 492-502.

Wang, R., Q. Yu, X. Wang, B. Li, A. Ciotkowska, B. Rutz, Y. Wang, C. G. Stief, and M. Hennenberg. 2020. 'Rac1 silencing, NSC23766 and EHT1864 reduce growth and actin organization of bladder smooth muscle cells', *Life Sci*, 261: 118468.

Ward, I. M., K. Minn, K. G. Jorda, and J. Chen. 2003. 'Accumulation of checkpoint protein 53BP1 at DNA breaks involves its binding to phosphorylated histone H2AX', *J Biol Chem*, 278: 19579-82.

Wartlick, F., A. Bopp, C. Henninger, and G. Fritz. 2013. 'DNA damage response (DDR) induced by topoisomerase II poisons requires nuclear function of the small GTPase Rac', *Biochim Biophys Acta*, 1833: 3093-103.

Waters, C. A., N. T. Strande, D. W. Wyatt, J. M. Pryor, and D. A. Ramsden. 2014. 'Nonhomologous end joining: a good solution for bad ends', *DNA Repair (Amst)*, 17: 39-51.

Wechsler, T., B. P. Chen, R. Harper, K. Morotomi-Yano, B. C. Huang, K. Meek, J. E. Cleaver, D. J. Chen, and M. Wabl. 2004. 'DNA-PKcs function regulated specifically by protein phosphatase 5', *Proc Natl Acad Sci U S A*, 101: 1247-52.

Weis, K. 2003. 'Regulating access to the genome: nucleocytoplasmic transport throughout the cell cycle', *Cell*, 112: 441-51.

Welch, H. C., W. J. Coadwell, L. R. Stephens, and P. T. Hawkins. 2003. 'Phosphoinositide 3-kinase-dependent activation of Rac', *FEBS Lett*, 546: 93-7.

Wells, C. M., M. Walmsley, S. Ooi, V. Tybulewicz, and A. J. Ridley. 2004. 'Rac1-deficient macrophages exhibit defects in cell spreading and membrane ruffling but not migration', *J Cell Sci*, 117: 1259-68.

Wennerberg, K., and C. J. Der. 2004. 'Rho-family GTPases: it's not only Rac and Rho (and I like it)', *J Cell Sci*, 117: 1301-12.

Wennerberg, K., K. L. Rossman, and C. J. Der. 2005. 'The Ras superfamily at a glance', *J Cell Sci*, 118: 843-6.

Wertheimer, E., A. Gutierrez-Uzquiza, C. Rosemblit, C. Lopez-Haber, M. S. Sosa, and M. G. Kazanietz. 2012. 'Rac signaling in breast cancer: a tale of GEFs and GAPs', *Cell Signal*, 24: 353-62.

White, D. E., D. Negorev, H. Peng, A. V. Ivanov, G. G. Maul, and F. J. Rauscher, 3rd. 2006. 'KAP1, a novel substrate for PIKK family members, colocalizes with numerous damage response factors at DNA lesions', *Cancer Res*, 66: 11594-9.

White, D., I. U. Rafalska-Metcalf, A. V. Ivanov, A. Corsinotti, H. Peng, S. C. Lee, D. Trono, S. M. Janicki, and F. J. Rauscher, 3rd. 2012. 'The ATM substrate KAP1 controls DNA repair in heterochromatin: regulation by HP1 proteins and serine 473/824 phosphorylation', *Mol Cancer Res*, 10: 401-14.

Williams, C. L. 2003. 'The polybasic region of Ras and Rho family small GTPases: a regulator of protein interactions and membrane association and a site of nuclear localization signal sequences', *Cell Signal*, 15: 1071-80.

Wilson, T. E., U. Grawunder, and M. R. Lieber. 1997. 'Yeast DNA ligase IV mediates non-homologous DNA end joining', *Nature*, 388: 495-8.

Wilstermann, A. M., and N. Osheroff. 2003. 'Stabilization of eukaryotic topoisomerase II-DNA cleavage complexes', *Curr Top Med Chem*, 3: 321-38.

Woroniuk, A., A. Porter, G. White, D. T. Newman, Z. Diamantopoulou, T. Waring, C. Rooney, D. Strathdee, D. J. Marston, K. M. Hahn, O. J. Sansom, T. Zech, and A. Malliri. 2018. 'STEF/TIAM2-mediated Rac1 activity at the nuclear envelope regulates the perinuclear actin cap', *Nat Commun*, 9: 2124.

Xia, Z., M. Dickens, J. Raingeaud, R. J. Davis, and M. E. Greenberg. 1995. 'Opposing effects of ERK and JNK-p38 MAP kinases on apoptosis', *Science*, 270: 1326-31.

Xie, W., S. Nagarajan, S. J. Baumgart, R. L. Kosinsky, Z. Najafova, V. Kari, M. Hennion, D. Indenbirken, S. Bonn, A. Grundhoff, F. Wegwitz, A. Mansouri, and S. A. Johnsen. 2017. 'RNF40 regulates gene expression in an epigenetic context-dependent manner', *Genome Biol*, 18: 32.

Xu, Y., H. Zhang, V. T. Nguyen, N. Angelopoulos, J. Nunes, A. Reid, L. Buluwela, L. Magnani, J. Stebbing, and G. Giamas. 2015. 'LMTK3 Represses Tumor Suppressor-like Genes through Chromatin Remodeling in Breast Cancer', *Cell Rep*, 12: 837-49.

Yan, Y., P. M. Greer, P. T. Cao, R. H. Kolb, and K. H. Cowan. 2012. 'RAC1 GTPase plays an important role in gamma-irradiation induced G2/M checkpoint activation', *Breast Cancer Res*, 14: R60.

Yan, Y., A. L. Hein, A. Etekpo, K. M. Burchett, C. Lin, C. A. Enke, S. K. Batra, K. H. Cowan, and M. M. Ouellette. 2014. 'Inhibition of RAC1 GTPase sensitizes pancreatic cancer cells to gamma-irradiation', *Oncotarget*, 5: 10251-70.

Yang, Y. S., and T. E. Hughes. 2001. 'Cre stoplight: a red/green fluorescent reporter of Cre recombinase expression in living cells', *Biotechniques*, 31: 1036, 38, 40-1.

Yannone, S. M., I. S. Khan, R. Z. Zhou, T. Zhou, K. Valerie, and L. F. Povirk. 2008. 'Coordinate 5' and 3' endonucleolytic trimming of terminally blocked blunt DNA double-strand break

ends by Artemis nuclease and DNA-dependent protein kinase', *Nucleic Acids Res*, 36: 3354-65.

Yao, C., K. P. Yu, W. Philbrick, B. H. Sun, C. Simpson, C. Zhang, and K. Insogna. 2017. 'Breast cancer-associated gene 3 interacts with Rac1 and augments NF-kappaB signaling in vitro, but has no effect on RANKL-induced bone resorption in vivo', *Int J Mol Med*, 40: 1067-77.

Yokoyama, K., G. W. Goodwin, F. Ghomashchi, J. A. Glomset, and M. H. Gelb. 1991. 'A protein geranylgeranyltransferase from bovine brain: implications for protein prenylation specificity', *Proc Natl Acad Sci U S A*, 88: 5302-6.

Yoo, S., and W. S. Dynan. 1999. 'Geometry of a complex formed by double strand break repair proteins at a single DNA end: recruitment of DNA-PKcs induces inward translocation of Ku protein', *Nucleic Acids Res*, 27: 4679-86.

Yoon, C. H., K. H. Hyun, R. K. Kim, H. Lee, E. J. Lim, H. Y. Chung, S. An, M. J. Park, Y. Suh, M. J. Kim, and S. J. Lee. 2011. 'The small GTPase Rac1 is involved in the maintenance of stemness and malignancies in glioma stem-like cells', *FEBS Lett*, 585: 2331-8.

Yoshida, T., Y. Zhang, L. A. Rivera Rosado, J. Chen, T. Khan, S. Y. Moon, and B. Zhang. 2010. 'Blockade of Rac1 activity induces G1 cell cycle arrest or apoptosis in breast cancer cells through downregulation of cyclin D1, survivin, and X-linked inhibitor of apoptosis protein', *Mol Cancer Ther*, 9: 1657-68.

Yu, Q., C. Gratzke, Y. Wang, X. Wang, B. Li, F. Strittmatter, A. Herlemann, R. Wang, A. Tamalunas, R. Waidelich, C. G. Stief, and M. Hennenberg. 2019. 'New strategies for inhibition of non-adrenergic prostate smooth muscle contraction by pharmacologic intervention', *Prostate*, 79: 746-56.

Yu, Y., A. Arora, W. Min, C. M. Roifman, and E. Grunebaum. 2009. 'EdU incorporation is an alternative non-radioactive assay to [(3)H]thymidine uptake for in vitro measurement of mice T-cell proliferations', *J Immunol Methods*, 350: 29-35.

Yue, X., C. Zhang, Y. Zhao, J. Liu, A. W. Lin, V. M. Tan, J. M. Drake, L. Liu, M. N. Boateng, J. Li, Z. Feng, and W. Hu. 2017. 'Gain-of-function mutant p53 activates small GTPase Rac1 through SUMOylation to promote tumor progression', *Genes Dev*, 31: 1641-54.

Zannini, L., D. Delia, and G. Buscemi. 2014. 'CHK2 kinase in the DNA damage response and beyond', *J Mol Cell Biol*, 6: 442-57.

Zerial, M., and H. McBride. 2001. 'Rab proteins as membrane organizers', *Nat Rev Mol Cell Biol*, 2: 107-17.

Zgheib, O., Y. Huyen, R. A. DiTullio, Jr., A. Snyder, M. Venere, E. S. Stavridi, and T. D. Halazonetis. 2005. 'ATM signaling and 53BP1', *Radiother Oncol*, 76: 119-22.

Zhang, B., Y. Zhang, and E. Shacter. 2004. 'Rac1 inhibits apoptosis in human lymphoma cells by stimulating Bad phosphorylation on Ser-75', *Mol Cell Biol*, 24: 6205-14.

Zhang, Y., J. Zhou, X. Cao, Q. Zhang, C. U. Lim, R. L. Ullrich, S. M. Bailey, and H. L. Liber. 2007. 'Partial deficiency of DNA-PKcs increases ionizing radiation-induced mutagenesis and telomere instability in human cells', *Cancer Lett*, 250: 63-73.

Zheng, H., S. Li, P. Hsu, and C. K. Qu. 2013. 'Induction of a tumor-associated activating mutation in protein tyrosine phosphatase Ptpn11 (Shp2) enhances mitochondrial metabolism, leading to oxidative stress and senescence', *J Biol Chem*, 288: 25727-38.

Zheng, Y. 2001. 'Dbl family guanine nucleotide exchange factors', *Trends Biochem Sci*, 26: 724-32.

Zhou, B. B., P. Chaturvedi, K. Spring, S. P. Scott, R. A. Johanson, R. Mishra, M. R. Mattern, J. D. Winkler, and K. K. Khanna. 2000. 'Caffeine abolishes the mammalian G(2)/M DNA damage checkpoint by inhibiting ataxia-telangiectasia-mutated kinase activity', *J Biol Chem*, 275: 10342-8.

Zhou, T., C. H. Wang, H. Yan, R. Zhang, J. B. Zhao, C. F. Qian, H. Xiao, and H. Y. Liu. 2016. 'Inhibition of the Rac1-WAVE2-Arp2/3 signaling pathway promotes radiosensitivity via downregulation of cofilin-1 in U251 human glioma cells', *Mol Med Rep*, 13: 4414-20.

Zhou, Z. W., M. Kirtay, N. Schneble, G. Yakoub, M. Ding, T. Rudiger, K. Siniuk, R. Lu, Y. N. Jiang, T. L. Li, C. Kaether, A. Barzilai, and Z. Q. Wang. 2020. 'NBS1 interacts with Notch signaling in neuronal homeostasis', *Nucleic Acids Res*, 48: 10924-39.

Ziegler, V., C. Henninger, I. Simiantonakis, M. Buchholzer, M. R. Ahmadian, W. Budach, and G. Fritz. 2017. 'Rho inhibition by lovastatin affects apoptosis and DSB repair of primary human lung cells in vitro and lung tissue in vivo following fractionated irradiation', *Cell death & disease*, 8: e2978.

Ziv, Y., D. Bielopolski, Y. Galanty, C. Lukas, Y. Taya, D. C. Schultz, J. Lukas, S. Bekker-Jensen, J. Bartek, and Y. Shiloh. 2006. 'Chromatin relaxation in response to DNA double-strand breaks is modulated by a novel ATM- and KAP-1 dependent pathway', *Nat Cell Biol*, 8: 870-6.

Zondag, G. C., E. E. Evers, J. P. ten Klooster, L. Janssen, R. A. van der Kammen, and J. G. Collard. 2000. 'Oncogenic Ras downregulates Rac activity, which leads to increased Rho activity and epithelial-mesenchymal transition', *J Cell Biol*, 149: 775-82.

Zou, L., and S. J. Elledge. 2003. 'Sensing DNA damage through ATRIP recognition of RPA-ssDNA complexes', *Science*, 300: 1542-8.

Zoughlami, Y., A. M. van Stalborgh, P. B. van Hennik, and P. L. Hordijk. 2013. 'Nucleophosmin1 is a negative regulator of the small GTPase Rac1', *PLoS One*, 8: e68477.

Zuleger, N., S. Boyle, D. A. Kelly, J. I. de las Heras, V. Lazou, N. Korfali, D. G. Batrakou, K. N. Randles, G. E. Morris, D. J. Harrison, W. A. Bickmore, and E. C. Schirmer. 2013. 'Specific nuclear envelope transmembrane proteins can promote the location of chromosomes to and from the nuclear periphery', *Genome Biol*, 14: R14.

7 Appendix

7.1 Additional figures

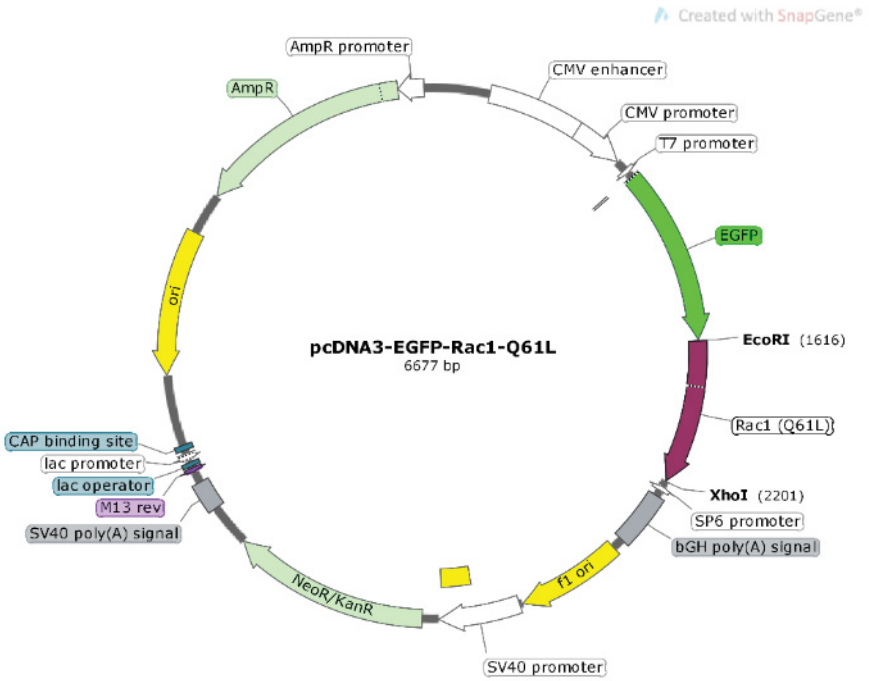

Figure 7.1: Map of constitutively active *RAC1* plasmid.
The sequence was provided from the manufacturer and loaded into SnapGene® to create the map.

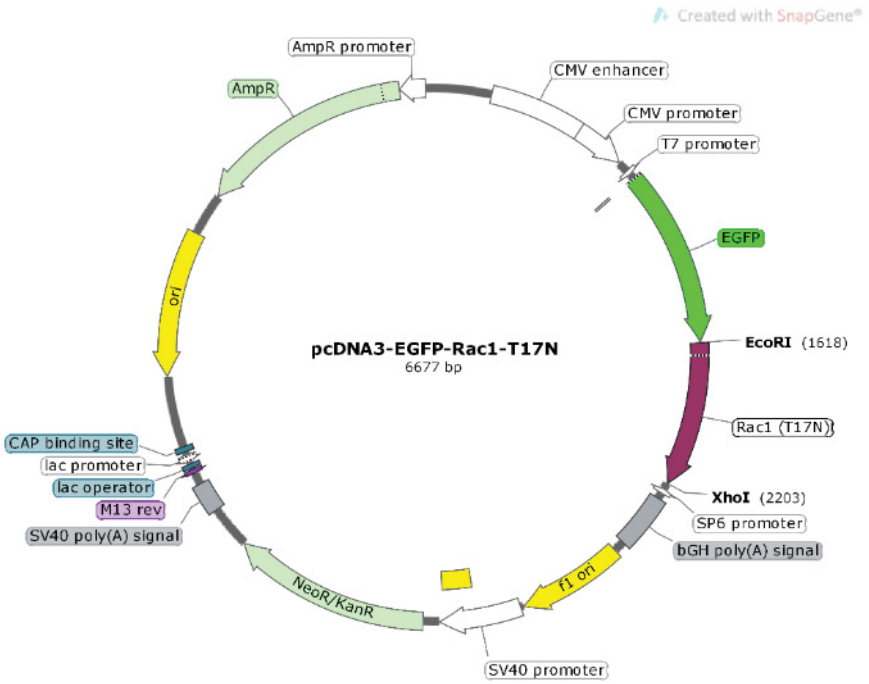

Figure 7.2: Map of dominant-negative *RAC1* plasmid.
The sequence was provided from the manufacturer and loaded into SnapGene® to create the map.

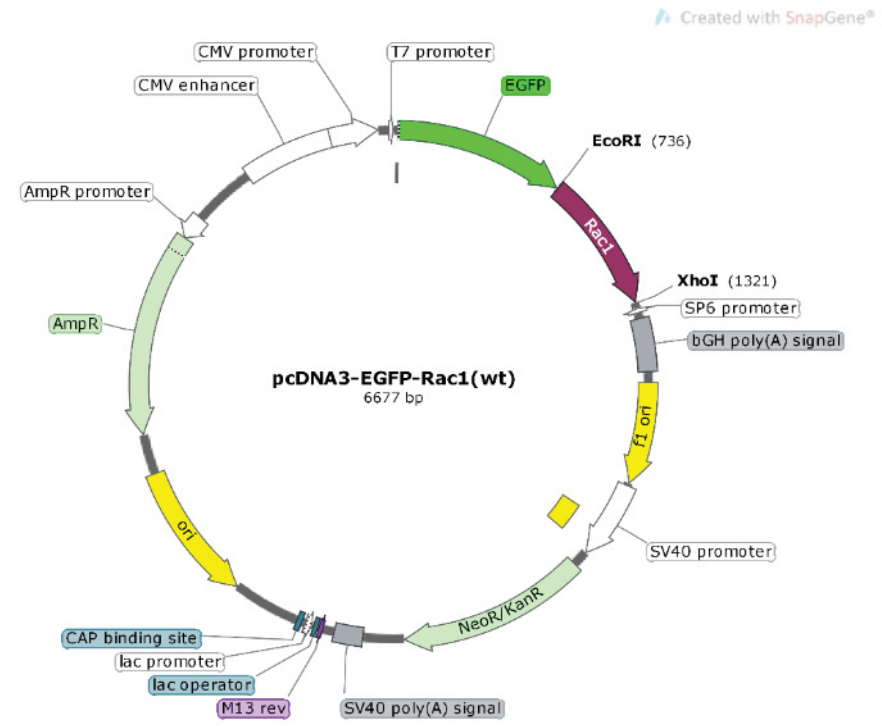

Figure 7.3: Map of wild-type *RAC1* plasmid.
The sequence was provided from the manufacturer and loaded into SnapGene® to create the map.

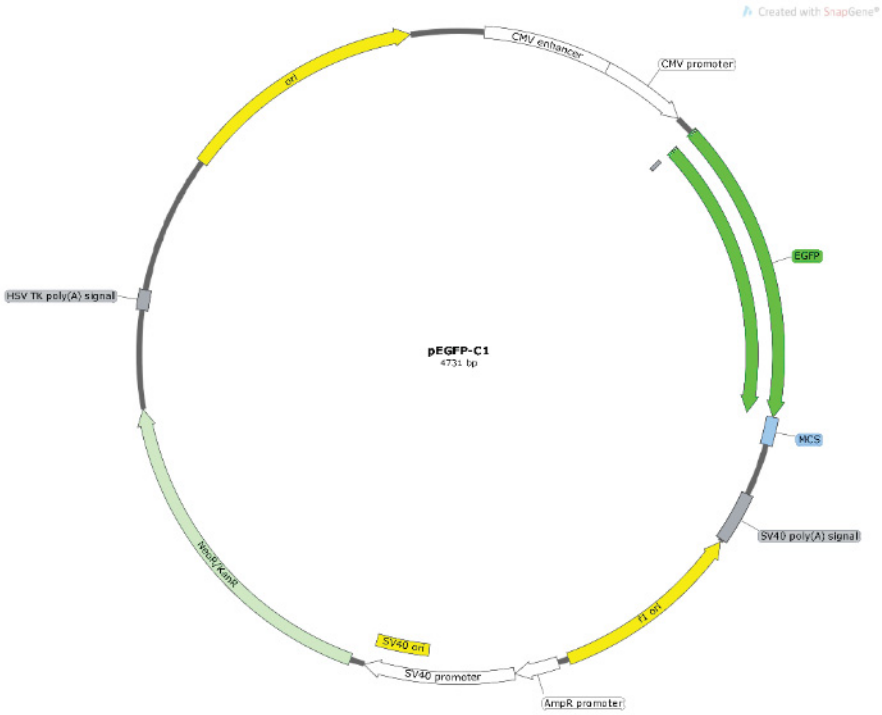

Figure 7.4: Map of GFP plasmid.
The sequence was provided from the manufacturer and loaded into SnapGene® to create the map.

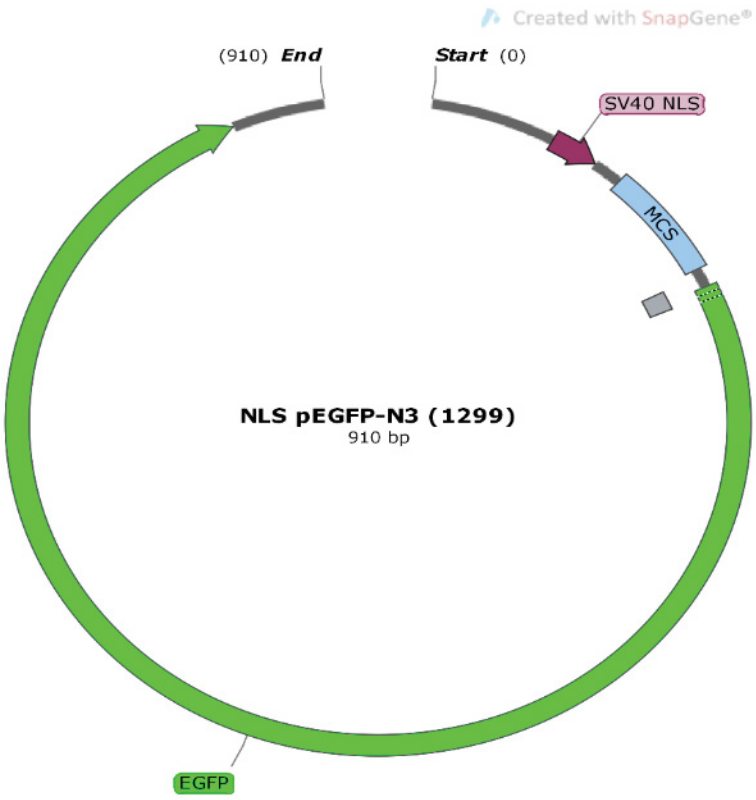

Figure 7.5: Map of GFP plasmid with SV40 NLS.
The sequence was provided from the manufacturer and loaded into SnapGene® to create the map.

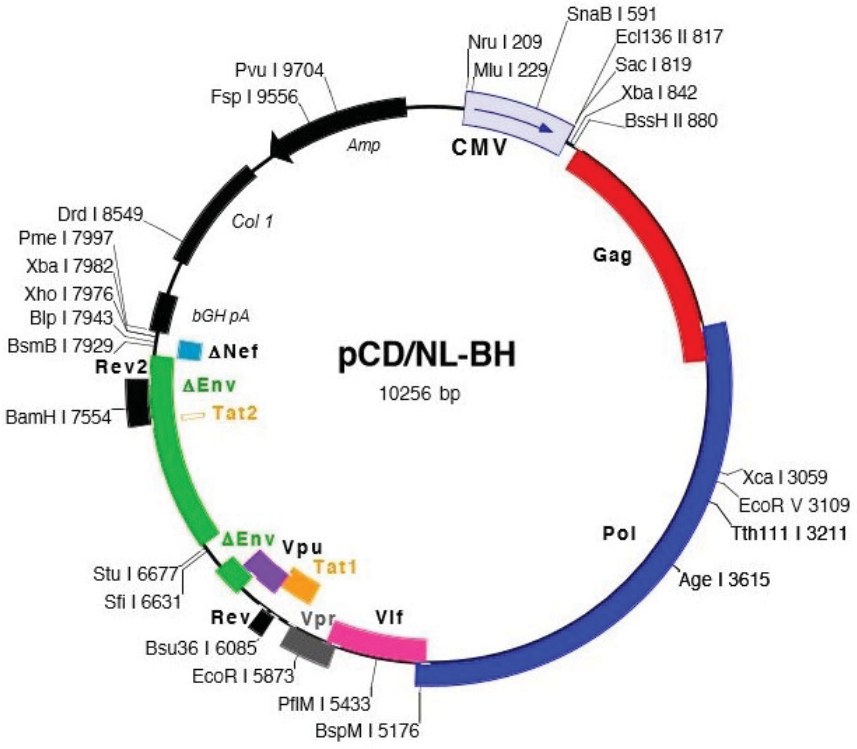

Figure 7.6: Map of pCD/NL-BH.

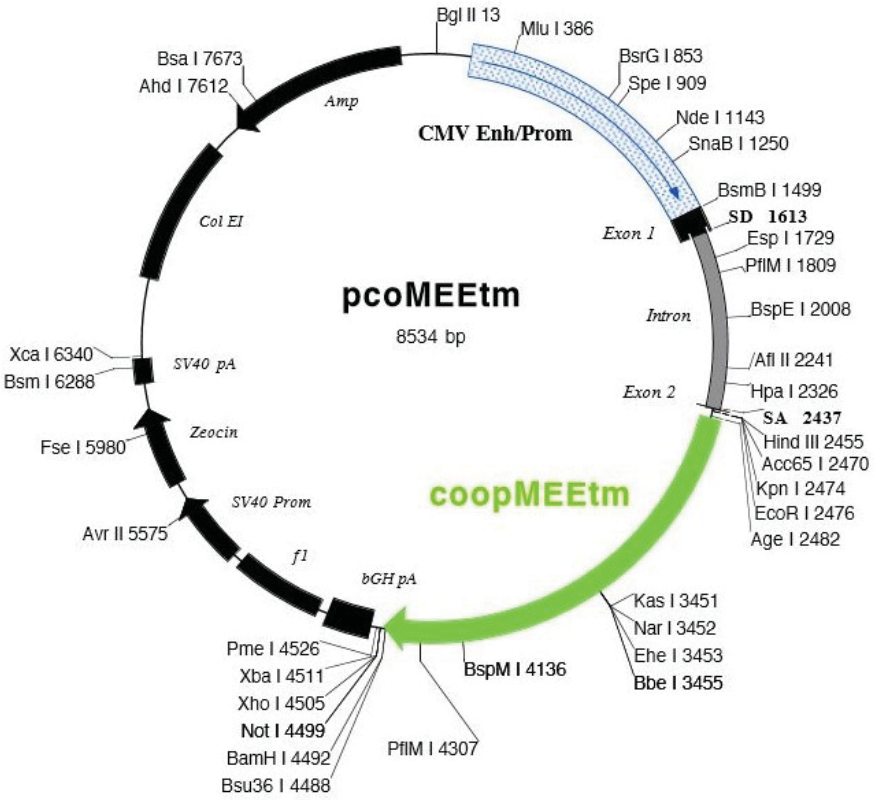

Figure 7.7: Map of pcoMEEtm.

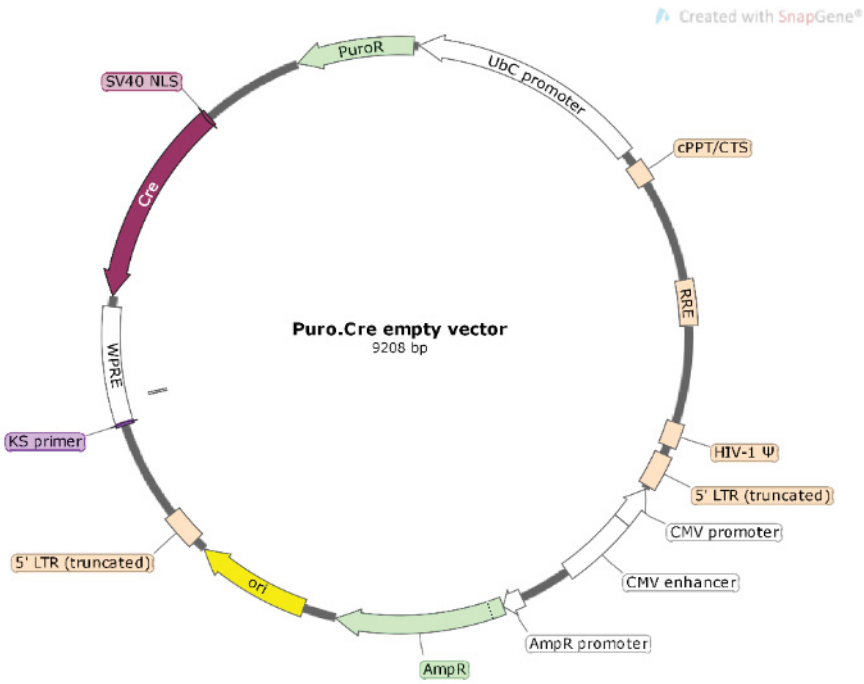

Figure 7.8: Map of Puro.Cre empty vector.
The sequence was provided from the manufacturer and loaded into SnapGene® to create the map.

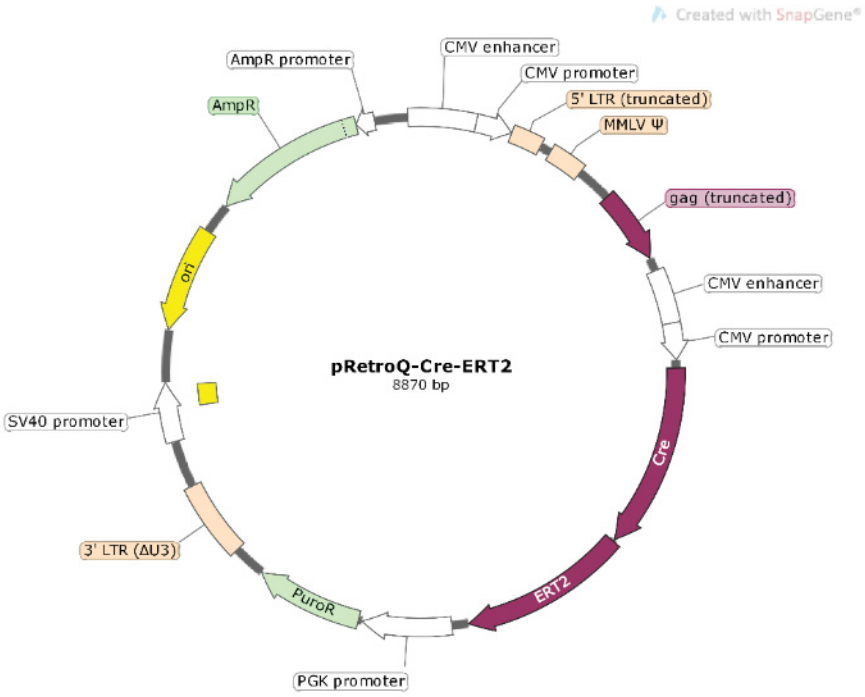

Figure 7.9: Map of pRetroQ-Cre-ERT2.
The sequence was provided from the manufacturer and loaded into SnapGene® to create the map.

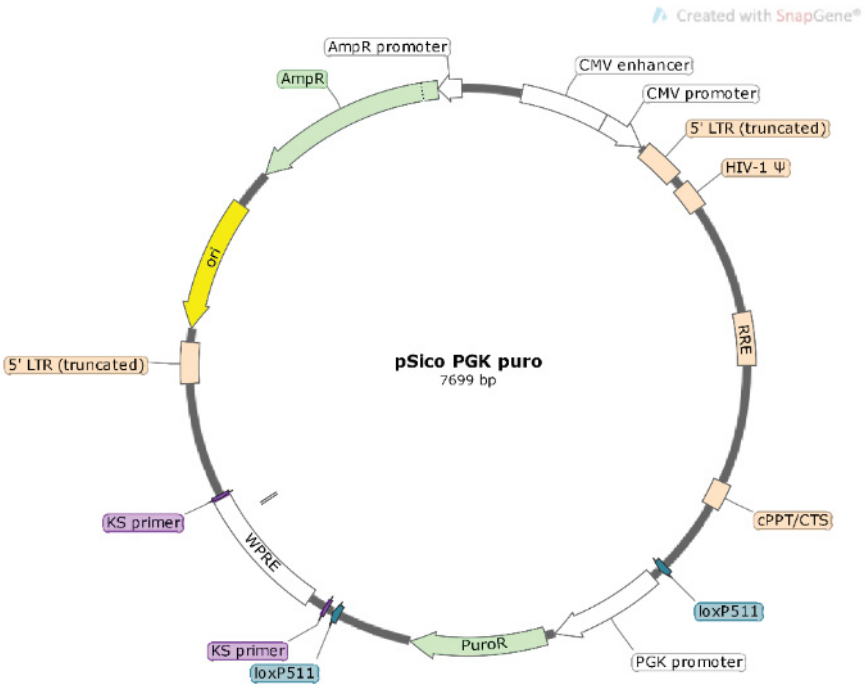

Figure 7.10: Map of pSico PGK puro.
The sequence was provided from the manufacturer and loaded into SnapGene® to create the map.

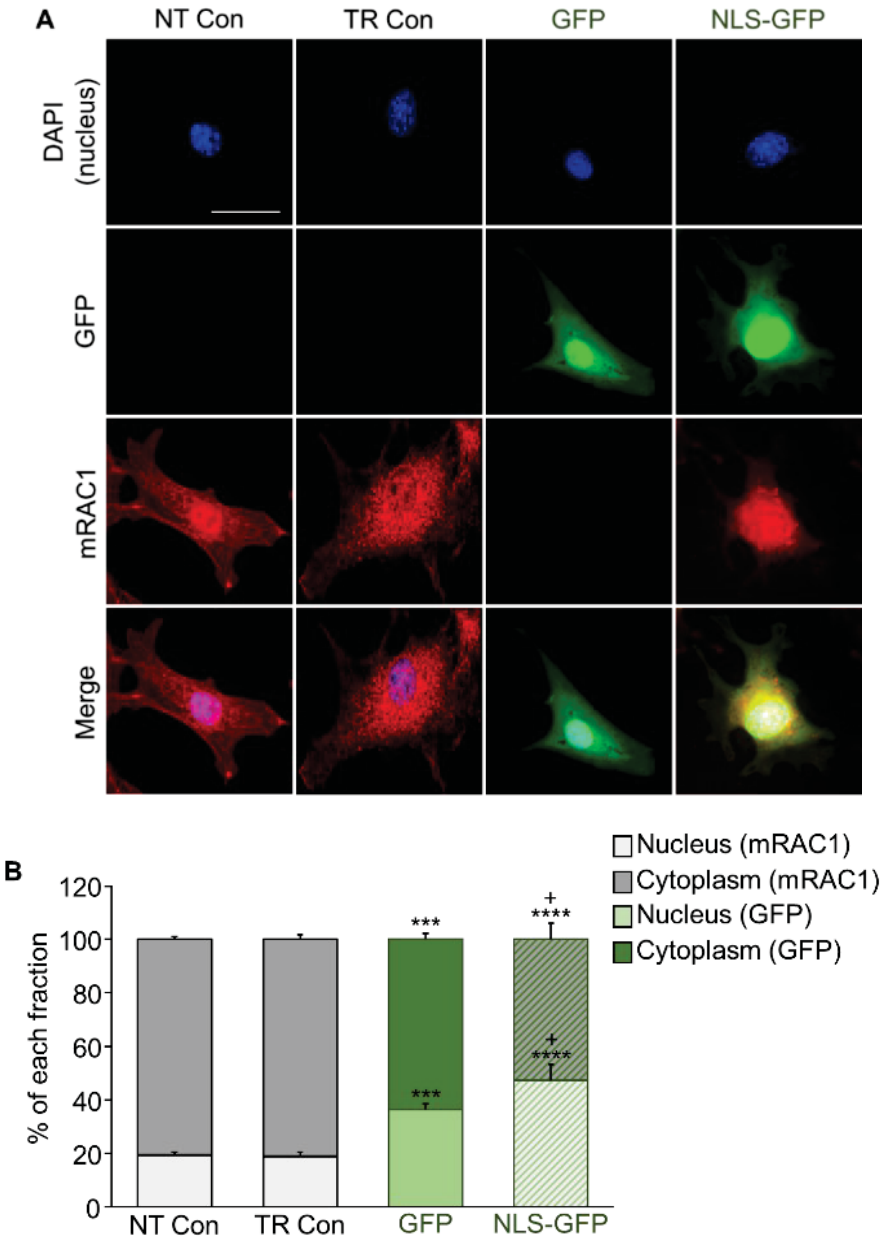

Figure 7.11: Fluorescence-based analysis of mRAC1 protein as well as GFP protein (with and without NLS) localization in non-transfected vs. transfected cells.
MEF were transiently transfected with *GFP* or *NLS-GFP* expression vector. Transfection control cells (TR Con) were treated with TransIT-X2. Control cells (NT Con) were non-transfected. **A** Pictures were taken 24 h after transfection. Representative microscopical pictures are shown; blue: DAPI-stained nuclei, green: GFP fluorescence, red: fluorescence-coupled antibody against primary antibody directed against intrinsic mRAC1. Scale bar: 25 µm. **B** Quantification of the fluorescence. Fluorescence intensity for cytoplasm and nucleus were quantified by measuring the fluorescence intensity of GFP-coupled hRAC1. The total fluorescence of each cell was set to 100 % (mean+SD; n=3 with 50 cells counted per experiment; ***$p \leq 0.001$, ****$p \leq 0.0001$ compared to control (NT Con); one-way ANOVA with Dunnett post-hoc test; $^{+}p \leq 0.05$ compared to GFP; T-Test, unpaired, two-sided). The data underlying the graph are shown in Table 7.43 of the appendix. Abbreviations: NT Con: non-transfected control cells, TR Con: control cells treated with TransIT-X2, GFP: green fluorescent protein, NLS-GFP: green fluorescent protein with additional NLS.

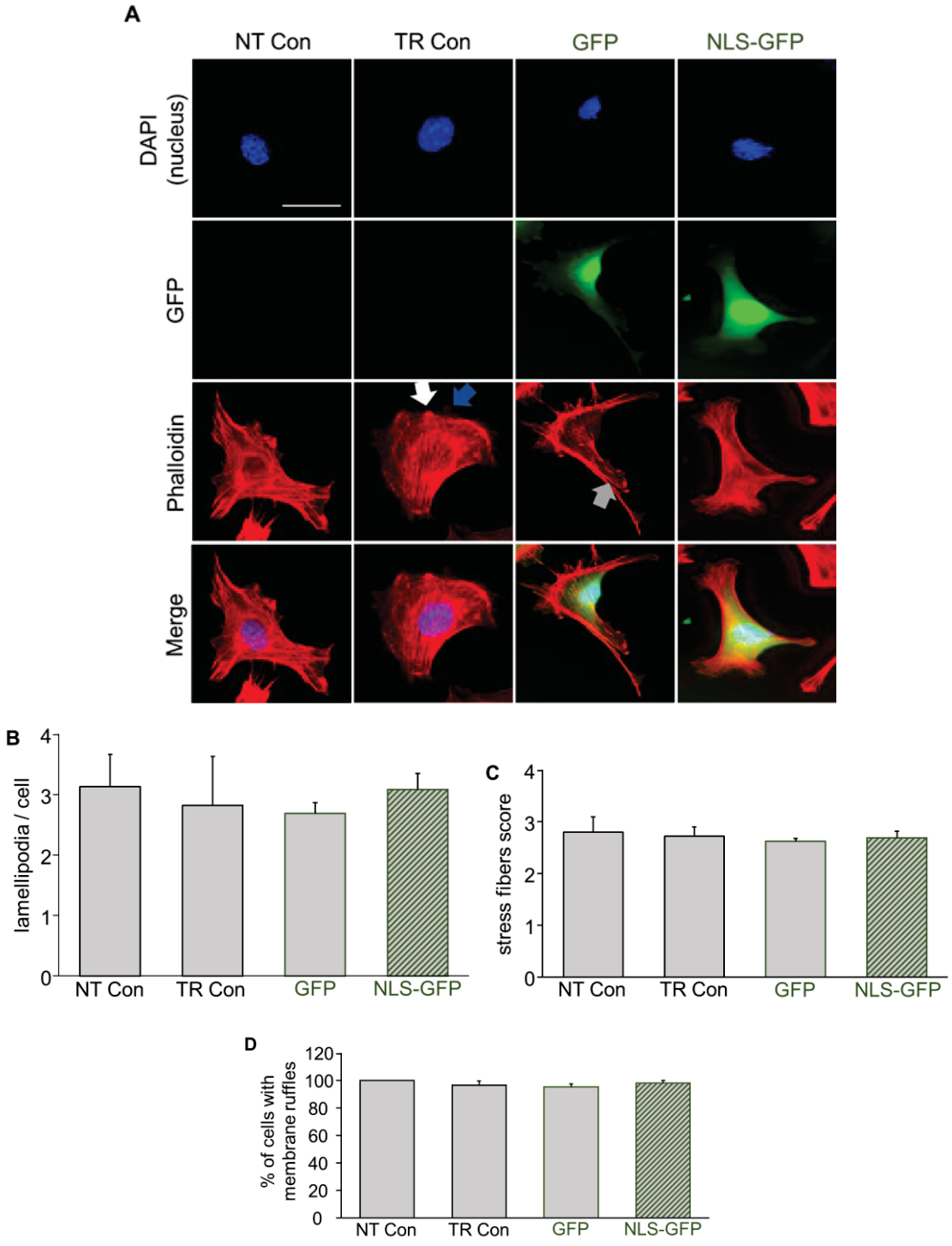

Figure 7.12: Cytoskeleton-staining in non-transfected cells and cells transfected with *GFP* or *NLS-GFP* expression vector.
MEF were transiently transfected with *GFP* or *NLS-GFP* expression vector. Transfection control cells (TR Con) were treated with TransIT-X2. Control cells (NT Con) were non-transfected. **A** 24 h after transfection cells were stained with Phalloidin-TRITC. Representative microscopical fluorescence pictures are shown; blue: DAPI-stained nuclei, green: GFP signal, red: cytoskeleton stained with Phalloidin-TRITC, white arrow: membrane ruffles, blue arrow: lamellipodia, grey arrow: stress fibers. Scale bar: 25 µm. **B** Quantification of lamellipodia formation. Lamellipodia of each cell were counted (mean+SD; n=3 with 50 cells counted per experiment). The data underlying the graph are shown in Table 7.44 of the appendix. **C** Quantification of stress fibers score. Stress fibers score of each cell was rated (mean+SD; n=3 with 50 cells counted per

experiment). The data underlying the graph are shown in Table 7.45 of the appendix. **D** Quantification of cells with membrane ruffles. Presence or absence of membrane ruffles was counted for each cell (mean+SD; n=3 with 50 cells counted per experiment). The data underlying the graph are shown in Table 7.46 of the appendix. Abbreviations: NT Con: non-transfected control cells, TR Con: control cells treated with TransIT-X2, GFP: green fluorescent protein, NLS-GFP: green fluorescent protein with additional NLS.

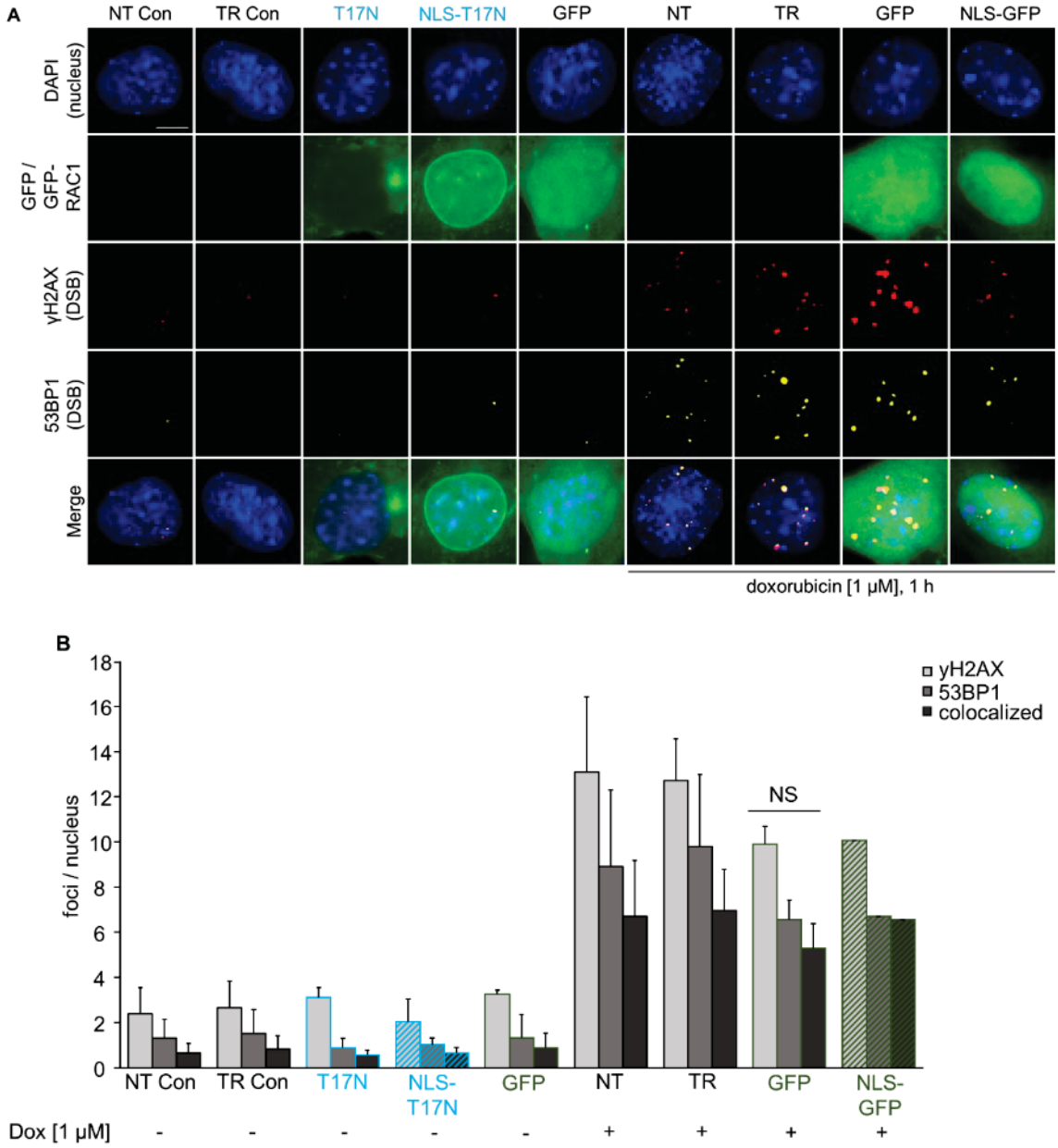

Figure 7.13: Influence of GFP-hRAC1(T17N) and GFP-NLS-hRAC1(T17N) expression itself on basal γH2AX and 53BP1 foci formation.
MEF were transiently transfected with *GFP-hRAC1(T17N)*, *GFP-NLS-hRAC1(T17N)*, *GFP*, or *NLS-GFP* expression vector. Transfection control cells (TR Con) were treated with TransIT-X2. Control cells (NT Con) were non-transfected. Next day cells were treated with Dox [1 µM] for 1 h. **A** After the end of the Dox treatment, cells were fixed and staining of γH2AX and 53BP1 foci was carried out as described in methods. Representative microscopical fluorescence pictures are shown; blue: DAPI-stained nuclei, green: GFP signal, red: γH2AX (Ser139), yellow: 53BP1. Scale

bar: 10 µm. **B** Quantification of γH2AX and 53BP1 foci formation, as well as colocalization of these foci. Foci of each cell were counted (mean+SD; n=1 - 38 with 50 nuclei counted per experiment). The data underlying the graph are shown in Table 7.47 of the appendix. Abbreviations: NT Con, NT: non-transfected cells, TR Con, TR: cells treated with transfection reagent (TransIT-X2), T17N: dominant-negative RAC1, NLS-T17N: dominant-negative RAC1 with additional NLS, GFP: green fluorescent protein, NLS-GFP: green fluorescent protein with NLS, NS: not significant.

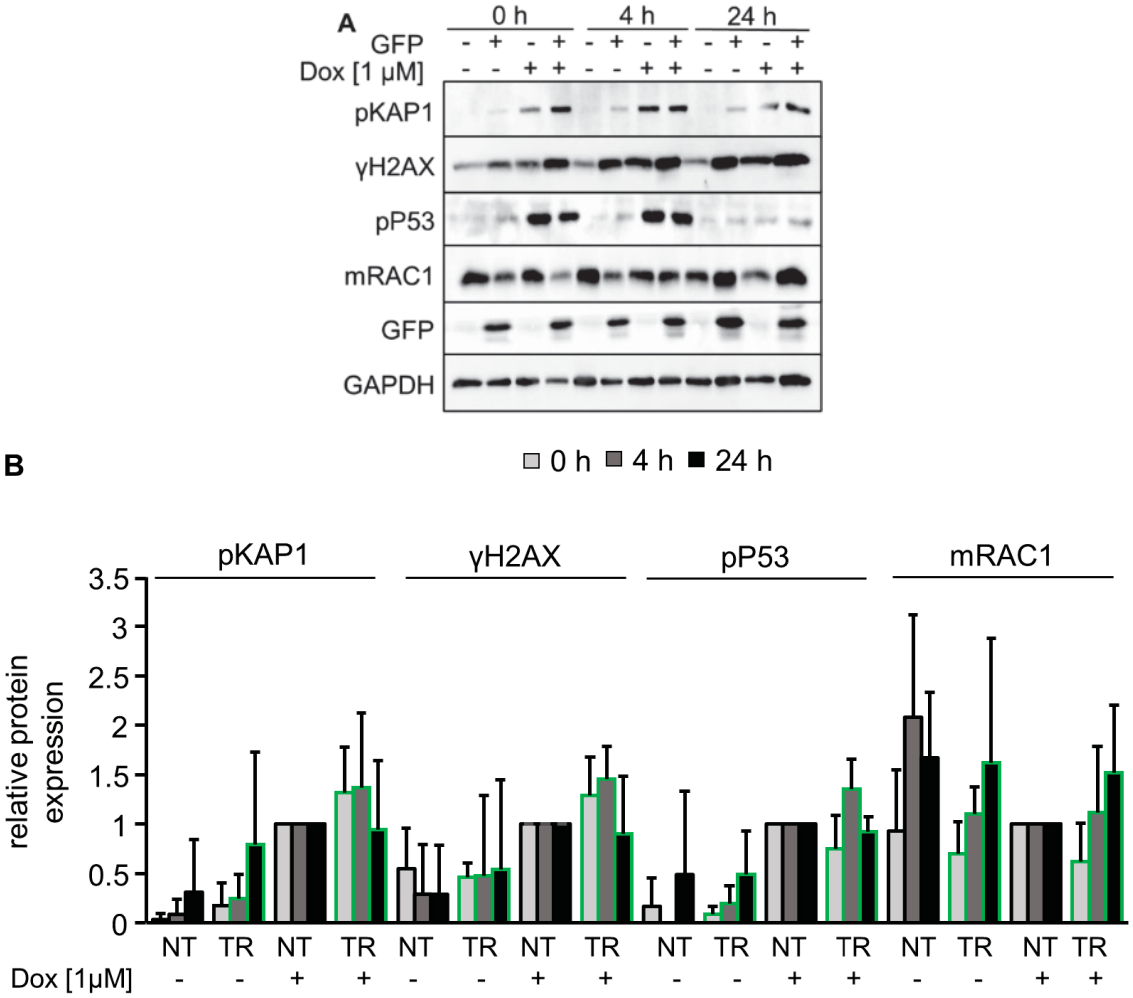

Figure 7.14: Western blot analysis in non-transfected cells and cells expressing GFP after doxorubicin treatment.
A MEF were transiently transfected with *GFP* expression vector or left un-transfected. 24 h after transfection cells were 2 h pulse-treated with 1 µM Dox. Cells were harvested after the indicated time-points. Afterwards cells were lysed, and protein extracts were analyzed by western blot analysis as described in methods. GAPDH was used as reference protein. **B** Change in protein expression in transfected and non-transfected cells after Dox treatment was quantified as described in methods. The protein expression of non-transfected cells (NT) treated with Dox was set to 1 (mean+SD; n=3). The data underlying the graph are shown in Table 7.48 of the appendix. Abbreviations: NT: non-transfected cells, TR: cells transfected with *GFP* expression vector.

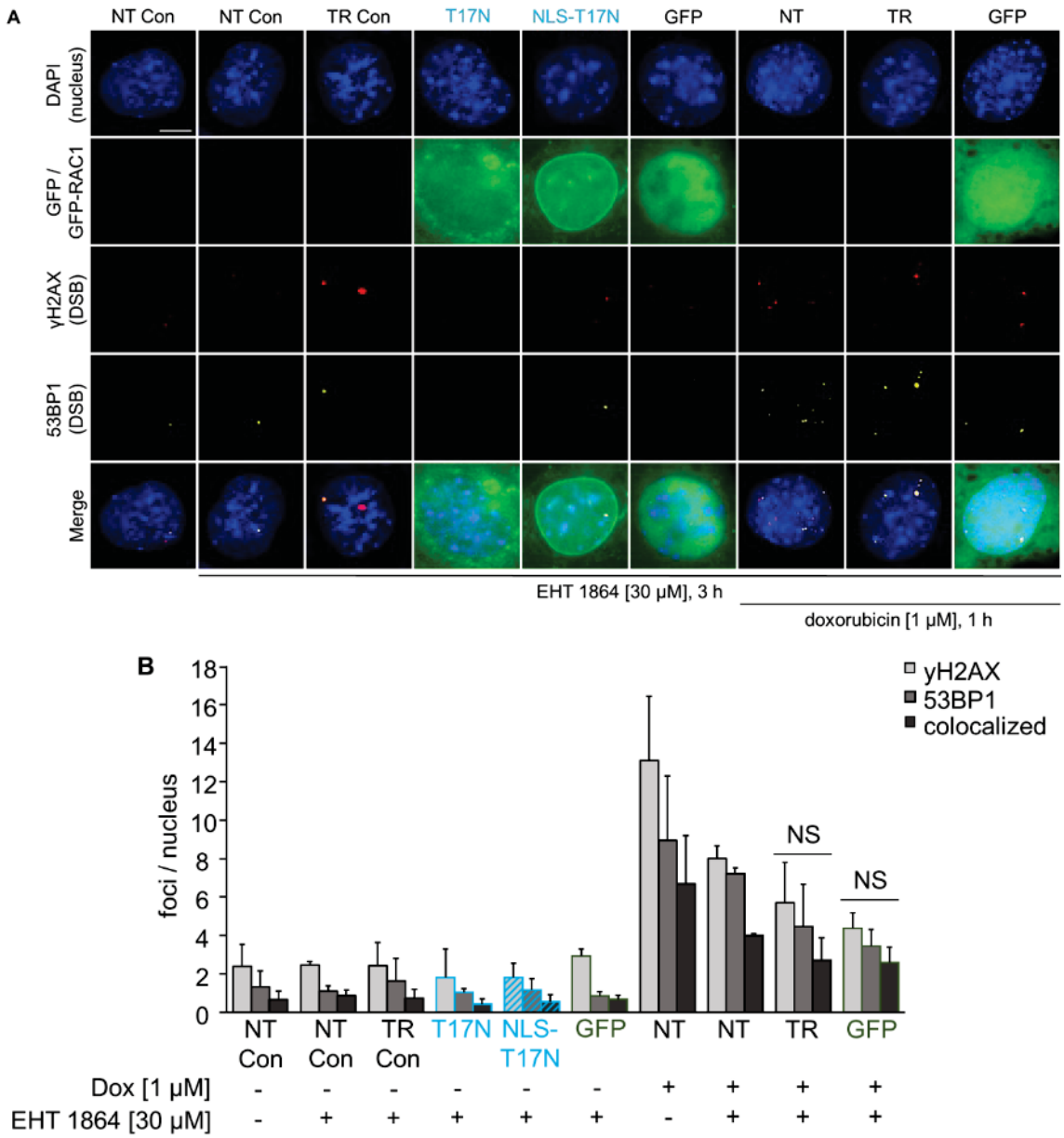

Figure 7.15: Influence of the transfection itself and EHT 1864 treatment on basal γH2AX and 53BP1 foci formation.
MEF were transiently transfected with *GFP-hRAC1(T17N)*, *GFP-NLS-hRAC1(T17N)*, or *GFP* expression vector. Transfection control cells (TR Con, TR) were treated with TransIT-X2. Control cells (NT Con, NT) were non-transfected. 24 h after transfection cells were pre-treated with 30 µM EHT 1864 for 3 h prior to treatment with Dox [1 µM, 1 h]. **A** After the end of the Dox treatment, cells were fixed and staining of γH2AX and 53BP1 foci was carried out as described in methods. Representative microscopical fluorescence pictures are shown; blue: DAPI-stained nuclei, green: GFP signal, red: γH2AX (Ser139), yellow: 53BP1. Scale bar: 10 µm. **B** Quantification of γH2AX and 53BP1 foci formation, as well as colocalization of these foci. Foci of each cell were counted (mean+SD; n=3 - 28 with 50 nuclei counted per experiment). The data underlying the graph are shown in Table 7.49 of the appendix. Abbreviations: NT Con, NT: non-transfected cells, TR Con, TR: cells treated with TransIT-X2, T17N: dominant-negative RAC1, NLS-T17N: dominant-negative RAC1 with additional NLS, GFP: green fluorescent protein, NS: not significant (vs NT + EHT 1864 + Dox).

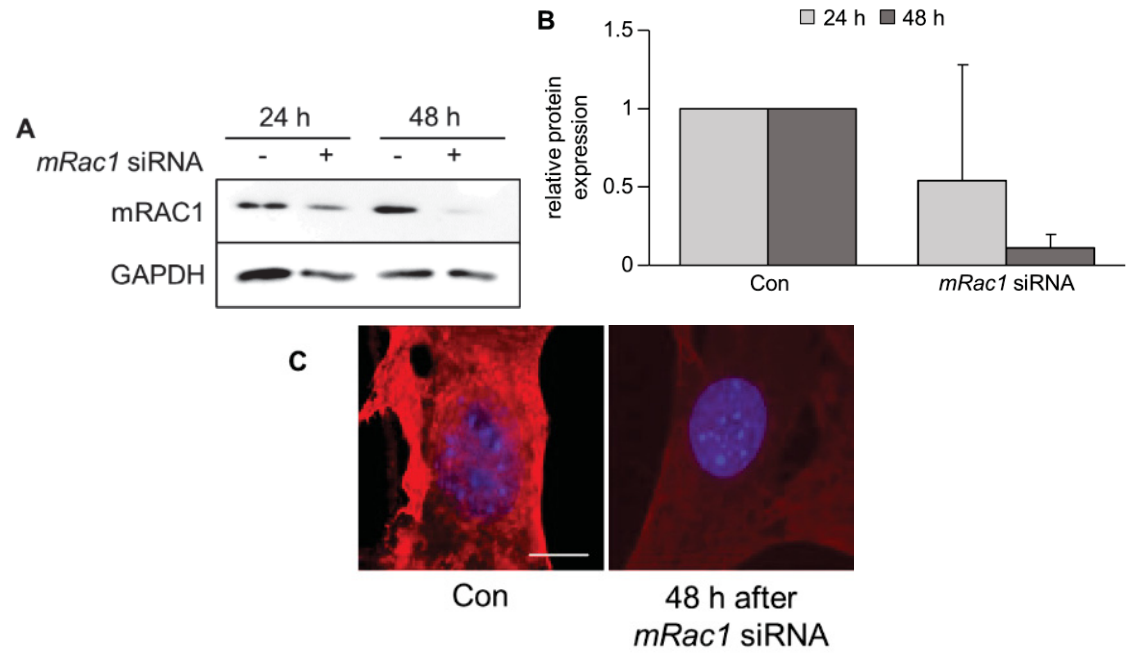

Figure 7.16: Transfection with *mRac1* siRNA efficiently reduced intrinsic mRAC1 protein expression.
A Cells were analyzed 24 h and 48 h after transfection with siRNA against *mRac1*. Cells were lysed and protein extracts were analyzed by western blot analysis as described in methods. GAPDH was used as reference protein. Scale bar: 25 µm. **B** Quantification of mRAC1 protein expression in non-transfected control cells and *mRac1* siRNA transfected cells. The protein expression of control cells was set to 1 (mean+SD; n=2). The data underlying the graph are shown in Table 7.50 of the appendix. Abbreviations: Con: non-transfected control cells, *mRac1* siRNA: cells transfected with siRNA against the murine *Rac1.* **C** Immunofluorescence-staining of mRAC1 48 h after transfection with *mRac1* siRNA. Abbreviations: Con: non-transfected control cells, *mRac1* siRNA: cells transfected with siRNA against murine *Rac1*.

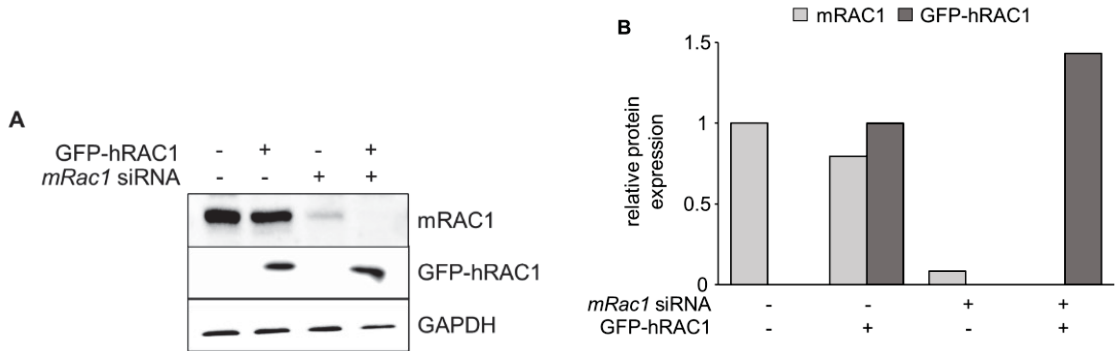

Figure 7.17: Transfection with *mRac1* siRNA efficiently reduced intrinsic mRAC1 protein expression while expression of human GFP-RAC1 was not affected.
A Cells were transfected with *mRac1* siRNA/human *GFP-RAC1* expression vector only, co-transfected with *mRac1* siRNA and human *GFP-RAC1* expression vector or left non-transfected. Cells were harvested 48 h after transfection with *mRac1* siRNA. Afterwards, cells were lysed, and protein extracts were analyzed by western blot analysis as described in methods. GAPDH was used as reference protein. **B** Change in mRAC1 and GFP-hRAC1 protein expression in non-transfected and transfected cells was quantified. The protein expression of control cells was set to 1 (mRAC1); the protein expression of only *GFP-hRAC1* expression vector transfected cells was set to 1 (GFP-hRAC1) (mean; n=1). The data underlying the graph are shown in Table 7.51

of the appendix. Abbreviations: *mRac1* siRNA: cells transfected siRNA against murine *Rac1*, GFP-hRAC1: cells transfected with *GFP-hRAC1* expression vector.

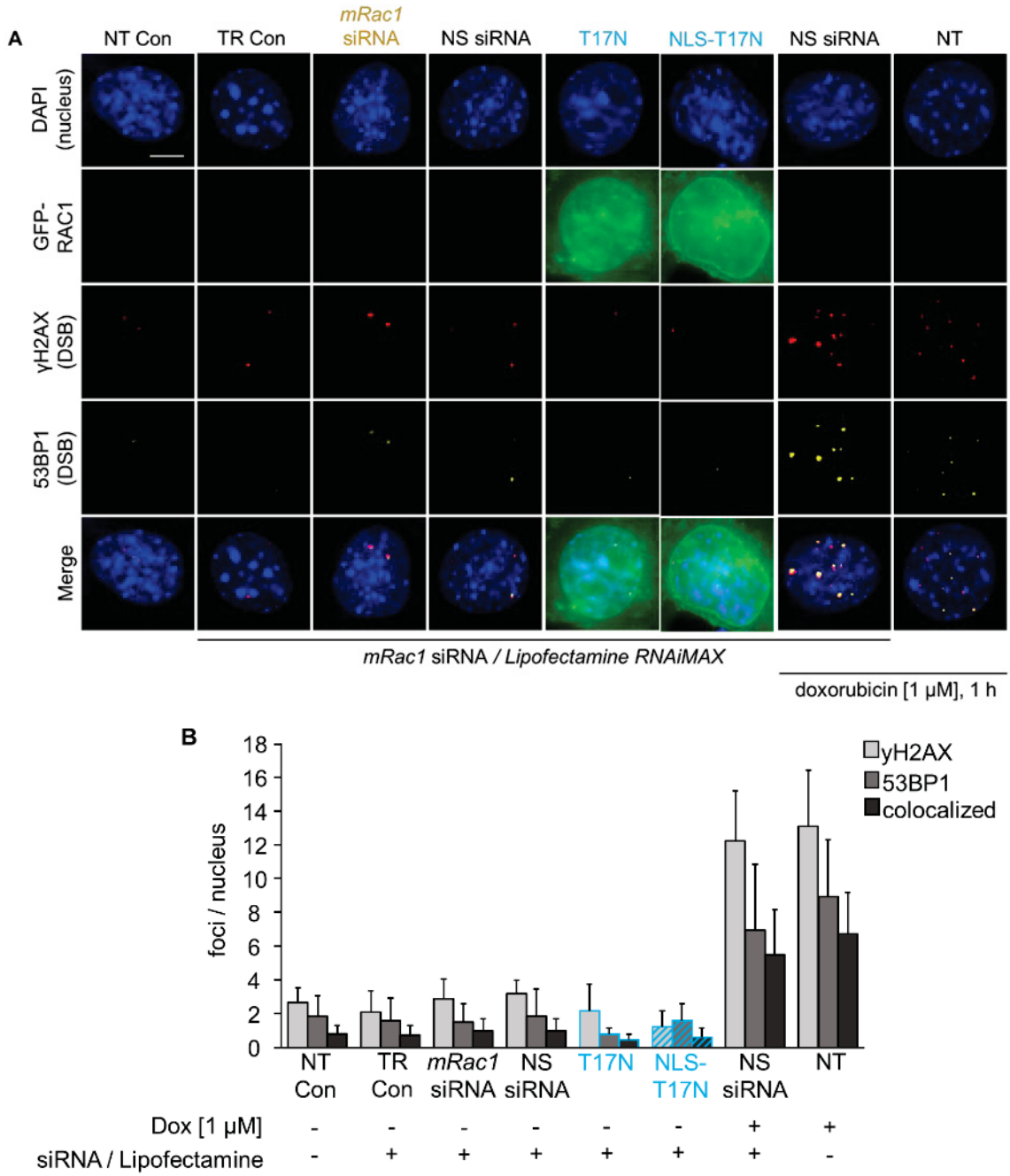

Figure 7.18: Influence of single and double transfection on basal γH2AX and 53BP1 foci formation.
mRac1 knockdown was achieved by transfection with *mRac1* siRNA. The treatment scheme is shown in material and methods (Figure 2.1 E, F). Cells were additionally transfected with *GFP-hRAC1(T17N)* or *GFP-NLS-hRAC1(T17N)* expression vector. **A** After the end of the Dox treatment, cells were fixed and staining of γH2AX and 53BP1 foci was carried out as described in methods. Representative microscopical fluorescence pictures are shown; blue: DAPI-stained nuclei, green: GFP signal, red: γH2AX (Ser139), yellow: 53BP1. Scale bar: 10 µm. **B** Quantification of γH2AX and 53BP1 foci formation, as well as colocalization of these foci. Foci of each cell were counted (mean+SD; n=2 - 28 with 50 nuclei counted per experiment). The data underlying the graph are shown in Table 7.52 of the appendix. Abbreviations: NT Con, NT: non-

transfected cells, TR Con: cells treated with transfection reagent (Lipofectamine RNAiMAX), *mRac1* siRNA: siRNA against murine *Rac1*, NS siRNA: non-silencing siRNA, T17N: dominant-negative RAC1, NLS-T17N: dominant-negative RAC1 with additional NLS.

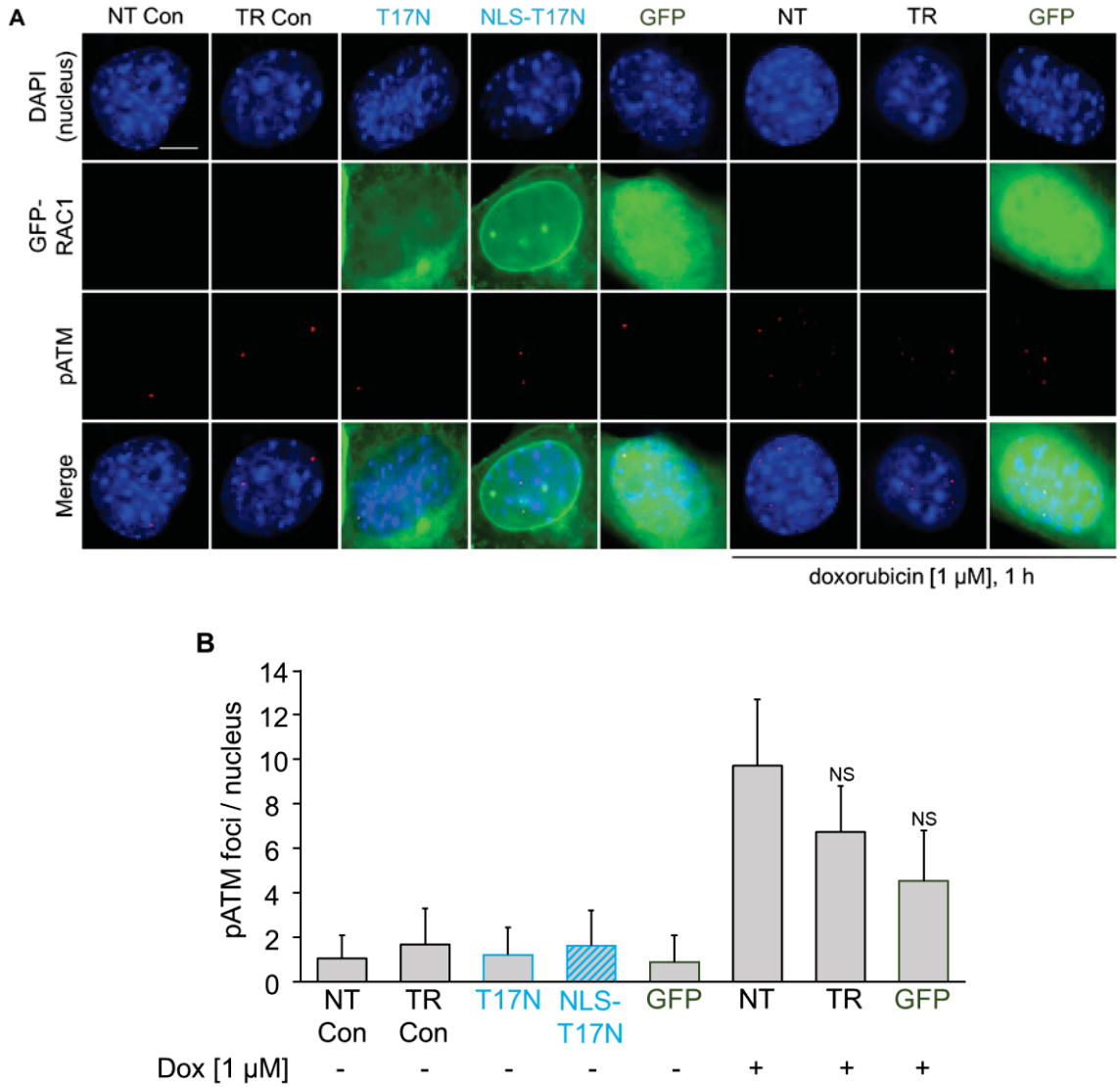

Figure 7.19: Influence of dominant-negative hRAC1 expression on basal pATM foci formation.
Cells were transiently transfected with *GFP-hRAC1(T17N)*, *GFP-NLS-hRAC1(T17N)*, or *GFP* expression vector. Transfection control cells (TR Con, TR) were treated with TransIT-X2. Control cells (NT Con, NT) were non-transfected. 24 h after transfection cells were treated with Dox [1 µM, 1 h]. **A** After the end of the Dox treatment, cells were fixed and staining of pATM foci was carried out as described in methods. Representative microscopical fluorescence pictures are shown; blue: DAPI-stained nuclei, green: GFP signal, red: pATM. **B** Quantification of pATM foci formation. Foci of each cell were counted (mean+SD; n=2 - 18 with 50 nuclei counted per experiment). The data underlying the graph are shown in Table 7.53 of the appendix. Scale bar: 10 µm. Abbreviations: NT Con, NT: non-transfected cells, TR Con, TR: cells treated with TransIT-X2, T17N: dominant-negative RAC1, NLS-T17N: dominant-negative RAC1 with additional NLS, GFP: green fluorescent protein, NS: not significant.

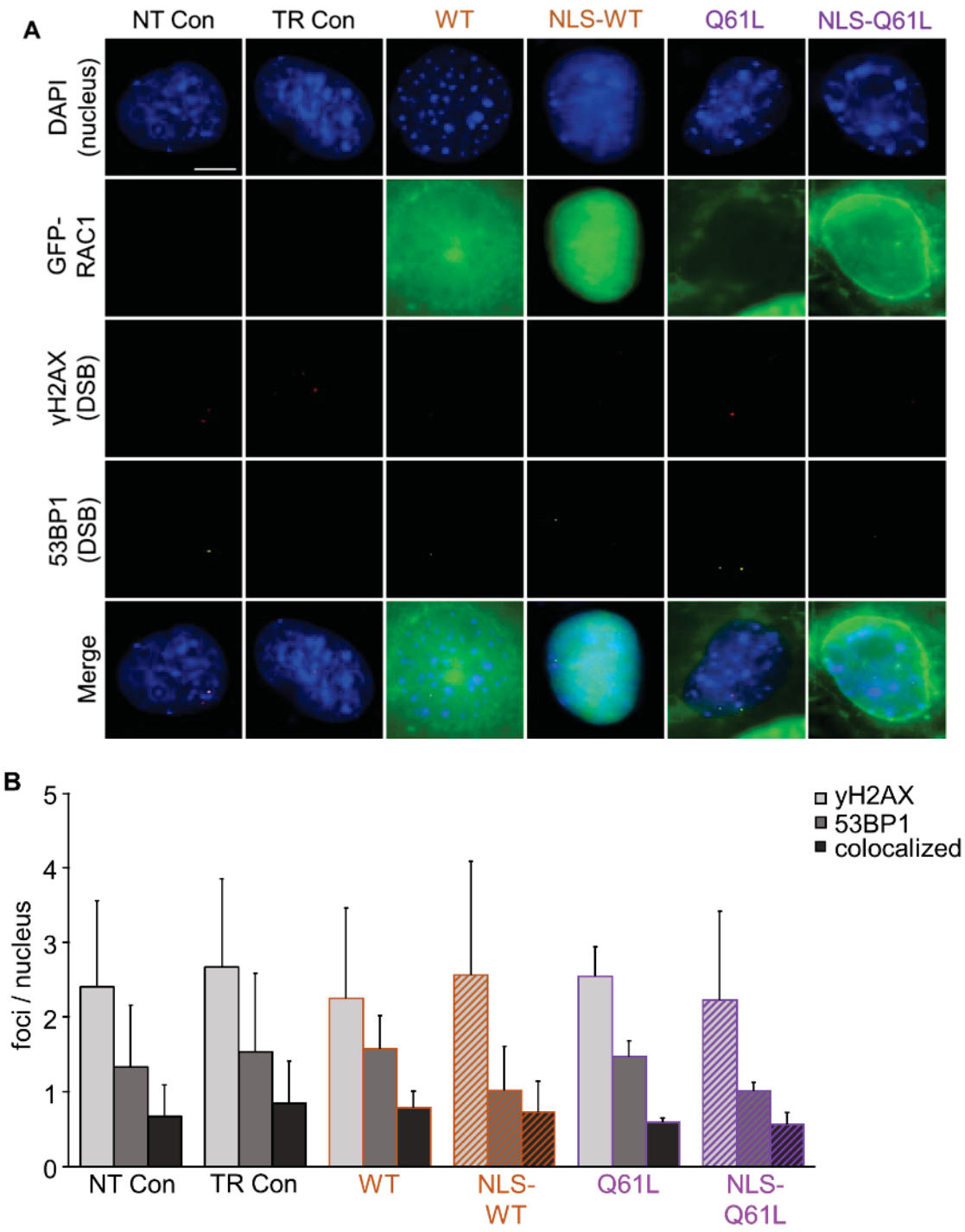

Figure 7.20: Influence of human GFP-RAC1 expression itself on basal γH2AX and 53BP1 foci formation.

MEF were transiently transfected with *GFP-hRAC1(WT)*, *GFP-NLS-hRAC1(WT)*, *GFP-hRAC1(Q61L)*, or *GFP-NLS-hRAC1(Q61L)* expression vector. Transfection control cells (TR Con) were treated with TransIT-X2. Control cells (NT Con) were non-transfected. **A** 24 h after transfection, cells were fixed and staining of γH2AX and 53BP1 foci was carried out as described in methods. Representative microscopical fluorescence pictures are shown; blue: DAPI-stained nuclei, green: GFP signal, red: γH2AX (Ser139), yellow: 53BP1. Scale bar: 10 µm. **B** Quantification of γH2AX and 53BP1 foci counts, as well as colocalization of these foci. Foci of each cell were counted (mean+SD; n=3 - 25 with 50 nuclei counted per experiment). The data underlying the graph are shown in Table 7.54 of the appendix. Abbreviations: NT Con: non-

transfected cells, TR Con: cells treated with transfection reagent (TransIT-X2), WT: wild-type RAC1, NLS-WT: wild-type RAC1 with additional NLS, Q61L: constitutively active RAC1, NLS-Q61L: constitutively active RAC1 with additional NLS.

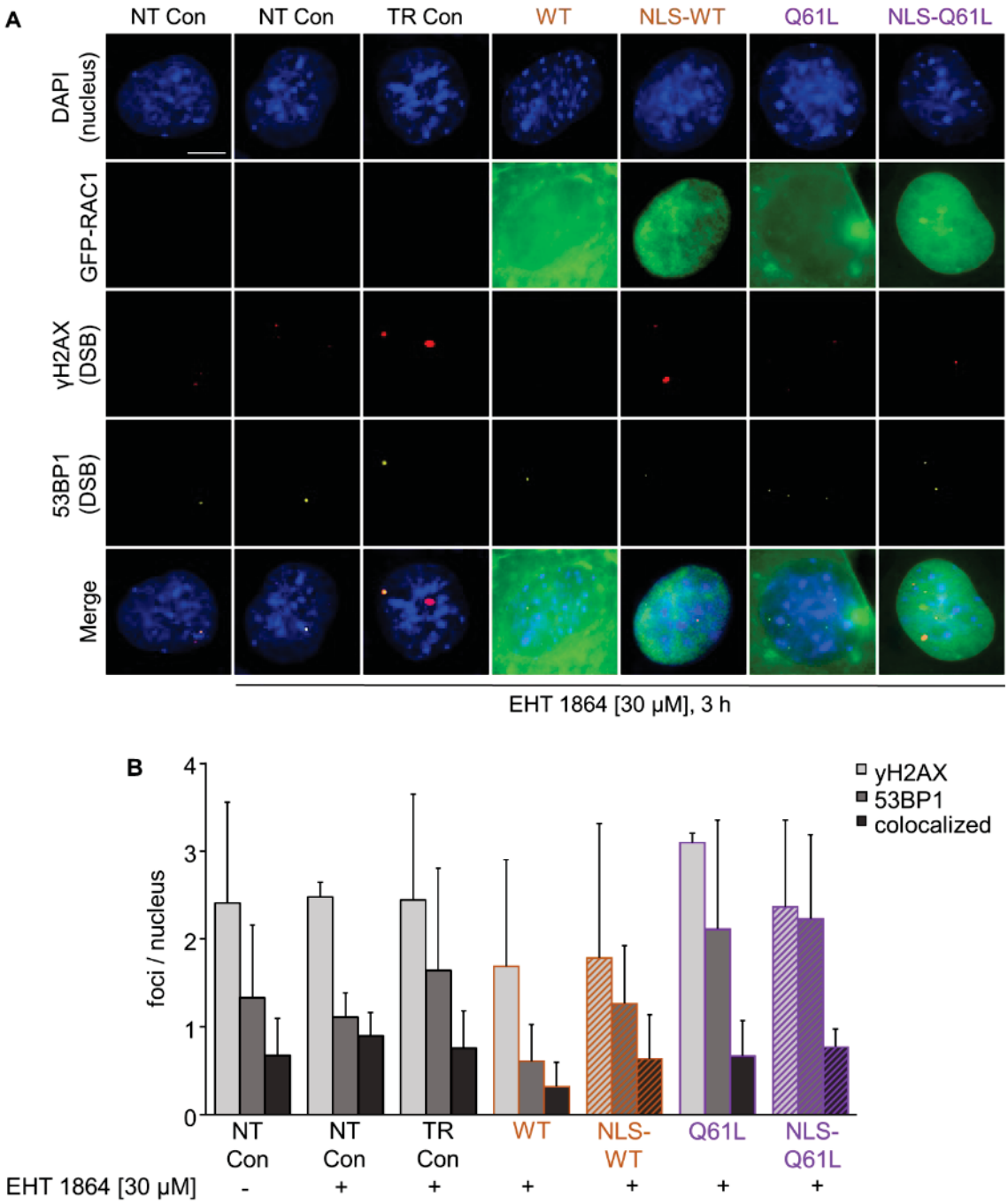

Figure 7.21: Influence of EHT 1864 treatment on basal γH2AX and 53BP1 foci formation. MEF were transiently transfected with *GFP-hRAC1(WT)*, *GFP-NLS-hRAC1(WT)*, *GFP-hRAC1(Q61L)*, or *GFP-NLS-hRAC1(Q61L)* expression vector. Transfection control cells (TR Con) were treated with TransIT-X2. Control cells (NT Con) were non-transfected. 24 h after transfection cells were treated with 30 µM EHT 1864 for 3 h. **A** 24 h after transfection, cells were fixed and staining of γH2AX and 53BP1 foci was carried out as described in methods. Representative microscopical fluorescence pictures are shown; blue: DAPI-stained nuclei, green: GFP signal, red: γH2AX (Ser139), yellow: 53BP1. Scale bar: 10 µm. **B** Quantification of γH2AX and 53BP1 foci formation, as well as colocalization of these foci. Foci of each cell were counted

(mean+SD; n=3 - 23 with 50 nuclei counted per experiment). The data underlying the graph are shown in Table 7.55 of the appendix. Abbreviations: NT Con: non-transfected cells, TR Con: cells treated with TransIT-X2, WT: wild-type RAC1, NLS-WT: wild-type RAC1 with additional NLS, Q61L: constitutively active RAC1, NLS-Q61L: constitutively active RAC1 with additional NLS.

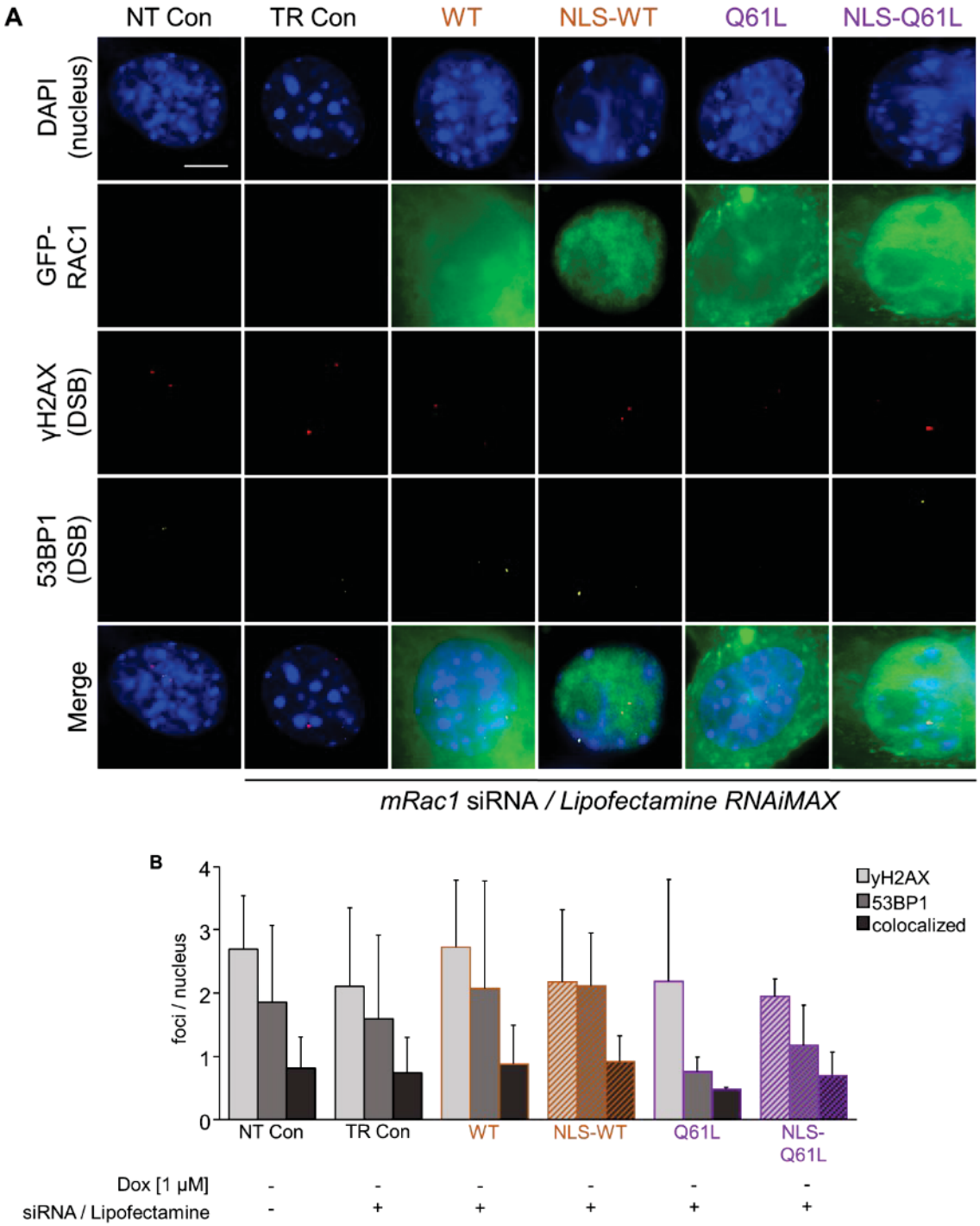

Figure 7.22: Influence of single and double transfection on basal γH2AX and 53BP1 foci formation.
mRac1 knockdown was achieved by transfection with *mRac1* siRNA. The treatment scheme is shown in material and methods (Figure 2.1 E, F). Cells were co-transfected with *GFP-hRAC1(WT)*, *GFP-NLS-hRAC1(WT)*, *GFP-hRAC1(Q61L)*, or *GFP-NLS-hRAC1(Q61L)*

expression vector. **A** 48 h after treatment with Lipofectamine RNAiMAX, cells were fixed and staining of γH2AX and 53BP1 foci was carried out as described in methods. Representative microscopical fluorescence pictures are shown; blue: DAPI-stained nuclei, green: GFP signal, red: γH2AX (Ser139), yellow: 53BP1. **B** Quantification of γH2AX and 53BP1 foci formation, as well as colocalization of these foci. Foci of each cell were counted (mean+SD; n=2 - 20 with 50 nuclei counted per experiment). The data underlying the graph are shown in Table 7.56 of the appendix. Scale bar: 10 µm. Abbreviations: NT Con: non-transfected cells, TR Con: cells treated with Lipofectamine RNAiMAX and TransIT-X2, WT: wild-type RAC1, NLS-WT: wild-type RAC1 with additional NLS, Q61L: constitutively active RAC1, NLS-Q61L: constitutively active RAC1 with additional NLS.

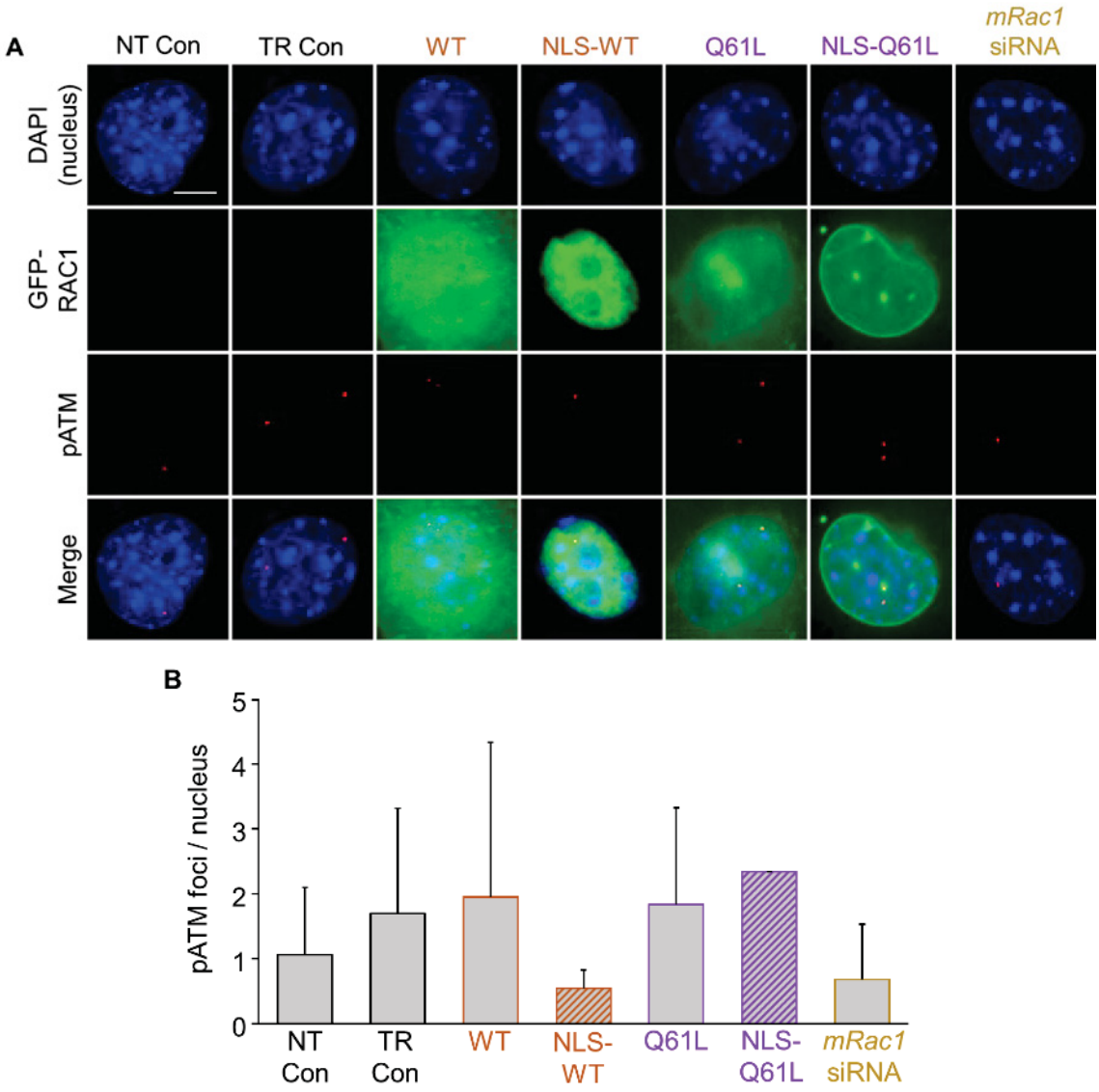

Figure 7.23: Influence of the transfection methods on basal pATM foci formation.
Cells were transiently transfected with *GFP-hRAC1(WT)*, *GFP-NLS-hRAC1(WT)*, *GFP-hRAC1(Q61L)*, or *GFP-NLS-hRAC1(Q61L)* expression vector or *mRac1* siRNA. Transfection control cells (TR Con) were treated with TransIT-X2. Control cells (NT Con) were non-transfected. **A** 24 h after transfection with *GFP-hRAC1* expression vectors or 48 h after transfection with *mRac1* siRNA cells were fixed and staining of pATM foci was carried out as described in methods. Representative microscopical fluorescence pictures are shown; blue: DAPI-stained nuclei, green: GFP signal, red: pATM. **B** Quantification of pATM foci formation. Foci

of each cell were counted (mean+SD; n=1 - 18 with 50 nuclei counted per experiment). The data underlying the graph are shown in Table 7.57 of the appendix. Scale bar: 10 µm. Abbreviations: NT Con, NT: non-transfected cells, TR Con, TR: cells treated with TransIT-X2, WT: wild-type RAC1, NLS-WT: wild-type RAC1 with additional NLS, Q61L: constitutively active RAC1, NLS-Q61L: constitutively active RAC1 with additional NLS, *mRac1* siRNA: siRNA against murine *Rac1*.

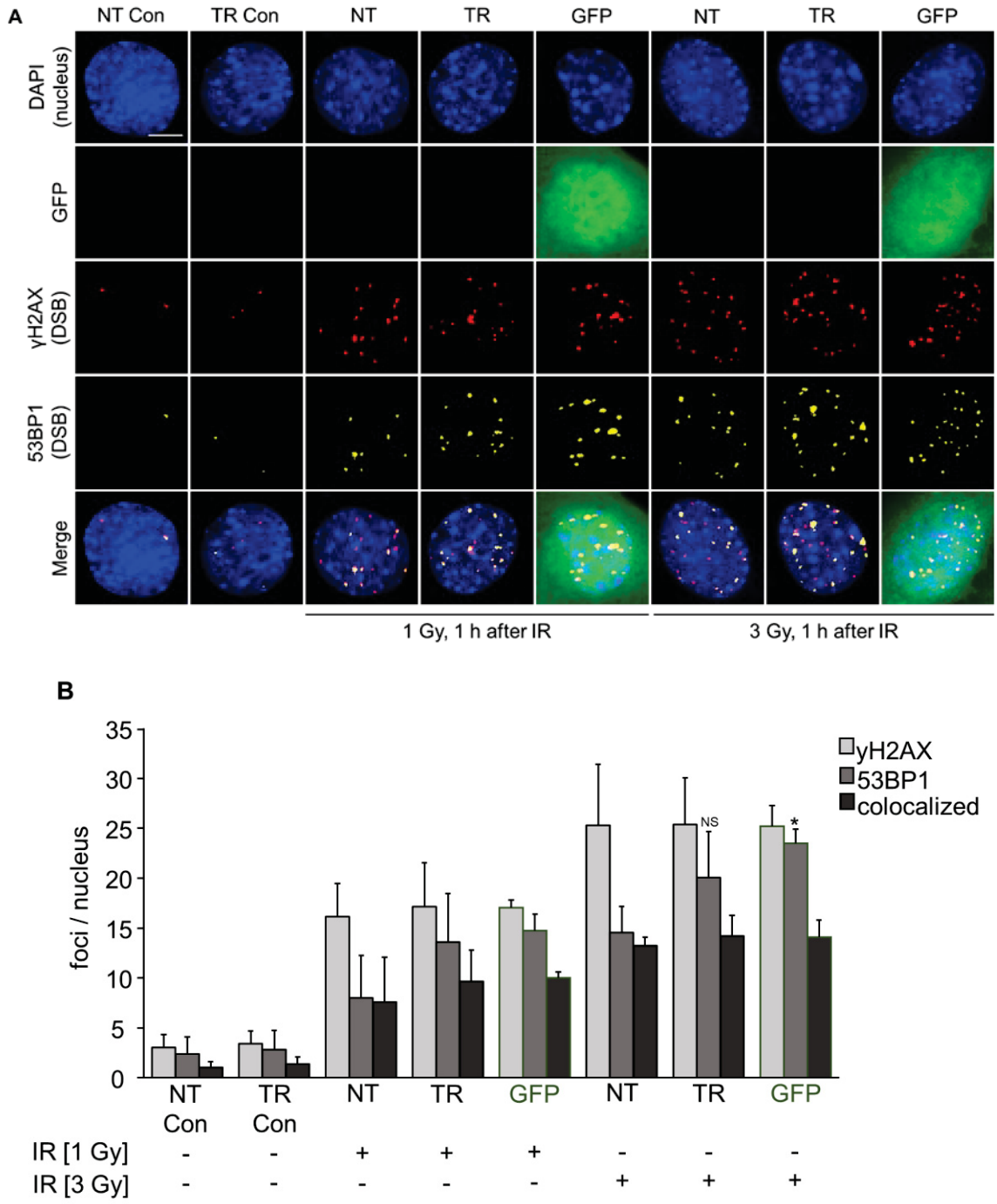

Figure 7.24: Influence of GFP as part of the plasmids on IR-induced foci formation.
Cells were transiently transfected with *GFP* expression vector. Transfection control cells (TR Con, TR) were treated with TransIT-X2. Control cells (NT Con, NT) were non-transfected. Cells were irradiated with 1 Gy or 3 Gy. 1 h after treatment with IR, cells were fixed and staining of γH2AX and 53BP1 foci was carried out as described in methods. **A** Representative microscopical

fluorescence pictures are shown; blue: DAPI-stained nuclei, green: GFP signal, red: γH2AX (Ser139), yellow: 53BP1. Scale bar: 10 µm. **B** Quantification of γH2AX and 53BP1 foci formation, as well as colocalization of these foci. Foci of each nucleus were counted (mean+SD; n=3 - 24 with 50 nuclei counted per experiment; *p ≤ 0.05 compared to IR [3 Gy] treated cells (TR), one-way ANOVA with Dunnett post-hoc test). The data underlying the graph are shown in Table 7.58 of the appendix. Abbreviations: NT Con, NT: non-transfected cells, TR Con, TR: cells treated with transfection reagent (TransIT-X2), GFP: green fluorescent protein, NS: not significant.

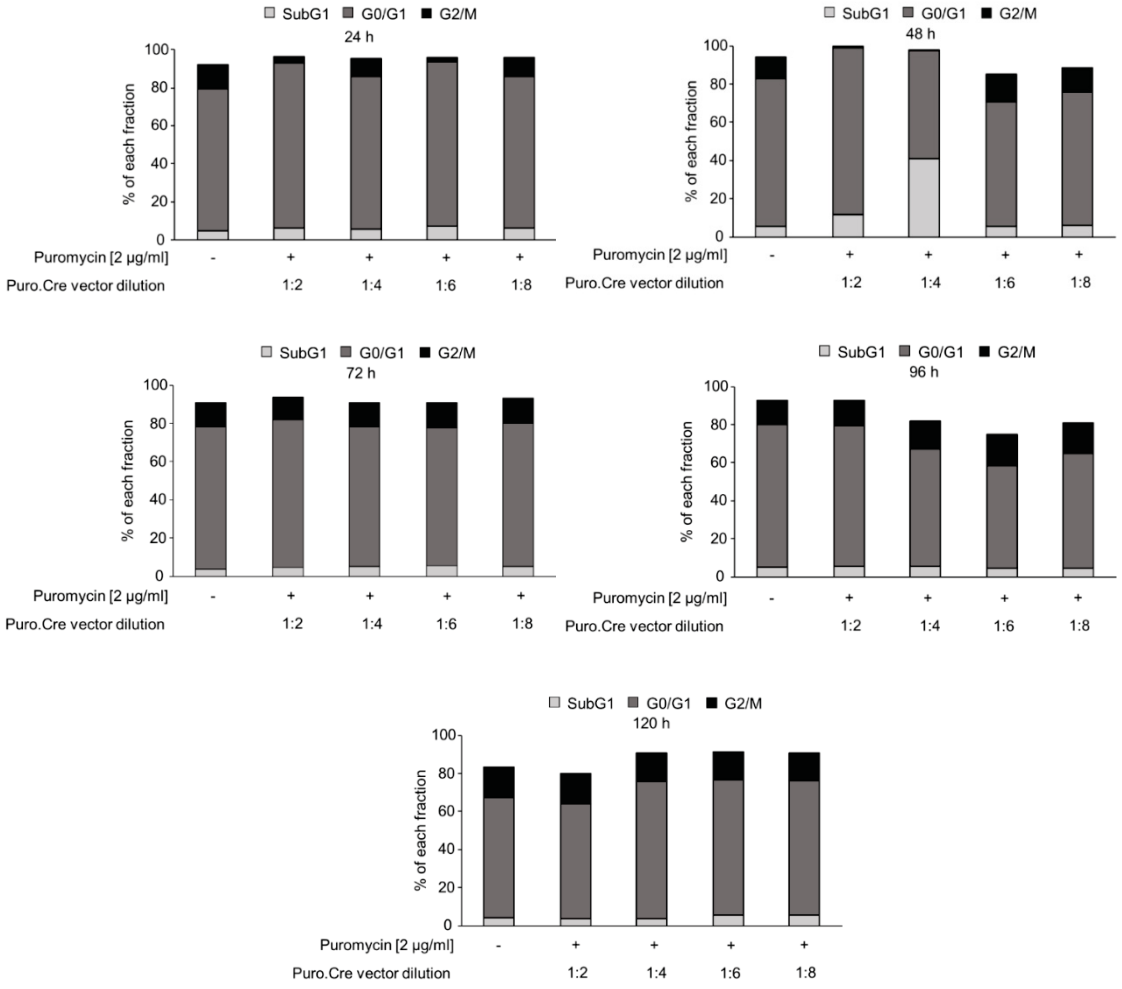

Figure 7.25: Flow cytometric analysis of cell cycle distribution and apoptosis after lentiviral transduction with diluted Puro.Cre vector in mouse embryonic fibroblasts without loxP sites (*Rac1*$^{wt/wt}$).
Cells were transduced with different dilutions of Puro.Cre vector and 24 h later treatment with puromycin was started. Cells were analyzed 24 h, 48 h, 72 h, 96 h, and 120 h after puromycin selection. Cells were lysed and the nuclei were stained with the DNA-intercalating agent propidium iodide. The cell cycle distribution was determined using a flow cytometer. Control cells (*Rac1*$^{wt/wt}$) were non-transduced. Shown is the evaluation of the different fractions (n=1). The data underlying the graph are shown in Table 7.59 of the appendix. Abbreviations: SubG1: apoptotic cell fraction, G0/G1: fraction of cells in state of quiescence/growth phase, G2/M: fraction of cells in growth phase (preparation for mitosis)/mitosis.

7.2 List of dates underlying the graphs

Table 7.1: Data from fluorescence-based quantification of doxorubicin-induced DNA double-strand breaks (γH2AX foci).
MEF were treated with 0 µM, 0.1 µM, 0.3 µM, 1 µM, or 3 µM Dox for 1 h. Pictures were taken after the end of the Dox treatment. The mean values on which Figure 3.2 B is based on are listed in the Table (n=3 with 50 nuclei counted per experiment*).*

doxorubicin [µM]	foci/nucleus mean ± SD	p value
0	4.62 ± 0.71	
0.1	6.42 ± 0.97	0.9725
0.3	9.67 ± 1.21	0.5469
1	17.31 ± 6.35	0.0305
3	29.22 ± 8.67	0.0004

Table 7.2: Data from western blot analysis of representative DDR-related proteins after doxorubicin treatment.
MEF were 2 h pulse-treated with 0 µM, 0.1 µM, 0.3 µM, 1 µM, or 3 µM Dox. Cells were harvested after the indicated time points. Afterwards, cells were lysed, and protein extracts were analyzed by western blot analysis as described in methods. The fluorescence intensities of the proteins were determined with ImageLab. 1 µM Dox treatment was set to 1. The mean values on which Figure 3.3 B is based on are listed in the Table (n=3).

pKAP1 0 h	Experiment 1 Protein normalized	Experiment 2 Protein normalized	Experiment 3 Protein normalized	mean ± SD	p value
0 µM Dox	0.12	0.00	0.12	0.08 ± 0.07	
0.1 µM Dox	0.27	0.01	0.14	0.11 ± 0.08	0.9908
0.3 µM Dox	0.87	0.40	0.36	0.51 ± 0.22	0.0025
1 µM Dox	1.00	1.00	1.00	1.00 ± 0.00	<0.0001
3 µM Dox	0.99	0.94	0.96	0.96 ± 0.03	<0.0001
pKAP1 4 h	Experiment 1 Protein normalized	Experiment 2 Protein normalized	Experiment 3 Protein normalized	mean ± SD	p value
0 µM Dox	0.13	0.00	0.06	0.09 ± 0.05	
0.1 µM Dox	0.41	0.08	0.11	0.20 ± 0.18	0.9977
0.3 µM Dox	0.87	0.61	0.36	0.69 ± 0.38	0.5735
1 µM Dox	1.00	1.00	1.00	1.00 ± 0.00	0.2558
3 µM Dox	2.66	1.47	0.58	1.57 ± 1.05	0.0434
pKAP1 24 h	Experiment 1 Protein normalized	Experiment 2 Protein normalized	Experiment 3 Protein normalized	mean ± SD	p value
0 µM Dox	0.62	0.04	0.47	0.38 ± 0.30	
0.1 µM Dox	0.62	0.04	0.57	0.41 ± 0.32	0.9999
0.3 µM Dox	1.34	0.24	1.25	0.94 ± 0.61	0.3919
1 µM Dox	1.00	1.00	1.00	1.00 ± 0.00	0.3135
3 µM Dox	0.47	1.76	0.98	1.07 ± 0.65	0.2378

γH2AX 0 h	Experiment 1 Protein normalized	Experiment 2 Protein normalized	Experiment 3 Protein normalized	mean ± SD	p value
0 µM Dox	0.53	0.38	0.52	0.48 ± 0.09	
0.1 µM Dox	0.35	0.31	0.38	0.35 ± 0.03	0.8346
0.3 µM Dox	0.32	0.92	0.76	0.66 ± 0.31	0.6446
1 µM Dox	1.00	1.00	1.00	1.00 ± 0.00	0.0290
3 µM Dox	1.80	1.26	1.74	1.60 ± 0.30	0.0002
γH2AX 4 h	Experiment 1 Protein normalized	Experiment 2 Protein normalized	Experiment 3 Protein normalized	mean ± SD	p value
0 µM Dox	0.24	0.00	0.25	0.25 ± 0.01	
0.1 µM Dox	0.84	1.01	0.21	0.69 ± 0.42	0.9753
0.3 µM Dox	1.14	0.72	0.22	0.69 ± 0.46	0.9753
1 µM Dox	1.00	1.00	1.00	1.00 ± 0.00	0.8656
3 µM Dox	1.54	5.21	1.13	2.62 ± 2.25	0.1241
γH2AX 24 h	Experiment 1 Protein normalized	Experiment 2 Protein normalized	Experiment 3 Protein normalized	mean ± SD	p value
0 µM Dox	1.39	1.02	0.93	1.11 ± 0.24	
0.1 µM Dox	1.07	1.18	1.18	1.14 ± 0.06	0.9982
0.3 µM Dox	0.73	0.91	0.80	0.82 ± 0.09	0.1860
1 µM Dox	1.00	1.00	1.00	1.00 ± 0.00	0.8466
3 µM Dox	1.51	1.53	1.03	1.36 ± 0.28	0.2831
pP53 0 h	Experiment 1 Protein normalized	Experiment 2 Protein normalized	Experiment 3 Protein normalized	mean ± SD	p value
0 µM Dox	0.05	0.00	0.41	0.16 ± 0.23	
0.1 µM Dox	0.14	0.28	0.10	0.17 ± 0.09	>0.9999
0.3 µM Dox	0.45	0.68	0.61	0.58 ± 0.12	0.0554
1 µM Dox	1.00	1.00	1.00	1.00 ± 0.00	0.0007
3 µM Dox	1.64	1.25	1.84	1.57 ± 0.30	<0.0001
pP53 4 h	Experiment 1 Protein normalized	Experiment 2 Protein normalized	Experiment 3 Protein normalized	mean ± SD	p value
0 µM Dox	0.01	0.00	0.30	0.16 ± 0.21	
0.1 µM Dox	0.20	0.00	0.16	0.12 ± 0.11	0.9843
0.3 µM Dox	0.57	0.28	0.44	0.43 ± 0.15	0.0858
1 µM Dox	1.00	1.00	1.00	1.00 ± 0.00	<0.0001
3 µM Dox	1.50	1.53	1.57	1.53 ± 0.04	<0.0001
pP53 24 h	Experiment 1 Protein normalized	Experiment 2 Protein normalized	Experiment 3 Protein normalized	mean ± SD	p value
0 µM Dox	0.15	0.00	0.10	0.08 ± 0.07	
0.1 µM Dox	0.34	0.12	0.22	0.23 ± 0.11	0.9781
0.3 µM Dox	0.37	0.44	0.08	0.30 ± 0.19	0.9216
1 µM Dox	1.00	1.00	1.00	1.00 ± 0.00	0.0798
3 µM Dox	3.50	1.97	1.80	2.42 ± 0.94	0.0002

Table 7.3: Data from western blot analysis of doxorubicin-induced P53 and H2AX phosphorylation after pre-treatment with EHT 1864.
MEF were pre-treated for 1 h with 10 µM EHT 1864 and afterwards treated with 1 µM Dox for 2 h. Cells were harvested after the end of the Dox treatment. Afterwards cells were lysed, and protein extracts were analyzed by western blot analysis as described in methods. The fluorescence intensities of the proteins were determined with ImageLab. 1 µM Dox treatment was set to 1. The mean values on which Figure 3.4 B is based on are listed in the Table (n=3).

pP53 0 h	Experiment 1 Protein normalized	Experiment 2 Protein normalized	Experiment 3 Protein normalized	mean ± SD	p value
Con	0.00	0.00	0.10	0.03 ± 0.05	
EHT 1864 [10µM]	0.00	0.00	0.05	0.02 ± 0.03	
Dox [1µM]	1.00	1.00	1.00	1.00 ± 0.00	
EHT 1864 [10µM] + Dox [1µM]	0.77	5.17	2.27	2.24 ± 2.54	0.5243
γH2AX 0 h	Experiment 1 Protein normalized	Experiment 2 Protein normalized	Experiment 3 Protein normalized	mean ± SD	p value
Con	0.04	0.00	0.00	0.01 ± 0.02	
EHT 1864 [10µM]	0.21	0.00	0.00	0.07 ± 0.12	
Dox [1µM]	1.00	1.00	1.00	1.00 ± 0.00	
EHT 1864 [10µM] + Dox [1µM]	0.81	1.06	2.27	1.38 ± 0.78	0.5339

Table 7.4: Data from fluorescence-based quantification of doxorubicin-induced DNA double-strand breaks (γH2AX foci) after pre-treatment with EHT 1864.
MEF were pre-treated for 3 h with different doses of EHT 1864 [10 µM, 30 µM, or 100 µM] and afterwards treated for 1 h with 1 µM Dox. Pictures were taken after the end of the Dox treatment. The mean values on which Figure 3.5 B is based on are listed in the Table (n=1 with 50 nuclei counted).

	foci/nucleus mean
Con	6.56
EHT 1864 [100µM]	5.74
Dox [1µM]	17.88
EHT 1864 [10µM] + Dox [1µM]	10.74
EHT 1864 [30µM] + Dox [1µM]	12.88
EHT 1864 [100µM] + Dox [1µM]	12.18

Table 7.5: Data from western blot analysis of doxorubicin-induced representative DDR-related proteins after pre-treatment with EHT 1864.
MEF were pre-treated for 3 h with different doses of EHT 1864 [10 µM, 30 µM, or 100 µM] and afterwards treated with 1 µM Dox for 2 h. Cells were harvested after the end of the Dox treatment. Afterwards cells were lysed, and protein extracts were analyzed by western blot analysis as described in methods. The fluorescence intensities of the proteins were determined with ImageLab. 1 µM Dox treatment was set to 1. The mean values on which Figure 3.5 D is based on are listed in the Table (n=3).

pCHK1	Experiment 1 Protein normalized	Experiment 2 Protein normalized	Experiment 3 Protein normalized	mean ± SD	p value
Con	0.00	0.00	0.00	0.00 ± 0.00	
EHT 1864 [100µM]	0.00	0.00	0.00	0.00 ± 0.00	<0.0001
Dox [1µM]	1.00	1.00	1.00	1.00 ± 0.00	
EHT 1864 [10µM] + Dox [1µM]	0.45	0.43	0.03	0.30 ± 0.24	<0.0001
EHT 1864 [30µM] + Dox [1µM]	0.38	0.35	0.12	0.28 ± 0.14	<0.0001
EHT 1864 [100µM] + Dox [1µM]	0.18	0.16	0.17	0.17 ± 0.01	<0.0001
pP53	Experiment 1 Protein normalized	Experiment 2 Protein normalized	Experiment 3 Protein normalized	mean ± SD	p value
Con	0.00	0.00	0.00	0.00 ± 0.00	
EHT 1864 [100µM]	0.00	0.00	0.00	0.00 ± 0.00	0.0014
Dox [1µM]	1.00	1.00	1.00	1.00 ± 0.00	
EHT 1864 [10µM] + Dox [1µM]	0.03	0.02	0.75	0.27 ± 0.42	0.0136
EHT 1864 [30µM] + Dox [1µM]	0.01	0.01	0.75	0.26 ± 0.43	0.0124
EHT 1864 [100µM] + Dox [1µM]	0.00	0.00	0.05	0.02 ± 0.03	0.0016
γH2AX	Experiment 1 Protein normalized	Experiment 2 Protein normalized	Experiment 3 Protein normalized	mean ± SD	p value
Con	0.00	0.00	0.00	0.00 ± 0.00	
EHT 1864 [100µM]	0.00	0.00	0.00	0.00 ± 0.00	<0.0001
Dox [1µM]	1.00	1.00	1.00	1.00 ± 0.00	
EHT 1864 [10µM] + Dox [1µM]	0.83	1.04	0.67	0.85 ± 0.18	0.6404
EHT 1864 [30µM] + Dox [1µM]	0.78	0.90	0.29	0.66 ± 0.32	0.0661
EHT 1864 [100µM] + Dox [1µM]	0.35	0.36	0.25	0.32 ± 0.06	0.0006

pKAP1	Experiment 1 Protein normalized	Experiment 2 Protein normalized	Experiment 3 Protein normalized	mean ± SD	p value
Con	0.00	0.00	0.00	0.00 ± 0.00	
EHT 1864 [100µM]	0.00	0.00	0.35	0.12 ± 0.20	0.0020
Dox [1µM]	1.00	1.00	1.00	1.00 ± 0.00	
EHT 1864 [10µM] + Dox [1µM]	0.98	1.04	0.20	0.74 ± 0.47	0.6235
EHT 1864 [30µM] + Dox [1µM]	0.96	0.94	0.32	0.47 ± 0.36	0.6235
EHT 1864 [100µM] + Dox [1µM]	0.17	0.23	0.35	0.25 ± 0.09	0.0155

Table 7.6: Data from fluorescence-based quantification of doxorubicin-induced DNA double-strand breaks (γH2AX foci) after pre-treatment with EHT 1864.
MEF were pre-treated for 3 h with a single dose of EHT 1864 [30 µM] and afterwards treated with 1 µM Dox for 1 h. Pictures were taken after the end of the Dox treatment. The mean values on which Figure 3.6 B is based on are listed in the Table (n=6 with 50 nuclei counted per experiment).

	foci/nucleus mean ± SD	p value
Con	4.32 ± 1.73	
EHT 1864 [30µM]	4.52 ± 0.55	
Dox [1µM]	19.44 ± 3.08	
EHT 1864 [30µM] + Dox [1µM]	13.54 ± 1.64	0.0001

Table 7.7: Data from fluorescence-based quantification of intrinsic mRAC1 as well as GFP-hRAC1 distribution in cells expressing human GFP-RAC1 with and without additional NLS.
MEF were transiently transfected with *GFP-hRAC1(WT)*, *GFP-NLS-hRAC1(WT)*, *GFP-hRAC1(Q61L)*, *GFP-NLS-hRAC1(Q61L)*, *GFP-hRAC1(T17N), or GFP-NLS-hRAC1(T17N)* expression vector. Transfection control cells (TR Con) were treated with TransIT-X2. The mean values on which Figure 3.7 B is based on are listed in the Table (n=3 with 50 cells counted per experiment). Abbreviations: TR Con: control cells treated with transfection reagent (TransIT-X2), WT: wild-type RAC1, NLS-WT: wild-type RAC1 with additional NLS, Q61L: constitutively active RAC1, NLS-Q61L: constitutively active RAC1 with additional NLS, T17N: dominant-negative RAC1, NLS-T17N: dominant-negative RAC1 with additional NLS.

	nucleus [%] mean ± SD	cytoplasm [%] mean ± SD	p value nucleus vs TR Con (*) / GFP-hRAC1 (#)	p value cytoplasm vs TR Con (*) / GFP-hRAC1 (#)
TR Con	18.92 ± 1.54	81.08 ± 1.54		
WT	30.84 ± 2.56	69.16 ± 2.56	(*) 0.0192	(*) 0.0192
NLS-WT	86.53 ± 1.80	13.47 ± 1.80	(*) <0.0001 / (#) <0.0001	(*) <0.0001 / (#) <0.0001
Q61L	18.94 ± 0.96	81.06 ± 0.96	(*) >0.9999	(*) >0.9999
NLS-Q61L	37.03 ± 8.65	62.97 ± 8.65	(*) 0.0007 / (#) 0.0228	(*) 0.0007 / (#) 0.0228
T17N	18.25 ± 1.66	81.75 ± 1.66	(*) 0.9997	(*) 0.9997
NLS-T17N	36.16 ± 6.06	63.84 ± 6.06	(*) 0.0011 / (#) 0.0078	(*) 0.0011 / (#) 0.0078

Table 7.8: Data from influence of the different human *GFP-RAC1* mutants (with and without additional NLS) on the lamellipodia formation.
MEF were transiently transfected with *GFP-hRAC1(WT)*, *GFP-NLS-hRAC1(WT)*, *GFP-hRAC1(Q61L)*, *GFP-NLS-hRAC1(Q61L)*, *GFP-hRAC1(T17N)*, or *GFP-NLS-hRAC1(T17N)* expression vector. Transfection control cells were treated with TransIT-X2 (TR Con). 24 h after transfection, cells were stained with phalloidin-TRITC. The mean values on which Figure 3.9 B is based on are listed in the Table (n=3 with 50 cells counted per experiment). Abbreviations: TR Con: control cells treated with transfection reagent (TransIT-X2), WT: wild-type RAC1, NLS-WT: wild-type RAC1 with additional NLS, Q61L: constitutively active RAC1, NLS-Q61L: constitutively active RAC1 with additional NLS, T17N: dominant-negative RAC1, NLS-T17N: dominant-negative RAC1 with additional NLS.

	lamellipodia mean ± SD	p value vs TR Con (*) / GFP-hRAC1 (#)
TR Con	2.82 ± 0.81	
WT	2.14 ± 0.97	(*) 0.6515
NLS-WT	2.81 ± 0.97	(*) >0.9999 / (#) 0.4452
Q61L	5.59 ± 0.98	(*) <0.0001
NLS-Q61L	4.95 ± 0.49	(*) 0.0006 / (#) 0.3689
T17N	1.92 ± 0.62	(*) 0.3477
NLS-T17N	2.07 ± 0.22	(*) 0.5496 / (#) 0.7131

Table 7.9: Data from influence of the different human *GFP-RAC1* mutants (with and without additional NLS) on the stress fibers formation.
MEF were transiently transfected with *GFP-hRAC1(WT)*, *GFP-NLS-hRAC1(WT)*, *GFP-hRAC1(Q61L)*, *GFP-NLS-hRAC1(Q61L)*, *GFP-hRAC1(T17N)*, or *GFP-NLS-hRAC1(T17N)* expression vector. Transfection control cells (TR Con) were treated with TransIT-X2. 24 h after transfection, cells were stained with phalloidin-TRITC. The mean values on which Figure 3.9 C is based on are listed in the Table (n=3 with 50 cells counted per experiment). Abbreviations: TR Con: control cells treated with transfection reagent (TransIT-X2), WT: wild-type RAC1, NLS-WT: wild-type RAC1 with additional NLS, Q61L: constitutively active RAC1, NLS-Q61L: constitutively active RAC1 with additional NLS, T17N: dominant-negative RAC1, NLS-T17N: dominant-negative RAC1 with additional NLS.

	stress fibers mean ± SD	p value vs TR Con (*) / GFP-hRAC1 (#)
TR Con	2.72 ± 0.17	
WT	2.89 ± 0.23	(*) 0.5769
NLS-WT	2.80 ± 0.30	(*) 0.9771 / (#) 0.7012
Q61L	2.17 ± 0.17	(*) 0.0001
NLS-Q61L	2.46 ± 0.18	(*) 0.1484 / (#) 0.1124
T17N	3.06 ± 0.17	(*) 0.0283
NLS-T17N	2.67 ± 0.18	(*) 0.9979 / (#) 0.05

Table 7.10: Data from influence of the different human *GFP-RAC1* mutants (with and without additional NLS) on the membrane ruffles formation.
MEF were transiently transfected with *GFP-hRAC1(WT)*, *GFP-NLS-hRAC1(WT)*, *GFP-hRAC1(Q61L)*, *GFP-NLS-hRAC1(Q61L)*, *GFP-hRAC1(T17N)*, or *GFP-NLS-hRAC1(T17N)* expression vector. Transfection control cells (TR Con) were treated with TransIT-X2. 24 h after transfection, cells were stained with phalloidin-TRITC. The mean values on which Figure 3.9 D is based on are listed in the Table (n=3 with 50 cells counted per experiment). Abbreviations: TR Con: control cells treated with transfection reagent (TransIT-X2), WT: wild-type RAC1, NLS-WT: wild-type RAC1 with additional NLS, Q61L: constitutively active RAC1, NLS-Q61L: constitutively active RAC1 with additional NLS, T17N: dominant-negative RAC1, NLS-T17N: dominant-negative RAC1 with additional NLS.

	membrane ruffles [%] mean ± SD	p value vs TR Con (*) / GFP-hRAC1 (#)
TR Con	96.42 ± 3.28	
WT	96.00 ± 6.93	(*) 0.9998
NLS-WT	93.33 ± 11.55	(*) 0.8310 / (#) 0.7486
Q61L	90.67 ± 4.16	(*) 0.2288
NLS-Q61L	90.00 ± 0.55	(*) 0.1402 / (#) 0.7958
T17N	92.00 ± 5.29	(*) 0.5078
NLS-T17N	92.67 ± 2.31	(*) 0.6789 / (#) 0.8505

Table 7.11: Data from influence of mainly cytosolic and targeted nuclear expression of dominant-negative hRAC1 on doxorubicin-induced γH2AX and 53BP1 foci formation.
MEF were transiently transfected with *GFP-hRAC1(T17N)* or *GFP-NLS-hRAC1(T17N)* expression vector. Transfection control cells (TR Con, TR) were treated with TransIT-X2. 24 h after transfection cells were treated with Dox [1 µM] for 1 h. The mean values on which Figure 3.10 B is based on are listed in the Table (n=6 - 38 with 50 nuclei counted per experiment). Abbreviations: TR Con, TR: cells treated with TransIT-X2, T17N: dominant-negative RAC1, NLS-T17N: dominant-negative RAC1 with additional NLS.

	γH2AX foci/nucleus mean ± SD	53BP1 foci/nucleus mean ± SD	colocalization foci/nucleus mean ± SD
TR Con	2.67 ± 1.18	1.53 ± 1.06	0.85 ± 0.57
TR + Dox [1 µM]	12.73 ± 1.84	9.81 ± 3.18	6.97 ± 1.83
T17N + Dox [1 µM]	7.23 ± 1.49	5.72 ± 1.86	4.23 ± 1.32
NLS-T17N + Dox [1 µM]	7.58 ± 1.32	6.38 ± 3.09	3.72 ± 1.27
	p value γH2AX vs TR (*) / GFP-hRAC1 (#)	p value 53BP1 vs TR (*) / GFP-hRAC1 (#)	p value colocalization vs TR (*) / GFP-hRAC1 (#)
T17N + Dox [1 µM]	(*) <0.0001	(*) 0.0076	(*) 0.0015
NLS-T17N + Dox [1 µM]	(*) <0.0001 / (#) 0.6758	(*) 0.0275 / (#) 0.6635	(*) 0.0002 / (#) 0.5107

Table 7.12: Data from western blot analysis after doxorubicin treatment in dominant-negative hRAC1-expressing cells with and without additional NLS.
MEF were transiently transfected with *GFP-hRAC1(T17N)* or *GFP-NLS-hRAC1(T17N)* expression vector. 24 h after transfection cells were 2 h pulse-treated with 1 µM Dox. Cells were harvested after indicated time-points. Afterwards cells were lysed, and protein extracts were analyzed by western blot analysis as described in methods. The fluorescence intensities of the proteins were determined with ImageLab. Non-transfected cells treated with 1 µM Dox were set to 1. The mean values on which Figure 3.11 C - F is based on are listed in the Table (n=3). Abbreviations: NT Con, NT: non-transfected cells, T17N: dominant-negative RAC1, NLS-T17N: dominant-negative RAC1 with additional NLS.

pKAP1 0 h	Experiment 1 Protein normalized	Experiment 2 Protein normalized	Experiment 3 Protein normalized	mean ± SD	p value vs Dox (*) / GFP-hRAC1 + Dox (#)
NT Con	0.00	0.00	0.00	0.00 ± 0.00	
T17N	0.04	0.35	0.04	0.15 ± 0.18	
NLS-T17N	0.00	0.00	0.00	0.00 ± 0.00	
NT + 1 µM Dox	1.00	1.00	1.00	1.00 ± 0.00	
T17N + 1 µM Dox	0.30	0.79	0.53	0.54 ± 0.24	(*) 0.2803
NLS-T17N + 1 µM Dox	0.63	0.30	1.61	0.85 ± 0.68	(*) 0.9575 / (#) 0.4979
pKAP1 4 h	Experiment 1 Protein normalized	Experiment 2 Protein normalized	Experiment 3 Protein normalized	mean ± SD	p value vs Dox (*) / GFP-hRAC1 + Dox (#)
NT Con	0.00	0.00	0.00	0.00 ± 0.00	
T17N	0.05	0.52	0.08	0.22 ± 0.26	
NLS-T17N	0.00	0.00	0.00	0.00 ± 0.00	
NT + 1 µM Dox	1.00	1.00	1.00	1.00 ± 0.00	
T17N + 1 µM Dox	0.61	2.06	0.57	1.08 ± 0.85	(*) 0.9987
NLS-T17N + 1 µM Dox	0.57	1.26	0.93	0.92 ± 0.35	(*) 0.9987 / (#) 0.7781

pKAP1 24 h	Experiment 1 Protein normalized	Experiment 2 Protein normalized	Experiment 3 Protein normalized	mean ± SD	p value vs Dox (*) / GFP-hRAC1 + Dox (#)
NT Con	0.00	0.00	0.00	0.00 ± 0.00	
T17N	0.00	0.47	0.00	0.16 ± 0.27	
NLS-T17N	0.00	0.00	0.00	0.00 ± 0.00	
NT + 1 µM Dox	1.00	1.00	1.00	1.00 ± 0.00	
T17N + 1 µM Dox	0.58	0.20	0.77	0.52 ± 0.29	(*) 0.0137
NLS-T17N + 1 µM Dox	0.00	0.00	0.00	0.00 ± 0.00	(*) <0.0001 / (#) 0.0360
γH2AX 0 h	Experiment 1 Protein normalized	Experiment 2 Protein normalized	Experiment 3 Protein normalized	mean ± SD	p value vs Dox (*) / GFP-hRAC1 + Dox (#)
NT Con	0.59	0.00	0.71	0.43 ± 0.38	
T17N	0.00	0.00	0.34	0.11 ± 0.19	
NLS-T17N	0.00	0.21	0.00	0.07 ± 0.12	
NT + 1 µM Dox	1.00	1.00	1.00	1.00 ± 0.00	
T17N + 1 µM Dox	1.38	1.05	2.69	1.71 ± 0.87	(*) 0.3008
NLS-T17N + 1 µM Dox	0.00	1.08	1.02	0.76 ± 0.66	(*) 0.9559 / (#) 0.2063
NLS-T17N + 1 µM Dox	0.00	1.08	1.02	0.76 ± 0.66	(*) 0.9559 / (#) 0.2063
γH2AX 4 h	Experiment 1 Protein normalized	Experiment 2 Protein normalized	Experiment 3 Protein normalized	mean ± SD	p value vs Dox (*) / GFP-hRAC1 + Dox (#)
NT Con	0.12	0.45	0.00	0.19 ± 0.23	
T17N	0.42	1.06	0.40	0.63 ± 0.37	
NLS-T17N	0.00	0.22	0.00	0.06 ± 0.08	
NT + 1 µM Dox	1.00	1.00	1.00	1.00 ± 0.00	
T17N + 1 µM Dox	0.91	3.45	0.68	1.68 ± 1.54	(*) 0.6267
NLS-T17N + 1 µM Dox	0.94	0.81	0.21	0.65 ± 0.39	(*) 0.9502 / (#) 0.3243

γH2AX 24 h	Experiment 1 Protein normalized	Experiment 2 Protein normalized	Experiment 3 Protein normalized	mean ± SD	p value vs Dox (*) / GFP-hRAC1 + Dox (#)
NT Con	0.00	0.00	0.00	0.00 ± 0.00	
T17N	0.00	0.00	0.00	0.00 ± 0.00	
NLS-T17N	0.48	0.00	0.00	0.16 ± 0.28	
NT + 1 µM Dox	1.00	1.00	1.00	1.00 ± 0.00	
T17N + 1 µM Dox	0.00	0.00	0.00	0.00 ± 0.00	(*) 0.0009
NLS-T17N + 1 µM Dox	1.50	0.53	0.85	0.96 ± 0.50	(*) 0.9997 / (#) 0.0292
pP53 0 h	Experiment 1 Protein normalized	Experiment 2 Protein normalized	Experiment 3 Protein normalized	mean ± SD	p value vs Dox (*) / GFP-hRAC1 + Dox (#)
NT Con	0.00	0.00	0.07	0.04 ± 0.04	
T17N	0.22	0.00	0.23	0.15 ± 0.13	
NLS-T17N	0.00	0.00	0.00	0.00 ± 0.00	
NT + 1 µM Dox	1.00	1.00	1.00	1.00 ± 0.00	
T17N + 1 µM Dox	0.11	0.04	0.22	0.12 ± 0.09	(*) <0.0001
NLS-T17N + 1 µM Dox	1.20	0.91	0.73	0.95 ± 0.23	(*) 0.9746 / (#) 0.0043
pP53 4 h	Experiment 1 Protein normalized	Experiment 2 Protein normalized	Experiment 3 Protein normalized	mean ± SD	p value vs Dox (*) / GFP-hRAC1 + Dox (#)
NT Con	0.00	0.00	0.00	0.00 ± 0.00	
T17N	0.08	0.00	0.09	0.06 ± 0.05	
NLS-T17N	0.69	0.00	0.00	0.23 ± 0.40	
NT + 1 µM Dox	1.00	1.00	1.00	1.00 ± 0.00	
T17N + 1 µM Dox	0.59	0.73	0.69	0.67 ± 0.07	(*) 0.4711
NLS-T17N + 1 µM Dox	1.63	0.58	1.18	1.13 ± 0.53	(*) 0.9634 / (#) 0.2104

pP53 24 h	Experiment 1 Protein normalized	Experiment 2 Protein normalized	Experiment 3 Protein normalized	mean ± SD	p value vs Dox (*) / GFP-hRAC1 + Dox (#)
NT Con	0.00	0.00	0.16	0.05 ± 0.09	
T17N	0.00	0.00	0.28	0.09 ± 0.16	
NLS-T17N	0.00	0.00	0.00	0.00 ± 0.00	
NT + 1 µM Dox	1.00	1.00	1.00	1.00 ± 0.00	
T17N + 1 µM Dox	0.40	0.07	0.37	0.28 ± 0.18	(*) 0.0002
NLS-T17N + 1 µM Dox	0.39	0.00	0.00	0.13 ± 0.23	(*) <0.0001 / (#) 0.4240
mRAC1 0 h	Experiment 1 Protein normalized	Experiment 2 Protein normalized	Experiment 3 Protein normalized	mean ± SD	p value vs Dox (*) / GFP-hRAC1 + Dox (#)
NT Con	1.78	0.63	1.01	1.14 ± 0.59	(*) 0.9977
T17N	0.62	1.53	1.32	1.16 ± 0.48	(*) 0.9960
NLS-T17N	0.77	0.80	1.59	1.05 ± 0.46	(*) 0.9999 / (#) 0.7887
NT + 1 µM Dox	1.00	1.00	1.00	1.00 ± 0.00	
T17N + 1 µM Dox	0.52	2.05	2.19	1.58 ± 0.93	(*) 0.6092
NLS-T17N + 1 µM Dox	0.61	0.98	1.62	1.07 ± 0.51	(*) 0.9998 / (#) 0.4518
mRAC1 4 h	Experiment 1 Protein normalized	Experiment 2 Protein normalized	Experiment 3 Protein normalized	mean ± SD	p value vs Dox (*) / GFP-hRAC1 + Dox (#)
NT Con	0.84	2.02	0.97	1.27 ± 0.64	(*) 0.9710
T17N	0.69	1.27	0.21	0.72 ± 0.53	(*) 0.9665
NLS-T17N	0.81	1.80	1.02	1.21 ± 0.52	(*) 0.9900 / (#) 0.3168
NT + 1 µM Dox	1.00	1.00	1.00	1.00 ± 0.00	
T17N + 1 µM Dox	0.29	1.50	1.12	0.97 ± 0.62	(*) >0.9999
NLS-T17N + 1 µM Dox	0.30	0.94	2.10	1.11 ± 0.91	(*) 0.9997 / (#) 0.8365

mRAC1 24 h	Experiment 1 Protein normalized	Experiment 2 Protein normalized	Experiment 3 Protein normalized	mean ± SD	p value vs Dox (*) / GFP-hRAC1 + Dox (#)
NT Con	1.02	0.59	1.32	0.98 ± 0.37	(*) >0.9999
T17N	0.49	1.43	1.61	1.18 ± 0.60	(*) 0.9975
NLS-T17N	0.62	0.71	1.06	0.80 ± 0.23	(*) 0.9961 / (#) 0.3636
NT + 1 µM Dox	1.00	1.00	1.00	1.00 ± 0.00	
T17N + 1 µM Dox	0.50	0.35	3.17	1.34 ± 1.59	(*) 0.9639
NLS-T17N + 1 µM Dox	0.47	0.64	0.62	0.58 ± 0.09	(*) 0.9204 / (#) 0.4549

Table 7.13: Data from influence of pharmacological RAC1 inhibition on doxorubicin-induced foci formation in cells expressing GFP-hRAC1(T17N) GFP-NLS-hRAC1(T17N).
MEF were transiently transfected with *GFP-hRAC1(T17N)* or *GFP-NLS-hRAC1(T17N)* expression vector. Transfection control cells (TR Con, TR) were treated with TransIT-X2. 24 h after transfection cells were pre-treated with 30 µM EHT 1864 for 3 h prior to treatment with Dox [1 µM, 1 h]. The mean values on which Figure 3.12 B is based on are listed in the Table (n=3 - 38 with 50 nuclei counted per experiment). Abbreviations: TR Con, TR: cells treated with TransIT-X2, T17N: dominant-negative RAC1, NLS-T17N: dominant-negative RAC1 with additional NLS, $*^{1}$: One way ANOVA, $*^{2}$: Two way ANOVA, $\#^{T}$ vs T17N+Dox, $\#^{TED}$ vs T17N+EHT+Dox, $\#^{N-T}$ vs NLS-T17N+Dox.

	γH2AX foci/nucleus mean ± SD	53BP1 foci/nucleus mean ± SD	colocalization foci/nucleus mean ± SD
TR Con	2.61 ± 1.17	1.53 ± 1.06	0.85 ± 0.57
TR + Dox [1 µM]	12.44 ± 1.97	9.81 ± 3.18	6.97 ± 1.83
T17N + Dox [1 µM]	7.23 ± 1.49	5.72 ± 1.86	4.23 ± 1.32
NLS-T17N + Dox [1 µM]	7.58 ± 1.32	6.38 ± 3.09	3.72 ± 1.27
TR + EHT 1864 [30 µM] + Dox [1 µM]	5.89 ± 2.21	4.90 ± 1.95	2.96 ± 1.03
T17N + EHT 1864 [30 µM] + Dox [1 µM]	4.13 ± 1.25	4.51 ± 0.74	2.30 ± 0.44
NLS-T17N + EHT 1864 [30 µM] + Dox [1 µM]	5.45 ± 2.64	4.98 ± 3.55	3.10 ± 1.85

	p value γH2AX vs TR (^{*1},^{*2}) / GFP-hRAC1 ($\#^{T}$, $\#^{TED}$, $\#^{N-T}$)	p value 53BP1 vs TR (^{*1},^{*2}) / GFP-hRAC1 ($\#^{T}$, $\#^{TED}$, $\#^{N-T}$)	p value colocalization vs TR (^{*1},^{*2}) / GFP-hRAC1 ($\#^{T}$, $\#^{TED}$, $\#^{N-T}$)
T17N + Dox [1 µM]	(^{*1}) <0.0001	(^{*1}) 0.0076	(^{*1}) 0.0015
NLS-T17N + Dox [1 µM]	(^{*1}) <0.0001 / ($\#^{T}$) 0.6758	(^{*1}) 0.0275 / ($\#^{T}$) 0.6635	(^{*1}) 0.0002 / ($\#^{T}$) 0.5107
TR + EHT 1864 [30 µM] + Dox [1 µM]	(^{*2}) <0.0001	(^{*2}) <0.0001	(^{*2}) <0.0001
T17N + EHT 1864 [30 µM] + Dox [1 µM]	(^{*2}) <0.0001 / ($\#^{T}$) 0.2681	(^{*2}) 0.0014 / ($\#^{T}$) 0.9998	(^{*2}) <0.0001 / ($\#^{T}$) 0.5431
NLS-T17N + EHT 1864 [30 µM] + Dox [1 µM]	(^{*2}) <0.0001 / ($\#^{TED}$) 0.9979 / ($\#^{N-T}$) 0.8027	(^{*2}) 0.0049 / ($\#^{TED}$) >0.9999 / ($\#^{N-T}$) 0.9992	(^{*2}) <0.0001 / ($\#^{TED}$) 0.9997 / ($\#^{N-T}$) 0.9999

Table 7.14: Data from influence of pharmacological RAC1 inhibition on doxorubicin-induced DDR in cells expressing human dominant-negative GFP-RAC1.
MEF were transiently transfected with *GFP-hRAC1(T17N)* expression vector. 24 h after transfection cells were pre-treated with EHT 1864 [3 h, 30 µM] prior to treatment with 1 µM Dox for 2 h. Cells were harvested after the end of the Dox treatment. Afterwards cells were lysed, and protein extracts were analyzed by western blot analysis as described in methods. The fluorescence intensities of the proteins were determined with ImageLab. Non-transfected cells treated with 1 µM Dox were set to 1. The mean values on which Figure 3.13 B is based on are listed in the Table (n=1 - 2). Abbreviations: Con: non-transfected control cells, T17N: dominant-negative RAC1.

pKAP1	Experiment 1 Protein normalized	Experiment 2 Protein normalized	mean ± SD
Con	0.00	0.00	0.00 ± 0.00
T17N	0.00	0.00	0.00 ± 0.00
EHT 1864 [30 µM]	0.00	0.00	0.00 ± 0.00
T17N + EHT 1864 [30 µM]	0.00	0.00	0.00 ± 0.00
1 µM Dox	1.00	1.00	1.00 ± 0.00
T17N + 1 µM Dox	1.10	0.37	0.73 ± 0.52
EHT 1864 [30 µM] + 1 µM Dox	1.96	1.90	1.93 ± 0.05
T17N + EHT 1864 [30 µM] + 1 µM Dox	1.30	0.33	0.81 ± 0.69
pP53	Experiment 1 Protein normalized	Experiment 2 Protein normalized	mean ± SD
Con	0.00		
T17N	0.00		
EHT 1864 [30 µM]	0.00		
T17N + EHT 1864 [30 µM]	0.00		
1 µM Dox	1.00		
T17N + 1 µM Dox	1.12		
EHT 1864 [30 µM] + 1 µM Dox	0.00		
T17N + EHT 1864 [30 µM] + 1 µM Dox	0.00		

mRAC1	Experiment 1 Protein normalized	Experiment 2 Protein normalized	mean ± SD
Con	0.58	0.57	0.57 ± 0.01
T17N	0.62	0.50	0.56 ± 0.08
EHT 1864 [30 µM]	0.89	0.56	0.72 ± 0.23
T17N + EHT 1864 [30 µM]	0.89	0.85	0.87 ± 0.03
1 µM Dox	1.00	1.00	1.00 ± 0.00
T17N + 1 µM Dox	0.82	0.61	0.71 ± 0.10
EHT 1864 [30 µM] + 1 µM Dox	0.92	1.50	1.21 ± 0.41
T17N + EHT 1864 [30 µM] + 1 µM Dox	1.16	0.34	0.75 ± 0.58

Table 7.15: Data from influence of GFP-hRAC1(T17N) with or without additional NLS on doxorubicin-induced foci formation in *mRac1* silenced MEF.
mRac1 knockdown was achieved by transfection with *mRac1* siRNA. The treatment scheme is shown in material and methods (Figure 2.1 E, F). Cells were additionally transfected with *GFP-hRAC1(T17N)* or *GFP-NLS-hRAC1(T17N)* expression vector. The mean values on which Figure 3.14 B is based on are listed in the Table (n=3 - 38 with 50 nuclei counted per experiment). Abbreviations: TR Con, TR: cells treated with TransIT-X2 only or with Lipofectamine RNAiMAX and TransIT-X2, T17N: dominant-negative RAC1, NLS-T17N: dominant-negative RAC1 with additional NLS, *mRac1* siRNA: siRNA against murine *Rac1,* ^{*1}: One way ANOVA, ^{*2}: Two way ANOVA, $\#^{T}$ vs T17N+Dox, $\#^{TsiD}$ vs T17N+siRNA+Dox, $\#^{N-T}$ vs NLS-T17N+Dox.

	γH2AX foci/nucleus mean ± SD	53BP1 foci/nucleus mean ± SD	colocalization foci/nucleus mean ± SD
TR Con	2.62 ± 1.11	1.42 ± 0.95	0.84 ± 0.53
TR + Dox [1 µM]	12.58 ± 1.91	9.81 ± 3.18	6.97 ± 1.83
T17N + Dox [1 µM]	7.23 ± 1.49	5.72 ± 1.86	4.23 ± 1.32
NLS-T17N + Dox [1 µM]	7.58 ± 1.32	6.38 ± 3.09	3.72 ± 1.27
TR + *mRac1* siRNA+ Dox [1 µM]	5.09 ± 1.32	3.92 ± 1.96	2.45 ± 1.19
T17N + *mRac1* siRNA+ Dox [1 µM]	5.36 ± 1.93	4.36 ± 3.08	2.51 ± 1.65
NLS-T17N + *mRac1* siRNA+ Dox [1 µM]	6.50 ± 2.16	5.45 ± 2.96	3.09 ± 1.07
	p value γH2AX vs TR (^{*1},^{*2}) / GFP-hRAC1 ($\#^{T}$, $\#^{TsiD}$, $\#^{N-T}$)	p value 53BP1 vs TR (^{*1},^{*2}) / GFP-hRAC1 ($\#^{T}$, $\#^{TsiD}$, $\#^{N-T}$)	p value colocalization vs TR (^{*1},^{*2}) / GFP-hRAC1 ($\#^{T}$, $\#^{TsiD}$, $\#^{N-T}$)
T17N + Dox [1 µM]	(^{*1}) <0.0001	(^{*1}) 0.0076	(^{*1}) 0.0015
NLS-T17N + Dox [1 µM]	(^{*1}) <0.0001 / ($\#^{T}$) 0.6759	(^{*1}) 0.0275 / ($\#^{T}$) 0.6635	(^{*1}) 0.0002 / ($\#^{T}$) 0.5107
TR + *mRac1* siRNA+ Dox [1 µM]	(^{*2}) <0.0001	(^{*2}) <0.0001	(^{*2}) <0.0001
T17N + *mRac1* siRNA+ Dox [1 µM]	(^{*2}) <0.0001 / ($\#^{T}$) 0.7295	(^{*2}) <0.0001 / ($\#^{T}$) 0.9982	(^{*2}) <0.0001 / ($\#^{T}$) 0.5837
NLS-T17N + *mRac1* siRNA+ Dox [1 µM]	(^{*2}) <0.0001 / ($\#^{TsiD}$) 0.9974 / ($\#^{N-T}$) 0.9968	(^{*2}) 0.0127 / ($\#^{TsiD}$) >0.9999 / ($\#^{N-T}$) >0.9999	(^{*2}) <0.0001 / ($\#^{TsiD}$) >0.9999 / ($\#^{N-T}$) 0.9999

Table 7.16: Data from comparison of GFP-hRAC1(T17N) with and without additional NLS, EHT 1864, and *mRac1* siRNA on doxorubicin induced γH2AX and 53BP1 foci formation.
Cells were transfected with *GFP-hRAC1(T17N)* or *GFP-NLS-hRAC1(T17N)* expression vector. Transfection control cells (TR Con) were treated with TransIT-X2 only or with Lipofectamine RNAiMAX and TransIT-X2 (TR). 24 h after transfection cells were pre-treated with 30 µM EHT 1864 for 3 h prior to treatment with Dox [1 µM, 1 h] or were only treated with Dox [1 µM, 1 h]. *mRac1* knockdown was achieved by transfection with *mRac1* siRNA. The treatment scheme is shown in material and methods (Figure 2.1 E, F). Cells were additionally transfected with *GFP-hRAC1(T17N)* or *GFP-NLS-hRAC1(T17N)* expression vector. The mean values on which Figure 3.15 is based on are listed in the Table (n=3 - 38 with 50 nuclei counted per experiment). Abbreviations: TR Con: cells treated with TransIT-X2, TR: cells treated with TransIT-X2 only or with Lipofectamine RNAiMAX and TransIT-X2, T17N: dominant-negative RAC1, NLS-T17N: dominant-negative RAC1 with additional NLS, mRac1 *siRNA: siRNA against murine* Rac1, $*^1$: One way ANOVA, $*^2$: Two way ANOVA, $\#^T$ vs T17N+Dox, $\#^{TED}$ vs T17N+EHT+Dox, $\#^{TsiD}$ vs T17N+siRNA+Dox, $\#^{N-T}$ vs NLS-T17N+Dox.

	γH2AX foci/nucleus mean ± SD	53BP1 foci/nucleus mean ± SD	colocalization foci/nucleus mean ± SD
TR Con	2.67 ± 1.18	1.53 ± 1.06	0.85 ± 0.57
TR + Dox [1 µM]	12.73 ± 1.84	9.81 ± 3.18	6.97 ± 1.83
T17N + Dox [1 µM]	7.23 ± 1.49	5.72 ± 1.86	4.23 ± 1.32
NLS-T17N + Dox [1 µM]	7.58 ± 1.32	6.38 ± 3.09	3.72 ± 1.27
TR + EHT 1864 [30 µM] + Dox [1 µM]	5.89 ± 2.21	4.90 ± 1.95	2.96 ± 1.03
T17N + EHT 1864 [30 µM] + Dox [1 µM]	4.13 ± 1.25	4.51 ± 0.74	2.30 ± 0.44
NLS-T17N + EHT 1864 [30 µM] + Dox [1 µM]	5.45 ± 2.64	4.98 ± 3.55	3.10 ± 1.85
TR + *mRac1* siRNA + Dox [1 µM]	5.09 ± 1.32	3.72 ± 1.84	2.45 ± 1.19
T17N + *mRac1* siRNA + Dox [1 µM]	5.36 ± 1.93	4.36 ± 3.08	2.51 ± 1.65
NLS-T17N + *mRac1* siRNA + Dox [1 µM]	6.50 ± 2.16	5.45 ± 2.96	3.09 ± 1.07
	p value γH2AX vs TR ($*^1$,$*^2$) / GFP-hRAC1 ($\#^T$, $\#^{TED}$, $\#^{TsiD}$, $\#^{N-T}$)	p value 53BP1 vs TR ($*^1$,$*^2$) / GFP-hRAC1 ($\#^T$, $\#^{TED}$, $\#^{TsiD}$, $\#^{N-T}$)	p value colocalization vs TR ($*^1$,$*^2$) / GFP-hRAC1 ($\#^T$, $\#^{TED}$, $\#^{TsiD}$, $\#^{N-T}$)
T17N + Dox [1 µM]	($*^1$) <0.0001	($*^1$) 0.0076	($*^1$) 0.0015
NLS-T17N + Dox [1 µM]	($*^1$) <0.0001 / ($\#^T$) 0.6758	($*^1$) 0.0275 / ($\#^T$) 0.6635	($*^1$) 0.0002 / ($\#^T$) 0.5107
TR + EHT 1864 [30 µM] + Dox [1 µM]	($*^2$) <0.0001	($*^2$) <0.0001	($*^2$) <0.0001
T17N + EHT 1864 [30 µM] + Dox [1 µM]	($*^2$) <0.0001 / ($\#^T$) 0.3171	($*^2$) 0.0006 / ($\#^T$) >0.9999	($*^2$) <0.0001 / ($\#^T$) 0.6389
NLS-T17N + EHT 1864 [30 µM] + Dox [1 µM]	($*^2$) <0.0001 / ($\#^{TED}$) 0.9999 / ($\#^{N-T}$) 0.8956	($*^2$) 0.0027 / ($\#^{TED}$) >0.9999 / ($\#^{N-T}$) >0.9999	($*^2$) <0.0001 / ($\#^{TED}$) >0.9999 / ($\#^{N-T}$) >0.9999
TR + *mRac1* siRNA + Dox [1 µM]	($*^2$) <0.0001	($*^2$) <0.0001	($*^2$) <0.0001
T17N + *mRac1* siRNA + Dox [1 µM]	($*^2$) <0.0001 / ($\#^T$) 0.9230	($*^2$) <0.0001 / ($\#^T$) >0.9999	($*^2$) <0.0001 / ($\#^T$) 0.6796
NLS-T17N + *mRac1* siRNA + Dox [1 µM]	($*^2$) <0.0001 / ($\#^{TsiD}$) >0.9999 / ($\#^{N-T}$) >0.9999	($*^2$) 0.0103 / ($\#^{TsiD}$) 0.9994 / ($\#^{N-T}$) >0.9999	($*^2$) <0.0001 / ($\#^{TsiD}$) >0.9999 / ($\#^{N-T}$) >0.9999

Table 7.17: Data from influence of human dominant-negative GFP-RAC1 (with and without additional NLS) on doxorubicin-induced pATM foci formation.
Cells were transiently transfected with *GFP-hRAC1(T17N)* or *GFP-NLS-hRAC1(T17N)* expression vector. Transfection control cells (TR Con, TR) were treated with transfection reagent (TransIT-X2). 24 h after transfection cells were treated with Dox [1 µM, 1 h]. The mean values on which Figure 3.16 B is based on are listed in the Table (n=3 - 18 with 50 nuclei counted per experiment). Abbreviations: TR Con, TR: cells treated with TransIT-X2, T17N: dominant-negative RAC1, NLS-T17N: dominant-negative RAC1 with additional NLS.

	pATM foci/nucleus mean ± SD	p value vs TR (*) / T17N (#)
TR Con	1.69 ± 1.62	
TR + Dox [1 µM]	6.74 ± 2.07	
T17N + Dox [1 µM]	6.37 ± 1.55	(*) 0.9816
NLS-T17N + Dox [1 µM]	5.53 ± 1.11	(*) 0.6245 / (#)0.4879

Table 7.18: Data influence of wild-type and constitutively active hRAC1 (with and without additional NLS) expression on doxorubicin-induced foci formation.
MEF were transiently transfected with *GFP-hRAC1(WT)*, *GFP-NLS-hRAC1(WT)*, *GFP-hRAC1(Q61L)*, or *GFP-NLS-hRAC1(Q61L)* expression vector. Transfection control cells (TR Con, TR) were treated with TransIT-X2. 24 h after transfection cells were 1 h pulse treated with Dox [1 µM]. The mean values on which Figure 3.17 B is based on are listed in the Table (n=6 - 38 with 50 nuclei counted per experiment). Abbreviations: TR Con, TR: cells treated with TransIT-X2, WT: wild-type RAC1, NLS-WT: wild-type RAC1 with additional NLS, Q61L: constitutively active RAC1, NLS-Q61L: constitutively active RAC1 with additional NLS.

	γH2AX foci/nucleus mean ± SD	53BP1 foci/nucleus mean ± SD	colocalization foci/nucleus mean ± SD
TR Con	2.67 ± 1.18	1.53 ± 1.06	0.85 ± 0.57
TR + Dox [1 µM]	12.73 ± 1.84	9.81 ± 3.18	6.97 ± 1.83
WT + Dox [1 µM]	10.07 ± 1.19	7.73 ± 1.96	5.32 ± 1.23
NLS-WT + Dox [1 µM]	10.63 ± 2.68	8.42 ± 3.13	5.88 ± 1.85
Q61L + Dox [1 µM]	12.32 ± 1.97	9.38 ± 2.56	6.73 ± 1.66
NLS-Q61L + Dox [1 µM]	6.54 ± 2.45	4.96 ± 1.75	3.34 ± 1.59
	p value γH2AX vs TR (*) / GFP-hRAC1 (#)	p value 53BP1 vs TR (*) / GFP-hRAC1 (#)	p value colocalization vs TR (*) / GFP-hRAC1 (#)
WT + Dox [1 µM]	(*) 0.0021	(*) 0.2092	(*) 0.0433
NLS-WT + Dox [1 µM]	(*) 0.0381 / (#) 0.6263	(*) 0.6766 / (#) 0.6374	(*) 0.3985 / (#) 0.5276
Q61L + Dox [1 µM]	(*) 0.9831	(*) 0.9959	(*) 0.9967
NLS-Q61L + Dox [1 µM]	(*) <0.0001 / (#) 0.0006	(*) 0.0002 / (#) 0.0044	(*) <0.0001 / (#) 0.0033

Table 7.19: Data from western blot analysis after doxorubicin treatment in wild-type hRAC1-expressing cells with and without additional NLS.
MEF were transiently transfected with *GFP-hRAC1(WT)* or *GFP-NLS-hRAC1(WT)* expression vector. 24 h after transfection cells were 2 h pulse-treated with 1 µM Dox. Cells were harvested after indicated time-points. Afterwards cells were lysed, and protein extracts were analyzed by western blot analysis as described in methods. The fluorescence intensities of the proteins were determined with ImageLab. Non-transfected cells treated with 1 µM Dox were set to 1. The mean values on which Figure 3.18 C - F is based on are listed in the Table (n=3). Abbreviations: NT Con, NT: non-transfected cells, WT: wild-type RAC1, NLS-WT: wild-type RAC1 with additional NLS.

pKAP1 0 h	Experiment 1 Protein normalized	Experiment 2 Protein normalized	Experiment 3 Protein normalized	mean ± SD	p value vs Dox (*) / GFP-hRAC1 +Dox (#)
NT Con	0.01	0.00	0.00	0.00 ± 0.01	
WT	0.06	0.03	0.18	0.09 ± 0.08	
NLS-WT	0.00	0.00	0.00	0.00 ± 0.00	
NT + 1 µM Dox	1.00	1.00	1.00	1.00 ± 0.00	
WT + 1 µM Dox	0.06	0.38	0.47	0.30 ± 0.22	(*) 0.0203
NLS-WT + 1 µM Dox	0.63	0.89	1.31	0.95 ± 0.35	(*) 0.9534 / (#) 0.05
pKAP1 4 h	Experiment 1 Protein normalized	Experiment 2 Protein normalized	Experiment 3 Protein normalized	mean ± SD	p value vs Dox (*) / GFP-hRAC1 +Dox (#)
NT Con	0.02	0.00	0.00	0.01 ± 0.01	
WT	0.02	0.06	0.00	0.02 ± 0.03	
NLS-WT	0.00	0.00	0.00	0.00 ± 0.00	
NT + 1 µM Dox	1.00	1.00	1.00	1.00 ± 0.00	
WT + 1 µM Dox	0.77	0.31	0.06	0.38 ± 0.36	(*) 0.2514
NLS-WT + 1 µM Dox	1.37	0.31	0.00	0.56 ± 0.72	(*) 0.4508 / (#) 0.7183

pKAP1 24 h	Experiment 1 Protein normalized	Experiment 2 Protein normalized	Experiment 3 Protein normalized	mean ± SD	p value vs Dox (*) / GFP-hRAC1 +Dox (#)
NT Con	0.06	0.00	0.02	0.03 ± 0.03	
WT	0.19	0.09	0.03	0.07 ± 0.10	
NLS-WT	0.00	0.00	0.00	0.00 ± 0.00	
NT + 1 µM Dox	1.00	1.00	1.00	1.00 ± 0.00	
WT + 1 µM Dox	0.17	0.42	0.09	0.22 ± 0.17	(*) 0.0042
NLS-WT + 1 µM Dox	0.49	0.00	0.00	0.16 ± 0.28	(*) 0.0029 / (#) 0.7669
γH2AX 0 h	Experiment 1 Protein normalized	Experiment 2 Protein normalized	Experiment 3 Protein normalized	mean ± SD	p value vs Dox (*) / GFP-hRAC1 +Dox (#)
NT Con	0.16	0.00	0.00	0.05 ± 0.09	
WT	0.00	0.19	0.00	0.06 ± 0.11	
NLS-WT	0.00	0.00	0.00	0.00 ± 0.00	
NT + 1 µM Dox	1.00	1.00	1.00	1.00 ± 0.00	
WT + 1 µM Dox	0.99	1.17	1.00	1.05 ± 0.10	(*) 0.8184
NLS-WT + 1 µM Dox	0.90	1.15	0.82	0.96 ± 0.17	(*) 0.8774 / (#) 0.4735
γH2AX 4 h	Experiment 1 Protein normalized	Experiment 2 Protein normalized	Experiment 3 Protein normalized	mean ± SD	p value vs Dox (*) / GFP-hRAC1 +Dox (#)
NT Con	0.16	0.33	0.26	0.25 ± 0.09	
WT	0.54	0.18	0.52	0.41 ± 0.20	
NLS-WT	0.00	0.99	0.00	0.33 ± 0.57	
NT + 1 µM Dox	1.00	1.00	1.00	1.00 ± 0.00	
WT + 1 µM Dox	0.91	1.21	1.25	1.22 ± 0.18	(*) 0.0709
NLS-WT + 1 µM Dox	0.00	0.00	0.00	0.00 ± 0.00	(*) <0.0001 / (#) 0.0003

γH2AX 24 h	Experiment 1 Protein normalized	Experiment 2 Protein normalized	Experiment 3 Protein normalized	mean ± SD	p value vs Dox (*) / GFP-hRAC1 +Dox (#)
NT Con	0.00	0.00	0.00	0.00 ± 0.00	
WT	0.00	0.04	0.00	0.01 ± 0.03	
NLS-WT	0.00	0.00	0.00	0.00 ± 0.00	
NT + 1 µM Dox	1.00	1.00	1.00	1.00 ± 0.00	
WT + 1 µM Dox	0.00	0.00	0.00	0.00 ± 0.00	(*) 0.1749
NLS-WT + 1 µM Dox	0.00	2.02	0.19	0.74 ± 1.11	(*) 0.8419 / (#) 0.3125
pP53 0 h	Experiment 1 Protein normalized	Experiment 2 Protein normalized	Experiment 3 Protein normalized	mean ± SD	p value vs Dox (*) / GFP-hRAC1 +Dox (#)
NT Con	0.00	0.00	0.03	0.01 ± 0.02	
WT	0.00	0.09	0.11	0.07 ± 0.06	
NLS-WT	0.00	0.00	0.00	0.00 ± 0.00	
NT + 1 µM Dox	1.00	1.00	1.00	1.00 ± 0.00	
WT + 1 µM Dox	0.05	0.38	0.10	0.18 ± 0.18	(*) 0.0144
NLS-WT + 1 µM Dox	0.12	0.76	0.00	0.29 ± 0.41	(*) 0.0267 / (#) 0.6924
pP53 4 h	Experiment 1 Protein normalized	Experiment 2 Protein normalized	Experiment 3 Protein normalized	mean ± SD	p value vs Dox (*) / GFP-hRAC1 +Dox (#)
NT Con	0.00	0.00	0.04	0.01 ± 0.02	
WT	0.00	0.09	0.11	0.07 ± 0.06	
NLS-WT	0.00	0.00	0.00	0.00 ± 0.00	
NT + 1 µM Dox	1.00	1.00	1.00	1.00 ± 0.00	
WT + 1 µM Dox	0.06	0.40	0.20	0.22 ± 0.17	(*) 0.0264
NLS-WT + 1 µM Dox	0.66	0.33	1.24	0.74 ± 0.46	(*) 0.4691 / (#) 0.1402

pP53 24 h	Experiment 1 Protein normalized	Experiment 2 Protein normalized	Experiment 3 Protein normalized	mean ± SD	p value vs Dox (*) / GFP-hRAC1 +Dox (#)
NT Con	0.00	0.10	0.10	0.07 ± 0.06	
WT	0.00	0.29	0.07	0.12 ± 0.15	
NLS-WT	0.00	0.00	0.00	0.00 ± 0.00	
NT + 1 µM Dox	1.00	1.00	1.00	1.00 ± 0.00	
WT + 1 µM Dox	0.19	0.84	0.08	0.37 ± 0.41	(*) 0.0322
NLS-WT + 1 µM Dox	0.12	0.00	0.00	0.04 ± 0.07	(*) 0.8419 / (#) 0.2413
mRAC1 0 h	Experiment 1 Protein normalized	Experiment 2 Protein normalized	Experiment 3 Protein normalized	mean ± SD	p value vs Dox (*) / GFP-hRAC1 +Dox (#)
NT Con	0.29	2.23	0.31	0.94 ± 1.12	
WT	1.47	1.26	1.94	1.56 ± 0.35	
NLS-WT	1.70	1.88	0.73	1.44 ± 0.62	
NT + 1 µM Dox	1.00	1.00	1.00	1.00 ± 0.00	
WT + 1 µM Dox	1.35	1.82	2.34	1.83 ± 0.49	(*) 0.0234
NLS-WT + 1 µM Dox	0.86	0.91	1.11	0.96 ± 0.13	(*) 0.9797 / (#) 0.0410
mRAC1 4 h	Experiment 1 Protein normalized	Experiment 2 Protein normalized	Experiment 3 Protein normalized	mean ± SD	p value vs Dox (*) / GFP-hRAC1 +Dox (#)
NT Con	1.14	1.51	1.02	1.22 ± 0.26	
WT	2.01	1.37	0.70	0.36 ± 0.66	
NLS-WT	1.36	1.03	1.26	1.22 ± 0.17	
NT + 1 µM Dox	1.00	1.00	1.00	1.00 ± 0.00	
WT + 1 µM Dox	1.49	0.46	0.21	0.72 ± 0.68	(*) 0.6163
NLS-WT + 1 µM Dox	0.50	0.55	0.53	0.53 ± 0.07	(*) 0.3144 / (#) 0.6554

mRAC1 24 h	Experiment 1 Protein normalized	Experiment 2 Protein normalized	Experiment 3 Protein normalized	mean ± SD	p value vs Dox (*) / GFP-hRAC1 +Dox (#)
NT Con	2.06	0.99	0.95	1.34 ± 0.63	
WT	1.13	0.46	1.34	0.98 ± 0.46	
NLS-WT	0.47	0.52	0.58	0.52 ± 0.06	
NT + 1 µM Dox	1.00	1.00	1.00	1.00 ± 0.00	
WT + 1 µM Dox	0.70	0.62	0.18	0.50 ± 0.28	(*) 0.0432
NLS-WT + 1 µM Dox	0.74	0.46	0.31	0.50 ± 0.22	(*) 0.0432 / (#) >0.9999

Table 7.20: Data from western blot analysis after doxorubicin treatment in constitutively active hRAC1-expressing cells with and without additional NLS.
MEF were transiently transfected with *GFP-hRAC1(Q61L)* or *GFP-NLS-hRAC1(Q61L)* expression vector. 24 h after transfection cells were 2 h pulse-treated with 1 µM Dox. Cells were harvested after indicated time-points. Afterwards cells were lysed, and protein extracts were analyzed by western blot analysis as described in methods. The fluorescence intensities of the proteins were determined with ImageLab. Non-transfected cells treated with 1 µM Dox were set to 1. The mean values on which Figure 3.19 C - F is based on are listed in the Table (n=3). Abbreviations: NT Con, NT: non-transfected cells, Q61L: constitutively active RAC1, NLS-Q61L: constitutively active RAC1 with additional NLS.

pKAP1 0 h	Experiment 1 Protein normalized	Experiment 2 Protein normalized	Experiment 3 Protein normalized	mean ± SD	p value vs Dox (*) / GFP-hRAC1 +Dox (#)
NT Con	0.00	0.00	0.00	0.00 ± 0.00	
Q61L	0.07	0.04	0.00	0.04 ± 0.04	
NLS-Q61L	0.00	0.00	0.00	0.00 ± 0.00	
NT + 1 µM Dox	1.00	1.00	1.00	1.00 ± 0.00	
Q61L + 1 µM Dox	0.37	0.34	1.69	0.80 ± 0.77	(*) 0.9345
NLS-Q61L + 1 µM Dox	0.12	0.36	2.23	0.90 ± 1.15	(*) 0.9830 / (#) 0.9064

pKAP1 4 h	Experiment 1 Protein normalized	Experiment 2 Protein normalized	Experiment 3 Protein normalized	mean ± SD	p value vs Dox (*) / GFP-hRAC1 +Dox (#)
NT Con	0.00	0.00	0.00	0.00 ± 0.00	
Q61L	0.09	0.02	0.55	0.22 ± 0.28	
NLS-Q61L	0.00	0.00	0.00	0.00 ± 0.00	
NT + 1 µM Dox	1.00	1.00	1.00	1.00 ± 0.00	
Q61L + 1 µM Dox	1.17	0.23	1.26	0.89 ± 0.57	(*) 0.9572
NLS-Q61L + 1 µM Dox	0.56	0.43	1.81	0.94 ± 0.76	(*) 0.9869 / (#) 0.9317
pKAP1 24 h	Experiment 1 Protein normalized	Experiment 2 Protein normalized	Experiment 3 Protein normalized	mean ± SD	p value vs Dox (*) / GFP-hRAC1 +Dox (#)
NT Con	0.00	0.00	0.00	0.00 ± 0.00	
Q61L	0.00	0.04	0.36	0.13 ± 0.19	
NLS-Q61L	0.00	0.00	0.00	0.00 ± 0.00	
NT + 1 µM Dox	1.00	1.00	1.00	1.00 ± 0.00	
Q61L + 1 µM Dox	0.39	0.85	0.53	0.59 ± 0.24	(*) 0.6255
NLS-Q61L + 1 µM Dox	1.41	1.92	0.00	1.11 ± 0.99	(*) 0.9626 / (#) 0.4266
γH2AX 0 h	Experiment 1 Protein normalized	Experiment 2 Protein normalized	Experiment 3 Protein normalized	mean ± SD	p value vs Dox (*) / GFP-hRAC1 +Dox (#)
NT Con	0.77	0.74	0.00	0.50 ± 0.44	
Q61L	1.67	0.79	0.00	0.82 ± 0.84	
NLS-Q61L	0.15	0.00	0.00	0.05 ± 0.09	
NT + 1 µM Dox	1.00	1.00	1.00	1.00 ± 0.00	
Q61L + 1 µM Dox	0.85	0.65	3.10	1.54 ± 1.36	(*) 0.6834
NLS-Q61L + 1 µM Dox	0.43	1.28	0.00	0.57 ± 0.65	(*) 0.7786 / (#) 0.3275

γH2AX 4 h	Experiment 1 Protein normalized	Experiment 2 Protein normalized	Experiment 3 Protein normalized	mean ± SD	p value vs Dox (*) / GFP-hRAC1 +Dox (#)
NT Con	0.26	0.09	0.00	0.12 ± 0.13	
Q61L	1.00	0.26	0.40	0.55 ± 0.39	
NLS-Q61L	0.00	0.00	0.00	0.00 ± 0.00	
NT + 1 µM Dox	1.00	1.00	1.00	1.00 ± 0.00	
Q61L + 1 µM Dox	3.00	0.49	4.50	2.66 ± 2.03	(*) 0.2675
NLS-Q61L + 1 µM Dox	2.90	1.29	1.41	1.87 ± 0.90	(*) 0.6394 / (#) 0.5711
γH2AX 24 h	Experiment 1 Protein normalized	Experiment 2 Protein normalized	Experiment 3 Protein normalized	mean ± SD	p value vs Dox (*) / GFP-hRAC1 +Dox (#)
NT Con	0.00	0.00	0.00	0.00 ± 0.00	
Q61L	0.00	0.04	0.00	0.01 ± 0.03	
NLS-Q61L	0.05	0.00	0.00	0.02 ± 0.03	
NT + 1 µM Dox	1.00	1.00	1.00	1.00 ± 0.00	
Q61L + 1 µM Dox	0.00	0.00	0.00	0.00 ± 0.00	(*) 0.1177
NLS-Q61L + 1 µM Dox	1.03	0.00	1.86	0.96 ± 0.93	(*) 0.9943 / (#) 0.1583
pP53 0 h	Experiment 1 Protein normalized	Experiment 2 Protein normalized	Experiment 3 Protein normalized	mean ± SD	p value vs Dox (*) / GFP-hRAC1 +Dox (#)
NT Con	0.00	0.00	0.08	0.03 ± 0.05	
Q61L	0.63	0.31	0.17	0.37 ± 0.24	
NLS-Q61L	0.09	0.00	0.00	0.03 ± 0.05	
NT + 1 µM Dox	1.00	1.00	1.00	1.00 ± 0.00	
Q61L + 1 µM Dox	0.82	0.35	1.15	0.77 ± 0.44	(*) 0.5062
NLS-Q61L + 1 µM Dox	0.53	0.78	0.54	0.62 ± 0.14	(*) 0.2174 / (#) 0.6037

pP53 4 h	Experiment 1 Protein normalized	Experiment 2 Protein normalized	Experiment 3 Protein normalized	mean ± SD	p value vs Dox (*) / GFP-hRAC1 +Dox (#)
NT Con	0.00	0.00	0.02	0.01 ± 0.01	
Q61L	0.18	0.13	0.19	0.17 ± 0.03	
NLS-Q61L	0.00	0.00	0.00	0.00 ± 0.00	
NT + 1 µM Dox	1.00	1.00	1.00	1.00 ± 0.00	
Q61L + 1 µM Dox	0.81	1.56	0.86	1.08 ± 0.42	(*) 0.9093
NLS-Q61L + 1 µM Dox	0.37	0.75	0.43	0.52 ± 0.20	(*) 0.1210 / (#) 0.1054
pP53 24 h	Experiment 1 Protein normalized	Experiment 2 Protein normalized	Experiment 3 Protein normalized	mean ± SD	p value vs Dox (*) / GFP-hRAC1 +Dox (#)
NT Con	0.00	0.00	0.35	0.12 ± 0.20	
Q61L	0.92	0.28	0.65	0.62 ± 0.32	
NLS-Q61L	0.00	0.00	0.00	0.00 ± 0.00	
NT + 1 µM Dox	1.00	1.00	1.00	1.00 ± 0.00	
Q61L + 1 µM Dox	0.22	0.31	0.81	0.45 ± 0.32	(*) 0.5469
NLS-Q61L + 1 µM Dox	1.25	2.28	0.00	1.18 ± 1.14	(*) 0.9280 / (#) 0.3458
mRAC1 0 h	Experiment 1 Protein normalized	Experiment 2 Protein normalized	Experiment 3 Protein normalized	mean ± SD	p value vs Dox (*) / GFP-hRAC1 +Dox (#)
NT Con	0.03	1.11	1.01	0.72 ± 0.59	
Q61L	2.62	0.56	1.65	1.62 ± 1.04	
NLS-Q61L	1.20	1.31	0.71	1.07 ± 0.32	
NT + 1 µM Dox	1.00	1.00	1.00	1.00 ± 0.00	
Q61L + 1 µM Dox	0.12	0.44	5.85	2.14 ± 3.22	(*) 0.6945
NLS-Q61L + 1 µM Dox	0.92	1.72	0.79	1.14 ± 0.50	(*) 0.9940 / (#) 0.6232

mRAC1 4 h	Experiment 1 Protein normalized	Experiment 2 Protein normalized	Experiment 3 Protein normalized	mean ± SD	p value vs Dox (*) / GFP-hRAC1 +Dox (#)
NT Con	0.44	0.34	1.74	0.84 ± 0.78	
Q61L	2.54	0.19	3.95	2.22 ± 1.90	
NLS-Q61L	0.68	1.96	0.84	1.16 ± 0.70	
NT + 1 µM Dox	1.00	1.00	1.00	1.00 ± 0.00	
Q61L + 1 µM Dox	4.41	0.10	2.24	2.25 ± 2.15	(*) 0.4277
NLS-Q61L + 1 µM Dox	0.70	1.01	1.63	1.12 ± 0.47	(*) 0.9902 / (#) 0.4214
mRAC1 24 h	Experiment 1 Protein normalized	Experiment 2 Protein normalized	Experiment 3 Protein normalized	mean ± SD	p value vs Dox (*) / GFP-hRAC1 +Dox (#)
NT Con	0.31	2.06	0.67	1.01 ± 0.93	
Q61L	0.32	0.26	0.96	0.51 ± 0.39	
NLS-Q61L	1.27	0.45	0.79	0.84 ± 0.41	
NT + 1 µM Dox	1.00	1.00	1.00	1.00 ± 0.00	
Q61L + 1 µM Dox	0.64	0.70	0.69	0.67 ± 0.04	(*) 0.5393
NLS-Q61L + 1 µM Dox	2.09	1.44	0.70	1.41 ± 0.70	(*) 0.4102 / (#) 0.1415

Table 7.21: Data from influence of pharmacological RAC1 inhibition on doxorubicin-induced foci formation in cells expressing cytosolic or nuclear human GFP-RAC1(WT).
MEF were transiently transfected with *GFP-hRAC1(WT)* or *GFP-NLS-hRAC1(WT)* expression vector. Transfection control cells (TR Con, TR) were treated with TransIT-X2. 24 h after transfection cells were pre-treated with 30 µM EHT 1864 for 3 h prior to treatment with Dox [1 µM, 1 h]. The mean values on which Figure 3.20 B is based on are listed in the Table (n=3 - 38 with 50 nuclei counted per experiment). Abbreviations: TR Con, TR: cells treated with TransIT-X2, WT: wild-type RAC1, NLS-WT: wild-type RAC1 with additional NLS, ^{*1}: One way ANOVA, ^{*2}: Two way ANOVA, $\#^{WT}$ vs WT + Dox, $\#^{WTED}$ vs WT + EHT + Dox, $\#^{N\text{-}WT}$ vs NLS-WT + Dox.

	γH2AX foci/nucleus mean ± SD	53BP1 foci/nucleus mean ± SD	colocalization foci/nucleus mean ± SD
TR Con	2.61 ± 1.17	1.53 ± 1.06	0.85 ± 0.57
TR + Dox [1 µM]	12.44 ± 1.97	9.81 ± 3.18	6.97 ± 1.83
WT + Dox [1 µM]	10.07 ± 1.19	7.73 ± 1.96	5.32 ± 1.23
NLS-WT + Dox [1 µM]	10.63 ± 2.68	8.42 ± 3.13	5.88 ± 1.85
TR + EHT 1864 [30 µM] + Dox [1 µM]	5.89 ± 2.21	4.90 ± 1.95	2.96 ± 1.03
WT + EHT 1864 [30 µM] + Dox [1 µM]	5.55 ± 1.69	2.57 ± 0.88	2.07 ± 1.00
NLS-WT + EHT 1864 [30 µM] + Dox [1 µM]	4.01 ± 2.30	4.40 ± 1.63	2.20 ± 1.01
	p value γH2AX vs TR (^{*1}, ^{*2}) / GFP-hRAC1 ($\#^{WT}$, $\#^{WTED}$, $\#^{N\text{-}WT}$)	p value 53BP1 vs TR (^{*1}, ^{*2}) / GFP-hRAC1 ($\#^{WT}$, $\#^{WTED}$, $\#^{N\text{-}WT}$)	p value colocalization vs TR (^{*1}, ^{*2}) / GFP-hRAC1 ($\#^{WT}$, $\#^{WTED}$, $\#^{N\text{-}WT}$)
WT + Dox [1 µM]	(^{*1}) 0.0108	(^{*1}) 0.1942	(^{*1}) 0.05
NLS-WT + Dox [1 µM]	(^{*1}) 0.0827 / ($\#^{WT}$) 0.6263	(^{*1}) 0.5115 / ($\#^{WT}$) 0.6374	(^{*1}) 0.3024 / ($\#^{WT}$) 0.5276
TR + EHT 1864 [30 µM] + Dox [1 µM]	(^{*2}) <0.0001	(^{*2}) <0.0001	(^{*2}) 0.1600
WT + EHT 1864 [30 µM] + Dox [1 µM]	(^{*2}) <0.0001 / ($\#^{WT}$) 0.0121	(^{*2}) <0.0001 / ($\#^{WT}$) 0.0422	(^{*2}) 0.9047 / ($\#^{WT}$) 0.9999
NLS-WT + EHT 1864 [30 µM] + Dox [1 µM]	(^{*2}) <0.0001 / ($\#^{WTED}$) 0.9946 / ($\#^{N\text{-}WT}$) <0.0001	(^{*2}) 0.0008 / ($\#^{WTED}$) 0.9971 / ($\#^{N\text{-}WT}$) 0.3041	(^{*2}) 0.9186 / ($\#^{WTED}$) >0.9999 / ($\#^{N\text{-}WT}$) 0.9997

Table 7.22: Data from influence of pharmacological RAC1 inhibition on doxorubicin-induced foci formation in cells expressing cytosolic or nuclear human GFP-RAC1(Q61L). MEF were transiently transfected with *GFP-hRAC1(Q61L)* or *GFP-NLS-hRAC1(Q61L)* expression vector. Transfection control cells (TR Con, TR) were treated with TransIT-X2. 24 h after transfection cells were pre-treated with 30 µM EHT 1864 for 3 h prior to treatment with Dox [1 µM, 1 h]. The mean values on which Figure 3.21 B is based on are listed in the Table (n=3 - 38 with 50 nuclei counted per experiment). Abbreviations: TR Con, TR: cells treated with TransIT-X2, Q61L: constitutively active RAC1, NLS-Q61L: constitutively active RAC1 with additional NLS, ^{*1}: One way ANOVA, ^{*2}: Two way ANOVA, $\#^{Q}$ vs Q61L + Dox, $\#^{QED}$ vs Q61L + EHT + Dox, $\#^{N-Q}$ vs NLS-Q61L + Dox.

	γH2AX foci/nucleus mean ± SD	53BP1 foci/nucleus mean ± SD	colocalization foci/nucleus mean ± SD
TR Con	2.61 ± 1.17	1.53 ± 1.06	0.85 ± 0.57
TR + Dox [1 µM]	12.44 ± 1.97	9.81 ± 3.18	6.97 ± 1.83
Q61L + Dox [1 µM]	12.32 ± 1.97	9.38 ± 2.56	6.73 ± 1.66
NLS-Q61L + Dox [1 µM]	6.54 ± 2.45	4.96 ± 1.75	3.34 ± 1.59
TR + EHT 1864 [30 µM] + Dox [1 µM]	5.89 ± 2.21	4.90 ± 1.95	2.96 ± 1.03
Q61L + EHT 1864 [30 µM] + Dox [1 µM]	7.40 ± 2.65	4.82 ± 1.18	3.20 ± 1.30
NLS-Q61L + EHT 1864 [30 µM] + Dox [1 µM]	6.07 ± 1.65	4.82 ± 1.30	2.62 ± 0.49
	p value γH2AX vs TR (^{*1},^{*2}) / GFP-hRAC1 ($\#^{Q}$, $\#^{QED}$, $\#^{N-Q}$)	p value 53BP1 vs TR (^{*1},^{*2}) / GFP-hRAC1 ($\#^{Q}$, $\#^{QED}$, $\#^{N-Q}$)	p value colocalization vs TR (^{*1},^{*2}) / GFP-hRAC1 ($\#^{Q}$, $\#^{QED}$, $\#^{N-Q}$)
Q61L + Dox [1 µM]	(^{*1}) 0.9867	(^{*1}) 0.9246	(^{*1}) 0.9338
NLS-Q61L + Dox [1 µM]	(^{*1}) <0.0001 / ($\#^{Q}$) 0.0006	(^{*1}) 0.0011 / ($\#^{Q}$) 0.0044	(^{*1}) <0.0001 / ($\#^{Q}$) 0.0033
TR + EHT 1864 [30 µM] + Dox [1 µM]	(^{*2}) <0.0001	(^{*2}) <0.0001	(^{*2}) <0.0001
Q61L + EHT 1864 [30 µM] + Dox [1 µM]	(^{*2}) <0.0001 / ($\#^{Q}$) 0.0038	(^{*2}) 0.0025 / ($\#^{Q}$) 0.1152	(^{*2}) <0.0001 / ($\#^{Q}$) 0.0050
NLS-Q61L + EHT 1864 [30 µM] + Dox [1 µM]	(^{*2}) <0.0001 / ($\#^{QED}$) 0.9985 / ($\#^{N-Q}$) >0.9999	(^{*2}) 0.0025 / ($\#^{QED}$) >0.9999 / ($\#^{N-Q}$) >0.9999	(^{*2}) <0.0001 / ($\#^{QED}$) >0.9999 / ($\#^{N-Q}$) 0.9997

Table 7.23: Data from influence of pharmacological RAC1 inhibition on doxorubicin-induced DDR in cells expressing human GFP-RAC1(WT)
MEF were transiently transfected with *GFP-hRAC1(WT)* expression vector. 24 h after transfection cells were pre-treated with EHT 1864 [3 h, 30 µM] prior to treatment with 1 µM Dox for 2 h. Cells were harvested after the end of the Dox treatment. Afterwards cells were lysed, and protein extracts were analyzed by western blot analysis as described in methods. The fluorescence intensities of the proteins were determined with ImageLab. Non-transfected cells treated with 1 µM Dox were set to 1. The mean values on which Figure 3.22 B is based on are listed in the Table (n=1). Abbreviations: Con: non-transfected control cells, WT: wild-type RAC1.

	pKAP1 Protein normalized	pP53 Protein normalized	mRAC1 Protein normalized
Con	0.00	0.00	1.77
WT	0.00	0.00	1.39
EHT 1894 [30 µM]	0.00	0.00	1.20
WT + EHT 1894 [30 µM]	0.00	0.00	1.75
Dox [1 µM]	1.00	1.00	1.00
WT + Dox [1 µM]	0.37	0.87	1.74
EHT 1894 [30 µM] + Dox [1 µM]	0.25	0.22	0.77
WT + EHT 1894 [30 µM] + Dox [1 µM]	0.27	2.15	0.82

Table 7.24: Data from influence of pharmacological RAC1 inhibition on doxorubicin-induced DDR in cells expressing human GFP-RAC1(Q61L)
MEF were transiently transfected with *GFP-hRAC1(Q61L)* expression vector. 24 h after transfection cells were pre-treated with EHT 1864 [3 h, 30 µM] prior to treatment with 1 µM Dox for 2 h. Cells were harvested after the end of the Dox treatment. Afterwards cells were lysed, and protein extracts were analyzed by western blot analysis as described in methods. The fluorescence intensities of the proteins were determined with ImageLab. Non-transfected cells treated with 1 µM Dox were set to 1. The mean values on which Figure 3.23 B is based on are listed in the Table (n=1). Abbreviations: Con: non-transfected control cells, Q61L: constitutively active RAC1.

	pKAP1 Protein normalized	pP53 Protein normalized	mRAC1 Protein normalized
Con	0.00	0.00	0.92
Q61L	0.00	0.00	1.03
EHT 1894 [30 µM]	0.00	0.00	1.07
Q61L + EHT 1894 [30 µM]	0.00	0.00	0.97
Dox [1 µM]	1.00	1.00	1.00
Q61L + Dox [1 µM]	2.10	0.71	1.31
EHT 1894 [30 µM] + Dox [1 µM]	1.97	0.43	0.74
Q61L + EHT 1894 [30 µM] + Dox [1 µM]	3.76	0.04	1.16

Table 7.25: Data from influence of GFP-hRAC1(WT) with or without additional NLS on doxorubicin-induced foci formation in *mRac1* silenced MEF.
mRac1 knockdown was achieved by transfection with *mRac1* siRNA. The treatment scheme is shown in material and methods (Figure 2.1 E, F). Cells were additionally transfected with *GFP-hRAC1(WT)* or *GFP-NLS-hRAC1(WT)* expression vector. The mean values on which Figure 3.24 B is based on are listed in the Table (n=3 - 38 with 50 nuclei counted per experiment). Abbreviations: TR Con, TR: cells treated with TransIT-X2 only or with Lipofectamine RNAiMAX and TransIT-X2, WT: wild-type RAC1, NLS-WT: wild-type RAC1 with additional NLS, $*^1$: One way ANOVA, $*^2$: Two way ANOVA, $\#^{WT}$ vs WT + Dox, $\#^{WTsiD}$ vs WT + siRNA + Dox, $\#^{N\text{-}WT}$ vs NLS-WT + Dox.

	γH2AX foci/nucleus mean ± SD	53BP1 foci/nucleus mean ± SD	colocalization foci/nucleus mean ± SD
TR Con	2.62 ± 1.11	1.42 ± 0.95	0.84 ± 0.53
TR + Dox [1 µM]	12.58 ± 1.91	9.81 ± 3.18	6.97 ± 1.83
WT + Dox [1 µM]	10.07 ± 1.19	7.37 ± 1.96	5.32 ± 1.23
NLS-WT + Dox [1 µM]	10.63 ± 2.68	8.42 ± 3.13	5.88 ± 1.85
TR + *mRac1* siRNA+ Dox [1 µM]	5.09 ± 1.32	3.92 ± 1.96	2.45 ± 1.19
WT + *mRac1* siRNA+ Dox [1 µM]	6.89 ± 2.50	3.25 ± 1.84	2.25 ± 1.44
NLS-WT + *mRac1* siRNA+ Dox [1 µM]	5.16 ± 1.35	4.33 ± 3.66	2.35 ± 1.29
	p value γH2AX vs TR ($*^1$,$*^2$) / GFP-hRAC1 ($\#^{WT}$, $\#^{WTsiD}$, $\#^{N\text{-}WT}$)	p value 53BP1 vs TR ($*^1$,$*^2$) / GFP-hRAC1 ($\#^{WT}$, $\#^{WTsiD}$, $\#^{N\text{-}WT}$)	p value colocalization vs TR ($*^1$,$*^2$) / GFP-hRAC1 ($\#^{WT}$, $\#^{WTsiD}$, $\#^{N\text{-}WT}$)
WT + Dox [1 µM]	($*^1$) 0.0108	($*^1$) 0.1105	($*^1$) 0.05
NLS-WT + Dox [1 µM]	($*^1$) 0.0827 / ($\#^{WT}$) 0.6263	($*^1$) 0.5115 / ($\#^{WT}$) 0.4762	($*^1$) 0.3024 / ($\#^{WT}$) 0.5276
TR + *mRac1* siRNA+ Dox [1 µM]	($*^2$) <0.0001	($*^2$) <0.0001	($*^2$) <0.0001
WT + *mRac1* siRNA+ Dox [1 µM]	($*^2$) <0.0001 / ($\#^{WT}$) 0.1294	($*^2$) <0.0001 / ($\#^{WT}$) 0.2222	($*^2$) <0.0001 / ($\#^{WT}$) 0.0269
NLS-WT + *mRac1* siRNA+ Dox [1 µM]	($*^2$) <0.0001 / ($\#^{WTsiD}$) 0.9677 / ($\#^{N\text{-}WT}$) 0.0001	($*^2$) 0.0006 / ($\#^{WTsiD}$) >0.9999 / ($\#^{N\text{-}WT}$) 0.2646	($*^2$) <0.0001 / ($\#^{WTsiD}$) >0.9999 / ($\#^{N\text{-}WT}$) 0.0065

Table 7.26: Data from influence of GFP-hRAC1(Q61L) with or without additional NLS on doxorubicin-induced foci formation in *mRac1* silenced MEF.

mRac1 knockdown was achieved by transfection with *mRac1* siRNA. The treatment scheme is shown in material and methods (Figure 2.1 E, F). Cells were additionally transfected with *GFP-hRAC1(Q61L)* or *GFP-NLS-hRAC1(Q61L)* expression vector. The mean values on which Figure 3.25 B is based on are listed in the Table (n=3 - 38 with 50 nuclei counted per experiment). Abbreviations: TR Con, TR: cells treated with TransIT-X2 only or with Lipofectamine RNAiMAX and TransIT-X2, Q61L: constitutively active RAC1, NLS-Q61L: constitutively active RAC1 with additional NLS, $*^{1}$: One way ANOVA, $*^{2}$: Two way ANOVA, $\#^{Q}$ vs Q61L + Dox, $\#^{QsiD}$ vs Q61L + siRNA + Dox, $\#^{N-Q}$ vs NLS-Q61L + Dox.

	γH2AX foci/nucleus mean ± SD	53BP1 foci/nucleus mean ± SD	colocalization foci/nucleus mean ± SD
TR Con	2.62 ± 1.11	1.42 ± 0.95	0.84 ± 0.53
TR + Dox [1 µM]	12.58 ± 1.91	9.81 ± 3.18	6.97 ± 1.83
Q61L + Dox [1 µM]	12.32 ± 1.97	9.38 ± 2.56	6.73 ± 1.66
NLS-Q61L + Dox [1 µM]	6.54 ± 2.45	4.96 ± 1.75	3.34 ± 1.59
TR + *mRac1* siRNA+ Dox [1 µM]	5.09 ± 1.32	3.92 ± 1.96	2.45 ± 1.19
Q61L + *mRac1* siRNA+ Dox [1 µM]	2.49 ± 0.55	2.63 ± 3.13	1.39 ± 1.46
NLS-Q61L + *mRac1* siRNA+ Dox [1 µM]	9.00 ± 0.91	10.84 ± 2.01	5.69 ± 0.41
	p value γH2AX vs TR ($*^{1}$,$*^{2}$) / GFP-hRAC1 ($\#^{Q}$, $\#^{QsiD}$, $\#^{N-Q}$)	p value 53BP1 vs TR ($*^{1}$,$*^{2}$) / GFP-hRAC1 ($\#^{Q}$, $\#^{QsiD}$, $\#^{N-Q}$)	p value colocalization vs TR ($*^{1}$,$*^{2}$) / GFP-hRAC1 ($\#^{Q}$, $\#^{QsiD}$, $\#^{N-Q}$)
Q61L + Dox [1 µM]	($*^{1}$) 0.9867	($*^{1}$) 0.9246	($*^{1}$) 0.9338
NLS-Q61L + Dox [1 µM]	($*^{1}$) <0.0001 / ($\#^{Q}$) 0.0006	($*^{1}$) 0.0011 / ($\#^{Q}$) 0.0044	($*^{1}$) <0.0001 / ($\#^{Q}$) 0.0033
TR + *mRac1* siRNA+ Dox [1 µM]	($*^{2}$) <0.0001	($*^{2}$) <0.0001	($*^{2}$) <0.0001
Q61L + *mRac1* siRNA+ Dox [1 µM]	($*^{2}$) <0.0001 / ($\#^{Q}$) <0.0001	($*^{2}$) 0.0001 / ($\#^{Q}$) 0.0077	($*^{2}$) <0.0001 / ($\#^{Q}$) <0.0001
NLS-Q61L + *mRac1* siRNA+ Dox [1 µM]	($*^{2}$) 0.0182 / ($\#^{QsiD}$) 0.0025 / ($\#^{N-Q}$) 0.7186	($*^{2}$) 0.9992 / ($\#^{QsiD}$) 0.0107 / ($\#^{N-Q}$) 0.0466	($*^{2}$) 0.8426 / ($\#^{QsiD}$) 0.0432 / ($\#^{N-Q}$) 0.5070

Table 7.27: Data from comparison of GFP-hRAC1(WT) with and without additional NLS, EHT 1864, and *mRac1* siRNA on doxorubicin induced γH2AX and 53BP1 foci formation. Cells were transfected with *GFP-hRAC1(WT)* or *GFP-NLS-hRAC1(WT)* expression vector. Transfection control cells were treated with TransIT-X2 (TR Con, TR), or with Lipofectamine RNAiMAX and TransIT-X2 (TR). 24 h after transfection cells were pre-treated with 30 µM EHT 1864 for 3 h prior to treatment with Dox [1 µM, 1 h] or were only treated with Dox [1 µM, 1 h]. *mRac1* knockdown was achieved by transfection with *mRac1* siRNA. The treatment scheme is shown in material and methods (Figure 2.1 E, F). Cells were additionally transfected with *GFP-hRAC1(WT)* or *GFP-NLS-hRAC1(WT)* expression vector. The mean values on which Figure 3.26 is based on are listed in the Table (n=3 - 38 with 50 nuclei counted per experiment). Abbreviations: TR Con: cells treated with TransIT-X2, TR: cells treated with TransIT-X2 only or with Lipofectamine RNAiMAX and TransIT-X2, WT: wild-type RAC1, NLS-WT: wild-type RAC1 with additional NLS, mRac1 *siRNA: siRNA against murine* Rac1, $*^1$: One way ANOVA, $*^2$: Two way ANOVA, $\#^{WT}$ vs WT + Dox, $\#_W{}^{TED}$ vs WT + EHT + Dox, $\#^{WTsiD}$ vs WT + siRNA + Dox, $\#^{N\text{-}WT}$ vs NLS-WT + Dox.

	γH2AX foci/nucleus mean ± SD	53BP1 foci/nucleus mean ± SD	colocalization foci/nucleus mean ± SD
TR Con	2.67 ± 1.18	1.53 ± 1.06	0.85 ± 0.57
TR + Dox [1 µM]	12.73 ± 1.84	9.81 ± 3.18	6.97 ± 1.83
WT + Dox [1 µM]	10.07 ± 1.19	7.73 ± 1.96	5.32 ± 1.23
NLS-WT + Dox [1 µM]	10.63 ± 2.68	8.42 ± 3.13	5.88 ± 1.85
TR + EHT 1864 [30 µM] + Dox [1 µM]	5.89 ± 2.21	4.90 ± 1.95	2.96 ± 1.03
WT + EHT 1864 [30 µM] + Dox [1 µM]	5.55 ± 1.69	2.57 ± 0.88	2.07 ± 1.00
NLS-WT + EHT 1864 [30 µM] + Dox [1 µM]	4.01 ± 2.30	4.40 ± 1.63	2.20 ± 1.01
TR + *mRac1* siRNA+ Dox [1 µM]	5.09 ± 1.32	3.92 ± 1.96	2.45 ± 1.19
WT + *mRac1* siRNA+ Dox [1 µM]	6.89 ± 2.50	3.25 ± 1.84	2.25 ± 1.44
NLS-WT + *mRac1* siRNA+ Dox [1 µM]	5.16 ± 1.35	4.33 ± 3.66	2.35 ± 1.29
	p value γH2AX vs TR ($*^1$,$*^2$) / GFP-hRAC1 ($\#^{WT}$, $\#^{WTED}$, $\#^{WTsiD}$, $\#^{N\text{-}WT}$)	p value 53BP1 vs TR ($*^1$,$*^2$) / GFP-hRAC1 ($\#^{WT}$, $\#^{WTED}$, $\#^{WTsiD}$, $\#^{N\text{-}WT}$)	p value colocalization vs TR ($*^1$,$*^2$) / GFP-hRAC1 ($\#^{WT}$, $\#^{WTED}$, $\#^{WTsiD}$, $\#^{N\text{-}WT}$)
WT + Dox [1 µM]	($*^1$) 0.0104	($*^1$) 0.1807	($*^1$) 0.05
NLS-WT + Dox [1 µM]	($*^1$) 0.0775 / ($\#^{WT}$) 0.6263	($*^1$) 0.4829 / ($\#^{WT}$) 0.6374	($*^1$) 0.2818 / ($\#^{WT}$) 0.5276
TR + EHT 1864 [30 µM] + Dox [1 µM]	($*^2$) <0.0001	($*^2$) <0.0001	($*^2$) <0.0001
WT + EHT 1864 [30 µM] + Dox [1 µM]	($*^2$) <0.0001 / ($\#^{WT}$) 0.0086	($*^2$) <0.0001/ ($\#^{WT}$) 0.0393	($*^2$) <0.0001 / ($\#^{WT}$) 0.0104
NLS-WT + EHT 1864 [30 µM] + Dox [1 µM]	($*^2$) <0.0001 / ($\#^{WTED}$) 0.9994 / ($\#^{N\text{-}WT}$) <0.0001	($*^2$) 0.0004 / ($\#^{WTED}$) 0.9998 / ($\#^{N\text{-}WT}$) 0.3530	($*^2$) <0.0001 / ($\#^{WTED}$) >0.9999 / ($\#^{N\text{-}WT}$) 0.0021
TR + *mRac1* siRNA + Dox [1 µM]	($*^2$) <0.0001	($*^2$) <0.0001	($*^2$) <0.0001
WT + *mRac1* siRNA + Dox [1 µM]	($*^2$) <0.0001 / ($\#^{WT}$) 0.2828	($*^2$) <0.0001 / ($\#^{WT}$) 0.1508	($*^2$) <0.0001 / ($\#^{WT}$) 0.0225
NLS-WT + *mRac1* siRNA + Dox [1 µM]	($*^2$) <0.0001 / ($\#^{WTsiD}$) 0.9975 / ($\#^{N\text{-}WT}$) 0.0005	($*^2$) 0.0003 / ($\#^{WTsiD}$) >0.9999 / ($\#^{N\text{-}WT}$) 0.3224	($*^2$) <0.0001 / ($\#^{WTsiD}$) >0.9999 / ($\#^{N\text{-}WT}$) 0.0043

Table 7.28: Data from comparison of GFP-hRAC1(Q61L) with and without additional NLS, EHT 1864, and *mRac1* siRNA on doxorubicin induced γH2AX and 53BP1 foci formation.
Cells were transfected with *GFP-hRAC1(Q61L)* or *GFP-NLS-hRAC1(Q61L)* expression vector. Transfection control cells were treated with TransIT-X2 (TR Con, TR), or with Lipofectamine RNAiMAX and TransIT-X2 (TR). 24 h after transfection cells were pre-treated with 30 µM EHT 1864 for 3 h prior to treatment with Dox [1 µM, 1 h] or were only treated with Dox [1 µM, 1 h]. *mRac1* knockdown was achieved by transfection with *mRac1* siRNA. The treatment scheme is shown in material and methods (Figure 2.1 E, F). Cells were additionally transfected with *GFP-hRAC1(Q61L)* or *GFP-NLS-hRAC1(Q61L)* expression vector. The mean values on which Figure 3.27 is based on are listed in the Table (n=3 - 38 with 50 nuclei counted per experiment). Abbreviations: TR Con: cells treated with TransIT-X2, TR: cells treated with TransIT-X2 only or with Lipofectamine RNAiMAX and TransIT-X2, Q61L: constitutively active RAC1, NLS-Q61L: constitutively active RAC1 with additional NLS, mRac1 *siRNA: siRNA against murine* Rac1, $*^1$: One way ANOVA, $*^2$: Two way ANOVA, $\#^{Q}$ vs Q61L + Dox, $\#^{QED}$ vs Q61L + EHT + Dox, $\#^{N-Q}$ vs NLS-Q61L + Dox.

	γH2AX foci/nucleus mean ± SD	53BP1 foci/nucleus mean ± SD	colocalization foci/nucleus mean ± SD
TR Con	2.67 ± 1.18	1.53 ± 1.06	0.85 ± 0.57
TR + Dox [1 µM]	12.73 ± 1.84	9.81 ± 3.18	6.97 ± 1.83
Q61L + Dox [1 µM]	12.32 ± 1.97	9.38 ± 2.56	6.73 ± 1.66
NLS-Q61L + Dox [1 µM]	6.54 ± 2.45	4.96 ± 1.75	3.34 ± 1.59
TR + EHT 1864 [30 µM] + Dox [1 µM]	5.89 ± 2.21	4.90 ± 1.95	2.96 ± 1.03
Q61L + EHT 1864 [30 µM] + Dox [1 µM]	7.40 ± 2.65	4.82 ± 1.18	3.20 ± 1.30
NLS-Q61L + EHT 1864 [30 µM] + Dox [1 µM]	6.07 ± 1.65	4.82 ± 1.30	2.62 ± 0.49
TR + *mRac1* siRNA+ Dox [1 µM]	5.09 ± 1.32	3.92 ± 1.96	2.45 ± 1.19
Q61L + *mRac1* siRNA+ Dox [1 µM]	2.49 ± 0.55	2.63 ± 3.13	1.39 ± 1.46
NLS-Q61L + *mRac1* siRNA+ Dox [1 µM]	9.00 ± 0.91	10.84 ± 2.01	5.69 ± 0.41
	p value γH2AX vs TR ($*^1$,$*^2$) / GFP-hRAC1 ($\#^{Q}$, $\#^{QED}$, $\#^{N-Q}$)	p value 53BP1 vs TR ($*^1$,$*^2$) / GFP-hRAC1 ($\#^{Q}$, $\#^{QED}$, $\#^{N-Q}$)	p value colocalization vs TR ($*^1$,$*^2$) / GFP-hRAC1 ($\#^{Q}$, $\#^{QED}$, $\#^{N-Q}$)
Q61L + Dox [1 µM]	($*^1$) 0.9849	($*^1$) 0.9149	($*^1$) 0.9252
NLS-Q61L + Dox [1 µM]	($*^1$) <0.0001 / ($\#^{Q}$) 0.0006	($*^1$) 0.0011 / ($\#^{Q}$) 0.0044	($*^1$) <0.0001 / ($\#^{Q}$) 0.0033
TR + EHT 1864 [30 µM] + Dox [1 µM]	($*^2$) <0.0001	($*^2$) <0.0001	($*^2$) <0.0001
Q61L + EHT 1864 [30 µM] + Dox [1 µM]	($*^2$) <0.0001 / ($\#^{Q}$) 0.0020	($*^2$) 0.0010 / ($\#^{Q}$) 0.1129	($*^2$) <0.0001 / ($\#^{Q}$) 0.0031
NLS-Q61L + EHT 1864 [30 µM] + Dox [1 µM]	($*^2$) <0.0001 / ($\#^{QED}$) >0.9999 / ($\#^{N-Q}$) >0.9999	($*^2$) 0.0010 / ($\#^{QED}$) >0.9999 / ($\#^{N-Q}$) >0.9999	($*^2$) <0.0001 / ($\#^{QED}$) >0.9999 / ($\#^{N-Q}$) >0.9999
TR + *mRac1* siRNA+ Dox [1 µM]	($*^2$) <0.0001	($*^2$) <0.0001	($*^2$) <0.0001
Q61L + *mRac1* siRNA+ Dox [1 µM]	($*^2$) <0.0001 / ($\#^{Q}$) <0.0001	($*^2$) <0.0001 / ($\#^{Q}$) 0.0065	($*^2$) <0.0001 / ($\#^{Q}$) <0.0001
NLS-Q61L + *mRac1* siRNA+ Dox [1 µM]	($*^2$) 0.0200 / ($\#^{QsiD}$) 0.0086 / ($\#^{N-Q}$) 0.9125	($*^2$) 0.9989 / ($\#^{QsiD}$) 0.0094 / ($\#^{N-Q}$) 0.0491	($*^2$) 0.7365 / ($\#^{QsiD}$) 0.0355 / ($\#^{N-Q}$) 0.5739

Table 7.29: Data from influence of human GFP-RAC1 expression and *mRac1* gene silencing on doxorubicin-induced pATM foci formation.
Cells were transiently transfected with *GFP-hRAC1(WT)*, *GFP-NLS-hRAC1(WT)*, *GFP-hRAC1(Q61L)*, or *GFP-NLS-hRAC1(Q61L)* expression vector or *mRac1* siRNA. Transfection control cells (TR Con, TR) were treated with transfection reagent (TransIT-X2). 24 h after transfection with *GFP-hRAC1* expression vectors or 48 h after transfection with *mRac1* siRNA cells were treated with Dox [1 µM, 1 h]. The mean values on which Figure 3.28 B is based on are listed in the Table (n=1 - 18 with 50 nuclei counted per experiment). Abbreviations: TR Con, TR: cells treated with TransIT-X2, WT: wild-type RAC1, NLS-WT: wild-type RAC1 with additional NLS, Q61L: constitutively active RAC1, NLS-Q61L: constitutively active RAC1 with additional NLS, *mRac1* siRNA: siRNA against murine *Rac1*.

	pATM foci/nucleus mean ± SD	p value vs TR (*)
TR Con	1.69 ± 1.62	
TR + Dox [1 µM]	6.74 ± 0.07	
WT + Dox [1 µM]	5.81 ± 0.99	(*) 0.9154
NLS-WT + Dox [1 µM]	6.47 ± 0.52	
Q61L + Dox [1 µM]	5.16 ± 2.98	(*) 0.6263
NLS-Q61L + Dox [1 µM]	5.96	
mRac1 siRNA + Dox [1 µM]	10.08 ± 4.29	(*) 0.05

Table 7.30: Data from influence of GFP-hRAC1(WT) with or without additional NLS on IR-induced γH2AX and 53BP1 foci formation.
Cells were transiently transfected with *GFP-hRAC1(WT)* or *GFP-NLS-hRAC1(WT)* expression vector. Transfection control cells (TR Con, TR) were treated with TransIT-X2. 24 h after transfection cells were irradiated [1 Gy, 3 Gy]. The mean values on which Figure 3.29 B is based on are listed in the Table (n=3 - 18 with 50 nuclei counted per experiment). Abbreviations: TR Con, TR: cells treated with TransIT-X2, WT: wild-type RAC1, NLS-WT: wild-type RAC1 with additional NLS, $*^1$: vs 1 Gy, $*^3$: vs 3 Gy.

	γH2AX foci/nucleus mean ± SD	53BP1 foci/nucleus mean ± SD	colocalization foci/nucleus mean ± SD
TR Con	3.41 ± 1.26	2.83 ± 1.93	1.37 ± 0.68
TR + IR [1 Gy]	17.16 ± 4.41	13.61 ± 4.88	9.69 ± 3.11
WT + IR [1 Gy]	14.70 ± 3.21	13.78 ± 1.90	9.75 ± 2.68
NLS-WT + IR [1 Gy]	15.45 ± 3.74	9.92 ± 2.06	9.26 ± 1.61
TR + IR [3 Gy]	25.39 ± 4.67	20.06 ± 4.63	14.24 ± 2.05
WT + IR [3 Gy]	20.93 ± 2.99	14.25 ± 5.30	9.77 ± 3.91
NLS-WT + IR [3 Gy]	16.89 ± 1.18	11.92 ± 1.59	10.35 ± 0.20
	p value γH2AX vs TR ($*^1$, $*^3$) / GFP-hRAC1 ($\#^1$, $\#^3$)	p value 53BP1 vs TR ($*^1$, $*^3$) / GFP-hRAC1 ($\#^1$, $\#^3$)	p value colocalization vs TR ($*^1$, $*^3$) / GFP-hRAC1 ($\#^1$, $\#^3$)
WT + IR [1 Gy]	($*^1$) 0.6280	($*^1$) 0.9999	($*^1$) >0.9999
NLS-WT + IR [1 Gy]	($*^1$) 0.8325 / ($\#^1$) 0.8051	($*^1$) 0.3587 / ($\#^1$) 0.0755	($*^1$) 0.9896 / ($\#^1$) 0.7995
WT + IR [3 Gy]	($*^3$) 0.1762	($*^3$) 0.0727	($*^3$) 0.0023
NLS-WT + IR [3 Gy]	($*^3$) 0.0030 / ($\#^3$) 0.0951	($*^3$) 0.0077 / ($\#^3$) 0.5062	($*^3$) 0.0082 / ($\#^3$) 0.8102

Table 7.31: Data from influence of GFP-hRAC1(Q61L) with or without additional NLS on IR-induced γH2AX and 53BP1 foci formation.
Cells were transiently transfected with *GFP-hRAC1(Q61L)* or *GFP-NLS-hRAC1(Q61L)* expression vector. Transfection control cells (TR Con, TR) were treated with TransIT-X2. 24 h after transfection cells were irradiated [1 Gy, 3 Gy]. The mean values on which Figure 3.30 B is based on are listed in the Table (n=3 - 18 with 50 nuclei counted per experiment). Abbreviations: TR Con, TR: cells treated with TransIT-X2, Q61L: constitutively active RAC1, NLS-Q61L: constitutively active RAC1 with additional NLS, *[1]: vs 1 Gy, *[3]: vs 3 Gy.

	γH2AX foci/nucleus mean ± SD	53BP1 foci/nucleus mean ± SD	colocalization foci/nucleus mean ± SD
TR Con	3.41 ± 1.26	2.83 ± 1.93	1.37 ± 0.68
TR + IR [1 Gy]	17.16 ± 4.41	13.61 ± 4.88	9.69 ± 3.11
Q61L + IR [1 Gy]	17.37 ± 0.77	10.91 ± 5.38	7.93 ± 3.33
NLS-Q61L + IR [1 Gy]	14.29 ± 4.79	11.46 ± 2.82	8.14 ± 2.30
TR + IR [3 Gy]	25.39 ± 4.67	20.06 ± 4.63	14.24 ± 2.05
Q61L + IR [3 Gy]	22.04 ± 5.39	17.33 ± 9.00	12.34 ± 3.95
NLS-Q61L + IR [3 Gy]	22.48 ± 3.66	17.93 ± 3.93	13.68 ± 0.34
	p value γH2AX vs TR (*[1], *[3]) / GFP-hRAC1 (#[1], #[3])	p value 53BP1 vs TR (*[1], *[3]) / GFP-hRAC1 (#[1], #[3])	p value colocalization vs TR (*[1], *[3]) / GFP-hRAC1 (#[1], #[3])
Q61L + IR [1 Gy]	(*[1]) 0.9996	(*[1]) 0.6541	(*[1]) 0.6286
NLS-Q61L + IR [1 Gy]	(*[1]) 0.5078 / (#[1]) 0.3332	(*[1]) 0.7885 / (#[1]) 0.8830	(*[1]) 0.7131 / (#[1]) 0.9327
Q61L + IR [3 Gy]	(*[3]) 0.4555	(*[3]) 0.6945	(*[3]) 0.3124
NLS-Q61L + IR [3 Gy]	(*[3]) 0.5691 / (#[3]) 0.9125	(*[3]) 0.8253 / (#[3]) 0.9208	(*[3]) 0.9502 / (#[3]) 0.5897

Table 7.32: Data from influence of GFP-hRAC1(T17N) with or without additional NLS on IR-induced γH2AX and 53BP1 foci formation.
Cells were transiently transfected with *GFP-hRAC1(T17N)* or *GFP-NLS-hRAC1(T17N)* expression vector. Transfection control cells (TR Con, TR) were treated with TransIT-X2. 24 h after transfection cells were irradiated [1 Gy, 3 Gy]. The mean values on which Figure 3.31 B is based on are listed in the Table (n=3 - 18 with 50 nuclei counted per experiment). Abbreviations: TR Con, TR: cells treated with TransIT-X2, T17N: dominant-negative RAC1, NLS-T17N: dominant-negative RAC1 with additional NLS, *[1]: vs 1 Gy, *[3]: vs 3 Gy.

	γH2AX foci/nucleus mean ± SD	53BP1 foci/nucleus mean ± SD	colocalization foci/nucleus mean ± SD
TR Con	3.41 ± 1.26	2.83 ± 1.93	1.37 ± 0.68
TR + IR [1 Gy]	17.16 ± 4.41	13.61 ± 4.88	9.69 ± 3.11
T17N + IR [1 Gy]	14.14 ± 0.13	8.35 ± 3.09	6.51 ± 1.57
NLS-T17N + IR [1 Gy]	11.07 ± 3.56	11.57 ± 4.62	7.23 ± 2.24
TR + IR [3 Gy]	25.39 ± 4.67	20.06 ± 4.63	14.24 ± 2.05
T17N + IR [3 Gy]	23.86 ± 6.25	16.20 ± 6.32	12.43 ± 3.10
NLS-T17N + IR [3 Gy]	22.19 ± 5.48	20.70 ± 3.92	14.01 ± 2.25

	p value γH2AX vs TR (*1, *3) / GFP-hRAC1 (#1, #3)	p value 53BP1 vs TR (*1, *3) / GFP-hRAC1 (#1, #3)	p value colocalization vs TR (*1, *3) / GFP-hRAC1 (#1, #3)
T17N + IR [1 Gy]	(*1) 0.4423	(*1) 0.1390	(*1) 0.1416
NLS-T17N + IR [1 Gy]	(*1) 0.0302 / (#1) 0.2098	(*1) 0.8076 / (#1) 0.3724	(*1) 0.3223 / (#1) 0.6721
T17N + IR [3 Gy]	(*3) 0.9120	(*3) 0.3687	(*3) 0.3438
NLS-T17N + IR [3 Gy]	(*3) 0.5369 / (#3) 0.7454	(*3) 0.9921 / (#3) 0.3538	(*3) 0.9961 / (#3) 0.5144

Table 7.33: Data from real-time qPCR analysis of *mRac1* knockout efficiency after lentiviral transduction with Puro.Cre vector in mouse embryonic fibroblasts with *mRac1* flanked by loxP sites (*Rac1*$^{flx/flx}$).
Cells were transduced with two concentrations of Puro.Cre vector (undiluted, 1:2 diluted) with and without protamine phosphate. Control cells (*Rac1*$^{flx/flx}$) are non-transduced. 24 h later puromycin selection was started. 144 h post transduction cells were analyzed by real-time qPCR. The mean values on which Figure 3.33 is based on are listed in the Table (n=5 - 7 in duplicates). Abbreviations: Con: non-transduced control cells (*Rac1*$^{flx/flx}$), PP: protamine phosphate, *1: One way ANOVA, *2: Two way ANOVA.

	knockout efficiency [%] mean ± SD	p value vs Con (*1, *2) / dilution w/o PP (#)
Con	1.88 ± 2.26	
undiluted vector	50.04 ± 20.74	(*1) 0.0005
1:2 diluted vector	38.25 ± 19.49	(*1) 0.0050 / (#) 0.2946
undiluted vector + PP	44.31 ± 21.20	(*2) 0.0009 / (#) 0.9884
1:2 diluted vector + PP	45.40 ± 17.71	(*2) 0.0010 / (#) 0.9741

Table 7.34: Data from flow cytometric analysis of cell cycle distribution and apoptosis after lentiviral transduction with Puro.Cre vector in mouse embryonic fibroblasts with *mRac1* flanked by loxP sites *(Rac1*$^{flx/flx}$*)*.
Cells were transduced with undiluted Puro.Cre vector and analyzed 144 h after puromycin selection. Control cells (*Rac1*$^{flx/flx}$) are non-transduced. Cells were lysed and the nuclei were stained with the DNA-intercalating agent propidium iodide. The cell cycle distribution was determined using a flow cytometer. The mean values on which Figure 3.34 is based on are listed in the Table (n=1). Abbreviations: Con: non-transduced control cells (*Rac1*$^{flx/flx}$), potential KO: cells transduced with Puro.Cre and selected with puromycin.

	SubG1 [%] mean	G1 [%] mean	G2/M [%] mean
Con	16.48	44.94	7.05
potential KO	91.33	4.83	0.52

Table 7.35: Data from real-time qPCR analysis of the *mRac1* knockout efficiency after lentiviral transduction with Puro.Cre vector in not properly attached mouse embryonic fibroblasts (*Rac1*$^{flx/flx}$).
Cells were transduced with undiluted Puro.Cre vector. 24 h later puromycin selection was started. 24 h - 144 h after transduction cells were washed with PBS and collected for real-time qPCR. Control cells (*Rac1*$^{flx/flx}$) were non-transduced. The mean values on which Figure 3.35 is based on are listed in the Table (n=1 - 4 in duplicates).

	24 h knockout efficiency [%] mean	48 h knockout efficiency [%] mean	72 h knockout efficiency [%] mean	96 h knockout efficiency [%] mean	144 h knockout efficiency [%] mean ± SD
0 µg/ml Puromycin	0.3	0.59	87.29		
1 µg/ml Puromycin	0.15	3.36	5.58	15.59	
2 µg/ml Puromycin	0.57	8.93	13.58	8.49	70.94 ± 31.86

Table 7.36: Data from impact of transduction itself and/or puromycin treatment on cell death in MEF *(Rac1*$^{flx/flx}$*)* transduced with Puro vector (puromycin resistance only).
MEF *(Rac1*$^{flx/flx}$*)* were transduced with Puro vector and harvested 96 h later. Meanwhile puromycin selection was performed [2 µg/ml]. Cells were lysed and the nuclei were stained with the DNA-intercalating agent propidium iodide. The cell cycle distribution was determined using a flow cytometer. Shown is the evaluation of the different fractions. The mean values on which Figure 3.36 is based on are listed in the Table (n=3).

	SubG1 [%] mean ± SD	G1 [%] mean ± SD	G2/M [%] mean ± SD
Puro vector	14.27 ± 9.08	63.75 ± 13.41	8.41 ± 0.08
Puro vector + Puromycin [2 µg/ml]	25.09 ± 16.90	48.06 ± 17.03	12.28 ± 2.88
	SubG1 p value vs Puro vector	G1 p value vs Puro vector	G2/M p value vs Puro vector
Puro vector + Puromycin [2 µg/ml]	0.3840	0.2782	0.0806

Table 7.37: Data from flow cytometric analysis of cell cycle distribution after lentiviral transduction with Puro.Cre vector and treatment with pan caspase inhibitor QVD.
MEF (*Rac1*$^{flx/flx}$) were plated on collagen-coated dishes, transduced with Puro.Cre vector and 24 h later permanently treated with QVD and puromycin. Cells were harvested after indicated time-points. Cells were lysed and the nuclei were stained with the DNA-intercalating agent propidium iodide. The cell cycle distribution was determined using a flow cytometer. Control cells (*Rac1*$^{flx/flx}$) were non-transduced. The mean values on which Figure 3.37 is based on are listed in the Table (n=1). Abbreviations: Con: control cells, virus: lentivirus containing Puro.Cre vector, QVD: Q-VD-OPh hydrate (pan caspase inhibitor).

24 h	SubG1 [%] mean	G1 [%] mean	G2/M [%] mean
Con	6.18	46.46	44.48
virus	37.73	25.76	35.70
virus + QVD [10 µM]	9.37	32.28	57.14

48 h	SubG1 [%] mean	G1 [%] mean	G2/M [%] mean
Con	4.39	62.49	31.07
virus	68.91	16.39	14.52
virus + QVD [10 µM]	22.41	39.71	36.85
72 h	SubG1 [%] mean	G1 [%] mean	G2/M [%] mean
Con	7.72	63.33	27.59
virus	58.89	24.27	16.22
virus + QVD [10 µM]	54.64	35.67	10.53
96 h	SubG1 [%] mean	G1 [%] mean	G2/M [%] mean
Con	29.32	53.11	17.33
virus	56.28	31.36	12.21
virus + QVD [10 µM]	55.97	29.85	14.19
120 h	SubG1 [%] mean	G1 [%] mean	G2/M [%] mean
Con	28.82	52.68	18.38
virus	77.42	17.98	4.84
virus + QVD [10 µM]	70.11	23.54	7.41

Table 7.38: Data from real-time qPCR analysis of *mRac1* knockout after lentiviral transduction with Puro.Cre vector and permanent treatment with a pan caspase inhibitor. MEF (*Rac1*$^{flx/flx}$) were transduced with undiluted Puro.Cre vector. 24 h later puromycin selection and QVD treatment were started. 24 h - 120 h after transduction cells were harvested for real-time qPCR. Control cells (*Rac1*$^{flx/flx}$) were non-transduced. The mean values on which Figure 3.38 is based on are listed in the Table (n=1 in duplicates). Abbreviations: Con: control cells, virus: lentivirus containing Puro.Cre vector, QVD: Q-VD-OPh hydrate (pan caspase inhibitor).

	24 h knockout efficiency [%] mean	48 h knockout efficiency [%] mean	72 h knockout efficiency [%] mean	96 h knockout efficiency [%] mean	120 h knockout efficiency [%] mean
Con	0.47				
virus	10.22	27.41	69.97	30.62	3.75
virus + QVD [10 µM]	14.12	24.93	10.97	8.57	11.56

Table 7.39: Data from real-time qPCR analysis of *mRac1* knockout after transfection with Cre Recombinase Gesicles in mouse embryonic fibroblasts (*Rac1*$^{flx/flx}$). MEF (*Rac1*$^{flx/flx}$) were transfected with Cre Recombinase Gesicles (10 µl and 25 µl). 48 h after transfection cells were analyzed by real-time qPCR. Control cells (*Rac1*$^{flx/flx}$) were non-transfected. The mean values on which Figure 3.39 is based on are listed in the Table (n=1 in duplicates).

properly attached cells	knockout efficiency [%] mean
0 µl Puro Cre Gesicles	0.25
10 µl Puro Cre Gesicles	5.92
25 µl Puro Cre Gesicles	19.56
lose attached cells	knockout efficiency [%] mean
10 µl Puro Cre Gesicles	13.46
25 µl Puro Cre Gesicles	3.32

Table 7.40: Data from influence of tamoxifen (4-OHT) treatment on expression of *mRac1* in stable Cre.ER expressing cells.
Cells were treated with 1 µM tamoxifen (4-OHT) for 5 min, 45 min, 90 min, 3 h, 6 h, 24 h, or 48 h. Cells treated for 24 h and 48 h were harvested after treatment, the other samples were post-incubated for 24 h before they were harvested. The mRNA expression of *mRac1*-wild-type was examined using quantitative real-time PCR. The relative mRNA expression of untreated, non-transduced cells was set to 1. The mean values on which Figure 3.42 is based on are listed in the Table (n=1 in duplicates).

	Cre.ER #1 *Rac1*-WT mean ± SEM	Cre.ER #4 *Rac1*-WT mean ± SEM
Con	1.00 ± 0.05	1.00 ± 0.13
5 min + tamoxifen [1 µM]	0.48 ± 0.11	0.63 ± 0.17
45 min + tamoxifen [1 µM]	0.57 ± 0.05	0.56 ± 0.09
90 min + tamoxifen [1 µM]	0.61 ± 0.02	0.66 ± 0.05
3 h + tamoxifen [1 µM]	1.22 ± 0.19	0.61 ± 0.03
6 h + tamoxifen [1 µM]	0.50 ± 0.03	0.50 ± 0.15
24 h + tamoxifen [1 µM]	0.64 ± 0.04	0.68 ± 0.11
48 h + tamoxifen [1 µM]	0.90 ± 0.05	1.01 ± 0.03

Table 7.41: Data from influence of tamoxifen (4-OHT) treatment on expression of *mRac1* in stable Cre.ER expressing MEF (*Rac1*$^{flx/flx}$).
Cells were treated with 1 µM, 10 µM, or 100 µM Tam (4-OHT) for 5 min, or 45 min and post-incubated for 24 h. The mRNA expression of *mRac1*-wild-type was examined using real-time RT-qPCR. The relative mRNA expression of untreated, non-transduced cells was set to 1. The mean values on which Figure 3.43 A, B is based on are listed in the Table (n=2 in duplicates).

	Cre.ER #1 *Rac1*-WT, 5 min mean ± SD	Cre.ER #1 *Rac1*-WT, 45 min mean ± SD	Cre.ER #4 *Rac1*-WT, 5 min mean ± SD	Cre.ER #4 *Rac1*-WT, 45 min mean ± SD
tamoxifen [0 µM]	1.00 ± 0.00	1.00 ± 0.00	1.00 ± 0.00	1.00 ± 0.00
tamoxifen [1 µM]	1.00 ± 0.02	0.96 ± 0.87	0.99 ± 0.08	0.93 ± 0.30
tamoxifen [10 µM]	1.20 ± 0.32	6.54 ± 7.08	1.03 ± 0.58	0.42 ± 0.30
tamoxifen [100 µM]	6.57 ± 8.50	17.91 ± 25.05	0.97 ± 0.97	0.56 ± 0.26

Table 7.42: Data from influence of tamoxifen (4-OHT) treatment on expression of *mRac1* in stable Cre.ER expressing MEF (*Rac1*$^{flx/flx}$).
Cells were treated with 1 µM Tam (4-OHT) on two consecutive days or three times (Monday, Wednesday, Friday) per week for two weeks. The mRNA expression of *mRac1*-wild-type was examined using real-time RT-qPCR. The relative mRNA expression of untreated, non-transduced cells was set to 1. The mean values on which Figure 3.43 C is based on are listed in the Table (n=2 in duplicates). Abbreviations: 2x: treatment on two consecutive days, 2x3x: treatment three times per week for two weeks.

	Cre.ER #1 *Rac1*-WT mean ± SD	Cre.ER #4 *Rac1*-WT mean ± SD
Con	1.00 ± 0.00	1.00 ± 0.00
2x tamoxifen [1 µM]	1.45 ± 1.56	0.46 ± 0.20
2x3x tamoxifen [1 µM]	0.16 ± 0.03	0.93 ± 0.78

Table 7.43: Data from fluorescence-based analysis of mRAC1 as well as GFP protein (with and without NLS) localization in non-transfected vs. transfected cells.
MEF were transiently transfected with *GFP* or *NLS-GFP* expression vector. Transfection control cells (TR Con) were treated with TransIT-X2. Control cells (NT Con) were non-transfected. The mean values of the evaluation of Figure 7.11 B is listed in the Table (n=3 with 50 cells counted per experiment). Abbreviations: NT Con: non-transfected control cells, TR Con: control cells treated with TransIT-X2, GFP: green fluorescent protein, NLS-GFP: green fluorescent protein with additional NLS.

	nucleus [%] mean ± SD	cytoplasm [%] mean ± SD	p value nucleus vs TR Con (*) / GFP (#)	p value cytoplasm vs NT Con (*) / GFP (#)
NT Con	19.43 ± 1.06	80.57 ± 1.06		
TR Con	18.92 ± 1.54	81.08 ± 1.54	(*) 0.9946	(*) 0.9946
GFP	36.34 ± 2.16	63.66 ± 2.16	(*) 0.0006	(*) 0.0006
NLS-GFP	47.36 ± 5.82	52.64 ± 5.82	(*) <0.0001 / (#) 0.0371	(*) <0.0001 / (#) 0.0371

Table 7.44: Data from cytoskeleton-staining in non-transfected cells and cells transfected with *GFP* or *NLS-GFP* expression vector.
MEF were transiently transfected with *GFP* or *NLS-GFP* expression vector. Transfection control cells (TR Con) were treated with TransIT-X2. Control cells (NT Con) were non-transfected. 24 h after transfection, cells were stained with phalloidin-TRITC. The mean values of the evaluation of Figure 7.12 B is listed in the Table (n=3 with 50 cells counted per experiment). Abbreviations: NT Con: non-transfected control cells, TR Con: control cells treated with TransIT-X2, GFP: green fluorescent protein, NLS-GFP: green fluorescent protein with additional NLS.

	lamellipodia mean ± SD	p value vs NT Con (*) / GFP (#)
NT Con	3.13 ± 0.53	
TR Con	2.82 ± 0.81	(*) 0.8078
GFP	2.96 ± 0.17	(*) 0.9807
NLS-GFP	3.08 ± 0.27	(*) 0.9994 / (#) 0.5503

Table 7.45: Data from cytoskeleton-staining in non-transfected cells and cells transfected with *GFP* or *NLS-GFP* expression vector.
MEF were transiently transfected with *GFP* or *NLS-GFP* expression vector. Transfection control cells (TR Con) were treated with TransIT-X2. Control cells (NT Con) were non-transfected. 24 h after transfection, cells were stained with phalloidin-TRITC. The mean values of the evaluation of Figure 7.12 C is listed in the Table (n=3 with 50 cells counted per experiment). Abbreviations: NT Con: non-transfected control cells, TR Con: control cells treated with TransIT-X2, GFP: green fluorescent protein, NLS-GFP: green fluorescent protein with additional NLS.

	stress fibers mean ± SD	p value vs NT Con (*) / GFP (#)
NT Con	2.80 ± 0.29	
TR Con	2.72 ± 0.17	(*) 0.7644
GFP	2.62 ± 0.06	(*) 0.4226
NLS-GFP	2.69 ± 0.13	(*) 0.7489 / (#) 0.4448

Table 7.46: Data from cytoskeleton-staining in non-transfected cells and cells transfected with *GFP* or *NLS-GFP* expression vector.

MEF were transiently transfected with *GFP* or *NLS-GFP* expression vector. Transfection control cells (TR Con) were treated with TransIT-X2. Control cells (NT Con) were non-transfected. 24 h after transfection, cells were stained with phalloidin-TRITC. The mean values of the evaluation of Figure 7.12 D is listed in the Table (n=3 with 50 cells counted per experiment). Abbreviations: NT Con: non-transfected control cells, TR Con: control cells treated with TransIT-X2, GFP: green fluorescent protein, NLS-GFP: green fluorescent protein with additional NLS.

	Membrane ruffles [%] mean ± SD	p value vs NT Con (*) / GFP (#)
NT Con	100.00 ± 0.00	
TR Con	96.42 ± 3.28	(*) 0.1425
GFP	95.33 ± 2.31	(*) 0.1540
NLS-GFP	98.00 ± 2.00	(*) 0.7272 / (#) 0.2047

Table 7.47: Data from influence of GFP-hRAC1(T17N) and GFP-NLS-hRAC1(T17N) expression itself on basal γH2AX and 53BP1 foci formation.

MEF were transiently transfected with *GFP-hRAC1(T17N)*, *GFP-NLS-hRAC1(T17N)*, *GFP*, or *NLS-GFP* expression vector. Transfection control cells (TR Con, TR) were treated with TransIT-X2. Control cells (NT Con, NT) were non-transfected. Next day cells were treated with Dox [1 µM] for 1 h. The mean values of the evaluation of Figure 7.13 B is listed in the Table (n=1 - 38 with 50 cells counted per experiment). Abbreviations: NT Con, NT: non-transfected cells, TR Con, TR: cells treated with transfection reagent (TransIT-X2), T17N: dominant-negative RAC1, NLS-T17N: dominant-negative RAC1 with additional NLS, GFP: green fluorescent protein, NLS-GFP: green fluorescent protein with NLS.

	γH2AX foci/nucleus mean ± SD	53BP1 foci/nucleus mean ± SD	colocalization foci/nucleus mean ± SD
NT Con	2.41 ± 1.15	1.33 ± 0.83	0.68 ± 0.42
TR Con	2.67 ± 1.18	1.53 ± 1.06	0.85 ± 0.57
T17N	3.12 ± 0.44	0.89 ± 0.42	0.57 ± 0.20
NLS-T17N	2.05 ± 1.00	1.03 ± 0.30	0.67 ± 0.23
GFP	3.27 ± 0.18	1.33 ± 1.03	0.89 ± 0.64
NT + Dox [1 µM]	13.11 ± 3.32	8.92 ± 3.37	6.71 ± 2.47
TR + Dox [1 µM]	12.73 ± 1.84	9.81 ± 3.18	6.97 ± 1.83
GFP + Dox [1 µM]	9.90± 0.81	6.57 ± 0.86	5.30 ± 1.10
NLS-GFP+ Dox [1 µM]	10.08	6.70	6.56
	p value γH2AX vs NT Con (*) / NT (#)	p value 53BP1 vs NT Con (*) / NT (#)	p value colocalization vs NT Con (*) / NT (#)
TR Con	(*) 0.8832	(*) 0.9049	(*) 0.6407
T17N	(*) 0.7572	(*) 0.8937	(*) 0.9927
NLS-T17N	(*) 0.9727	(*) 0.9711	(*) >0.9999
GFP	(*) 0.7515	(*) >0.9999	(*) 0.9595
TR + Dox [1 µM]	(#) 0.5489	(#) 0.4666	(#) 0.8544
GFP + Dox [1 µM]	(#) 0.1701	(#) 0.5382	(#) 0.5906

Table 7.48: Data from western blot analysis in non-transfected cells and cells expressing GFP after doxorubicin treatment.
MEF were transiently transfected with *GFP* expression vector or left un-transfected. 24 h after transfection cells were 2 h pulse-treated with 1 µM Dox. Cells were harvested after indicated time-points. Afterwards cells were lysed, and protein extracts were analyzed by western blot analysis as described in methods. The fluorescence intensities of the proteins were determined with ImageLab. Non-transfected cells treated with 1 µM Dox were set to 1. The mean values on which Figure 7.14 B is based on are listed in the Table (n=3). Abbreviations: Con: non-transfected control cells, GFP: green fluorescent protein.

pKAP1 0 h	Experiment 1 Protein normalized	Experiment 2 Protein normalized	Experiment 3 Protein normalized	mean ± SD	p value vs Dox
Con	0.10	0.00	0.00	0.03 ± 0.06	
GFP	0.44	0.00	0.07	0.17 ± 0.23	
1 µM Dox	1.00	1.00	1.00	1.00 ± 0.00	
GFP + 1 µM Dox	1.11	1.84	1.00	1.32 ± 0.46	0.3565
pKAP1 4 h	Experiment 1 Protein normalized	Experiment 2 Protein normalized	Experiment 3 Protein normalized	mean ± SD	p value vs Dox
Con	0.26	0.00	0.00	0.09 ± 0.15	
GFP	0.24	0.00	0.49	0.24 ± 0.24	
1 µM Dox	1.00	1.00	1.00	1.00 ± 0.00	
GFP + 1 µM Dox	0.87	1.00	2.24	1.37 ± 0.76	0.5710
pKAP1 24 h	Experiment 1 Protein normalized	Experiment 2 Protein normalized	Experiment 3 Protein normalized	mean ± SD	p value vs Dox
Con	0.93	0.00	0.00	0.31 ± 0.53	
GFP	1.82	0.00	0.55	0.79 ± 0.93	
1 µM Dox	1.00	1.00	1.00	1.00 ± 0.00	
GFP + 1 µM Dox	1.50	0.15	1.17	0.94 ± 0.70	0.9988
γH2AX 0 h	Experiment 1 Protein normalized	Experiment 2 Protein normalized	Experiment 3 Protein normalized	mean ± SD	p value vs Dox
Con	0.11	0.60	0.93	0.55 ± 0.41	
GFP	0.38	0.40	0.62	0.46 ± 0.14	
1 µM Dox	1.00	1.00	1.00	1.00 ± 0.00	
GFP + 1 µM Dox	1.74	1.06	1.06	1.29 ± 0.39	0.5107
γH2AX 4 h	Experiment 1 Protein normalized	Experiment 2 Protein normalized	Experiment 3 Protein normalized	mean ± SD	p value vs Dox
Con	0.00	0.00	0.87	0.29 ± 0.50	
GFP	0.00	0.00	1.41	0.47 ± 0.81	
1 µM Dox	1.00	1.00	1.00	1.00 ± 0.00	
GFP + 1 µM Dox	1.65	1.08	1.64	1.46 ± 0.33	0.5704

γH2AX 24 h	Experiment 1 Protein normalized	Experiment 2 Protein normalized	Experiment 3 Protein normalized	mean ± SD	p value vs Dox)
Con	0.00	0.00	0.86	0.29 ± 0.50	
GFP	0.00	0.04	1.58	0.54 ± 0.90	
1 µM Dox	1.00	1.00	1.00	1.00 ± 0.00	
GFP + 1 µM Dox	0.51	0.62	1.57	0.90 ± 0.58	0.9933
pP53 0 h	Experiment 1 Protein normalized	Experiment 2 Protein normalized	Experiment 3 Protein normalized	mean ± SD	p value vs Dox
Con	0.00	0.00	0.50	0.17 ± 0.29	
GFP	0.00	0.13	0.13	0.09 ± 0.08	
1 µM Dox	1.00	1.00	1.00	1.00 ± 0.00	
GFP + 1 µM Dox	1.02	0.86	0.36	0.75 ± 0.34	0.4382
pP53 4 h	Experiment 1 Protein normalized	Experiment 2 Protein normalized	Experiment 3 Protein normalized	mean ± SD	p value vs Dox
Con	0.00	0.00	0.00	0.00 ± 0.00	
GFP	0.00	0.22	0.36	0.19 ± 0.18	
1 µM Dox	1.00	1.00	1.00	1.00 ± 0.00	
GFP + 1 µM Dox	1.51	1.01	1.55	1.36 ± 0.30	0.0852
24 h	Experiment 1 Protein normalized	Experiment 2 Protein normalized	Experiment 3 Protein normalized	mean ± SD	p value vs Dox
Con	0.00	0.00	1.46	0.49 ± 0.84	
GFP	0.00	0.61	0.86	0.49 ± 0.44	
1 µM Dox	1.00	1.00	1.00	1.00 ± 0.00	
GFP + 1 µM Dox	1.08	0.92	0.77	0.92 ± 0.15	0.9936
mRAC1 0 h	Experiment 1 Protein normalized	Experiment 2 Protein normalized	Experiment 3 Protein normalized	mean ± SD	p value vs Dox
Con	0.22	1.29	1.27	0.93 ± 0.61	
GFP	0.81	0.95	0.32	0.69 ± 0.33	
1 µM Dox	1.00	1.00	1.00	1.00 ± 0.00	
GFP + 1 µM Dox	0.60	1.02	0.24	0.62 ± 0.39	0.5394
mRAC1 4 h	Experiment 1 Protein normalized	Experiment 2 Protein normalized	Experiment 3 Protein normalized	mean ± SD	p value vs Dox
Con	1.29	1.69	3.26	2.08 ± 1.04	
GFP	0.79	1.19	1.32	1.10 ± 0.27	
1 µM Dox	1.00	1.00	1.00	1.00 ± 0.00	
GFP + 1 µM Dox	0.59	0.88	1.87	1.11 ± 0.67	0.9929

mRAC1 24 h	Experiment 1 Protein normalized	Experiment 2 Protein normalized	Experiment 3 Protein normalized	mean ± SD	p value vs Dox
Con	2.39	1.09	1.52	1.67 ± 0.67	
GFP	1.33	0.54	3.00	1.67 ± 1.26	
1 µM Dox	1.00	1.00	1.00	1.00 ± 0.00	
GFP + 1 µM Dox	1.99	0.74	1.83	1.52 ± 0.68	0.7646

Table 7.49: Data from influence of the transfection itself and EHT 1864 treatment on basal γH2AX and 53BP1 foci formation.
MEF were transiently transfected with *GFP-hRAC1(T17N)*, *GFP-NLS-hRAC1(T17N)*, or *GFP* expression vector Transfection control cells (TR Con, TR) were treated with TransIT-X2. Control cells (NT Con, NT) were non-transfected. 24 h after transfection cells were pre-treated with 30 µM EHT 1864 for 3 h prior to treatment with Dox [1 µM, 1 h]. The mean values of the evaluation of Figure 7.15 B is listed in the Table (n=3 - 28 with 50 nuclei counted per experiment). Abbreviations: NT Con, NT: non-transfected cells, TR Con, TR: cells treated with TransIT-X2, T17N: dominant-negative RAC1, NLS-T17N: dominant-negative RAC1 with additional NLS, GFP: green fluorescent protein, $\#^{D}$ vs NT + Dox, $\#^{ED}$ vs NT + EHT + Dox.

	γH2AX foci/nucleus mean ± SD	53BP1 foci/nucleus mean ± SD	colocalization foci/nucleus mean ± SD
NT Con	2.41 ± 1.15	1.33 ± 0.83	0.68 ± 0.42
NT Con + EHT 1864 [30 µM]	2.48 ± 0.17	1.11 ± 0.28	0.90 ± 0.26
TR Con + EHT 1864 [30 µM]	2.44 ± 1.20	1.64 ± 1.16	0.76 ± 0.42
T17N + EHT 1864 [30 µM]	1.82 ± 1.47	1.05 ± 0.16	0.42 ± 0.29
NLS-T17N + EHT 1864 [30 µM]	1.83 ± 0.72	1.17 ± 0.57	0.57 ± 0.35
GFP + EHT 1864 [30 µM]	2.92 ± 0.37	0.85 ± 0.22	0.67 ± 0.22
NT + Dox [1 µM]	13.11 ± 3.32	8.92 ± 3.37	6.71 ± 2.47
NT + EHT 1864 [30 µM] + Dox [1 µM]	8.02 ± 0.64	7.20 ± 0.32	4.10 ± 0.10
TR + EHT 1864 [30 µM] + Dox [1 µM]	5.72 ± 2.09	4.47 ± 2.19	2.70 ± 1.19
GFP + EHT 1864 [30 µM] + Dox [1 µM]	4.39 ± 0.80	3.46 ± 0.84	2.57 ± 0.83

	p value γH2AX vs NT Con (*) / NT (#^{D}, #^{ED}) / GFP-hRAC1 (+)	p value 53BP1 vs NT Con (*) / NT (#) / GFP-hRAC1 (+)	p value colocalization vs NT Con (*) / NT (#) / GFP-hRAC1 (+)
NT Con + EHT 1864 [30 µM]	(*) >0.9999	(*) 0.9996	(*) 0.9911
TR Con + EHT 1864 [30 µM]	(*) >0.9999	(*) 0.9419	(*) 0.9976
T17N + EHT 1864 [30 µM]	(*) 0.9851	(*) 0.9994	(*) 0.9730
NLS-T17N + EHT 1864 [30 µM]	(*) 0.9868 / (+) >0.9999	(*) 0.9997/ (+) >0.9999	(*) 0.9996/ (+) >0.9999
GFP + EHT 1864 [30 µM]	(*) 0.9932	(*) 0.9891	(*) >0.9999
NT + EHT 1864 [30 µM] + Dox [1 µM]	(#^{D}) 0.0004	(#^{D}) 0.8545	(#^{D}) 0.0312
TR + EHT 1864 [30 µM] + Dox [1 µM]	(#^{D}) 0.0001 / (#^{ED}) 0.6885	(#^{D}) <0.0001/ (#^{ED}) 0.6689	(#^{D}) <0.0001/ (#^{ED}) 0.8686
GFP + EHT 1864 [30 µM] + Dox [1 µM]	(#^{D}) <0.0001/ (#^{ED}) 0.4397	(#^{D}) 0.0015/ (#^{ED}) 0.6226	(#^{D}) <0.0001/ (#^{ED}) 0.9563

Table 7.50: Data from transfection with *mRac1* siRNA efficiently reduced intrinsic mRAC1 protein expression.
Cells were analyzed 24 h and 48 h after transfection with siRNA against *mRac1*. Cells were lysed and protein extracts were analyzed by western blot analysis as described in methods. The fluorescence intensities of the proteins were determined with ImageLab. Non-transfected cells were set to 1. The mean values on which **Figure 7.16** B is based on are listed in the Table (n=2). Abbreviations: Con: non-transfected control cells, *mRac1* siRNA: cells transfected siRNA against murine *Rac1*.

mRAC1 24 h	Experiment 1 Protein normalized	Experiment 2 Protein normalized	mean ± SD
Con	1.00	1.00	1.00 ± 0.00
mRac1 siRNA	1.06	0.02	0.54 ± 0.74
mRAC1 48 h	Experiment 1 Protein normalized	Experiment 2 Protein normalized	mean ± SD
Con	1.00	1.00	1.00 ± 0.00
mRac1 siRNA	0.17	0.05	0.11 ± 0.90

Table 7.51: Data from transfection with *mRac1* siRNA efficiently reduced intrinsic mRAC1 protein expression while expression of human GFP-RAC1 was not affected.
Cells were transfected with *mRac1* siRNA/human *GFP-RAC1* expression vector only, co-transfected with *mRac1* siRNA and human *GFP-RAC1* expression vector or left non-transfected. Cells were harvested 48 h after transfection with *mRac1* siRNA. Afterwards, cells were lysed, and protein extracts were analyzed by western blot analysis as described in methods. The fluorescence intensities of the proteins were determined with ImageLab. The protein expression of control cells was set to 1 (mRAC1); the protein expression of cells transfected only with *GFP-hRAC1* expression vector was set to 1 (GFP-hRAC1). The mean values on which Figure 7.17 B is based on are listed in the Table (n=1). Abbreviations: Con: non-transfected control cells, GFP-hRAC1: cells transfected with *GFP-hRAC1* expression vector, *mRac1* siRNA: cells transfected siRNA against murine *Rac1.*

mRAC1 48 h	Experiment 1 Protein normalized
Con	1.00
GFP-hRAC1	0.79
mRac1 siRNA	0.08
GFP-hRAC1 + *mRac1* siRNA	0.00
GFP-hRAC1 48 h	Experiment 1 Protein normalized
Con	0.00
GFP-hRAC1	1.00
mRac1 siRNA	0.00
GFP-hRAC1 + *mRac1* siRNA	1.40

Table 7.52: Data from influence of single and double transfection on basal γH2AX and 53BP1 foci formation.
mRac1 knockdown was achieved by transfection with *mRac1* siRNA. The treatment scheme is shown in material and methods (Figure 2.1 E, F). Cells were additionally transfected with *GFP-hRAC1(T17N)* or *GFP-NLS-hRAC1(T17N)* expression vector. The mean values of the evaluation of Figure 7.18 B is listed in the Table (n=2 - 28 with 50 nuclei counted per experiment). Abbreviations: NT Con, NT: non-transfected cells, TR Con, TR: cells treated with transfection reagent (Lipofectamine RNAiMAX), *mRac1* siRNA: siRNA against murine *Rac1*, NS siRNA: non-silencing siRNA, T17N: dominant-negative RAC1, NLS-T17N: dominant-negative RAC1 with additional NLS.

	γH2AX foci/nucleus mean ± SD	53BP1 foci/nucleus mean ± SD	colocalization foci/nucleus mean ± SD
NT Con	2.69 ± 0.85	1.85 ± 1.21	0.81 ± 0.49
TR Con	2.10 ± 1.24	1.59 ± 1.32	0.74 ± 0.56
mRac1 siRNA	2.89 ± 1.17	1.51 ± 1.06	1.00 ± 0.66
NS siRNA	3.20 ± 0.75	1.87 ± 1.59	1.00 ± 0.68
T17N + *mRac1* siRNA	2.17 ± 1.55	0.78 ± 0.35	0.47 ± 0.31
NLS-T17N + *mRac1* siRNA	1.19 ± 0.95	1.59 ± 0.98	0.61 ± 0.55
NS siRNA + Dox [1 µM]	12.24 ± 2.95	6.95 ± 3.88	5.49 ± 2.67
NT + Dox [1 µM]	13.11 ± 3.32	8.92 ± 3.37	6.71 ± 2.47

	p value γH2AX vs NT Con (*) / NT (#) / GFP-hRAC1 (+)	p value 53BP1 vs NT Con (*) / NT (#) / GFP-hRAC1 (+)	p value colocalization vs NT Con (*) / NT (#) / GFP-hRAC1 (+)
TR Con	(*) 0.5034	(*) 0.9926	(*) 0.9996
mRac1 siRNA	(*) 0.9951	(*) 0.9635	(*) 0.9081
NS siRNA	(*) 0.7541	(*) >0.9999	(*) 0.9460
T17N + *mRac1* siRNA	(*) 0.9714	(*) 0.6606	(*) 0.9201
NLS-T17N + *mRac1* siRNA			
NS siRNA + Dox [1 µM]	(#) 0.7669	(#) 0.2177	(#) 0.3183

Table 7.53: Data from influence of dominant-negative hRAC1 expression on basal pATM foci formation.
Cells were transiently transfected with *GFP-hRAC1(T17N)*, *GFP-NLS-hRAC1(T17N)* or *GFP* expression vector. Transfection control cells (TR Con, TR) were treated with TransIT-X2. Control cells (NT Con, NT) were non-transfected. 24 h after transfection cells were treated with Dox [1 µM, 1 h]. The mean values of the evaluation of Figure 7.19 B is listed in the Table (n=2 - 18 with 50 nuclei counted per experiment). Abbreviations: NT Con, NT: non-transfected cells, TR Con, TR: cells treated with TransIT-X2, T17N: dominant-negative RAC1, NLS-T17N: dominant-negative RAC1 with additional NLS.

	pATM foci/nucleus mean ± SD	p value vs NT Con (*) / NT (#)
NT Con	1.06 ± 1.03	
TR Con	1.69 ± 1.62	(*) 0.5098
T17N	1.22 ± 1.24	(*) 0.9993
NLS-T17N	1.61 ± 1.61	(*) 0.9398
GFP	0.89 ± 1.20	
NT + Dox [1 µM]	9.72 ± 2.96	
TR + Dox [1 µM]	6.74 ± 2.07	(#) 0.0714
GFP + Dox [1 µM]	4.53 ± 2.28	

Table 7.54: Data from influence of human GFP-RAC1 expression itself on basal γH2AX and 53BP1 foci formation.
MEF were transiently transfected with *GFP-hRAC1(WT)*, *GFP-NLS-hRAC1(WT)*, *GFP-hRAC1(Q61L)*, or *GFP-NLS-hRAC1(Q61L)* expression vector. Transfection control cells (TR Con, TR) were treated with TransIT-X2. Control cells (NT Con, NT) were non-transfected. The mean values of the evaluation of Figure 7.20 B is listed in the Table (n=3 - 25 with 50 cells counted per experiment). Abbreviations: NT Con: non-transfected cells, TR Con: cells treated with transfection reagent (TransIT-X2), WT: wild-type RAC1, NLS-WT: wild-type RAC1 with additional NLS, Q61L: constitutively active RAC1, NLS-Q61L: constitutively active RAC1 with additional NLS.

	γH2AX foci/nucleus mean ± SD	53BP1 foci/nucleus mean ± SD	colocalization foci/nucleus mean ± SD
NT Con	2.41 ± 1.15	1.33 ± 0.83	0.68 ± 0.42
TR Con	2.67 ± 1.18	1.53 ± 1.06	0.85 ± 0.57
WT	2.25 ± 1.20	1.57 ± 0.44	0.79 ± 0.22
NLS-WT	2.56 ± 1.52	1.02 ± 0.59	0.73 ± 0.41
Q61L	2.55 ± 0.39	1.47 ± 0.22	0.59 ± 0.06
NLS-Q61L	2.23 ± 1.19	1.01 ± 0.12	0.57 ± 0.15

	p value γH2AX vs NT Con	p value 53BP1 vs NT Con	p value colocalization vs NT Con
TR Con	0.9377	0.9378	0.6889
WT	0.9997	0.9949	0.9971
NLS-WT	0.9997	0.9835	0.9998
Q61L	0.9997	0.9997	0.9986
NLS-Q61L	0.9997	0.9810	0.9971

Table 7.55: Data from influence of EHT 1864 treatment on basal γH2AX and 53BP1 foci formation.
MEF were transiently transfected with *GFP-hRAC1(WT)*, *GFP-NLS-hRAC1(WT)*, *GFP-hRAC1(Q61L)*, or *GFP-NLS-hRAC1(Q61L)* expression vector. Transfection control cells (TR Con, TR) were treated with TransIT-X2. Control cells (NT Con, NT) were non-transfected. 24 h after transfection cells were treated with 30 µM EHT 1864 for 3 h. The mean values of the evaluation of Figure 7.21 B is listed in the Table (n=3 - 23 with 50 nuclei counted per experiment). Abbreviations: NT Con: non-transfected cells, TR Con: cells treated with TransIT-X2, WT: wild-type RAC1, NLS-WT: wild-type RAC1 with additional NLS, Q61L: constitutively active RAC1, NLS-Q61L: constitutively active RAC1 with additional NLS.

	γH2AX foci/nucleus mean ± SD	53BP1 foci/nucleus mean ± SD	colocalization foci/nucleus mean ± SD
NT Con	2.14 ± 1.15	1.33 ± 0.83	0.68 ± 0.42
NT Con + EHT 1864 [30 µM]	2.48 ± 0.17	1.11 ± 0.28	0.90 ± 0.26
TR Con + EHT 1864 [30 µM]	2.44 ± 1.20	1.64 ± 1.16	0.76 ± 0.42
WT + EHT 1864 [30 µM]	1.69 ± 1.21	0.61 ± 0.42	0.32 ± 0.28
NLS-WT + EHT 1864 [30 µM]	1.78 ± 1.53	1.26 ± 0.66	0.63 ± 0.50
Q61L + EHT 1864 [30 µM]	3.09 ± 0.11	2.11 ± 1.24	0.67 ± 0.40
NLS-Q61L + EHT 1864 [30 µM]	2.02 ± 0.91	2.23 ± 0.95	0.77 ± 0.21
	p value γH2AX vs NT Con (*) / GFP-hRAC1 (#)	p value 53BP1 vs NT Con (*) / GFP-hRAC1 (#)	p value colocalization vs NT Con (*) / GFP-hRAC1 (#)
NT Con + EHT 1864 [30 µM]	(*) >0.9999	(*) 0.9996	(*) 0.9934
TR Con + EHT 1864 [30 µM]	(*) >0.9999	(*) 0.9641	(*) 0.9993
WT + EHT 1864 [30 µM]	(*) 0.9754	(*) 0.9104	(*) 0.8710
NLS-WT + EHT 1864 [30 µM]	(*) 0.9907 / (#) >0.9999	(*) 0.9999 / (#) 0.9994	(*) 0.9998 / (#) 0.9993
Q61L + EHT 1864 [30 µM]	(*) 0.9843	(*) 0.8608	(*) > 0.9999
NLS-Q61L + EHT 1864 [30 µM]	(*) 0.9994 / (#) 0.9922	(*) 0.8876 / (#) >0.9999	(*) 0.9997 / (#) >0.9999

Table 7.56: Data from influence of single and double transfection on basal γH2AX and 53BP1 foci formation.
mRac1 knockdown was achieved by transfection with *mRac1* siRNA. The treatment scheme is shown in material and methods (Figure 2.1 E, F). Cells were additionally transfected with *GFP-hRAC1(WT)*, *GFP-NLS-hRAC1(WT)*, *GFP-hRAC1(Q61L)*, or *GFP-NLS-hRAC1(Q61L)* expression vector. The mean values of the evaluation of Figure 7.22 B is listed in the Table (n=2 - 20 with 50 nuclei counted per experiment). Abbreviations: NT Con: non-transfected cells, TR Con: cells treated with Lipofectamine RNAiMAX and TransIT-X2, WT: wild-type RAC1, NLS-WT: wild-type RAC1 with additional NLS, Q61L: constitutively active RAC1, NLS-Q61L: constitutively active RAC1 with additional NLS.

	γH2AX foci/nucleus mean ± SD	53BP1 foci/nucleus mean ± SD	colocalization foci/nucleus mean ± SD
NT Con	2.69 ± 0.85	1.85 ± 1.21	0.81 ± 0.49
TR Con	2.10 ± 1.24	1.59 ± 1.32	0.74 ± 0.56
WT + *mRac1* siRNA	2.72 ± 1.06	2.07 ± 1.70	0.87 ± 0.62
NLS-WT + *mRac1* siRNA	2.17 ± 1.14	2.11 ± 0.84	0.92 ± 0.40
Q61L + *mRac1* siRNA	2.18 ± 1.61	0.76 ± 0.23	0.48 ± 0.03
NLS-Q61L + *mRac1* siRNA	1.94 ± 0.28	1.17 ± 0.64	0.69 ± 0.38
	p value γH2AX vs NT Con (*) / GFP-hRAC1 (#)	p value 53BP1 vs NT Con (*) / GFP-hRAC1 (#)	p value colocalization vs NT Con (*) / GFP-hRAC1 (#)
TR Con	(*) 0.9993	(*) 0.9992	(*) 0.9996
WT + *mRac1* siRNA	(*) >0.9999	(*) 0.9997	(*) 0.9998
NLS-WT + *mRac1* siRNA	(*) 0.9959 / (#) >0.9999	(*) 0.9996 / (#) >0.9999	(*) 0.9996 / (#) >0.9999

Table 7.57: Data from influence of the transfection methods on basal pATM foci formation.
Cells were transiently transfected with *GFP-hRAC1(WT)*, *GFP-NLS-hRAC1(WT)*, *GFP-hRAC1(Q61L)*, or *GFP-NLS-hRAC1(Q61L)* expression vector or *mRac1* siRNA. Transfection control cells (TR Con) were treated with TransIT-X2. Control cells (NT Con) were non-transfected. 24 h after transfection with *GFP-hRAC1* expression vectors or 48 h after transfection with *mRac1* siRNA cells were fixed and staining of pATM foci was carried out as described in methods. The mean values of the evaluation of Figure 7.23 B is listed in the Table (n=1 - 18 with 50 nuclei counted per experiment). Abbreviations: NT Con: non-transfected cells, TR Con: cells treated with TransIT-X2, WT: wild-type RAC1, NLS-WT: wild-type RAC1 with additional NLS, Q61L: constitutively active RAC1, NLS-Q61L: constitutively active RAC1 with additional NLS, *mRac1* siRNA: siRNA against murine *Rac1*.

	pATM foci/nucleus mean ± SD	p value vs NT Con
NT Con	1.06 ± 1.03	
TR Con	1.69 ± 1.62	0.5417
WT	1.95 ± 2.38	0.7629
NLS-WT	0.54 ± 0.28	
Q61L	1.83 ± 1.49	0.8423
NLS-Q61L	2.34	
mRac1 siRNA	0.68 ± 0.85	0.9857

Table 7.58: Data from influence of GFP as part of the plasmids on IR-induced foci formation.

Cells were transiently transfected with *GFP* expression vector. Transfection control cells (TR Con, TR) were treated with TransIT-X2. Control cells (NT Con, NT) were non-transfected. Cells were irradiated with 1 Gy or 3 Gy. The mean values of the evaluation of Figure 7.24 B is listed in the Table (n=3 - 24 with 50 nuclei counted per experiment). Abbreviations: NT Con, NT: non-transfected cells, TR Con, TR: cells treated with transfection reagent (TransIT-X2), GFP: green fluorescent protein, *1: vs 1 Gy, *3: vs 3 Gy.

	γH2AX foci/nucleus mean ± SD	53BP1 foci/nucleus mean ± SD	colocalization foci/nucleus mean ± SD
NT Con	3.03 ± 1.32	2.38 ± 1.73	1.03 ± 0.60
TR Con	3.41 ± 1.26	2.83 ± 1.93	1.37 ± 0.68
NT + IR [1 Gy]	16.15 ± 3.32	7.99 ± 4.23	7.60 ± 4.50
TR + IR [1 Gy]	17.16 ± 4.41	13.61 ± 4.88	9.69 ± 3.11
GFP + IR [1 Gy]	17.05 ± 0.79	14.76 ± 1.65	9.99 ± 0.64
NT + IR [3 Gy]	25.31 ± 6.09	14.55 ± 2.59	13.27 ± 0.85
TR + IR [3 Gy]	25.39 ± 4.67	20.06 ± 4.63	14.24 ± 2.05
GFP + IR [3 Gy]	25.22 ± 2.08	23.48 ± 1.42	14.10 ± 1.71
	p value γH2AX vs NT (*1, *3)	p value 53BP1 vs NT (*1, *3)	p value colocalization vs NT (*1, *3)
TR + IR [1 Gy]	(*1) 0.8006	(*1) 0.0560	(*1) 0.3203
GFP + IR [1 Gy]	(*1) 0.9394	(*1) 0.0889	(*1) 0.4431
TR + IR [3 Gy]	(*3) >0.9999	(*3) 0.0629	(*3) 0.8982
GFP + IR [3 Gy]	(*3) >0.9999	(*3) 0.0139	(*3) 0.9849

Table 7.59: Data from flow cytometric analysis of cell cycle distribution and apoptosis after lentiviral transduction with diluted Puro.Cre vector in mouse embryonic fibroblasts without loxP sites (*Rac1*$^{wt/wt}$).

Cells were transduced with different dilutions of Puro.Cre vector and 24 h later treatment with puromycin was started. Cells were analyzed 24 h, 48 h, 72 h, 96 h, and 120 h after puromycin selection. Cells were lysed and the nuclei were stained with the DNA-intercalating agent propidium iodide. The cell cycle distribution was determined using a flow cytometer. Control cells (*Rac1*$^{wt/wt}$) were non-transduced. The mean values on which Figure 7.25 is based on are listed in the Table (n=1).

24 h	SubG1 [%] mean	G1 [%] mean	G2/M [%] mean
Con	4.82	74.35	12.89
1:2 vector dilution	6.11	86.75	3.27
1:4 vector dilution	5.57	80.45	9.33
1:6 vector dilution	7.28	86.21	2.52
1:8 vector dilution	6.13	79.92	9.90
48 h	SubG1 [%] mean	G1 [%] mean	G2/M [%] mean
Con	5.58	77.28	11.24
1:2 vector dilution	11.58	87.22	1.07
1:4 vector dilution	40.77	56.56	0.86
1:6 vector dilution	5.31	65.38	14.57
1:8 vector dilution	6.15	69.41	12.87

72 h	SubG1 [%] mean	G1 [%] mean	G2/M [%] mean
Con	3.70	74.29	13.02
1:2 vector dilution	4.55	77.49	11.86
1:4 vector dilution	5.17	72.85	12.78
1:6 vector dilution	5.29	72.45	13.17
1:8 vector dilution	4.96	75.00	13.30
96 h	SubG1 [%] mean	G1 [%] mean	G2/M [%] mean
Con	5.04	74.92	12.96
1:2 vector dilution	5.51	73.83	13.65
1:4 vector dilution	5.65	61.62	14.81
1:6 vector dilution	4.28	54.03	16.49
1:8 vector dilution	4.42	60.63	15.91
120 h	SubG1 [%] mean	G1 [%] mean	G2/M [%] Mean
Con	3.94	63.18	16.11
1:2 vector dilution	3.71	60.42	16.08
1:4 vector dilution	3.56	72.35	14.94
1:6 vector dilution	5.37	71.34	14.96
1:8 vector dilution	5.39	70.79	14.68

Eidesstattliche Erklärung

Ich versichere an Eides Statt, dass die Dissertation von mir selbstständig und ohne unzulässige Hilfe unter Beachtung der „Grundsätze zur Sicherung guter wissenschaftlicher Praxis an der Heinrich-Heine-Universität Düsseldorf“ erstellt worden ist. Ich erkläre außerdem, dass diese Dissertation, in dieser oder ähnlicher Form noch bei keiner anderen Institution eingereicht wurde. Ich habe keine vorherigen erfolglosen Promotionsversuche unternommen.

Düsseldorf, 08.12.2021 Rebekka Kitzinger

Danksagung

Die letzten Zeilen meiner Arbeit möchte ich all denen widmen die mich auf Weg zur Dissertation begleitet, unterstützt und zum Gelingen dieser Arbeit beigetragen haben.

Prof. Dr. Gerhard Fritz für die Möglichkeit meine Arbeit am Institut für Toxikologie anfertigen zu dürfen sowie für die Übernahme der Betreuung meiner Doktorarbeit.

Dr. Christian Henninger für die interessante Themenstellung und die Betreuung meiner Doktorarbeit.

Prof. Dr. Sebastian Wesselborg für die Bereitschaft das Zweitgutachten meiner Doktorarbeit zu übernehmen.

Dr. Constanze Wiek und **Dr. Katharina Roellecke** für die Einarbeitung in die virale Transduktion, die Beantwortung vieler Fragen und die Hilfestellung bei Problemen.

Allen **Mitarbeitern des Instituts für Toxikologie** für das angenehme Arbeitsklima. Ein besonderer Dank geht dabei an **Sandra Ohler** und **Kerstin de Mezzo** die immer ein offenes Ohr hatten und stets einen hilfreichen Rat bei Problemen hatten.

Alexandra Plumhoff und **Christine Wenz** für die Motivation und das Zuhören. Wenn man sich über die gleichen Sachen freuen und aufregen kann, wird einiges einfacher.

Der illustren Runde. Kulinarische Ausflüge mit euch lassen einen die Zeit vergessen und den Stress verfliegen.

Mein Dank gilt auch meiner **Familie**, die mich unterstützt, mich motiviert und angespornt hat.

Ron ganz besonderer Dank geht an dich, dafür das du immer an mich geglaubt hast, für deine Geduld und Unterstützung, insbesondere während der stressigen letzten Phase dieser Arbeit.

Vielen Dank!